THE UNIVERSITY
of EDINBURGH

Fundamental Aspects of Pickering Emulsion Stabilisation

David James French

Doctor of Philosophy
The University of Edinburgh
2016

Abstract

Much research has been carried out in recent years on Pickering emulsions, but understanding of the underlying physics requires considerable strengthening. This thesis seeks to address several fundamental aspects by presenting the results of recent experimental work.

This work has focused on a model oil-in-water emulsion system stabilised by fluorescent colloidal silica particles and using a mixture of dodecane and isopropyl myristate as the oil phase. The phase behaviour of the particle dispersions has been altered using sodium chloride and sodium iodide, whilst sodium hydroxide and hydrochloric acid have been used to adjust the pH of samples. Comparisons are also made to emulsions stabilised by commercially available fumed silica.

Conventionally, it was assumed that a weakly flocculating particle dispersion is required in order to generate a stable Pickering emulsion. It is shown in this work, however, that in some circumstances a weakly flocculating dispersion leads to the least stable emulsion. It is therefore argued that a more nuanced view of Pickering stabilisation is required, taking into account the factors affecting whether particles will adsorb to the interface during emulsification.

Very recently it has begun to be suspected that Pickering emulsions sometimes aggregate due to the sharing of particles between two droplets, an effect known as bridging. In this thesis it is also shown that particle bridges can form in Pickering emulsions at high shear, and that they can subsequently be broken by low shear or by modifying the particle wettability. For the first time, electron microscopy has been used to provide direct evidence of droplets sharing particles. A simple theoretical model is developed, based on collisions between partially coated droplets, which captures the trends observed experimentally. It is argued that particle bridging may have been overlooked in the literature, and that the shear history of emulsions is a crucial determinant of subsequent behaviour.

The deaggregation of bridged emulsions has been studied using a novel method where two different colours of particles are used. By starting with two emulsions which are bridged, each stabilised by a different colour of particle, and then using confocal microscopy to study them as they are mixed together and deaggregate, the processes involved in deaggregation can be elucidated. These experiments have also shown, for the first time, the dynamic nature of particles in Pickering emulsions; particles transfer readily between droplets when the samples are placed on a roller bank. It is found that a period of unbridging and rebridging takes place prior to deaggregation of the emulsions, and the timescale of deaggregation can be tuned by varying the particle wettability.

The two-colour method has also been applied to the study of Pickering emulsions which are repeatedly sheared. It is found that limited coalescence is not re-established simply by re-applying the shear rate which was used in the initial emulsification. This behaviour is attributed to the presence of an elastic shell of particles at the interface, which inhibits droplet breakup, and is in contrast to that of surfactant-stabilised emulsions, where increasing the stabiliser concentration makes droplets more liable to deform and breakup.

Finally, a short study has been carried out attempting to increase the scale of the experiments presented in this thesis to sample volumes of approximately one litre. This study has demonstrated the relevance of particle bridging to industrial emulsification processes.

Overall, experiments with carefully controlled model Pickering emulsions, including those using two colours of particles, have revealed the fundamental workings of these arrested systems.

Lay summary

Most people will be aware that oil and water don't generally mix. Some of these people will additionally be aware that oil and water can be made to mix by adding certain extra components, as occurs in salad dressings. When oil is mixed into water (or *vice versa*) in this way, the resulting liquid is called an emulsion, and consists of small droplets of one phase dispersed within the other phase. The additional components are known as emulsifiers, and are usually molecules which have one end which is soluble in water and one end which is soluble in oil, and it is this dichotomy in structure which allows them to encourage the formation of emulsions.

However, the third component does not need to be structurally heterogeneous. By simply taking up space on the interface between the oil and water, solid particles (*e.g.*, small grains of sand) can allow an emulsion to be formed. This is known as a Pickering emulsion and the droplets in such an emulsion are prevented from merging by the layers of particles at their surfaces. Interestingly, if the particles stick out far enough from the interface, they can be attached to two separate droplets at the same time. This phenomenon is known as particle bridging and radically alters the behaviour of the emulsion as it flows.

In this thesis, recent experimental work relating to several different aspects of particle-stabilised emulsions is presented. Whether the behaviour of emulsions is affected by the behaviour of the particles themselves (*e.g.*, if the particles stick together) is investigated, as are various factors affecting the presence of particle bridges in an emulsion, and whether particles can transfer between droplets.

This work describes several novel behaviours in Pickering emulsions and solidifies understanding of several others. It should therefore be relevant to anyone wishing to design a well controlled Pickering emulsion system.

Declaration

I declare that this thesis was composed by myself, that the work contained herein is my own except where explicitly stated otherwise in the text, and that this work has not been submitted for any other degree or professional qualification except as specified.

Work which has formed part of jointly authored publications has been included. The contribution of the candidate and the other authors to this work has been explicitly indicated below. I confirm that appropriate credit has been given within the thesis where reference has been made to the work of others.

A jointly authored publication forms the basis of Chapter 5. All experiments were carried out by the candidate, with help from Jill Foundling and Chris Stain whilst using the electron microscope. The published paper is:

D.J. French, P. Taylor, J. Fowler, and P.S. Clegg. Making and breaking bridges in a Pickering emulsion. *Journal of Colloid and Interface Science*, 441:30-38, 2015.

(*David James French, 2016*)

Acknowledgements

Many people have helped me through my PhD work, and I would like to thank some of them here. First of all, my supervisor, Paul Clegg, for his considerable enthusiasm, encouragement, help and scientific input throughout my PhD. Also, my industrial supervisors, Phil Taylor and Jeff Fowler at Syngenta, who have both also helped immensely.

I would also like to thank Andrew Schofield for synthesising the particles, Jill Foundling and Chris Stain at Syngenta for their help with the electron microscopy and Joe Forth for providing filtered dodecane. Andrew, Charlotte, James and Joe have proof read chapters of my thesis, which I am very grateful for. Also, the University of Edinburgh, EPSRC and Syngenta, who provided, amongst other useful things, money and a desk.

On a more personal note, I would like to thank everyone who has helped distract me from work over the last few years. The work of Machiavelli, Cato, Obliteron and Lanark has been also been incredibly helpful in this regard. Finally, my family, who have done so much for me, and Morvern, for her love, encouragement and support throughout.

Contents

Chapter 1

Introduction

1.1 Background

Pickering emulsions belong to a class of materials known as soft matter, which can be considered the area of science dealing with systems which do not conveniently fall into either crystals or simple fluids; soft matter can be thought of as the study of complex fluids. Soft matter is a broad topic, covering - amongst other subjects - liquid crystals, polymer solutions and living cells. This broad range of systems has a number of unifying features, however, such as a mesoscopic length scale and the importance of Brownian motion [1, 2]. This thesis seeks to provide some fundamental understanding of the physics involved in Pickering emulsions. Pickering emulsions are systems which have been arrested far from thermodynamic equilibrium, a fact which underlays much of their behaviour. Pickering emulsions open up a new spectrum of soft matter behaviour as a result of having two mesoscopic length scales. By relating the macroscopic properties of the emulsion to the microscopic properties of the colloidal particles, significant improvements in the knowledge and understanding of these systems should be possible, and should lead to improvements in the processing conditions used to create these emulsions industrially.

Emulsions are a common type of soft matter in which droplets of one liquid are dispersed within another. Examples include milk, vinaigrette and certain anaesthetics. To prevent the droplets of the dispersed phase from coalescing, some sort of barrier must be present on the interface between the two liquids.

This barrier can be mechanical, as in the case of surfactants, or electrostatic - if the interfaces can be made sufficiently charged then coalescence will not occur. Several types of surfactant exist, including amphiphilic surfactants and proteins - which are used as surfactants in biological systems. This thesis will deal with emulsions which have been stabilised by solid colloidal particles, also known as Pickering emulsions. The main system used is an oil-in-water (o/w) emulsion stabilised by colloidal silica, where the oil phase is a mixture of dodecane and isopropyl myristate and the ratio of the two oils is used to control the particle wettability. Fluorescent silica particles have been used so that imaging can be carried out with a confocal microscope.

Colloidal particles are generally in the nanometre-micrometre size range, which means that quantum effects can safely be ignored, and that thermal forces play a crucial rôle in their behaviour. On relatively short timescales gravity can also be neglected.

1.2 State of the art

1.2.1 Emulsions

When two immiscible liquids are brought into contact with each other, there is an energy penalty involved with creating the interface between them. This means that when the two liquids are mixed and droplets are formed, coalescence of the dispersed phase will occur, leading to macroscopic phase separation. The breakup of a droplet first requires the droplet to be deformed, and droplet deformation is opposed by the Laplace pressure, P_L, which for a spherical droplet is:

$$P_L = 2\frac{\sigma_{ow}}{r_o}, \tag{1.1}$$

where σ_{ow} is the oil-water interfacial tension and r_o is the radius of the droplet [3]. Typical Laplace pressures for oil-in-water emulsions are in the range of 10^3-10^6 Pa. To significantly deform a droplet, a stress greater than the Laplace pressure must be exerted upon it and so a relatively large velocity gradient must be applied to the system.

1.2.2 Pickering emulsions

Pickering emulsions have received considerable attention in recent years, despite being known about for over a century [4–6]. Solid particles which exhibit partial wettability with both of the fluid phases making up the emulsion are required; the particles reduce the free energy of the fluid-fluid interface and hence become kinetically trapped. It is therefore possible to create an emulsion stabilised solely by solid particles, where each droplet is coated with a layer of particles [7].

The three-phase contact angle, θ_w, is used to characterise the position of a particle at the oil-water interface, and is depicted in Fig. 1.1. Normally, θ_w is measured through the more polar liquid phase (*i.e.*, θ_w is low for hydrophilic particles and high for hydrophobic particles, with $\theta_w = 90°$ meaning that the particles are neutrally wetted) and is related to the solid-oil, solid-water and oil-water interfacial tensions by the Young equation:

$$\sigma_{so} = \sigma_{sw} + \sigma_{ow} \cos\theta_w. \tag{1.2}$$

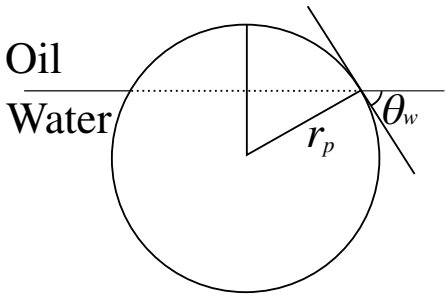

Figure 1.1 *A particle at a water-oil interface, showing the three-phase contact angle, θ_w.*

If a colloidal particle which has intermediate wettability with both liquids is placed on the liquid-liquid interface, as in Fig. 1.1, then it can behave like a surfactant. The interfacial area shared by the two liquids is reduced, and so the free energy of the interface is reduced as well.

The change in free energy, ΔG, occurring when a particle moves from its preferred phase to the oil-water interface is given by:

$$\Delta G = -\pi r_p^2 \sigma_{ow} (1 - |\cos\theta_w|)^2, \tag{1.3}$$

where r_p is the particle radius [8]. This change can be very large relative to the thermal energy, which means that if a particle once sequesters to the interface, it is very unlikely to be removed. A particle with radius 0.5 μm on a dodecane-water interface and a contact angle of 90° will have a trapping energy of approximately 10^6 k_BT (where k_B is Boltzmann's constant and T is the absolute temperature). This is in stark contrast to molecular surfactants, where $|\Delta G| \approx k_BT$, which tend to 'hop' on and off of the interface. Unless they are very small ($r_p \lesssim 10$ nm [9]), particles at an oil-water interface do not significantly reduce the interfacial tension, unlike molecular surfactants, and this distinction is important when considering the emulsification process. The reduction in interfacial tension caused by small solid particles at the interface has been referred to as a change in the "effective interfacial tension", in order to differentiate it from the "true" interfacial tension which exists at the bare fluid-fluid interface between particles [10].

Several factors which affect the stability of Pickering emulsions have previously been discussed in the literature. These include the oil:water ratio, concentration of particles and the particle wettability [11]; whether the particles are initially dispersed in the continuous or dispersed fluid phase, oil polarity and sample pH all have additional effects [12].

Furthermore, the specific surface chemistry of the particles will affect the three-phase contact angle, and hence will have an effect on emulsion stability. It is known that the drying temperature and time both affect the surface chemistry of fluorescent silica [13].

Various methods are available for characterising the properties of the emulsion. Most obviously, the size and polydispersity of the droplets is important, as is their shape. The stability of an emulsion can be characterised by the fraction of the dispersed phase which resolves - *i.e.,* which does not form droplets. The polydispersity of an emulsion can be characterised using the coefficient of variation (CV), which is defined as the standard deviation of the droplet size divided by the mean droplet size.

A theory relating the size of a droplet to the volume fractions of the emulsion components and the size of the particles was proposed by Binks *et al.* in 2001 [14]. The volume fraction of oil in the emulsion, ϕ_o, is given by:

$$\phi_o = \frac{4}{3}\pi r_o^3 n_o, \tag{1.4}$$

where n_o is the number density of droplets. Similarly, the volume fraction of particles is given by:

$$\phi_p = \frac{4}{3}\pi r_p^3 n_p, \tag{1.5}$$

where the subscript p denotes particles. Assuming that each droplet is covered by a hexagonally close-packed monolayer of monodisperse particles (which is not actually achievable at a curved interface, but is a good approximation when $r_o \gg r_p$, unless the particles aggregate strongly at the interface [15]), that all particles sequester to an interface and that the droplets are also monodisperse, the number of particles will be given by:

$$n_p = \frac{4\pi r_o^2 n_o}{\pi r_p^2}\frac{\sqrt{3}\pi}{6}, \tag{1.6}$$

where the numerical factor on the right is the packing fraction of hexagonally close-packed circles.

Combining Eq. (1.4), Eq. (1.5) and Eq. (1.6) yields the relation between droplet radius, constituent volume fractions and particle radius[1]:

$$r_o = \frac{2\pi}{\sqrt{3}}\frac{\phi_o r_p}{\phi_p}. \tag{1.7}$$

Binks *et al.* found that, for particles less than 1 μm in diameter, droplet diameter scaled linearly with particle diameter, with the gradient in good agreement with that expected from Eq. (1.7).

1.2.2.1 Limited coalescence

In the conventional picture of emulsification, immiscible liquids demix following shear until some barrier prevents further demixing. In Pickering emulsions, this barrier is mainly mechanical in nature, caused by the particles on two droplets preventing the droplets from coalescing. Demixing causes the system to move from a state of high interfacial area to a state of much lower interfacial area, until

[1]The numerical pre-factor has been corrected from Ref. [14].

the interfacial area is equal to that which can be stabilised by the particles, at which point the particles jam and coalescence is arrested [16, 17]. This process is known as limited coalescence and there is significant interest in probing its limits, situations in which the theory is not valid, and ways in which the process can be re-established.

1.2.2.2 Inversions

It is well known that various factors can dramatically change the properties of an emulsion. Binks *et al.* have shown that the volume fractions of the three components determine whether the emulsion will be water-in-oil, oil-in-water or a multiple emulsion [11]. The volume fractions of the constituents also affect the size and polydispersity of the final emulsion. Samples where the dispersed phase has a high volume fraction will have large droplets and a relatively low polydispersity [18].

The hydrophobicity of the particles determines their position on the interface. Hydrophobic particles tend to sit more into the oil phase, whilst hydrophilic particles will sit mostly in the water phase. This can affect which of the fluids becomes the dispersed phase and which becomes the continuous phase. Emulsions stabilised by hydrophilic particles are more likely to be oil-in-water [11]. This behaviour increases the packing fraction of particles at the interface. For a droplet with a radius of 100 μm an increase of 1 μm in the diameter of the particle shell can cause an increase in the number of particles in the shell of $\approx$ 2%. The switching between oil-in-water and water-in-oil type emulsions due to changes in hydrophilicity of particles is known as transitional inversion. Changes in the particle concentration can also induce a phase inversion - this has been attributed to a change in particle hydrophilicity caused by aggregation of inhomogeneous particles [11, 12].

Another factor which can change the type of emulsion is the oil:water ratio. Generally speaking, the minority phase is more likely to be the dispersed phase, as the majority phase will more quickly become fully connected when shearing ceases. The switching of dispersed and continuous phases as a result of varying the oil:water ratio is known as catastrophic inversion. The ratio at which catastrophic inversion occurs is dependent on the phase in which the particles are dispersed - the phase in which they are dispersed has a tendency to become the continuous phase [19]. This phenomenon will affect the likelihood of particles adsorbing at

the interface, and may be linked to contact angle hysteresis [7, 20].

In the current work, values of ϕ_o and ϕ_p have been chosen such that these inversion mechanisms are avoided.

1.2.2.3 Destabilising mechanisms

There are several mechanisms which can destabilise emulsions. The most obvious of these is coalescence, where two droplets merge together to form a larger droplet. Fully coated Pickering emulsion droplets are robust to coalescence because the particle layers create a mechanical barrier which the droplets cannot overcome. Partially coated droplets can also prevent coalescence, as attractive interactions between the particles can cause them to move to the areas of the droplet nearest to another droplet [21]. The effects of varying the particle-particle interactions on this mechanism are not currently clear, however.

Another process which can cause emulsion droplets to change in size is known as Ostwald ripening. Ostwald ripening occurs because the Laplace pressure of small droplets is larger than that of large droplets, which means that molecules of the dispersed phase dissolve more easily into the continuous phase from small droplets than large ones [3]. Therefore, fluid tends to move from small droplets to large droplets. However, when this happens in a Pickering emulsion, the curvature of the interface at the interstices between particles on the smaller droplets changes from positive to negative in order to maintain θ_w, as shown in Fig. 1.2. This results in the droplet having zero mean curvature and thereby prevents Ostwald ripening [22, 23]. However, if the surface coverage of the droplets is relatively low, Ostwald ripening may still occur, and so the surface coverage is important for stability against Ostwald ripening as well as coalescence [24].

When the densities of the dispersed and continuous phases are different, the dispersed phase will either rise or fall in the sample depending on which phase has the greater density. The terminal velocity, v_t, of a spherical object of radius, r_p, and density, ρ_p, sedimenting in a fluid of viscosity, η, and density, ρ_f, is given by:

$$v_t = \frac{2}{9}\frac{r_p^2(\rho_p - \rho_f)g}{\eta}, \tag{1.8}$$

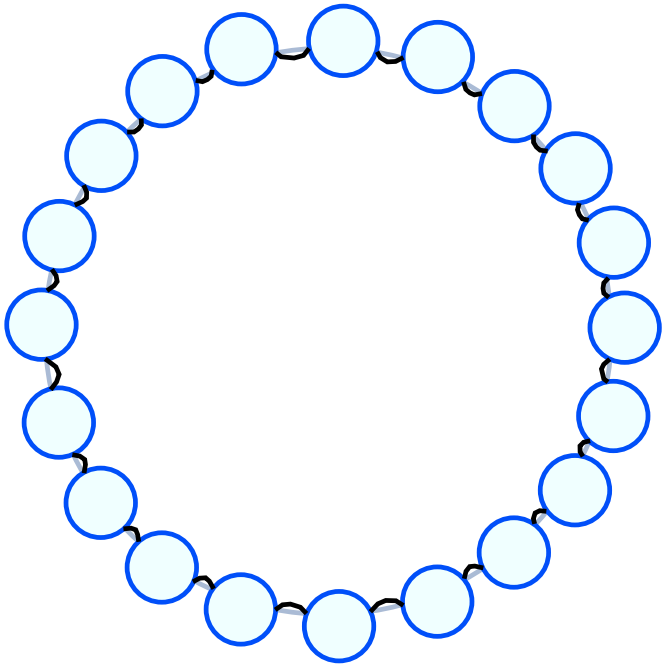

Figure 1.2 *Schematic showing why Pickering emulsions are resistant to Ostwald ripening. A fluid droplet is stabilised by particles (blue). The light grey line shows the initial droplet interface in the interstitial areas. Since the contact angle must be maintained, if the droplet reduces in volume slightly, the droplet interface will be given by the black lines. This causes the Laplace pressure to become negligible, and so further Ostwald ripening is prevented. Adapted from Ref. [22].*

where g is the acceleration due to gravity [25]. For oil-in-water emulsions the dispersed phase usually has the lower density, and so the droplets will rise to the top - a process known as creaming. As can be seen from Eq. (1.8), creaming can be suppressed by density matching the two liquid phases, by reducing droplet size or by increasing the viscosity of the continuous phase [26].

Finally, if the inter-droplet interactions in an emulsion are attractive, then the droplets will flocculate [27]. This is generally a reversible process, so that gentle shaking is sufficient to restore the emulsion to its dispersed state. Flocculation will also tend to increase the creaming rate, as the effective droplet radius is increased, but extensive flocculation can also lead to the emulsion forming a gel-like structure, which will lead to creaming being significantly hindered.

1.2.2.4 Particle bridging

One advantage of using solid colloidal particles rather than surfactants to stabilise emulsions is that some behavioural phenomena are possible with particles which are not possible with surfactants - a consequence of the two separate mesoscopic length scales in the system. For example, if the particles protrude further into the continuous phase than into the dispersed phase, then the particles can be adsorbed at the interfaces of two droplets simultaneously, a phenomenon known as particle bridging [28]. Clearly, such behaviour is capable of creating a network of droplets and radically altering the sample rheology. The presence of particle bridges in Pickering emulsions has been reported by various groups, but until now there has not been a systematic study of the ways in which they can be created and removed.

1.2.3 Theory of emulsification

It is clear that in order to generate a Pickering emulsion using immiscible fluids energy must be expended in order to increase the oil-water interfacial area. This is most commonly achieved by applying a shear to the sample. An overview of droplet breakup in both laminar and turbulent flows can be found in Ref. [29]. A brief theoretical description of the physics underlying emulsification by applying shear will be presented here.

In laminar flow the capillary number, Ca, is used to explain the relationship between interfacial area and shear rate. It is defined as the ratio of viscous forces to interfacial forces:

$$Ca = \frac{\eta \dot{\gamma} r_o}{\sigma_{ow}}, \tag{1.9}$$

where $\dot{\gamma}$ is the shear rate. If Ca is above a critical value, Ca_c, then a droplet will burst, reducing r_o and hence Ca [30]. At the same time, smaller droplets can coalesce, causing r_o and Ca to increase. In this way, Ca will tend towards Ca_c, the exact value of which depends on the viscosities of the dispersed and continuous phases, but which is approximately 0.2 in the experiments carried out here. Equation (1.9) can be re-expressed as:

$$A = \frac{3V_d}{Ca_c} \frac{\eta \dot{\gamma}}{\sigma_{ow}}, \tag{1.10}$$

where A is the total interfacial area and V_d is the total volume of the dispersed

phase.

Under turbulent conditions, however, droplet breakup is facilitated by stress from eddies and Eq. (1.9) is no longer valid. Instead, the maximum droplet diameter which will not break up, d_{max}, is given by Kolmogorov theory [31, 32], which states that:

$$d_{max} = C\frac{\sigma_{ow}^{3/5}}{\rho^{1/5}\epsilon^{2/5}}, \tag{1.11}$$

where ρ is the density of the continuous phase, ϵ is the energy dissipated *via* turbulence per unit volume and per unit time, and C is a proportionality constant, thought to be approximately 1 [33], and measured empirically as 0.86 by Vankova *et al.* using a narrow-gap homogeniser [34].

Equation (1.11) can also be re-expressed to give the interfacial area:

$$A = \frac{6V_d\rho^{1/5}\epsilon^{2/5}}{\sigma_{ow}^{3/5}}. \tag{1.12}$$

Several different emulsification devices - a rotor-stator, a vortex mixer and a continuous flow emulsifier - have been used to emulsify and shear samples in this work. These devices will be discussed in more detail in Chapter 2, and the continuous flow device will be discussed in Chapter 8.

The rotor-stator is capable of generating controlled shear rates over a large range, from 0-53 000 s^{-1}. The residence time, which is the length of time a droplet spends in the shear zone in a single pass, of the rotor-stator can be estimated as:

$$\tau_{res} \approx \frac{\delta_g}{r_{in}\omega}, \tag{1.13}$$

where δ_g is the width of the gap between the rotor and the stator, r_{in} is the inner radius of the stator and ω is the angular velocity of the rotor, in rad$\cdot s^{-1}$. The vortex mixer has a much larger shear zone than the rotor-stator, meaning that the droplets it creates have a longer lifetime, which can make it easier to get all the particles in a sample onto an oil-water interface. The shear rate in the vortex mixer is, however, unknown.

Sparks has estimated that $\approx$ 3% of the power supplied to the rotor-stator is dissipated in the fluid *via* turbulence [35], and that this dissipation occurs in a

relatively small volume surrounding the rotor and stator. Given the maximum power output and maximum shear rate, 750 W and 53 000 s^{-1} respectively, and assuming that the power dissipated is proportional to the square of the shear rate, ϵ can be estimated for the rotor-stator:

$$\epsilon = 0.03 \times 750 \left(\frac{\dot{\gamma}}{53\,000} \right)^2 \left(\frac{1}{(2 \times r_{in})^3} \right). \tag{1.14}$$

Whether the flow is laminar or turbulent can be determined from the Reynolds number, Re, given by:

$$Re = \frac{vl\rho}{\eta}, \tag{1.15}$$

where v is a characteristic velocity, here the tip velocity of the rotor, and l is a characteristic length scale, here the width of the gap between the rotor and the stator. If $Re \gtrsim 1000$, the flow will be turbulent [33].

It is not yet clear, however, how the solid layer of particles at a droplet's interface affects the interface's mechanical properties and Ca_c. This is an active area of research; recent work by Maurice *et al.* [36] and by Hermes and Clegg [37] is beginning to address this problem.

In practice the viscosity of the continuous phase depends on the particle volume fraction, which is not constant during the emulsification process. The ϕ_p values used in this work are all below 2.5%, however, and so the contribution to the viscosity from the colloidal particles is low.

1.2.4 Particle phase behaviour and emulsion stability

Equation (1.3) shows that a particle is most strongly held at the oil-water interface if the contact angle is 90° (*i.e.,* the particle protrudes equally into the two phases). This is accomplished by using particles of intermediate hydrophobicity, which means that the particles will not be particularly stable against flocculation in either of the two phases individually (*i.e.,* the particles will be too hydrophilic to be stable in the oil phase yet too hydrophobic to be stable in the aqueous phase). This causes problems because in order to form particle monolayers at the interface, and hence optimise particle usage, the particles are required to be well dispersed, which is difficult if the particles have a tendency to flocculate.

The tendency for weakly flocculating particles to achieve better stabilisation of

emulsions than non-flocculating particles was first reported in 1921 by Briggs, who also noted that strongly flocculating particles do not show the same stabilising behaviour [38]. This finding has been replicated for several experimental systems in recent years (*e.g.*, see Refs. [39–42]). However, Binks and Lumsdon have also demonstrated that the stabilising effect of weakly flocculating particles only occurs for certain salts - specifically they found that sodium chloride did not enhance the stability of toluene-in-water emulsions stabilised by 12 nm diameter silica particles [43]. It can therefore be seen that the picture of weakly flocculating particles being beneficial and strongly flocculating particles being detrimental to emulsion stability is an oversimplification.

Previous work in this area has been carried out by Binks *et al.,* but they used fumed silica particles which are not monodisperse and are not spherical [7, 39]. It is hoped, therefore, that the research presented in this thesis can place their work on a surer footing by directly visualising the particles at the interface using confocal microscopy, as well as extend it to new areas.

1.2.5 Particle interactions in bulk

The properties of a Pickering emulsion will be influenced by the behaviour of the particles stabilising it. For example, if the particles are able to quickly adsorb onto the oil-water interface then droplet coalescence will be suppressed at an earlier stage of phase separation and the result will be a finer emulsion. Also, if particles are prevented from aggregating then the particle layer covering a droplet will be a monolayer, whilst particle aggregation can lead to a thickening of the particle layer, which will affect both droplet size and stability [44].

The inter-particle potential is determined by several different mechanisms, the most important of which are the attractive van der Waals force and the repulsive force known as the electrical double layer interaction. The combined theory of van der Waals attractions and electrostatic repulsions is known as DLVO theory, after its main developers - Derjaguin, Landau, Verwey and Overbeek [45, 46]. Van der Waals forces arise from temporary dipole interactions between atoms, and the van der Waals potential between two atoms, $V_A(z)$, varies with their separation, z, as:

$$V_A(z) = -\frac{C}{z^6}, \tag{1.16}$$

where C depends on the atoms' polarisability and has units of energy multiplied by distance raised to the sixth power. To calculate the potential between two colloidal particles, one must integrate $V_A(z)$ over the volumes of both particles. Doing so for spherical particles in a single fluid yields:

$$V_A(z) = -\frac{A_h}{6}\left(\frac{2R_1R_2}{z^2-(R_1+R_2)^2}+\frac{2R_1R_2}{z^2-(R_1-R_2)^2}+\ln\frac{z^2-(R_1+R_2)^2}{z^2-(R_1-R_2)^2}\right), \tag{1.17}$$

where R_1 and R_2 are the radii of the particles and A_h is the Hamaker constant [47]. The Hamaker constant is a property of the material and has a value of 6.5×10^{-21} J for silica in water [48]. When $R_1 = R_2 = r_p$, Eq. (1.17) reduces to:

$$V_A(z) = -\frac{A_h}{6}\left(\frac{2r_p^2}{z^2-4r_p^2}+\frac{2r_p^2}{z^2}+\ln\left(1-\frac{4r_p^2}{z^2}\right)\right). \tag{1.18}$$

When $r_p \gg z$, Eq. (1.18) further simplifies to:

$$V_A(z) = -\frac{A_h r_p}{12z}. \tag{1.19}$$

The van der Waals potential can be modified by altering the refractive index of the solvent. This is true because refraction and van der Waals forces are both related to the polarisability of a substance. The most common method of altering the refractive index of aqueous solutions is to add either salt or glycerol.

The particles' surface charge will affect how ions in the solvent are distributed. There will be an increased concentration of counterions around the particle, and a corresponding decrease in the concentration of co-ions [49]. The ions immediately adjacent to the particle (known as the Stern layer) will be strongly bound to the particle, whilst ions further away will be less strongly bound. If the particle moves, then it will drag the ions nearest to it along, but ions far from the particle will not move with it. Therefore, there exists a boundary, or slipping plane, which separates the ions which are dragged by the particle from those which are not, as shown in Fig. 1.3. The potential at this boundary is called the zeta potential, ζ, and is a useful measure of the particles' charge and stability - the greater the magnitude of the zeta potential, the less likely the particles are to aggregate. The zeta potential can be measured by applying an electric field to the dispersion

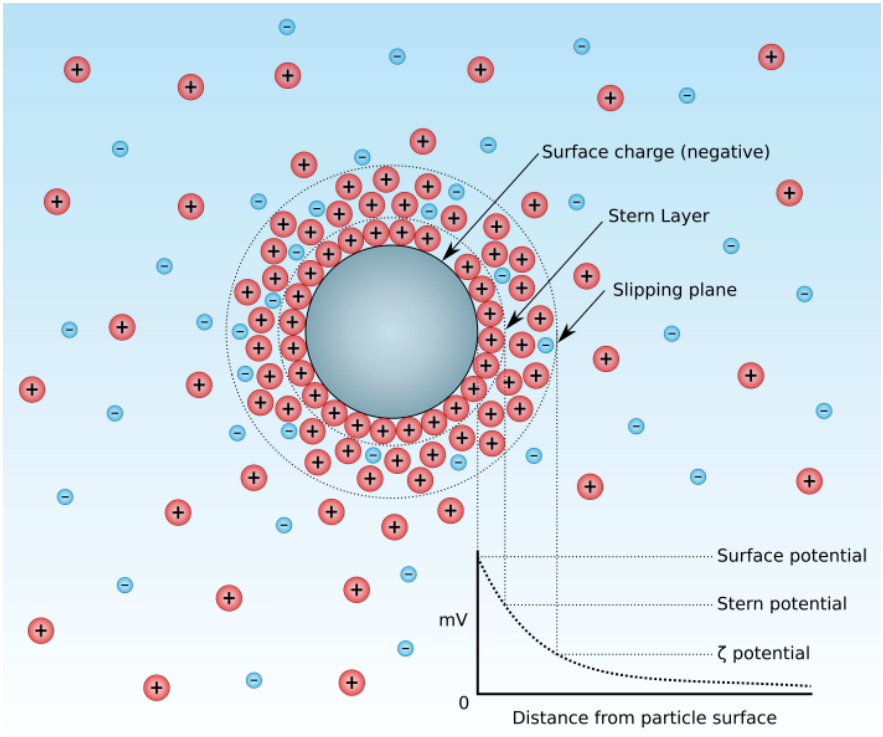

Figure 1.3 *Schematic showing how the zeta potential is defined. Taken from Ref. [50].*

and measuring the particles' velocity using light scattering.

The addition of salt to the sample can cause electrostatic interactions between particles to be screened [1]. Electrostatic screening is quantified by the Debye length, κ^{-1}, which is the distance over which electrostatic forces are considered important, and which is given by:

$$\kappa^{-1} = \sqrt{\frac{\epsilon_r \epsilon_0 k_B T}{2 N_A e^2 I}}, \tag{1.20}$$

where ϵ_r is the dielectric constant of the fluid, ϵ_0 is the relative permittivity of free space, N_A is Avogadro's number, e is the charge of an electron and I is the salt concentration in moles per cubic metre [47]. For monovalent salts in water at room temperature, Eq. (1.20) can be simplified to:

$$\kappa^{-1} = 0.304 I^{-\frac{1}{2}}\, nm, \tag{1.21}$$

where I is now in moles per litre [51].

The repulsive potential, $V_R(z)$, between two identical charged spheres is given by:

$$V_R(z) = 2\pi\epsilon_r\epsilon_0 r_p \psi^2 \exp(-\kappa z), \tag{1.22}$$

where ψ is the Stern potential of the particles [52]. DLVO theory combines Eq. (1.17) with Eq. (1.22) to give the overall potential, $V(z)$, as a function of the particle separation. Figure 1.4 shows some example interaction energies between colloidal particles at different salt concentrations.

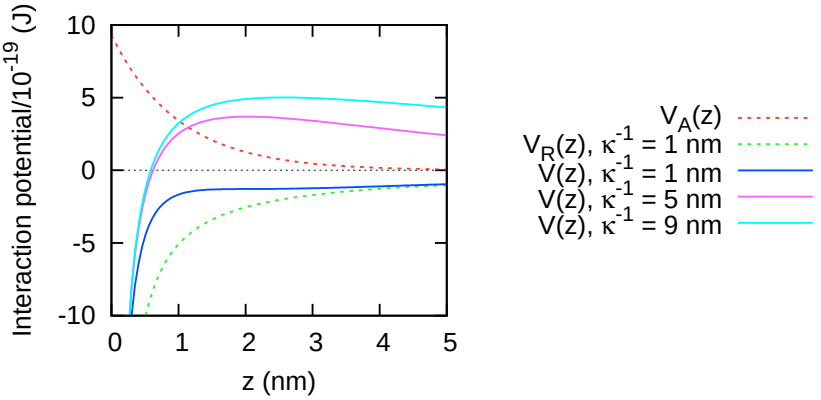

Figure 1.4 *Graphs showing the influence of the Debye length on the potential energy of interaction in a typical colloidal dispersion. For all plots,* $r_p = 100\ nm$, $T = 298\ K$, $A_h = 6.11 \times 10^{-20}\ J$, $\epsilon/\epsilon_0 = 78.5$ *and* $\psi = 50\ mV$.

Since it is expected that all particles are similarly charged, including salt is likely to reduce the repulsive forces between particles, making particle aggregation more likely. Electrostatic effects also affect the rate of droplet coalescence, because there is a charge on the surface of the oil droplets. Decoupling these effects from the inter-particle potentials will be important, since the interplay between droplet growth rate and the length of time it takes for a particle to diffuse to an interface will determine the eventual droplet size.

Adjusting the pH of the samples can also allow for electrostatic interactions to be modified. Fluorescent silica particles in solutions with a pH between 2 and 9 have negatively charged silanol groups (Si–O^-) and positively charged amino groups (NH_3^+) on their surfaces [53]. The amino groups are necessary to bind the fluorescent dye molecules to the silica. The ratio of these two groups will dictate the overall surface charge of a particle, and will be pH dependent. The pH at which silica has no net surface charge - the isoelectric point - has been reported at values ranging from 0.5 up to 3.7, although the majority of results are in the

region 2 ± 0.5 and variations from this value are likely due to factors such as the surface structure, particle size and presence of impurities [54]. Above pH 10 the solubility of silica increases dramatically, and colloidal silica breaks down [48].

The pH of the solution will affect the inter-particle potential, which means that it will be necessary to measure the zeta potential at a range of pH values. This information, along with sedimentation profiles, will be used to characterise the particle interactions. By comparing changes in these interactions with changes in macroscopic properties of the emulsions, the fundamental physics dictating emulsion behaviour will be deduced.

1.2.6 Particle-interface interactions

In order for Pickering stabilisation to occur, the particles must adsorb to the interface. At present little is known about the mechanics of particle-interface binding, although recent work by Kaz *et al.* has suggested that it may take several months for a particle to reach its equilibrium position [55]. However, these experiments used optical tweezers to minimise the forces acting on the particle as it became trapped and it is unknown whether these results have any serious implications for binding in the presence of the larger forces present in a vortex mixer, for example. The slow relaxation of particles at an interface does have interesting implications for the effect of colloidal interactions on emulsion properties, though, as the interactions will affect the relaxation dynamics.

If the particles are dispersed in the aqueous phase, then their charge can lead to a repulsive force between them and an oil-water interface, even if the interface is uncharged. This is because the relative permittivity of water is greater than that of dodecane, so the image charge observed by the particles in the oil is of the same sign as the particles [51, 56]. If a particle of charge, q, within a medium of relative permittivity, ϵ_w, is separated by a distance, d, from a plane surface of another medium of relative permittivity, ϵ_o, then the particle will experience a field from the surface equivalent to that from an image charge a distance d into the second medium and with charge:

$$q' = \frac{\epsilon_w - \epsilon_o}{\epsilon_w + \epsilon_o} q. \tag{1.23}$$

In the case of water and dodecane at 25℃, $\epsilon_w = 78.36$ [57] and $\epsilon_o = 2.02$ [58], and

so $q' \approx q$, meaning that the electrostatic contribution to the particle-interface interaction is repulsive.

1.2.7 Particles at liquid interfaces

When particles adsorb to an interface, they will change its physical properties. The particles can therefore impart new and useful behaviours on systems involving liquid interfaces. For example, milk is emulsion comprising fat globules in water, stabilised by solid casein proteins - without the proteins the fat globules would coalesce and the milk would phase separate. Solid nanoparticles also adsorb to lipid bilayers in cell membranes, which makes the interface more solid and can pose health risks [59].

1.2.7.1 Interactions between particles

The interactions between particles which have adsorbed to the oil-water interface will naturally influence the properties of a Pickering emulsion. However, the particle interactions at the interface may be very different from, and far more complex than, their interactions in a single fluid [60, 61]. In addition to the complications involved in applying DLVO interactions through two fluid phases with differing relative permittivities, new inter-particle interactions come into play as well. These new interactions are completely absent in either bulk phase and include capillary attractions and dipolar electrostatic interactions. If an anisotropic particle is placed at an isotropic oil-water interface (or if an isotropic particle is placed at an anisotropic interface), then the interface must deform in order to have a fixed contact angle at all points of the contact line [62]. If multiple particles are present at the interface, then the total interfacial area will be decreased if the deformed areas around each particle overlap, and this will lead to an attractive interaction between the particles. Although capillary attractions are most prominent for anisotropic particles, surface roughness can also lead to capillary attractions between spherical particles. Dipolar electrostatic interactions arise because the portion of the particle in contact with the non-polar phase can have a lower surface charge density than the portion of the particle in contact with the polar phase [63, 64]. However, the lack of ions in the non-polar fluid can lead to strongly repulsive interactions between particles at an interface.

Another important difference between bulk and interfacial particle interactions

is the dependence on θ_w which has to be considered at the interface. As shown in Ref. [60], van der Waals, electrostatic and dipolar interactions are all highly sensitive to the contact angle, particularly near the point of neutral wetting.

The properties of a monolayer of particles, and the interactions between the particles in the monolayer, at an oil-water interface can be probed by using a Langmuir trough to measure the surface pressure, Π, as a function of the two-dimensional density of particles at the interface [65]. The density of particles is varied by compressing the particle monolayer, and the pressure is measured using a Wilhelmy plate situated vertically at the edge of the trough. Such methods have been used to measure the long-range interactions between silica particles at an oil-water interface [66], and can be used to study the buckling behaviour of colloidal films under compression [67].

1.2.7.2 Contact angle determination

The three-phase contact angle is very important in determining the behaviour of the particle layer at the interface. However, experimental determination of θ_w is not straightforward. In particular, *in situ* determination of θ_w is very difficult. Therefore, θ_w is normally measured by placing millimetre-sized droplets of one fluid onto a surface which has been coated with the particles and which is surrounded by the other fluid, a technique known as the sessile drop method. Another complication is that the value of θ_w measured using the sessile drop method will depend upon the system history. For example, if a droplet is situated on a particle bed and has a contact angle of θ_w, when its volume is increased slightly, the contact line will remain pinned until a certain maximum contact angle, θ_A, is reached [68]. Similarly, if the volume of the droplet is reduced slowly, then the contact line will remain pinned until the contact angle reaches a minimum value, θ_R. These maximum and minimum values are known as the advancing and receding contact angles, respectively. The equilibrium contact angle will lie somewhere between θ_A and θ_R [69].

Several proposals have recently been made for more accurate and precise methods to empirically determine the contact angle. These include a method developed by Isa *et al.*, which they have termed freeze-fracture shadow-casting cryo-scanning electron microscopy (FreSCa) [70]. This technique involves forming a monolayer of particles at a flat oil-water interface before freezing the sample using liquid nitrogen and fracturing the sample along the interface. The particles can then

be observed directly using electron microscopy, allowing the contact angle to be measured. Good agreement has been exhibited between the contact angles measured using FreSCa and the point of transitional inversion when cationic surfactant was added to a dodecane-in-water emulsion stabilised by charged silica particles [71]. Horozov *et al.* have also developed a novel method for measuring the contact angle of particles at an oil-water interface [72]. Their technique involves creating a thin vertical film of fluid at which the particles are adsorbed, and surrounded by the other fluid. The thickness of the film will vary with height, being at a maximum at the ends of the film and at a minimum in its centre. If the particles "bridge" across the film (*i.e.*, they protrude from both of the film's interfaces), then they will move to an equilibrium position a distance, r_e, from the centre of the film. The value of r_e is determined by the thickness of the film and the need for the contact angle of the particle to be the same at both of the film's interfaces. By using interferometry, the thickness of the film at r_e, and hence θ_w, can be calculated.

1.2.8 Rheology

The viscoelastic properties of a fluid can be probed using a rheometer to apply a strain to the sample and measure the resultant stress [73, 74]. If the applied strain is sinusoidal then the resultant stress will normally be sinusoidal as well, although there can be a phase shift between the two, as shown in Fig. 1.5, with the phase shift denoted by δ. The ratio of the stress to the strain is known as the shear modulus, G^*.

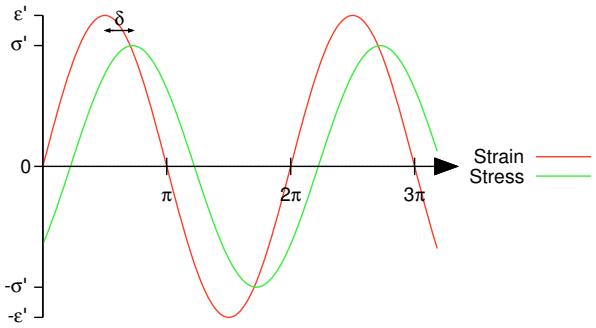

Figure 1.5 *A graph showing the relationship between an applied strain and the resulting stress for a viscoelastic fluid.*

For a perfectly elastic sample, this stress will be perfectly in phase with the applied strain ($\delta = 0$), whilst for a perfectly viscous sample the applied strain

and resultant stress will be perfectly out of phase ($\delta = \frac{\pi}{2}$). For a viscoelastic sample, however, $0 < \delta < \frac{\pi}{2}$. In this case it becomes useful to decompose G^* into two parts, G' and G'', which represent the elastic and the viscous components of the shear modulus, respectively. G' and G'' are defined as:

$$G' = \frac{\sigma'}{\epsilon'} \cos \delta, \tag{1.24}$$

$$G'' = \frac{\sigma'}{\epsilon'} \sin \delta, \tag{1.25}$$

where σ' is the amplitude of the stress and ϵ' is the amplitude of the measured applied strain. It can therefore be seen that:

$$G^* = G' + iG'', \tag{1.26}$$

and:

$$\frac{G''}{G'} = \tan \delta. \tag{1.27}$$

If $G' > G''$ then the sample can be said to have solid-like behaviour, whilst if $G'' > G'$ then the behaviour is liquid-like. For viscoelastic materials, δ is often strain-dependent, such that the material changes from being solid-like at low strains to liquid-like at high strains. The crossover point, where $G' = G''$, is used to define the yielding point of the material.

The rheology of various types of emulsions has been well studied in the past, but there is currently a lack of results pertaining to bridged emulsions.

1.3 Thesis outline, aims and objectives

Although Pickering emulsions were first studied by Ramsden and Pickering in the early 20th century [5, 6], little progress was made in the following decades. However, research into the behaviour of colloidal particles at liquid interfaces has undergone a revival in the last 15-20 years, and there are now books available on the subject [4]. This research paves the way for a fundamental understanding of the relationship between particle interactions and emulsion properties.

This thesis aims to strengthen understanding of the physics of Pickering emulsions by presenting experimental results from three key areas:

- The coupling between the phase behaviours of a particle dispersion and its resultant emulsion. In particular, whether it is always true that the most stable emulsion is formed from a weakly flocculating particle dispersion.

- Particle bridging in Pickering emulsions, including the conditions which are necessary for bridging to occur and the development of a simple theoretical model which explains experimental observations. This will be accomplished through a systematic study of the parameters which cause particle bridges to form.

- The dynamics of particles in a Pickering emulsion. By mixing together two emulsions, each stabilised by a different colour of particle, it becomes possible to study the dynamical behaviour of particles and droplets in a Pickering emulsion. Doing so should yield new insights into fundamental aspects of Pickering emulsion behaviour.

The rest of this thesis is laid out as follows. Chapter 2 describes the methods and materials used in the experimental work which are relevant to multiple chapters (methods specific to a single chapter are discussed in that chapter). The phase behaviour of the particle dispersions is described in Chapter 3, and this work is used to explain the experiments investigating the coupling between particle phase behaviour and emulsion phase behaviour in Chapter 4. A study of the parameters which affect the formation of particle bridges in (and their subsequent removal from) Pickering emulsions is presented in Chapter 5. Chapter 6 describes a novel method using two different colours of silica particles to study the deaggregation of bridged Pickering emulsions and in Chapter 7 the same technique is used to study the degree to which a Pickering emulsion is remixed during shear. In Chapter 8 some of the results from Chapter 5 are then replicated at a larger scale using a continuous flow setup, demonstrating the relevance of particle bridging to industrial emulsification. Finally, Chapter 9 contains a brief summary of the main results and proposals for further work.

Chapter 2

Materials and methods

2.1 Introduction

The work described in this thesis involves studying both colloidal dispersions and Pickering emulsions, as well as the coupling between their phase behaviours. As such, a large number of experimental techniques have been used to characterise the particle dispersions and emulsions separately, as well as the behaviour of the particles whilst they are stabilising an emulsion. This chapter serves as a brief introduction to these experimental techniques, and outlines typical protocols for some of them. Techniques which are only used in one chapter are generally discussed in that chapter.

2.2 Materials

2.2.1 Water

Water was distilled using a Fisons Fi-Streem 4 L still and then deionised using a Millipore Milli-Q reagent system, so that the water had a resistivity of at least 18 $M\Omega\,cm$. The interfacial tension of the resulting water with air, using a pendant drop method (see Section 2.3.5) was generally measured as 72 $mN\,m^{-1}$ at 19℃, in good agreement with literature values [57]. Unless otherwise stated, the water used in experiments was pure deionised water with a measured pH of ≈ 6.5.

2.2.2 Oils

Dodecane (Sigma-Aldrich, $\geq$ 99%) and isopropyl myristate (Sigma-Aldrich, $\geq$ 98%) were used as the oil phase in the experiments presented in this thesis. The density of dodecane was taken to be 750 $kg\,m^{-3}$, and that of isopropyl myristate to be 850 $kg\,m^{-3}$. The chemical structures of dodecane and isopropyl myristate are shown in Fig. 2.1. Unless otherwise stated, the dodecane used in this thesis was filtered through an alumina column twice to remove polar impurities [75]. Isopropyl myristate was used as received.

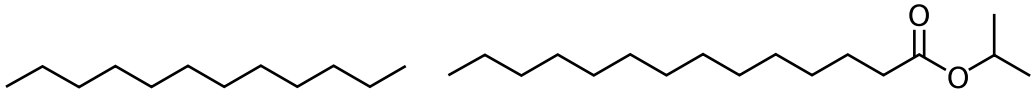

Figure 2.1 *The chemical structures of dodecane (left) and isopropyl myristate (right).*

2.2.3 Silica particles

The particles used in this work were, unless otherwise stated, synthesised by Dr. Andrew Schofield using a modified Stöber silica method which generates monodisperse, fluorescently labelled silica spheres [76, 77]. The physical properties of these particle dispersions will be described in more detail in Chapter 3. The particles have radii of approximately 400-500 nm, are monodisperse, spherical, charge-stabilised and are labelled using either fluorescein isothiocyanate (FITC) or Rhodamine B isothiocyanate (RITC). The synthesis procedure used was as in Ref. [78] for FITC-labelled particles and as in Ref. [79] for RITC-labelled particles.

The Stöber process forms particles by first hydrolysing tetraethyl orthosilicate (TEOS) to form silanol molecules which then undergo condensation reactions to form nanometre sized particles. The reaction which occurs is:

$$\mathrm{Si(OC_2H_5)_4 + 2H_2O \rightarrow SiO_2 + 4C_2H_5OH.} \tag{2.1}$$

The silica particles were washed at least ten times in distilled water to remove the ammonia and alcohol and were then dried in a pre-heated vacuum oven (Binder

9130-0029) for 1 h at a temperature of 170℃, rendering them hydrophobic enough to sequester to an oil-water interface [13]. The dried silica was then kept in a desiccator, to minimise the rate at which it absorbs water from the atmosphere.

Some samples were also prepared using a commercially available fumed silica, Aerosil OX50 (Degussa) [80]. The properties of the particles will be described in more detail in Chapter 3.

2.2.4 Other materials

Electrolytes and other materials used in this thesis, along with their source and purity, are listed in Table 2.1.

Table 2.1 *Suppliers and purities of the other materials used within this thesis.*

Material	Source	Purity
Sodium hydroxide	Fisher	98.73%
Hydrochloric acid	Fluka	1.0 M
Glycerol	Fisher	$\geq$ 98%
Sodium chloride	VWR	99.9%
Sodium iodide	Sigma-Aldrich	$\geq$ 99.5%
Sodium nitrate	Sigma-Aldrich	$\geq$ 99.0%

2.3 Experimental techniques

2.3.1 Sample preparation

Emulsions were prepared by mixing the oil phase with a dispersion of particles in water. Dispersions of silica were typically prepared as follows. Dried silica was added to 2.33 mL of water and dispersed using an ultrasonic probe (Sonics Vibracell VCX500). A typical dispersion protocol involved 1 s of sonication followed by 5 s of no sonication (in order to avoid overheating), repeated for a total time of 6 min. 0.67 mL of the oil phase, a mixture of dodecane and isopropyl myristate, was then added prior to the initial emulsification, which was carried out using a vortex mixer (Fisons Whirlimixer) until the resolved water was clear, or until further mixing did not decrease the opacity of the resolved water. Emulsification was carried out within 10 min of the particles being added

to the water. The volume fraction, Φ_{IM}, of isopropyl myristate in the oil phase is used to control particle wettability [81]. All sample preparation was carried out at room temperature.

Hydrochloric acid and sodium hydroxide were used to adjust the pH of some solutions, either prior to or following emulsification. If the pH was adjusted prior to emulsification, then the particles were dispersed in water at the appropriate pH before the oil was added. If the pH was adjusted following emulsification then the sample was emulsified as described in the previous paragraph, before a small amount of additional aqueous phase was added to the emulsified sample to bring the pH to the appropriate value.

When samples were to have salt added, the salt was added to the aqueous phase prior to the dispersion of the particles. Occasionally, the salt concentration of a sample was increased following emulsification by adding salt and gently shaking the sample to dissolve the salt.

Particle volume fractions have been calculated assuming a particle density of 1750 $kg\,m^{-3}$ for Stöber silica [77] and 2200 $kg\,m^{-3}$ for fumed silica [80].

Additional shearing was sometimes carried out using a rotor-stator (Kinematica Polytron PT3100 - inner diameter 5 mm, gap size 0.15 mm) at shear rates between 8 000 s^{-1} and 34 000 s^{-1}. A roller bank (Stuart Equipment SRT9 Roller Mixer) was used to apply low shear to samples and a shaker device (Stuart Equipment SF1 Flask Shaker, operating at 800 min^{-1} oscillations) was used to agitate some samples.

2.3.2 pH measurements

A Mettler-Toledo S20 SevenEasy pH meter was used to conduct measurements of solutions' pH.

2.3.3 Static light scattering

An ALV/CGS-3 goniometer and an ALV-5004 Multiple Tau Correlator were used to perform static light scattering measurements in order to measure the size of the Stöber silica particles. The form factor for spherical particles has minima

when:

$$q_p r_p = tan(q_p r_p), \tag{2.2}$$

where:

$$q_p = \frac{4\pi n}{\lambda} sin\left(\frac{\alpha}{2}\right), \tag{2.3}$$

and n is the refractive index of the solvent, λ is the wavelength of light being scattered and α is the scattering angle [82].

The first few solutions to Eq. (2.2) are $q_p r_p \approx 4.49, 7.73, 10.90$. By measuring the intensity of a laser beam scattered by a particle dispersion as a function of the scattering angle, the locations of the minima can be found and used to calculate r_p [83]. The particle dispersions were made with $\phi_p = 0.1\%$, so that the effects of multiple scattering were negligible, and dispersed using the ultrasonic probe. Measurements were initially taken for 10 s every 5° between 30° and 130°, in order to approximately locate the minima in the form factor. Measurements were then taken for 60 s every 0.5° in a region $\approx 10°$ either side of any minimum in the form factor. Gnuplot was used to fit a quadratic function near the minima, and the minimum point in the fitted line was used to calculate r_p.

2.3.4 Zeta potential measurements

The zeta potentials of particle dispersions were measured using a Malvern Nano-Z ZEN2600 Zetasizer. This apparatus measures the electrophoretic mobility, U_E, of the particles in the dispersion, and these values are used to calculate the zeta potentials by means of the Henry equation:

$$\zeta = \frac{3\eta U_E}{2\epsilon_w f(\kappa r_p)}, \tag{2.4}$$

where $f(\kappa r_p)$ is known as the Henry function [84]. The Henry function is a function of the Debye length and the particle radius. $f(\kappa r_p)$ varies from 1 when $\kappa r_p = 0$ to 1.5 when κr_p when $\kappa r_p = \infty$. For the particle dispersions for which the zeta potential has been measured in this work, $r_p \gg \kappa^{-1}$, and so $f(\kappa r_p)$ has been approximated to be 1.5. The temperature in the Zetasizer was set at 25℃ for all measurements.

The particle dispersions for zeta potential measurements were prepared by adding ≈ 0.005 g of particles to ≈ 3 mL of water containing 1 mM of sodium nitrate, and dispersing with the ultrasonic probe. The addition of the salt ensures that

$r_p \gg \kappa^{-1}$. Hydrochloric acid or sodium hydroxide was used to adjust the pH of samples. 1 mL of dispersion was then placed in a Zetasizer cell (DTS 1060 or DTS 1070), and the electrophoretic mobility was measured three times, with each measurement comprising at least 10 individual runs. Typically, this process would then be repeated using the same dispersion two more times, 2 h and 1 day later, with the particles being re-dispersed using the ultrasonic probe prior to each repetition.

2.3.5 Tensiometry and contact angle measurements.

Interfacial tension and contact angle measurements were made using a Krüss EasyDrop tensiometer (model 65 FM40Mk2). All experiments were carried out at room temperature, which was maintained at 19℃.

2.3.5.1 Interfacial tension

The tensiometer was used in the pendant drop setup to measure the interfacial tensions of the oil-water systems used in this thesis. In most of the experiments described in this thesis, a mixture of dodecane and isopropyl myristate was used as the oil phase in the emulsions, and the oil-water interfacial tension was measured as a function of the isopropyl myristate content of the oil phase. Water is more dense than the oils used in this thesis, and was therefore was used as the droplet. A cubic cuvette was filled with the oil phase, and a syringe with a flat steel needle (diameter = 1.832 mm) was used to insert a droplet of water of volume $\approx 25\ \mu L$ into the oil. Care was taken to avoid having air in the syringe during measurements, and for the water to be protruding slightly from the needle tip before immersion in the water.

2.3.5.2 Contact angles

Contact angle measurements were performed using the sessile drop method with the same apparatus. Particles were dispersed in water using a pulsed ultrasonic probe, with $\phi_p \approx 35\%$, and spin-coated onto glass coverslips. The spin-coating was carried out using a Cammax Precima spin-coater and 18 $mm \times 18\ mm$ glass coverslips. The coverslips were placed on the spin-coater, which uses a vacuum to hold them in place, and a pipette was used to add the particle dispersion onto

the slide. When the entire surface of the coverslip was covered with dispersion, the slide was spun for $\approx 5\ s$ at $\approx 2\ krpm$. The coverslips were then left to dry overnight before use. The particle-laden slides were placed in a cubic cuvette, into which the oil phase was then added, so that the particles contacted the oil prior to the water. Droplets of water (volume $\approx 50\ \mu L$) were then lowered onto the slide. Both advancing and receding contact angle measurements were made, and the average used as the equilibrium contact angle.

2.3.6 Particle size analyser

A Beckman Coulter LS 13 320 Particle Size Analyzer was used to measure the size distributions of particle dispersions, emulsion droplets and aggregates of droplets. The particle sizer uses laser diffraction to measure the size distribution of the sample. A helium-neon laser is directed at the sample within a sizing module, and the intensity of the scattered light is measured at multiple scattering angles. The Fraunhofer and Mie theories of light scattering are then used to calculate the size distribution of the sample.

The sizing module was filled using the continuous phase of the sample being studied, and drops of sample were added until the obscuration was within the suggested range. Three measurements were generally made for each sample, each lasting 1 min, and the average of the three runs was used. Unless otherwise stated, the volume-weighted size distribution has been used. The sizing module contains a magnetic stirrer bar to overcome problems associated with sample sedimentation or creaming, and this was always operated at 50% speed. All experiments were carried out at room temperature.

2.3.7 Microscopy

One of the advantages of studying colloidal systems is that the samples can be observed with optical techniques, including simple microscopy - in particular, the individual stabilisers in particle-stabilised emulsions can be directly observed, unlike in surfactant-stabilised emulsions. Additionally, because the silica particles can be fluorescently labelled, confocal microscopy can be used to observe the location of particles with a high degree of resolution in all three spatial dimensions; it is possible to resolve individual particles. Samples were prepared for microscopy

by pipetting a drop of the emulsion onto a glass cavity slide, diluting it in its continuous phase and covering with a glass coverslip. Epoxy resin was used to seal the slides in order to prevent evaporation and flow.

2.3.7.1 Optical microscopy

A Qimaging QICAM Fast 1394 monochromatic camera, attached to an Olympus BX50 optical microscope, was used to obtain bright-field micrographs of emulsions. Qimaging's QCapture Suite software was used to capture the images, which were exported as tiff files. The addition of scale bars and conversion to pdf format was accomplished using ImageMagick [85].

2.3.7.2 Confocal microscopy

A Zeiss LSM 700 confocal microscope was used to perform all of the confocal microscopy described in this work. A 10 mW, 488 nm solid-state laser was used to excite particles dyed with FITC and a 10 mW, 555 nm solid-state laser was used to excite particles dyed with RITC. Generally, the microscope was operated using a 10× objective, which is just powerful enough to resolve individual particles, but gives a large field-of-view. When two different colours of particles are used, it is possible with this lens to resolve individual red particles on an otherwise green droplet and *vice versa*. However, when it was necessary to resolve individual particles on a heterogeneous droplet, a 40× or 63× oil immersion objective lens was used. Zeiss' ZEN 2009 software was used to capture the images and add scale bars. The images were then exported as tiff files and converted to pdf files using ImageMagick.

2.3.7.3 Photography

Two digital cameras (Fujifilm Finepix S9600 and Canon DS26171) were used to take photographs of emulsions. Time-lapse photography was carried out by attaching a telescopic lens to the Qimaging QICAM Fast 1394 monochromatic camera and using Qimaging's QCapture Suite software.

Chapter 3

Phase behaviour of particle dispersions

3.1 Introduction

In order to study the coupling between particle phase behaviour and emulsion phase behaviour, the phase behaviour of aqueous particle dispersions has first been characterised. Several parameters have been used to modify the particle phase behaviour, and their effects will be outlined in this chapter. This will allow the changes in emulsion phase behaviour to be related, in Chapter 4, to those in the particle phase behaviour.

3.2 Methods and materials

The methods which are particular to this chapter will be discussed in this section. Methodology for techniques which are used in this chapter and in other chapters can be found in Chapter 2.

3.2.1 Sample preparation

The flocculation behaviour of the dispersions of silica can be seen from sedimentation profiles. A series of samples of FITC-labelled silica in dispersions

varying in sodium chloride concentration was prepared and their sedimentation behaviours studied using photography. Stokes' law can be used to calculate the particles' radius from their sedimentation velocity, which means that the degree of aggregation in a sample can be quantified [25]. The terminal velocity of a spherical particle of sedimenting in a fluid is given by Eq. (1.8). A theoretical understanding of colloidal gelation is still being developed but, for the purposes of the work carried out here, it is sufficient to assume that aggregated particles will sediment more quickly than dispersed particles [86, 87]. Clearly, if particles form aggregates then the aggregates will have a radius greater than the primary particles and so will sediment more quickly. For fractal aggregates the density of the aggregate is lower than that of the primary particles, but the effect of this on v_t will be small compared to that of increasing the radius. By measuring the terminal velocity of the particles, it should be possible to measure the apparent radius of the aggregates. Furthermore, because the particles are small enough to behave in a Brownian manner and are being observed on very long timescales (minutes to hours), it can also be assumed that they are always sedimenting at their terminal velocity. However, because differently sized particles sediment at different velocities, and the aggregates will be polydisperse and will grow with time, it is difficult to calculate a single effective radius for aggregating samples.

Dispersions of Stöber silica with various aqueous phase concentrations of sodium chloride and sodium iodide were observed during sedimentation, with $\phi_p = 0.35\%$. The dried particles and salt were dispersed in 15 mL of deionised water using the ultrasonic probe. Dispersions of fumed silica were also prepared and studied in a similar manner, but using a far lower value of ϕ_p (0.03%).

3.3 Physical properties of Stöber and fumed silica

3.3.1 Stöber silica

The synthesis of the fluorescent Stöber silica particles used in this work was carried out by Dr. Andrew Schofield following the procedure which was described in Chapter 2. A brief description of the particles' physical properties will be given here. The Stöber silica particles are charge-stabilised and fluorescently labelled.

The incorporation of a fluorescent dye into the particles necessitates the addition of 3-(aminopropyl)triethoxysilane (APS) to the particles. The APS is a coupling

agent, binding to both the silica and to a fluorescent molecule *via* an amine-isothiocyanate bond. The APS and the fluorescent dye are both approximately uniformly distributed throughout each particle. The APS is added in excess, and so is expected to be more important in determining the overall surface chemistry than the fluorescent dyes. The APS adds amino groups, which are positively charged below pH $\approx$ 9, to the particle surface. Additionally, there are silanol groups which are negatively charged above pH $\approx$ 2. The actual charge on the particle will depend on the ratio of silanol to amino groups, and will therefore vary with pH [53]. The FITC is uncharged, but the RITC adds a small amount of positive charge to the surface.

Static light scattering was used to measure the radius of the particles used in this work. Although the size varies slightly between different batches of particles, the radius of the particles is always between 400 and 500 nm, and the polydispersity is always low enough for the particles to crystallise, which means that CV is $\lesssim 10\%$ [88].

3.3.2 Fumed silica

The OX50 silica is very polydisperse, and the quoted specific surface area of the particles is $50 \pm 15\ m^2\, g^{-1}$, corresponding to a mean particle diameter of $\approx 55\ nm$. Figure 3.1 shows a transmission electron micrograph of the OX50 particles.

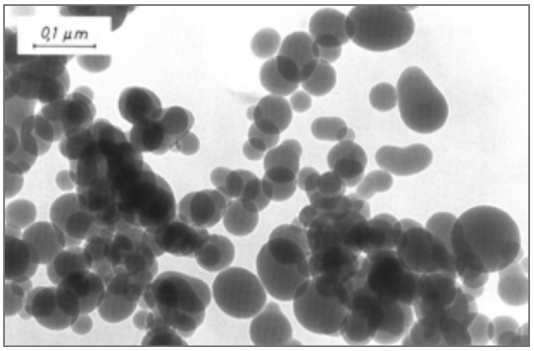

Figure 3.1 *Transmission electron micrograph of Aerosil OX50 particles. Taken from Ref. [80].*

3.4 Effects of varying salt concentration

Adding salt to the silica dispersions screens electrostatic interactions, making it more likely that two particles will overcome the electrostatic barrier between themselves and aggregate through van der Waals attractions.

It has been predicted theoretically that θ_w for silica particles at an oil-water interface will decrease (*i.e.,* the particles will become more hydrophilic) when the salt concentration of the aqueous phase is increased [84, 89]. Since the electrical double layer forms spontaneously, its formation must reduce the system's free energy. Therefore, when the salt concentration is increased, the system can lower its free energy by increasing the solid-water interfacial area, as this increases the contact area of the double layer. This increase in the solid-water interfacial area is accomplished by reducing θ_w. Furthermore, when the aqueous phase salt concentration is increased, γ_{ow} decreases and Eq. (1.2) shows that this will also contribute to a decrease in θ_w [90]. Fokkink and Ralston also show that θ_w is at a maximum at the isoelectric point of the solid surface, and that θ_w will increase as the magnitude of the surface potential is increased. Since the zeta potential of silica decreases as the salt concentration is increased [48], it might therefore be expected that θ_w would decrease as the salt concentration is increased. However, the decrease in zeta potential may not be indicative of a decrease in the surface potential, as a change in the ionic concentration will also affect the location of the slipping plane and hence the distance from the particle at which ζ is measured. It is also worth noting that the fluorescent dye added to the Stöber silica particles means that their wetting behaviour may be anomalous.

Some experimental data supporting these theoretical predictions are available for silica as well as for other oxides. Fokkink and Ralston reported that θ_w decreased in an air-water-silica system at pH 11 as the potassium nitrate concentration was increased, using silica which had been modified with trimethylchlorosilane [89]. Hanly *et al.* also reported a similar effect when the potassium nitrate concentration in an air-water-titania system was increased, using titania which had been modified using octadecyltrihydrosilane [91]. Serrano-Saldaña *et al.* have measured θ_w in a dodecane-brine-glass system and reported that θ_w decreases as the sodium chloride concentration of the brine is increased [90]. Barranco Jr. *et al.* measured θ_w as a function of sodium perchlorate concentration in both trichloroethylene-water-quartz and carbon tetrachloride-water-quartz systems and reported that θ_w decreased as the sodium perchlorate concentration was increased [92]. Phillips

and Riddiford reported no difference in the advancing contact angle and only a very small reduction in the receding contact angle in an air-water-siliconised glass system when the aqueous phase sodium chloride concentration was increased from 0 M to 2 M [93].

Literature values for the refractive indices and viscosities of solutions of sodium chloride and sodium iodide are given in Fig. 3.2.

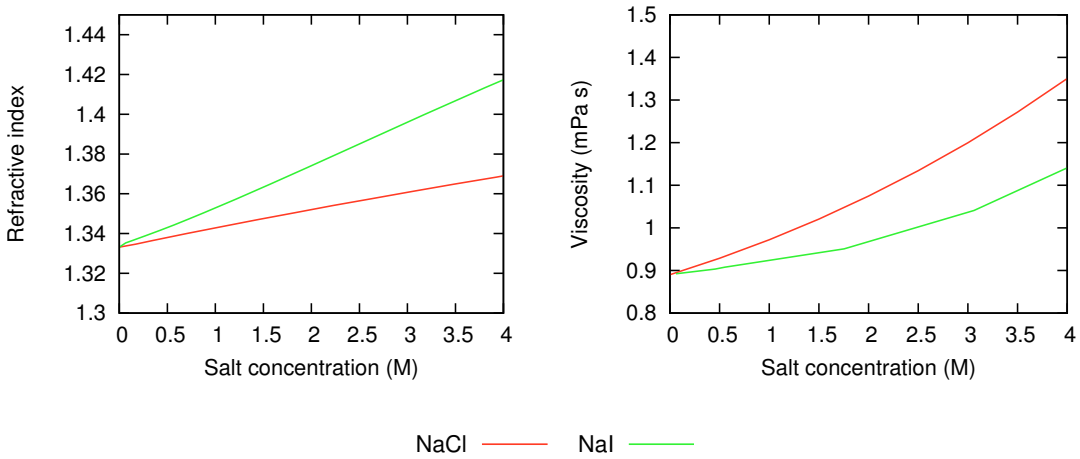

Figure 3.2 *Graphs showing the refractive indices (left) and viscosities (right) of solutions of sodium chloride and sodium iodide. The viscosities are measured at* 20 ℃ *and* 10^5 *Pa. Sodium chloride data taken from Ref. [57] and sodium iodide data taken from Ref. [94] (refractive indices) and Ref. [95] (viscosity).*

The increase in the viscosity of a solution containing sodium chloride relative to a solution containing an equal molarity of sodium iodide is because iodide ions are more chaotropic than chloride ions [96]. This means that the iodide ions interact more weakly with water than chloride ions, and are also more likely to adsorb at interfaces. The presence of iodide ions is likely to make the particles more hydrophobic, compared to the presence of chloride ions.

Particle sizing data, sedimentation behaviour and measurements of the three-phase contact angle have been used to characterise the effects of changing salt concentration on particle phase behaviour, and the results are presented below.

3.4.1 Characterisation of particle flocculation

Silica dispersions containing salt are expected to be more likely to aggregate, and so one can use the way the apparent particle size, as measured using light

scattering, evolves with time to quantify the degree and rate of aggregation in a dispersion.

3.4.1.1 Particle sizing

A Beckman Coulter particle size analyser (see Chapter 2) was used to track the apparent particle size in silica dispersions of different salt concentration with time. The particle size analyser was calibrated in the absence of particles, but at the appropriate salt concentration. A fresh dispersion of particles with a particle volume fraction of 0.3% was prepared without any salt for each experiment, and $\approx 1\ mL$ of this dispersion was added to the sizing module, so that the obscuration recorded by the size analyser was 10%, in the centre of the suggested range. The sizing module contains $\approx 20\ mL$ of aqueous phase prior to the addition of $\approx 1\ mL$ of particle dispersion, and therefore the change in salt concentration following addition of the particles is considered low enough to be neglected. This method also minimises the amount of aggregation which occurs prior to initial measurement, although the loading of the sample took $\approx$ 1-2 min, from first addition of the particles to starting the measurement. To prevent the particles from coating the inner walls of the module, the stirrer bar within the module was utilised at a constant rate (50%) over all the experiments.

Results for Stöber silica and sodium chloride are shown in Fig. 3.3 (left), for Stöber silica and sodium iodide in Fig. 3.3 (right) and those for fumed silica and sodium chloride in Fig. 3.4. As can be seen from these graphs, the Stöber silica particles begin aggregating immediately at all non-zero salt concentrations. When there is no added salt, the apparent particle size does not increase over the course of the experiment, which lasted 1 h, showing that the particles are indeed non-aggregating under these conditions (in fact, the particle size decreases slightly over the course of the experiment, as aggregates which were not initially fully dispersed are broken up). At non-zero salt concentrations, the apparent particle size increases relatively quickly over the first 5-10 min of the experiment, and then generally plateaus. For Stöber silica, and excluding the 0 mM case, the plateau value of the apparent particle size typically decreases as the salt concentration is increased, and this may be caused by the increased viscosity at higher salt concentrations leading to a greater shear stress in the stirred sample, thus decreasing the maximum aggregate size. At the highest sodium chloride concentration used here, 1000 mM, the apparent particle size starts to increase

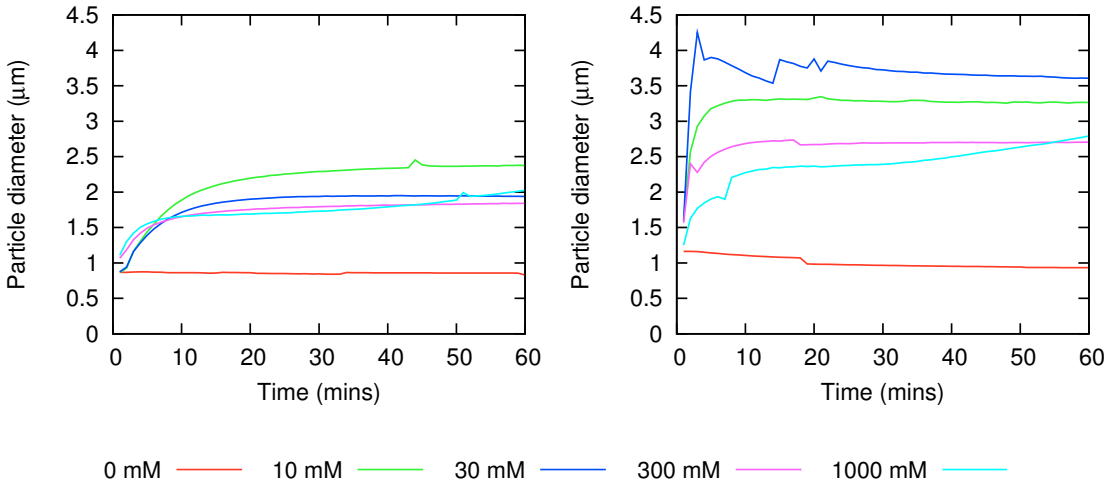

Figure 3.3 *Aggregation behaviour of dispersions of Stöber silica particles under shear at different sodium chloride (left) and sodium iodide (right) concentrations.*

again after $\approx 30\ min$, suggesting that the particle-particle interactions at this salt concentration are strong enough to overcome the shear rate and allow for the eventual development of larger particle aggregates. It is also worth noting that the first measured particle size in dispersions where the sodium chloride concentration was $\leq 30\ mM$ was negligibly different from the case with no added salt. In contrast, at sodium chloride concentrations $\geq 300\ mM$ the apparent particle size during the first measurement was noticeably greater than for the case with no added salt.

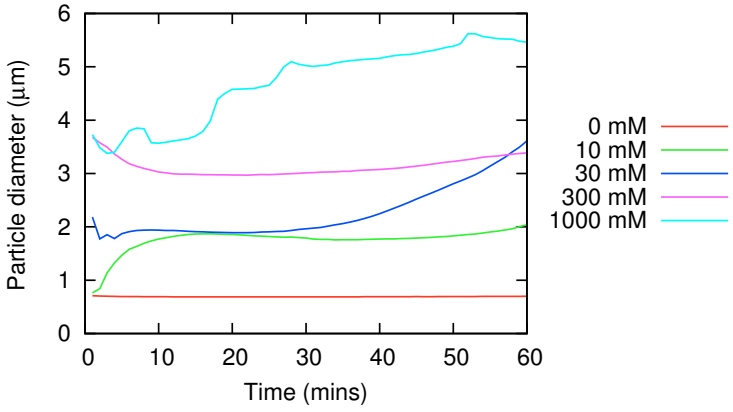

Figure 3.4 *Aggregation behaviour of OX50 silica at different sodium chloride concentrations.*

Figure 3.3 (right) shows that the aggregation behaviour in the samples containing

sodium iodide is qualitatively similar to the behaviour of samples containing sodium chloride. However, the rate of aggregation at short times is greater and the size of the aggregates in the plateau region is larger, which may be explained by the lower viscosity of sodium iodide solutions at a given molarity. However, as shown in Fig. 3.2, there is only a small difference between the viscosities of sodium chloride and sodium iodide solutions at concentrations below $\approx 500\ mM$. It therefore seems more likely that the observed differences in aggregation behaviour are due to ion specificity effects (*i.e.,* iodide ions are more chaotropic than chloride ions).

Figure 3.4 shows the results of similar experiments using fumed silica dispersions and sodium chloride. Clearly, the behaviour in these experiments is far noisier than in the experiments using Stöber silica, which is possibly a result of the fumed silica being smaller and more polydisperse. Interestingly, the size of the fumed silica aggregates increases with sodium chloride concentration, in contrast to the observed behaviour using Stöber silica. This suggests that the aggregation rate is far higher in the fumed silica samples, and that there is a greater difference in aggregation rate between low and high sodium chloride concentrations. It is also notable that, despite the smaller size of the fumed silica particles, the aggregates are larger than in the Stöber silica dispersions, although it should also be noted that the majority of the primary particles are smaller than the lowest size that the particle size analyser registers ($375\ nm$).

3.4.1.2 Sedimentation behaviour

When the aqueous phase had no salt added to it, the Stöber silica particles sedimented slowly initially, until $\approx 5\ h$ into the experiment, when the particles began to aggregate and sediment rapidly, with full sedimentation ($\approx 6\ cm$) taking approximately one further hour. This increase in the sedimentation rate is caused by the particles adsorbing water, which causes the particles to change from being positively charged to being negatively charged (as will be shown in Section 3.5.1), and the particles aggregate rapidly as they pass through the point of zero charge. The particles sediment $\approx 0.53\ cm$ in the first $275\ min$ of the experiment, and using Eq. (1.8) yields a value of $440\ nm$ for the particles' radius, which agrees well with light scattering measurements (measured $r_p = 430\ nm$).

As the particles aggregate, the clusters they form are polydisperse and hence sediment at different rates. This means that the interface between the sediment

and the supernatant is not sharp, and so Eq. (1.8) cannot be used to quantify the particle size. Instead, the average brightness, $b(t)$, of each vial has been measured using the Plot Profile feature in ImageJ for multiple photographs, where t is the time elapsed since the beginning of the experiment. A typical photograph from this experiment is shown in Fig. 3.5 (left). By plotting $\frac{b(t)}{b(t=0)}$ as a function of t, the sedimentation behaviour can be seen. Figure 3.5 (right) shows such a plot for Stöber silica in dispersions of sodium chloride. The sudden onset of sedimentation in the 0 mM sample can clearly be seen.

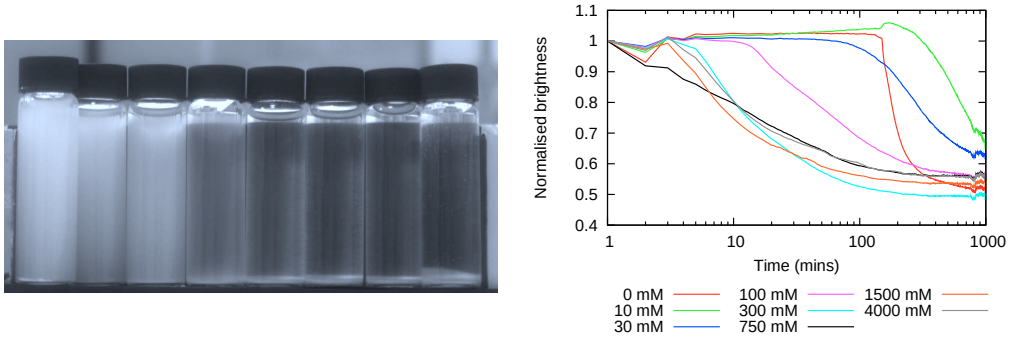

Figure 3.5 *Left: Photograph of Stöber silica dispersions during a sedimentation behaviour experiment. The time elapsed since the beginning of the experiment is* 120 *min. The sodium chloride concentrations are, from left to right,* 0 mM, 10 mM, 30 mM, 100 mM, 300 mM, 750 mM, 1500 mM *and* 4000 mM, *and in all samples,* $\phi_p = 0.35\%$; *Right: Graph showing the normalised brightness (a lower normalised brightness means that more particles have sedimented) as a function of time for the dispersions in the left hand image. The data are noisy at low and high times due to changing light conditions in the room.*

At higher salt concentrations, 10-30 mM, the dispersions are observed to sediment at approximately the same rate as in the sample without salt. However, unlike the dispersions with no salt, when the salt concentration is 10-30 mM, the particles do not all aggregate rapidly after ≈ 5 h, but gradually aggregate and sediment over the course of ≈ 20 h. However, because of the particle aggregation, there is not a sharp interface between the sediment and the supernatant.

At still-higher concentrations of sodium chloride, 300-3000 mM, the aggregation occurs immediately and the particles sediment rapidly, with sedimentation taking less than an hour. Again, there is no sharp sediment-supernatant interface, due to the polydispersity of the aggregates. It is obvious, however, that increasing the salt concentration causes an increase in the sedimentation rate.

Figure 3.6 (left) shows the results of a similar experiment using sodium iodide. No quantitative differences between dispersions containing sodium chloride and sodium iodide were observable.

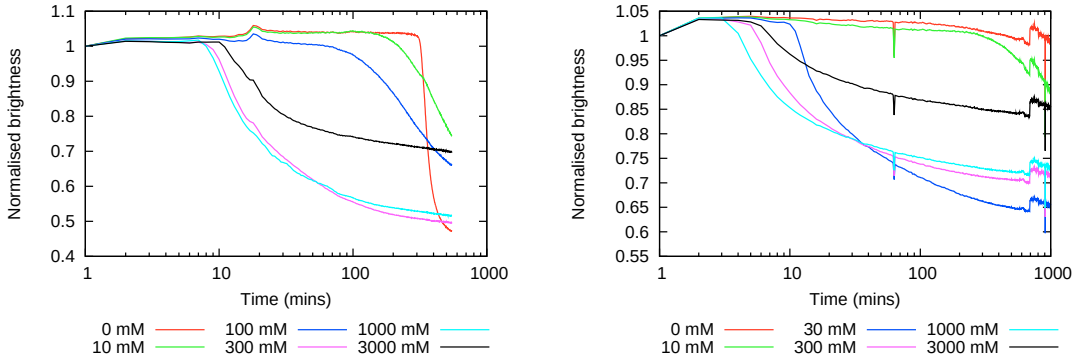

Figure 3.6 *Graphs showing the normalised brightness (with a lower normalised brightness indicating a greater degree of sedimentation) as a function of time for the dispersions of Stöber silica in sodium iodide solutions (left) and for fumed silica in sodium chloride (right). For the Stöber silica, $\phi_p = 0.35\%$, and for the fumed silica, $\phi_p = 0.03\%$. The data in the left graph have been truncated due to excessive noise at long times caused by changing light conditions in the room. In both cases, the 3000 mM sample is anomalous because it has already significantly sedimented by the time the experiment has started.*

In the case of fumed silica, the dispersions with sodium chloride concentrations $\geq$ 30 mM aggregate rapidly and sediment in $\approx$ 10-15 min. Figure 3.6 (right) shows the results of a sedimentation behaviour experiment using fumed silica particles in sodium chloride solutions. At lower salt concentrations, the particles are observed to sediment very slowly, as is to be expected from the small particle size. When the particle volume fraction is increased to 0.2%, all the dispersions with non-zero salt concentrations sediment rapidly, with the samples with the lower salt concentrations sedimenting most quickly, due to their lower viscosity.

3.4.1.3 Discussion: Flocculation

As expected, the Stöber silica dispersions with higher salt concentrations were observed to aggregate and sediment more quickly. The samples with no added salt were observed to sediment slowly initially, but aggregated and sedimented rapidly as the particles passed through the point of zero charge due to water adsorption at their surfaces. In the absence of salt, the Stöber silica particles are therefore non-flocculating. The degree of aggregation in a particle dispersion will depend

not only on the particle interactions but also on the shear stress in the fluid, and this will be important when considering the effects of particle flocculation during emulsification. Distinguishing between weakly and strongly flocculating particle dispersions is therefore difficult, but an important factor when considering the emulsification process will be whether the applied shear is capable of breaking up the particle aggregates. In this context, it is worthwhile noting the upward trend in the aggregate size of Stöber silica at experimental times greater than 30 min and when the salt concentration is 1 M, as shown in Fig. 3.3. In contrast, at salt concentrations $\leq$ 300 mM the aggregate size of Stöber silica is observed to plateau at a salt concentration-dependent value. Therefore, it is argued that at salt concentrations $\lesssim$ 300 mM the particle dispersions can be described as weakly flocculating.

3.4.2 Contact angles

Clearly the contact angle of the particles at the oil-water interface is an important determining factor in a Pickering emulsion's behaviour. However, measuring the contact angle directly is difficult, and the conventional sessile drop method is often unreliable. Nevertheless, this method has been used to measure contact angles as a function of the sodium chloride concentration of the aqueous phase.

Contact angles have been measured (for details, see Chapter 2) for the Stöber silica particles at different sodium chloride concentrations.

Measurements have been made of the contact angle of a water droplet on a slide which has been spin-coated with silica particles, surrounded by an oil phase with $\Phi_{IM} = 10\%$ for both the case where the water contains no salt and the case where the water contains 40 mM of sodium chloride. It is found that if the slides are dried under vacuum for 1 h at 50℃, then θ_w in the pure water case is 104(4)° but when the sodium chloride concentration is 40 mM, $\theta_w = 71(1)°$, as is shown in Fig. 3.7. It is noteworthy that the contact angle in the pure water case is greater than 90° despite the particles forming stable dispersions in water but not in dodecane. This discrepancy may be a result of surface roughness in the spin-coated particle layer, and measuring the roughness using profilometry would provide useful information in this regard.

Figure 3.8 shows how the three-phase contact angle depends on the oil phase's isopropyl myristate content. These experiments were conducted without adding

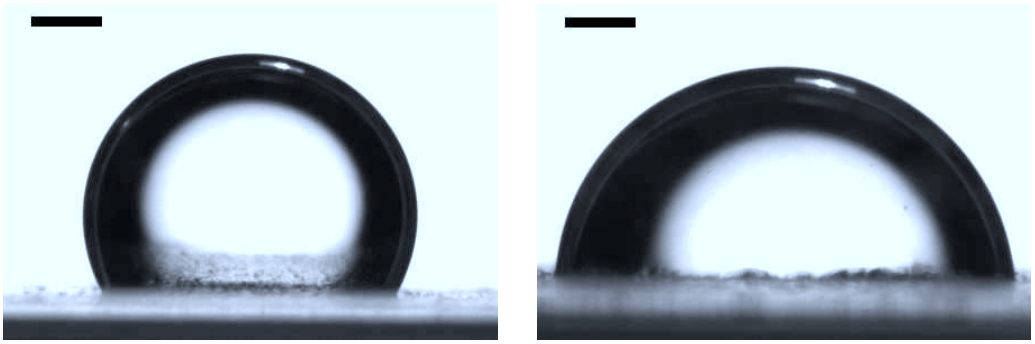

Figure 3.7 *Photographs showing advancing contact angles of water droplets on a slide which has been spin-coated with Stöber silica particles and dried at 50℃, surrounded by an oil phase with $\Phi_{IM} = 10\%$. In the left photograph the droplet is pure water, whilst in the right photograph the aqueous phase contains 40 mM of sodium chloride. The scale bars are 1 mm.*

salt to the aqueous phase and using pure deionised water (pH $\approx$ 6.5). These results show that $\theta_w > 90°$ for all but the 0% isopropyl myristate case, despite the silica particles forming stable dispersions in water but not in oil. This again suggests that surface roughness of the spin-coated particle layer is affecting the contact angles. Nevertheless, the increase in θ_w as Φ_{IM} increases corroborates the belief that increasing the oil phase's isopropyl myristate content increases the wettability of the particles by the oil phase, due to the increase in the dielectric constant of the oil.

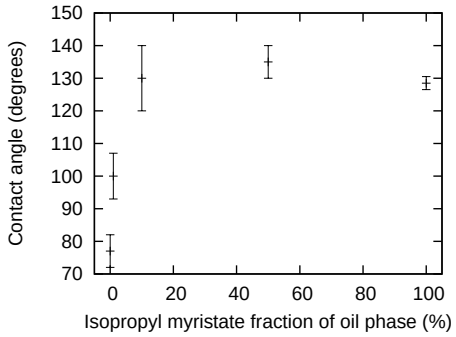

Figure 3.8 *Dependence of θ_w on the isopropyl myristate fraction of the oil phase.*

It has unfortunately not been possible to obtain reproducible measurements of the contact angle as a function of the sodium iodide concentration, or using fumed silica particles. Although reliable measurements of θ_w have proved elusive using the sessile drop method described here, other methods of measuring the contact

angle have been described in the literature and their utilisation may provide useful insight [70, 72].

3.5 Effects of varying pH

Adjusting the pH of the aqueous phase affects the charge on the silica's surface. The particle surface contains a mixture of positively charged amine groups and negatively charged silanol groups. The ratio at which these two groups are present will determine the net charge of the particle, and will be dependent on the pH [53]. This means that the pH of the sample will affect the rate at which particles aggregate.

Adjusting the pH also changes the Debye length of the sample, and so care is required to avoid these two effects being conflated.

The effects of varying the sample pH on the zeta potential and on the three-phase contact angle will now be described and explained.

3.5.1 Zeta potential

Measurements of the zeta potential have been used to characterise the effects of changing the pH of particle dispersions. The particles were dispersed using the ultrasonic probe in a solution at the desired pH value. Measurements were taken again using the same samples 2 h and 24 h later, with the particles being re-dispersed prior to these measurements. The zeta potential of fumed silica particles was observed to decrease from approximately 0 mV at pH 3 to approximately -40 mV at pH 4.5 and to then plateau at a value of approximately -45 mV between pH 6 and 10, as shown in Fig. 3.9 (left). The behaviour of FITC-labelled Stöber silica is slightly more complicated, however, as shown in Fig. 3.9 (right). When the dried particles are initially dispersed in water, their zeta potential is positive across the entire pH range studied here. When the pH is 3, $\zeta \approx 80$ mV and decreases almost linearly to ≈ 40 mV at pH 10. As the Stöber silica particles adsorb water, their zeta potential generally decreases, as shown by the green and blue points in Fig. 3.9 (right). This shows that the particles become more hydrophilic as they are immersed in water, and so will be less likely to adsorb to an oil-water interface. Water will also adsorb to the particles' surface when the

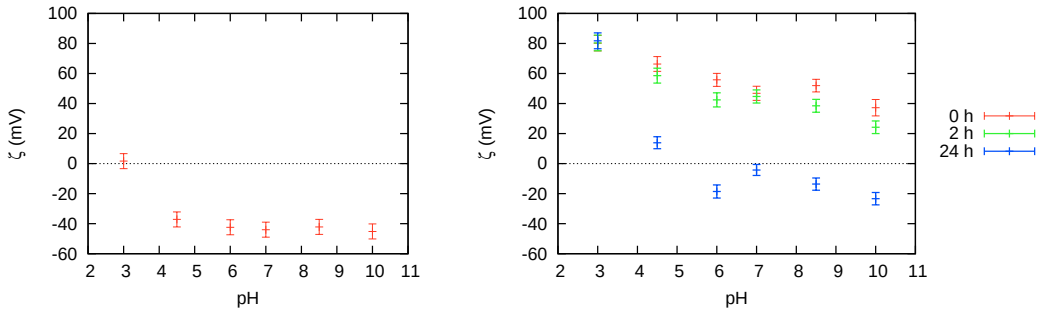

Figure 3.9 *Zeta potentials of fumed (left) and Stöber (right) silica, as a function of* pH. *In the Stöber silica graph, the different data sets refer to different immersion times in water. In the fumed silica experiments* $\phi_p = 0.005\%$ *and in the Stöber silica measurements* $\phi_p = 0.01\%$.

particles are stored in air, albeit far more slowly.

3.5.2 Contact angle

Measurements of θ_w were made at various pH values using filtered dodecane as the oil phase and Stöber silica which had been dried for 1 h under vacuum at 50°C. The results are shown in Fig. 3.10. Since the particles were immersed in water during the spin-coating and were then left to dry, it is difficult to predict where their isoelectric point, and hence the location of the expected peak in θ_w, will be. Nevertheless, the measured contact angles appear to be consistent with theoretical predictions [89]. Again, however, the measured contact angles are all above 90° despite the silica being hydrophilic.

3.6 Conclusions and future work

The effect of varying the salt concentration and changing the pH on the phase behaviour of dispersions of both Stöber and fumed silica has been studied.

The addition of salt to the particle dispersions is shown to cause flocculation of the particle dispersions, and greater flocculation rates are observed at higher salt concentrations. However, when the Stöber silica dispersions are simultaneously sheared the size of the aggregates peaks at relatively low salt concentrations, an effect which is thought to be caused by the increased viscosity of the dispersions at high salt concentrations. Sodium iodide is shown to cause a greater flocculation

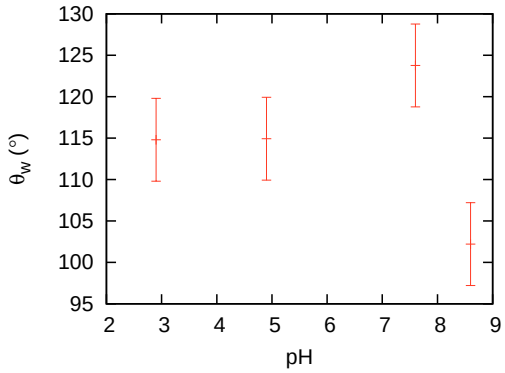

Figure 3.10 *The three-phase contact angle of Stöber silica as a function of pH. The oil phase used was filtered dodecane and the aqueous phase was deionised water with the* pH *adjusted using either hydrochloric acid or sodium hydroxide.*

rate and lead to larger particle aggregates in Stöber silica dispersions than sodium chloride, and this result has been attributed to the more chaotropic nature of iodide ions compared to chloride ions [96].

The three-phase contact angle of Stöber silica at an oil-water interface is shown to decrease when the sodium chloride concentration is increased from 0 mM to 40 mM, in agreement with both theoretical predictions [89] and experimental data from similar systems [89–93]. The contact angle has also been measured as a function of the aqueous phase pH, with no evident trend being observed. However, reliable contact angle measurements have generally proved elusive.

The zeta potentials of Stöber and fumed silica have been measured at a range of pH values. The zeta potential of Stöber silica decreases gradually from $\approx 80\ mV$ to $\approx 40\ mV$ as the pH is increased from 3 to 10, and also decreases with the length of time the particles have been immersed in water. In contrast, fumed silica has a more pronounced change in zeta potential from $\approx 5\ mV$ at pH 3 to $\approx -40\ mV$ at pH 4.5 and then remains at $\approx -45\ mV$ as the pH is increased further. The zeta potential of fumed silica does not change with immersion time in water. The general trend in the measured zeta potentials for fumed silica is in good agreement with published data for both silica [54] and metal oxides (although the isoelectric point can shift) [87, 91, 97, 98]. The measured zeta potentials for Stöber silica are shifted in the positive direction relative to those of the fumed silica due to the addition of APS to the particles, and decrease with immersion time in water, in good agreement with previous measurements [53].

In Chapter 4 these effects will be used to elucidate understanding of the changes in emulsion phase behaviour which are observed.

Chapter 4

The coupling between particle phase behaviour and emulsion phase behaviour in Pickering emulsions

4.1 Introduction

One key advantage of Pickering emulsions is that the particle phase behaviour can be used to influence the phase behaviour of the emulsion [11, 40]. Particle phase behaviour can be changed by tuning the surface chemistry of the particles, which allows for a richer variety of emulsion phase behaviours to be accessed than with molecular surfactants. For example, by tuning the interactions between the particles it is possible to create an emulsion comprising droplets which are themselves attractive or repulsive, which allows the physical properties of the emulsion, such as its rheological behaviour, to be tuned [37].

Another advantage of Pickering emulsions over surfactant-stabilised emulsions is that the molecular surfactants used to stabilise emulsions are often unstable or ineffective when placed in strong ionic solutions, leading to coalescence of the emulsion droplets. If an industrial application requires an emulsion's aqueous phase to have a high ionic strength (*e.g.,* the drilling fluids used in oil wells), then colloidal particles are likely to be a better emulsifier than conventional surfactants. The robustness of Pickering emulsions with high ionic strength aqueous phases is itself an under-researched area.

However, tuning the interactions between particles will affect the emulsification process as well as the properties of the final emulsion. It has often been stated that, in order to generate a stable emulsion, one must use flocculating particles. This is because the adsorption energy of the particles at the oil-water interface is at a maximum when the contact angle is 90°; but this typically means that the particles will not be stable as a dispersion in either phase, *i.e.,* the particles are too hydrophobic to be stable in the aqueous phase but are also too hydrophilic to be stable in the oil phase. This can lead to problems in the emulsification process at industrial scales, since it means that extra energy is required to prevent the particle dispersions aggregating.

This chapter looks at several different methods of modifying the phase behaviour of colloidal silica dispersions, as detailed in Chapter 3. The aim of the current chapter is to describe and explain the effects that these modifications have on the phase behaviour of the emulsions formed when these particle dispersions are mixed with oil. Photography, light scattering, bright-field microscopy and confocal microscopy have been used to characterise the emulsion phase behaviour.

Gautier *et al.* have previously studied the effects of changing both pH and the sodium chloride concentration of the aqueous phase in emulsions stabilised by silica and latex particles [99]. Gautier *et al.* observed several interesting phenomena, including bidisperse droplet populations at intermediate salt concentrations, a tenfold decrease in droplet size over the pH range 3-8 and droplet surface coverages which were substantially below that of hexagonal close packing at high pH and low salt concentrations. However, they studied a relatively small range of salt concentrations (all below 150 mM), did not use fluorescently labelled particles, and looked only at small silica particles ($r_p \approx 75\ nm$), which means that the particles could not be observed directly using optical microscopy.

Destribats *et al.* studied triglyceride oil-in-water emulsions stabilised by whey protein microgels at different pH values and salt concentrations [100]. They found that the droplet size of these emulsions peaked when the particles were charged and attributed this to a decrease in the fraction of particles which adsorb to the oil-water interface. When the particles were uncharged, or when the charge was screened by salt, complete adsorption of the particles occurred, leading to smaller droplets being formed. When the particles were uncharged they formed two-dimensional networks at the interface, whilst when the particles were charged they flocculated but did not form a continuous network. However, they looked only at two salt concentrations (0 mM and 150 mM), and the effects of larger

variations in the salt concentration are also interesting.

In order to extend the scope of the work of Gautier *et al.* and Destribats *et al.*, and to provide further insight, the work presented in this chapter will study a broader range of salt concentrations and pH values, using fluorescently labelled silica particles so that confocal microscopy can be used, and using higher particle volume fractions than those used by Gautier *et al.* The coupling between the phase behaviour of the particle dispersions and that of the final emulsions will also be discussed explicitly.

4.1.1 Salt, and flocculation of the particle dispersion

Briggs was seemingly the first to note that particle dispersions which weakly flocculate tend to be better at stabilising a Pickering emulsion [38], and this finding has been repeated by several groups in more recent years [39–43]. It is common to find in the literature statements such as the following from Binks and Whitby: "There are two important criteria for particles to effectively stabilise emulsions; the particles should be partially wet by both liquid phases and the particles should be weakly flocculating" [41] or the following from Binks and Lumsdon: "stable emulsions can only be formed if the particles are flocculated to some extent" [39]. More recently published articles have softened this position, however, and it has been proposed that flocculating particles are more likely to stabilise emulsions because particle aggregation alters θ_w. For example, Binks *et al.* have argued that particles behave "more hydrophobically (preferring w/o emulsions) when aggregated at higher concentrations since hydrophilic silanol groups [are] shielded and involved in siloxane bond formation between particles" [11, 101].

It is also unclear from the existing literature what exactly constitutes a "weakly" flocculating dispersion, nor when the flocculation becomes "strong". Chapter 3 presented characterisations of particle dispersions and these, together with the results presented in this chapter, should allow for a more rigorous assessment of this behaviour.

The apparent necessity for particles to flocculate in order to stabilise a Pickering emulsion is not ideal from an applications perspective, as it means that to generate a stable emulsion product, one must use an unstable particle dispersion, which means that more energy is required to disperse the particles, and can also put

time constraints on the emulsification process and means that the droplets are likely to aggregate, which is not always desirable. It would therefore be useful to discover and understand a system where a stable particle dispersion generated the most stable emulsion.

Increasing the salt concentration of the aqueous phase has several effects; the Debye length is reduced, meaning electrostatic interactions are more strongly screened, and also increases both the viscosity and refractive index of the water. Reducing the Debye length has several further effects. Firstly, the particles, if they are charged, are able to come closer together and are more likely to overcome the electrostatic barrier between one another and form aggregates (see Chapter 3). Secondly, the addition of salt to the aqueous phase also increases the rate of coalescence between oil droplets which are not fully coated with particles, as the oil droplets carry a slight charge. This is important, as a slower coalescence rate during the limited coalescence process allows the particles more time to adsorb to an oil-water interface, yielding smaller and more stable droplets. Finally, if the particles carry the opposite sign of charge to the oil-water interfaces, then adsorption will become easier, whilst the opposite is true if the particles and interfaces have similar charges.

The same references which claim that weakly flocculating particles are required to generate a stable emulsion also often claim that causing the particle dispersions to strongly flocculate will decrease emulsion stability. Detailed explanations for this are not usually given (*e.g.*, in Ref. [43] it is simply postulated that large particle aggregates may not adsorb as strongly as small particle aggregate), but the reason is presumably to do with the size of aggregates in strongly flocculating emulsions being large enough to prevent particle monolayers forming at the oil-water interface, reducing the efficacy of particle stabilisation.

It has been suggested that the surface chemistry of particle aggregates will differ from that of the primary particles, and that this is why aggregating particles are better at stabilising Pickering emulsions [11, 101]. Aggregates of silica particles may develop silanol bridges where the particles come into contact, and this will lower the number of exposed silanol groups. However, it is difficult to see how a small difference in the number of silanol groups could have a large effect on the average particle wettability, especially given that the changes in the silanol distribution would all be on the inner surfaces of particle aggregates and the external particle surfaces, which would still be exposed at the oil-water interface, would have the same surface silanol group density. The ease with which solvent

which has adsorbed to the interface of the particle can desorb when the particle comes into contact with the oil-water interface will also influence the probability of the particle adsorbing at the interface and remaining there. It is also possible that salt ions could adsorb to the surface of the particles, perhaps in place of water, and this would affect the particle wettability as well.

It is not necessary for the droplets to be fully coated by particles in order for an emulsion to be stable. This effect seems to require strongly charged particles and has been shown by, for example, Vignati *et al.*, who created silica-stabilised oil-in-water emulsions where the droplets had a surface coverage as low as 5% [21]. The mechanisms by which emulsions with such low droplet surface coverage are stable are not yet completely clear, although attractive particle-particle interactions may play a rôle, so that the particles on colliding droplets move to the the contact point and prevent coalescence. A build up of charge at droplet interfaces can also help prevent coalescence in the absence of particles [102].

This chapter will aim to discover if the conventional wisdom regarding Pickering stabilisation by weakly and strongly flocculating particle dispersions is true, and if it is not always true, the situations in which it is and is not correct.

4.1.2 pH

Changing the pH of the aqueous phase of a sample will alter the phase behaviour of the suspended particles (see Chapter 3), as well as the coalescence rate of the oil droplets. These changes can be characterised using the zeta potential of the particles and droplets. Marinova *et al.* have measured the zeta potential of droplets of various oils suspended in water, and found that the zeta potential decreases smoothly as pH increases [103]. The isoelectric point of the droplets was found to be at pH $\approx$ 2-3, and the zeta potential decreased to $\approx -75\ mV$ at pH 7 and then to $\approx -100\ mV$ at pH 9. This behaviour is attributed to the adsorption of negative hydroxyl ions at the oil-water interface.

Whether the pH is changed prior to or following emulsification may affect whether the portion of a particle protruding into the oil phase experiences a change in its surface charge. It is currently unclear how much rotational diffusion particles at an oil-water interface undergo, but it is quite plausible that the particles jam or that the contact line of the interface at the particle becomes pinned, so that the rotational diffusion rate of the particles is reduced. This would mean that

the portions of the particles which protrude into the oil phase are less likely to change their surface chemistry due to changes in the make-up of the aqueous phase, such as a change in pH, which would in turn increase the trapping energy of the particle because of a Janus effect [104]. This will be important because this portion of the particle will experience the strongest electrostatic repulsion from neighbouring particles, due to the lower dielectric constant of the oil relative to the water. By comparing the results of experiments where the pH is adjusted before emulsification has occurred with experiments where the pH is adjusted afterwards, elucidation into this area should be possible.

4.1.2.1 Particle charge

A further interesting aspect of using charge-stabilised hydrophilic particles to stabilise oil-in-water emulsions is that particles with higher charge will form more stable dispersions, where the particles are less likely to move to the interface and where the particles may also be less stable once they are adsorbed at the interface. The reduced dielectric constant of oils relative to water means that a charged particle in the aqueous phase will be repelled from the oil-water interface by image forces (see Eq. (1.23)), and that, if the particles do adsorb to the interface, the portions of the particles which extend into the oil phase will experience strongly repulsive forces due to the lack of electrostatic screening in the oil, although it is possible that recombination of surface groups with counter-ions will reduce the electrostatic effects here. This picture is made slightly more complicated by the fact that the interface itself carries a charge, and because the surface chemistry of the particles may change when they adsorb to the interface. The question thus arises: what is the optimum charge on particles being used as Pickering emulsion stabilisers? Further complications arise when one starts to consider the interactions between the particles once they have adsorbed at the interface - strongly charged particles will repel each other, potentially leaving large gaps in particle layer at the interface [28]. These gaps may make coalescence more likely, but droplets stabilised by strongly charged droplets will themselves repel, and so potentially be less likely to coalesce. This behaviour may explain the surprisingly high stability of sparsely covered droplets which has been reported by Vignati *et al.* [21].

More strongly charged particles will also be less likely to flocculate. Conventionally, therefore, they would be thought less likely to stabilise an emulsion, as it has

been thought necessary for the particle dispersion to weakly flocculate. It will therefore be interesting to consider the effects of changing the pH in this context.

4.1.3 Aggregation at the interface

Particles at the oil-water interface in a Pickering emulsion can form rigid layers which greatly enhance the stability of the emulsion against coalescence, even when the continuous phase is almost completely removed from the sample [105, 106]. The particle contact angle and the degree to which the particles aggregate at the interface will both affect the rigidity of the interface. The charge of silica particles means that their behaviour at the interface is especially interesting because the particles protrude to some extent into the oil phase, and so would be expected to repel due to the lack of electrostatic screening.

However, an understudied aspect of Pickering stabilisation is the link between the contact angle and the particle-particle interactions at the oil-water interface. Experimental work has been carried out on this topic by Horozov *et al.* [107] and theoretical work has been carried out by Law *et al.* [108]. Horozov *et al.* tuned the wettability of silica particles by silanising them using hexamethyldisilazane or dichlorodimethylsilane, and showed that when the particles had a contact angle of 65°, the particles aggregated at the interface, but that when the particles had a contact angle of 152°, a well-ordered monolayer with particle separations ≈ 5 times the particle diameter was formed. These findings are consistent with a simple picture where the interactions between the particles are considered to be dominated by the fluid phase by which they are preferentially wetted - *i.e.,* the interactions are considered to be similar to the bulk behaviour in water if the contact angle is low and are considered to be like the bulk behaviour in oil if the contact angle is high. This picture is naturally expected to break down at intermediate contact angles, although the lower dielectric constant of oils means that the interactions through the oil phase may be more important. However, a systematic study has yet to be carried out, and it is presently unclear what the relationships are between:

- Bulk particle interactions and interfacial particle interactions. For example, if a particle dispersion aggregates, do the particles also aggregate when they are placed on an oil-water interface, and *vice versa*? Given the results which Horozov *et al.* have shown, this behaviour will presumably be highly

sensitive to the contact angle.

- The particle-particle interactions at the interface and the stability of an emulsion. For example, if the particles strongly aggregate at the interface, the droplet will be less likely to deform during shear, but its interface will crack when it does deform, and this will have implications for the emulsion stability. Experiments carried out using two different colours of particle to stabilise an emulsion have been used to explore this area further, and will be described in Chapter 6 and Chapter 7.

Whether the particles aggregate when they have adsorbed at the interface will have a large effect on the rheological properties of the interface itself as well. If particles do aggregate at the interface, a network of particles on the surface of a droplet will presumably develop during the limited coalescence process. It is not clear if this will be beneficial to emulsion stability or not, and this chapter aims to begin addressing this.

4.2 Methods and materials

The methods which are particular to this chapter will be discussed in this section. Methodology for techniques which are used in this chapter and in other chapters can be found in Chapter 2.

4.2.1 Sample preparation: Salt

4.2.1.1 Stöber silica and sodium chloride

Eight emulsion samples were prepared, each with $\phi_p = 1.7\%$ and $\phi_o = 20\%$. The oil phase was a mixture of dodecane and isopropyl myristate, with $\Phi_{IM} = 10\%$. The sodium chloride concentrations of the eight samples were 0 mM, 10 mM, 30 mM, 100 mM, 300 mM, 750 mM, 1500 mM and 4000 mM - a range that covers non-flocculating, weakly flocculating and strongly flocculating dispersions (see Chapter 3). The dried particles and the salt were dispersed in water using the ultrasonic probe (1 s on, 4 s off for 60 cycles at an amplitude of 20%). The oil phase was then added and the samples were emulsified using a vortex mixer in 30 s bursts until either the aqueous phase was clear of particles, or

until the sample had been vortex mixed for a total of 3 min. The samples were then photographed regularly as the emulsion creamed and any remaining particles sedimented. Slides were prepared, with a drop of emulsion from each sample being diluted in some of the sample's continuous (aqueous) phase. Optical and confocal microscopy were then performed using the prepared slides, and light scattering was used to measure the emulsions' droplet size distributions. The droplet size has been used to characterise emulsion stability; an increase in the droplet size indicates that the emulsion is less stable, either because the particle trapping energy is lower or because the particles are not able to adsorb to the interface during emulsification. If, for a given sample preparation route, the droplet size is small, then the emulsification process has been more efficient than if the same preparation route led to a large droplet size. Since optimising the emulsion system so that the emulsification process requires as little energy as possible is desirable, droplet size can be used to compare the stability of emulsions which have followed the same preparation route.

4.2.1.2 Stöber silica and sodium iodide

Similar samples to those described above were made using sodium iodide as the salt rather than sodium chloride. The samples had the same molarities as above, and were prepared using the same protocol. Iodide ions are more chaotropic than chloride ions and so, for a given molarity using sodium iodide rather than sodium chloride gives the aqueous phase a higher refractive index and a lower viscosity (see Chapter 3). Since iodide ions are more chaotropic than chloride ions, they are more likely to adsorb to particle surfaces. This is likely to affect the contact angle of the particles at the interface, although for the reasons discussed in Chapter 3, this has not been demonstrated experimentally.

4.2.1.3 Fumed silica and sodium chloride

Five samples were prepared using the same protocol as above, but replacing the Stöber silica with OX50 fumed silica, and with $\phi_p = 0.07\%$. The sodium chloride concentrations used were 0 mM, 40 mM, 150 mM, 750 mM and 4000 mM, which again cover a range of non-flocculating, weakly flocculating and strongly flocculating particle dispersions (see Chapter 3).

4.2.2 Sample preparation: pH

Samples made to study the effects of changing pH were prepared in one of two ways; in both cases either hydrochloric acid or sodium hydroxide was used to alter the pH of the aqueous phase. In the first method, the particles were dispersed in the aqueous phase at the appropriate pH, then the oil phase was added and the sample was emulsified by vortex mixing until the aqueous phase was clear (or for a total mixing time of 3 min). In the second method, the samples were prepared and emulsified using pure deionised water as the aqueous phase, and then a small amount of additional aqueous phase was added to the sample to adjust the pH to the desired value. By comparing the emulsions prepared using these two methods, the effects of changing pH on the emulsification process itself can be studied. The pH range covered was 3-10.

4.3 Results and discussion

4.3.1 The effects of flocculating the particle dispersions by adding salt

Here, the results from experiments carried out by varying the salt concentration will be presented and discussed. First, the results from experiments using Stöber silica and sodium chloride will be presented, followed by the results of experiments with Stöber silica and sodium iodide and finally results obtained using fumed silica and sodium chloride. In particular, results which lie anent the conventional view presented in the literature will be emphasised and explanations for these discrepancies will be presented.

4.3.1.1 Stöber silica and sodium chloride

A photograph of the samples prepared using Stöber silica and sodium chloride can be seen in Fig. 4.1, and shows that the emulsion stability changes dramatically with sodium chloride concentration. No changes to the samples are observed if they are left for several weeks.

The size distributions of the emulsions in Fig. 4.1 are shown in Fig. 4.2, and

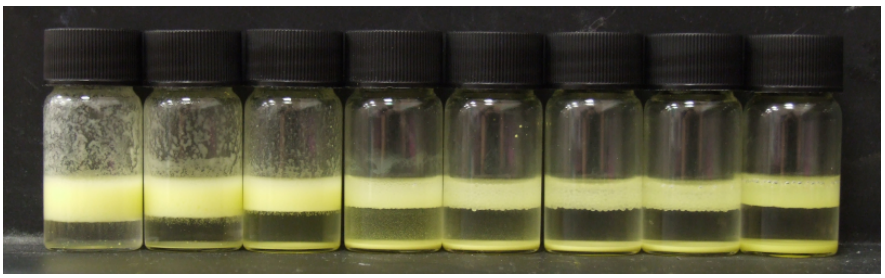

Figure 4.1 *Photograph showing emulsions stabilised by Stöber silica at various sodium chloride concentrations. The salt concentrations are, from left to right,* 0 mM, 10 mM, 30 mM, 100 mM, 300 mM, 750 mM, 1500 mM *and* 4000 mM. *The amount of free silica can clearly be seen to increase with salt concentration. The emulsion appears yellow due to the FITC dye in the silica particles, sedimented free silica is visible at the bottom of some vials and the clear phase below the emulsion is the resolved water.*

Fig. 4.3 shows the average droplet size from these samples. These graphs suggest that the droplet size is smallest when the sodium chloride concentration is 10 mM. However, as will be explained in Chapter 5, this is because the droplets in the 0 mM sample are aggregating due to particle bridging. It can therefore be seen that as the sodium chloride concentration is increased from 0 mM to 1500 mM, the emulsion droplets get continuously larger, and so the particles are becoming increasingly ineffectual.

Since an increase in droplet size indicates that the particles are not arresting the coalescence process as early as might be expected, which may happen because the particles do not adsorb to the interface at all or because the particle trapping energy has decreased, the changes in droplet size as the salt concentration is increased at constant particle volume fraction show that the emulsion stability is changing.

Bright-field microscopy confirms the light-scattering data which show that the droplet size of the resultant emulsion increases as the particles are made to weakly flocculate, as shown in Fig. 4.2, Fig. 4.3 and Fig. 4.4. In fact, the picture is slightly more complicated than Fig. 4.3 might initially suggest. At the lowest salt concentrations, $\lesssim 10\ mM$, the emulsion is relatively monodisperse. The apparent droplet size in the absence of salt is higher than the actual primary droplet size due to droplet aggregation caused by bridging, as will be discussed in Chapter 5. However, at a salt concentration of $\approx 30\ mM$, the emulsion becomes bidisperse, with two populations of droplets with mean diameters of $\approx 30\ \mu m$ and 100 μm.

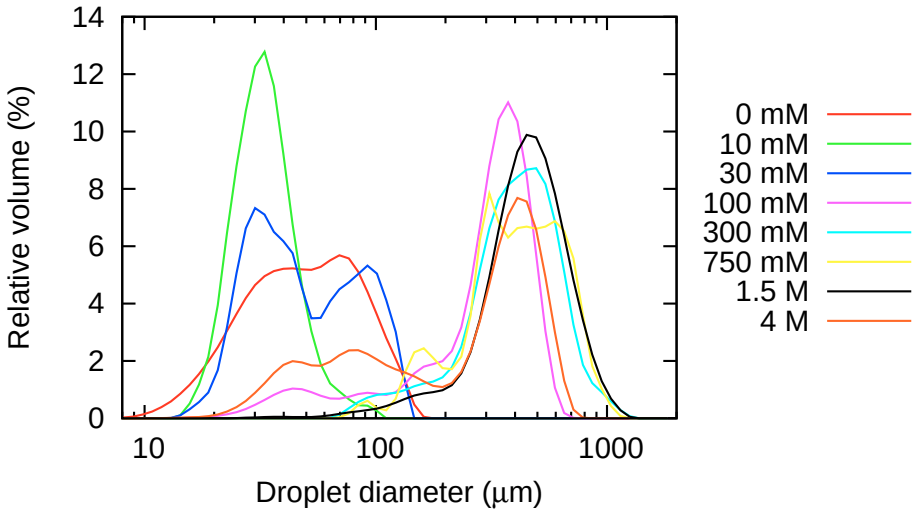

Figure 4.2 *Size distributions of emulsions stabilised by Stöber silica at various sodium chloride concentrations. In all samples,* $\phi_p = 1.7\%$, $\phi_o = 20\%$ *and* Φ_{IM}.

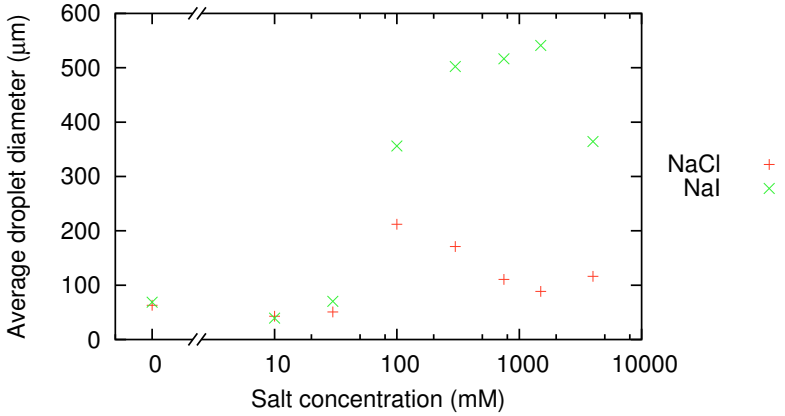

Figure 4.3 *Volume-weighted mean droplet size of emulsions at different sodium chloride and sodium iodide concentrations. In all samples,* $\phi_p = 1.7\%$, $\phi_o = 20\%$ *and* Φ_{IM}.

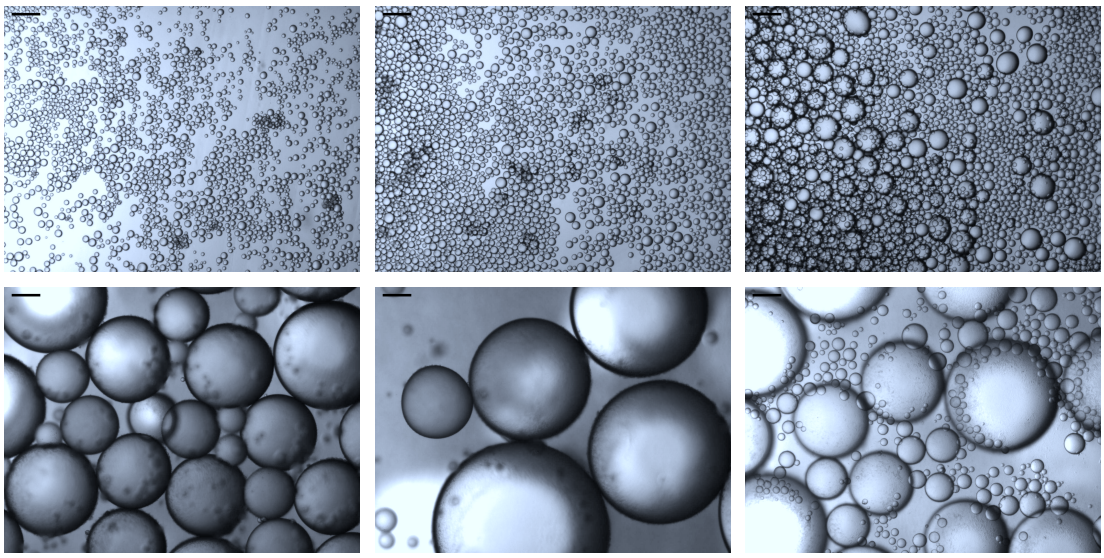

Figure 4.4 *Micrographs of emulsions at a variety of sodium chloride concentrations. The sodium chloride concentrations are, from left to right, Top row:* 0 mM, 10 mM *and* 30 mM*; Bottom row:* 100 mM, 300 mM *and* 4000 mM*. The scale bars are* 100 μm*.*

At still-higher salt concentrations the size distribution becomes monodisperse again, with droplet diameters centred on $\approx 500\ \mu m$ in the range 100-1500 mM, before becoming bidisperse again at the highest salt concentration studied here (4000 mM), where the droplet populations are centred around $\approx 80\ \mu m$ and $\approx 500\ \mu m$.

Sodium chloride will alter the contact angle, decreasing it initially (see Chapter 3), which will mean that particles are less strongly trapped at the oil-water interface. Therefore, as the limited coalescence process progresses, the particles may be ejected from the interface either during the coalescence events themselves, or soon afterwards because of pressure from their neighbours (*e.g.*, if the particles are jammed at the interface of a droplet which isn't spherical and is therefore trying to relax). This process could contribute to the increase in droplet size observed as the salt concentration is increased.

Surface coverage Optical and confocal microscopy also reveal differences in how the particles arrange themselves at a droplet's surface at different sodium chloride concentrations. At very low sodium chloride concentrations ($\lesssim 10\ mM$), the droplets are generally fully covered and the particles form a monolayer at the oil-water interface, as can be seen in Fig. 4.5. However, the confocal micrograph in Fig. 4.6 (left) shows that when the sodium chloride concentration is increased

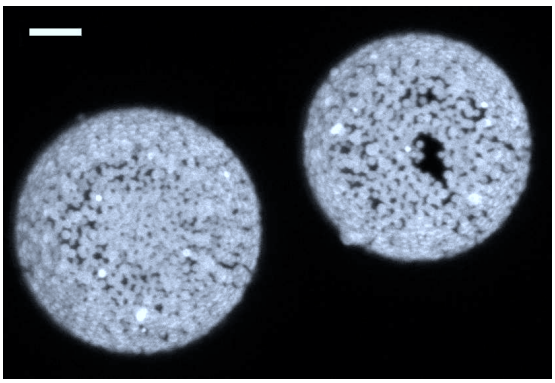

Figure 4.5 *Confocal micrograph projection showing the particle layers at two droplet interfaces. The image is a z-projection of* 14 *images, with a z-spacing of* 0.44 μm*, constructed using ImageJ. The sodium chloride concentration in this sample is* 10 mM *and the scale bar is* 5 μm*.*

to 30 mM, droplets where the surface coverage is well below that of close-packed spheres are observed. These droplets are generally the larger droplets in the sample, suggesting that there is a link between the appearance of a bidisperse size distribution at this salt concentration, and the lower surface coverage observed. It is also clear that the particles on the droplet in Fig. 4.6 (left) are aggregating whilst at the interface, which is perhaps to be expected as the particles flocculate in the bulk at this sodium chloride concentration (see Chapter 3). At sodium chloride concentrations greater than $\approx$ 100 mM, the particle layer at the oil-water interface is no longer a monolayer, but instead extends significantly into the aqueous phase, as shown in Fig. 4.6 (right) and Fig. 4.7. Clearly, the efficiency of the particle stabilisation is reduced here, and Eq. (1.3) no longer holds, even if all of the particles are at (or near) an oil-water interface.

It can also be seen from the photograph in Fig. 4.1 that in the sample with a sodium chloride concentration of 30 mM, not all of the particles adsorb to an interface, and a significant fraction of the particles are left in the aqueous phase and subsequently sediment. It is curious that, although not all of the particles adsorb to the oil-water interface, some droplets are left with large bare patches on their surfaces and are yet seemingly stable against further coalescence. One possible explanation is that the particle attractions are strong enough that particles on opposing droplets move towards each other when the droplets come into contact. Given the salt concentration in this sample, it seems unlikely that charged interfaces could be responsible for stabilising the droplets.

Overall, then, it can be seen that as the concentration of sodium chloride is

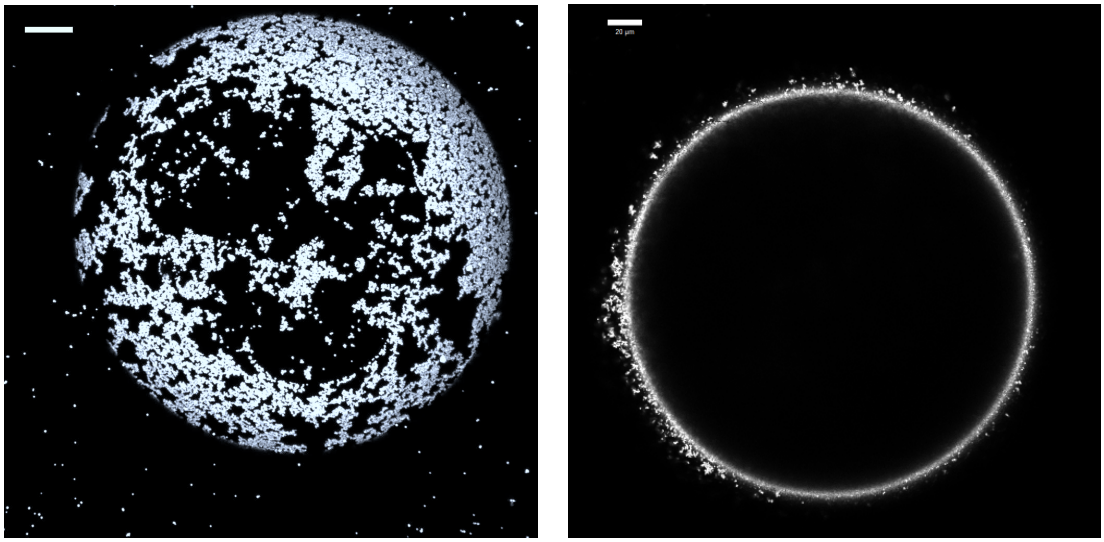

Figure 4.6 *Left: Confocal micrograph projection showing the packing of particles at the interface. The sodium chloride concentration in this sample is* 30 mM*. The image is a z-projection of* 42 *images, with a z-spacing of* 0.44 μm*, constructed using ImageJ; Right: Confocal micrograph showing the thickened particle layer at the interface in the* 100 mM *sample. The scale bars are both* 20 μm*.*

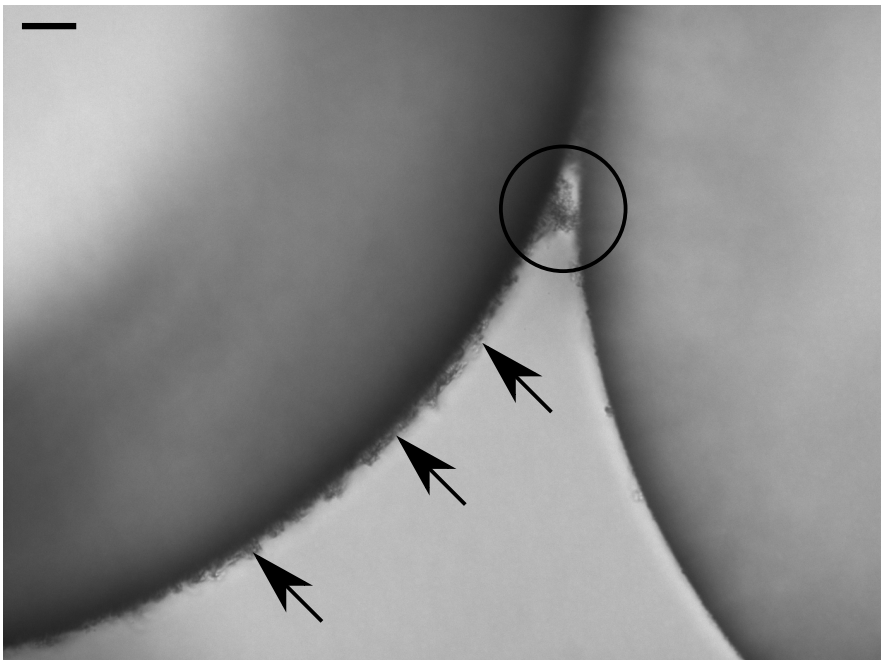

Figure 4.7 *Micrograph showing the thickening of the interfacial particle layer. The arrows indicate the thickened particle layer, which protrudes several micrometres into the continuous phase from the interface, and the circled area shows that the thickened particle layer can be shared by droplets. The sodium chloride concentration in this sample is* 300 mM *and the scale bar is* 10 μm*.*

increased, the droplets change from being fully coated by particles to not being fully coated by particles which aggregate at the interface, and then to being fully coated by particles, but with particle layers which extend into the continuous phase. This behaviour is summarised in the cartoon in Fig. 4.8. The change from being fully coated to not being fully coated appears to coincide with the change from a non-flocculating dispersion to a weakly flocculating dispersion, where the emulsification process is still capable of breaking up the particle aggregates. The transition to a system where the particles in the continuous phase form a network linking droplets together may then occur at the point where the emulsification process is no longer capable of fully disrupting particle aggregates. The increase in the coalescence rate as the sodium chloride concentration is increased may be responsible for the droplets becoming fully coated at higher salt concentrations, as non-fully coated droplets are less likely to be stable here.

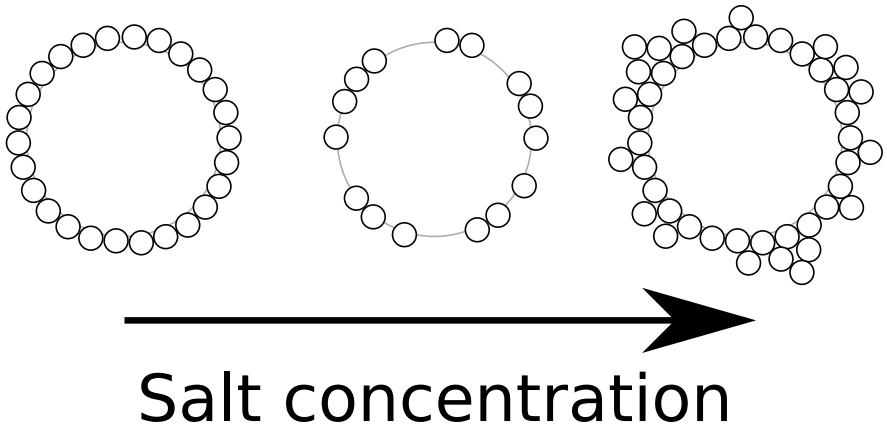

Figure 4.8 *Cartoon summarising the behaviour of droplets stabilised by Stöber silica as the salt concentration is increased. When the particles do not flocculate, the droplets are fully coated by a particle monolayer. Weakly flocculating particles aggregate at the interface and lead to a decrease in surface coverage of the droplets. Strongly flocculating particle dispersions lead to fully coated droplets, but with a thickened particle layer at the interface.*

As well as the thickening of the layer of particles at the interface, the amount of silica which remains in the aqueous phase following emulsification increases with sodium chloride concentration, as can be seen in the photograph of the samples in Fig. 4.1. This, together with the increased thickness of the particle layer at high salt concentrations, contributes to the increased droplet size. The increase in the packing fraction of the emulsions as the salt concentration increases from 0 mM to 30 mM is evidence of particle bridging in the low salt concentration samples, as will be discussed further in Chapter 5.

Discussion: Stöber silica and sodium chloride Oil-in-water Pickering emulsions stabilised by Stöber silica have been produced, and it has been observed that the most stable emulsions are formed when the aqueous phase contains no sodium chloride, that the least stable emulsions are formed when the aqueous phase has a sodium chloride concentration of $\approx 1000\ mM$ and that above this concentration the emulsion stability increases. A summary of this behaviour can be seen in the photographs in Fig. 4.9, which show emulsions similar to those in Fig. 4.1, but with $\phi_p = 1.1\%$ and $\Phi_{IM} = 0\%$. It can be seen here that at a sodium chloride concentration of 250 mM very large droplets ($r_o \approx 0.5\ mm$) are produced, meaning that only a very small proportion of the particles have become trapped at the interface. As detailed in Chapter 3 the three sodium chloride concentrations shown in these photographs (0 mM, 250 mM and 4000 mM) can be considered as non-flocculating, weakly flocculating and strongly flocculating particle dispersions, as can be ascertained from the rates at which the free silica sediments in each sample. It can therefore be seen that this system behaves in the opposite manner from that described by *e.g.,* Binks and Lumsdon [39]. This discrepancy is likely caused by the differing surface chemistry of the Stöber silica particles used here, which have non-native amino groups and fluorescent dye at their surface.

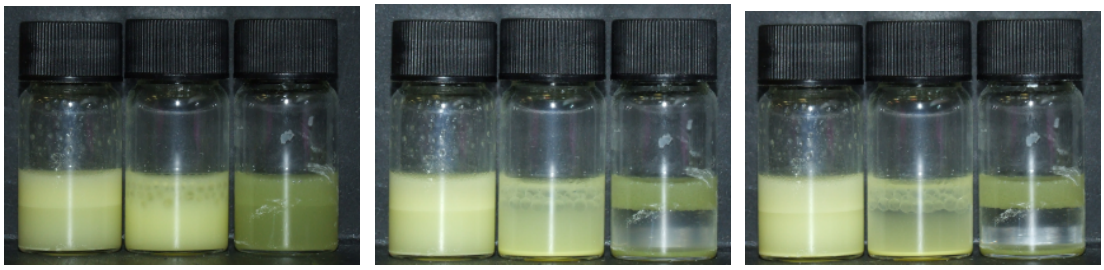

Figure 4.9 *Photographs of emulsions at a variety of salt concentrations. The samples in each photograph have salt concentrations of, from left to right,* 0 mM, 250 mM *and* 4000 mM. *In all three samples* $\phi_p = 1.1\%$, $\phi_o = 20\%$ *and* $\Phi_{IM} = 0\%$. *The time since emulsification in the three photographs is* 0, 40 *and* 80 *min.*

4.3.1.2 Stöber silica and sodium iodide

The results of experiments similar to those described in Section 4.3.1.1, but using sodium iodide rather than sodium chloride, will now be described.

Figure 4.10 shows a photograph of samples stabilised by Stöber silica at a variety of sodium iodide concentrations. The size distributions for these samples can

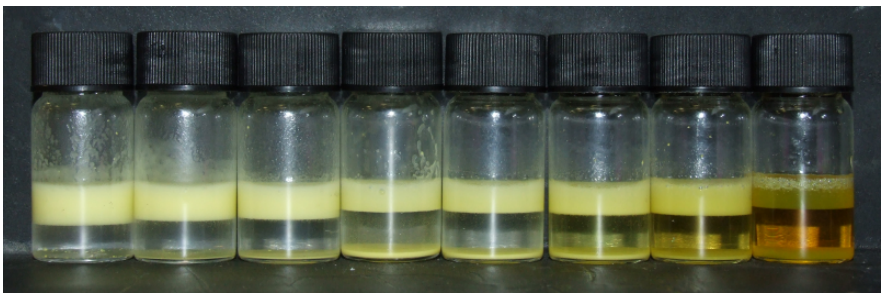

Figure 4.10 *Photograph showing emulsions stabilised by Stöber silica at various sodium iodide concentrations. The salt concentrations are, from left to right,* 0 mM, 10 mM, 30 mM, 100 mM, 300 mM, 750 mM, 1500 mM *and* 4000 mM. *The amount of free silica can clearly be seen to increase with salt concentration.*

be seen in Fig. 4.11, and a graph showing the volume-weighted mean droplet diameters for both sets of experiments is shown in Fig. 4.3. As can be seen from these graphs and the corresponding micrographs in Fig. 4.12, the effect of including sodium iodide is broadly similar to that of including sodium chloride, in that the average droplet size is lowest at small salt concentrations, passes through a peak at intermediate salt concentrations and decreases again at higher salt concentrations. However, there are several notable differences between the two sets of samples. Firstly, the mean droplet size in the emulsions containing sodium iodide is smaller at all salt concentrations, and considerably smaller at high salt concentrations. Secondly, bidisperse distributions are obvious at all sodium iodide concentrations in the range 30-4000 mM whereas bidisperse distributions are only observed at sodium chloride concentrations of 30 mM and 4000 mM, but not in between.

The dramatic difference in the size of the droplets in emulsions which contain the same molarity of sodium chloride and sodium iodide is initially surprising. As was shown in Chapter 3, the particle dispersions containing sodium iodide aggregate more strongly than dispersions containing an equal molarity of sodium chloride. In particular, particle sizing data (see Fig. 3.3) show that the dispersions containing sodium iodide aggregate more strongly than those containing sodium chloride when sheared. It seems likely that this stronger aggregation causes the observed difference in droplet size. The mechanism which causes this behaviour is not particularly clear, although it is possible that small aggregates of particles adsorb more easily to the interface than individual particles. Since the coalescence rate also increases as salt is added, a small difference in the particle adsorption

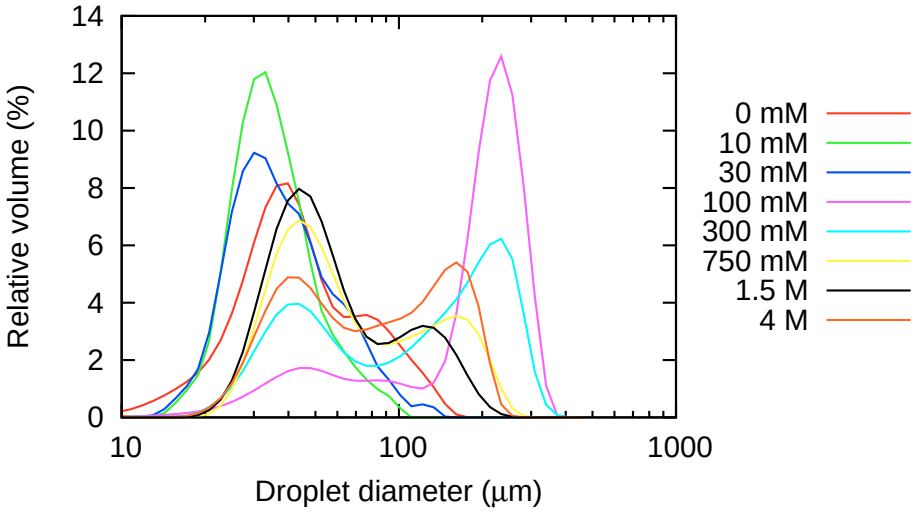

Figure 4.11 *Size distributions of emulsions stabilised by Stöber silica at various sodium iodide concentrations.*

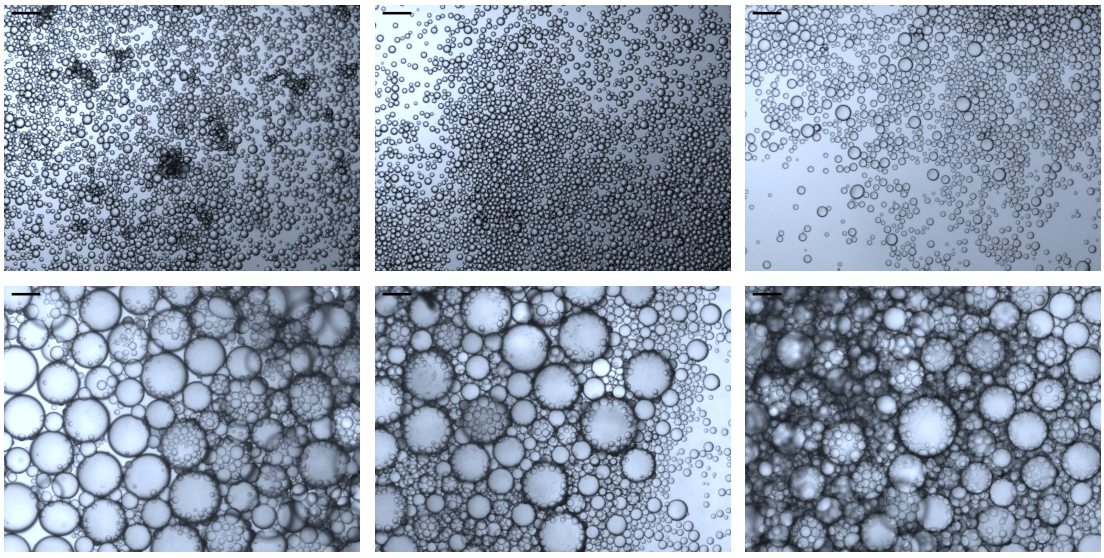

Figure 4.12 *Micrographs of emulsions stabilised by Stöber silica at a variety of sodium iodide concentrations. The salt concentrations are, from left to right, Top row: 0 mM, 10 mM and 30 mM; Bottom row: 100 mM, 300 mM and 1500 mM. The scale bars are 100 μm.*

rate may make a relatively large difference to the eventual droplet size. It is also possible that the increased aggregation strength of the particles causes the continuous phase to gel more quickly and easily when the shearing ends, which would dramatically decrease the coalescence rate so that more particles adsorb to an oil-water interface during decomposition, meaning that coalescence is arrested earlier.

Surface coverage As with the samples containing sodium chloride, changes in the surface coverage of emulsion droplets were observed as the sodium iodide concentration was increased. When no salt was added the droplets were generally fully covered, as before. At small sodium iodide concentrations ($\lesssim 30\ mM$), the surface coverage was observed to be a monolayer with very few gaps, as shown in Fig. 4.13. When the sodium iodide concentration is increased to 100-750 mM, the particle layer at the interface was again observed to thicken slightly in some places, as shown in Fig. 4.14, so that the particle aggregates protruded slightly into the continuous phase. In a similar fashion to the behaviour observed when sodium chloride was added, when the sodium iodide concentration was increased to $\geq 1500\ mM$, the particle aggregates were observed to protrude extensively into the continuous phase, to the extent that the emulsion droplets were almost all connected to each other by a network of aggregated particles, as can be seen in Fig. 4.15. This behaviour is similar to that observed by Yan and Masliyah, who studied the behaviour of emulsions stabilised by kaolinite clays as a function of the clay volume fraction and found that at higher clay volume fractions the majority of the clay remained in the continuous phase, forming a network which hindered the settling of the emulsion [109]. This network of particles in the continuous phase will act as a significant barrier against coalescence, and would possibly be capable of stabilising the emulsions even if the particles were not adsorbing to the interface, by gelling the continuous phase [7].

Despite the particles which are left in the continuous phase forming an open and branched network, it is clear that the particles which adsorb to the interface are able to fully coat the droplet surface in almost all cases - they don't form an open network on the interface. Since not all of the particles adsorb to an oil-water interface, but the droplets become fully covered by particles, the increase in droplet size observed at intermediate sodium iodide concentrations can be attributed to the increased coalescence rate between droplets, which is caused by the increased screening of electrostatic charge present at the droplet interfaces.

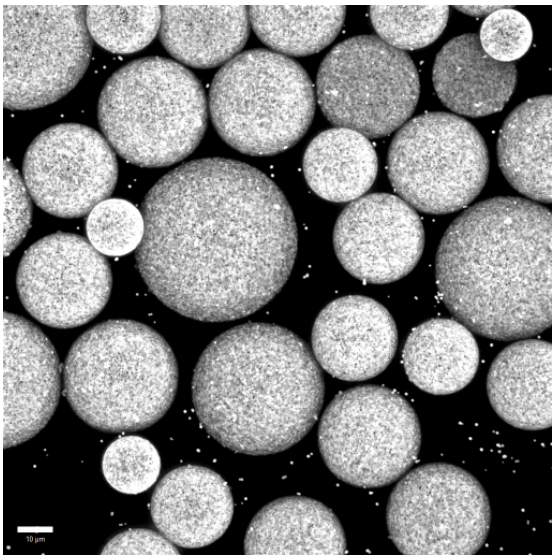

Figure 4.13 *Confocal micrograph showing surface coverage of emulsion droplets stabilised by Stöber silica, with a sodium iodide concentration of* 30 mM. *The image is a z-projection of* 17 *images, with a z-spacing of* 0.44 μm, *constructed using ImageJ. The scale bar is* 10 μm.

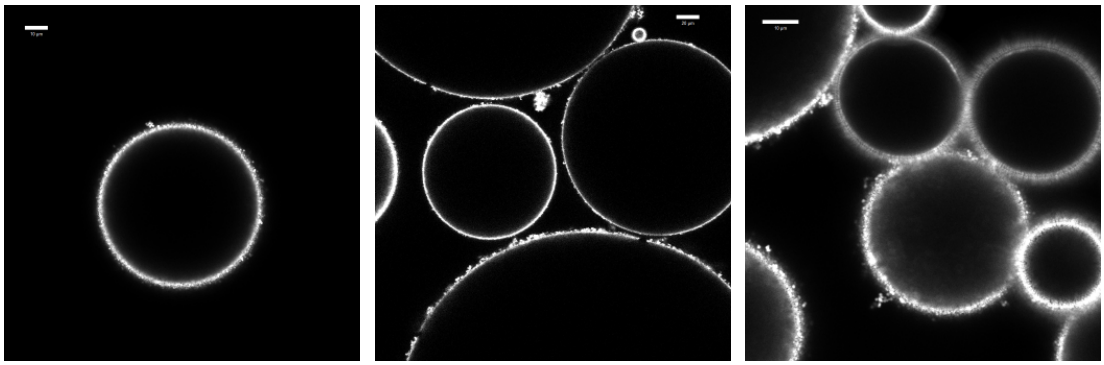

Figure 4.14 *Confocal micrographs of Pickering emulsion droplets stabilised by Stöber silica at sodium iodide concentrations of* 100-750 mM. *The sodium iodide concentrations are* 100 mM, 300 mM *and* 750 mM, *from left to right. The scale bars are* 10 μm *(left and right) and* 20 μm *(centre). The thickening of the particle layer at the droplets' interface as the salt concentration is increased can clearly be seen.*

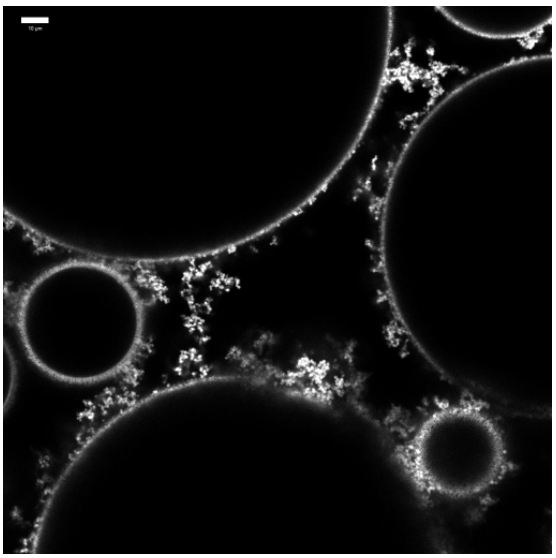

Figure 4.15 *Confocal micrographs showing a Pickering emulsion stabilised by Stöber silica, with a sodium iodide concentration of* 1500 mM. *A network of particles in the continuous phase can be seen to link the droplets together. The scale bar is* 10 μm.

Discussion: Stöber silica and sodium iodide Emulsions stabilised by Stöber silica have been studied at various sodium iodide concentrations. As with samples containing sodium chloride, the droplet size passes through a peak at intermediate salt concentrations. However, samples containing sodium iodide are observed to be more stable than those containing an equal concentration of sodium chloride, despite sodium iodide causing the particle dispersions to flocculate more strongly. This is attributed to the iodide ions being more chaotropic than chloride ions, which causes the particles to be more hydrophobic and hence more likely to be trapped at a droplet interface.

4.3.1.3 Fumed silica and sodium chloride

In order to compare and contrast the results obtained using Stöber silica, similar experiments have also been performed using fumed silica. Size distributions for these emulsions are shown in Fig. 4.16, and corresponding micrographs are shown in Fig. 4.17.

Surface coverage The fumed silica used here is not fluorescent, so confocal microscopy cannot be used to obtain a picture of how the particles organise at the

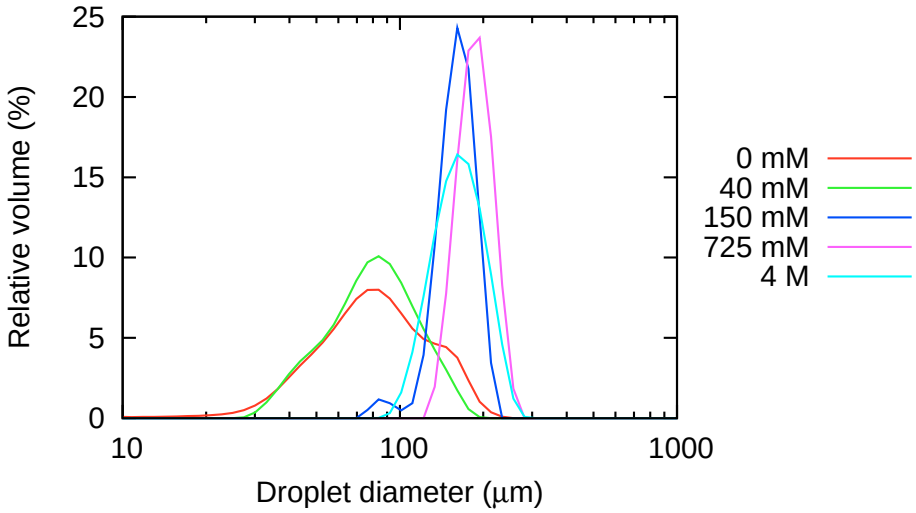

Figure 4.16 *Size distributions of emulsions stabilised by fumed silica particles at different sodium chloride concentrations.*

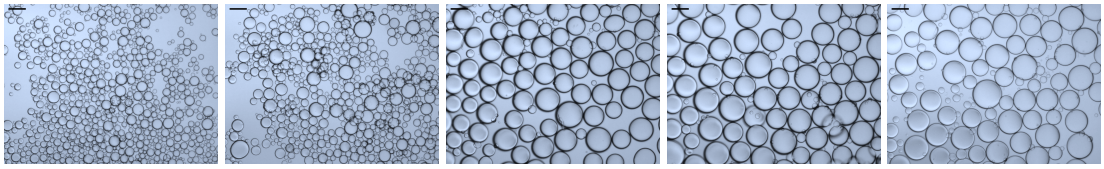

Figure 4.17 *Micrographs of Pickering emulsions stabilised by fumed silica at different sodium chloride concentrations. The salt concentrations in the micrographs are, from left to right,* 0 mM, 40 mM, 150 mM, 725 mM *and* 4000 mM, *and the scale bars are* 100 μm.

interface in these samples. However, the amount of silica left in the continuous phase of the fumed silica-stabilised emulsions following emulsification changes with salt concentration, as can be seen in the photograph in Fig. 4.18. In contrast to the samples stabilised by Stöber silica particles, the largest amount of free silica in the fumed silica samples is observed when the sample does not contain salt. At a sodium chloride concentration of 40 mM, there is no indication of free silica, whilst some can be observed at higher sodium chloride concentrations ($\approx$ 750-4000 mM). Given that the smallest droplets are observed when the sample contains no salt, it can be concluded that either the particle layers in the samples containing salt are not monolayers, but are slightly thickened, or that in the absence of salt the surface coverage is lower than that of close-packed spheres. Since the particles do not aggregate in the absence of salt, it seems unlikely that the particles would flocculate strongly enough at the interface to form a network. It is also possible that the polydispersity of the fumed silica

Figure 4.18 *Photograph showing Pickering emulsions stabilised by fumed silica at a variety of sodium chloride concentrations. The sodium chloride concentrations are, from left to right,* 0 mM, 40 mM, 150 mM, 750 mM *and* 4000 mM.

influences the behaviour, as the smaller particles may be left in the continuous phase whilst the larger particles adsorb to the interface, and this is an interesting topic for future investigation.

Discussion: Fumed silica and sodium chloride As can be seen from Fig. 4.16, Fig. 4.17 and Fig. 4.18 the droplet size in fumed silica-stabilised emulsions is lowest when the salt concentration is $\lesssim 40\ mM$, and when the salt concentration is 0 mM there are particles left in the aqueous phase. Therefore, it is argued that the stability of the fumed silica-stabilised emulsions passes through a maximum at intermediate salt concentrations, which contrasts with the behaviour observed for the Stöber silica particles in Section 4.3.1.1. In fact, the behaviour of the fumed silica-stabilised emulsions agrees qualitatively with the behaviour expected from the results of Binks *et al.* mentioned in Section 4.1.1 above. However, as was shown in Chapter 3, it is not entirely obvious that a dispersion of fumed silica with a sodium chloride concentration $\geq 10\ mM$ can be accurately described as "weakly flocculating". This suggests that the anomalous behaviour observed when using Stöber silica is due to their particular surface chemistry.

4.3.2 Discussion: Salt

There are clearly many different factors affecting the behaviour of the emulsions when salt is added, but it seems likely that the main reasons for the changes in droplet size seen here are the increase in coalescence rate between uncovered droplets and the aggregation of particles making it more difficult for a monolayer of particles to form at the interface.

Whilst it might be true of some, or even most, systems, it is not a universal fact that causing the particles to weakly flocculate will result in a more stable emulsion. Similarly, it is not always true that causing the particles to strongly flocculate will result in an emulsion which is less stable than an emulsion generated from a weakly flocculating particle dispersion.

It is not particularly clear from the existing literature as to what constitutes a "weakly" (or "strongly") flocculating particle dispersion. When considering Pickering emulsification, an added complication is that the dispersions usually undergo shear, and the applied shear rate will affect the flocculation behaviour. It is suggested here that "strongly flocculating" dispersions are those in which the flocculation is not overcome by the shear during emulsification. It is also necessary to note that at higher salt concentrations, the effect upon the viscosity is not negligible, and will lead to smaller aggregates being formed. This apparent reduction in the strength of the flocculation may be the reason that emulsions stabilised by Stöber silica at high salt concentrations are more stable than those at intermediate salt concentrations.

It is clear from the results presented here that a more nuanced view of Pickering stabilisation is required than has previously been presented in the literature. Whereas the requirements for Pickering stabilisation have usually been described in terms of the particle-particle interactions, the particle-interface interactions are also important to consider, as these will define whether the particles adsorb to the interface.

4.3.3 pH

Here, the results from the experiments carried out by varying the pH of the aqueous phase will be presented and discussed. First, the results from experiments using Stöber silica will be presented, followed by results obtained using fumed silica. In particular, results which do not fit the conventional view presented in the literature will be emphasised and explanations for these discrepancies will be presented. The idea that flocculating particles are necessary to stabilise a Pickering emulsion will also be tested here, with particle dispersions where $|\zeta| \gtrsim 20\ mV$ generally being considered stable and those where $|\zeta| \lesssim 20\ mV$ being considered unstable (see Chapter 3). This means that the fumed silica dispersions are unstable when the pH $\lesssim 3$, and the Stöber silica dispersions are unstable at pH $\approx$ 4-5.

4.3.3.1 Stöber silica

As mentioned above, two methods of adjusting the pH of samples were used: pre- and post-emulsification. The results of these two protocols will be discussed here, and any discrepancies between the two will be explained.

By emulsifying samples which have different pH values, the effects of particle charge on the emulsification process can be probed.

Pre-emulsification Figure 4.19 shows a series of emulsions stabilised by Stöber silica with different aqueous phase pH values, where the pH was adjusted prior to emulsification. Micrographs from these samples are shown in Fig. 4.20. Little difference between the emulsions is noticeable, with the exception of the sample at pH 3, which has a significant amount of free silica. This is not surprising because the particles in this sample have the highest positive zeta potential ($\approx 80\ mV$), and so would be expected to have the strongest repulsions between the particles and the oil-water interface due to image forces, which leads to the particles being less likely to adsorb to a droplet interface at this pH. Furthermore, the zeta potential of the oil droplets is very low here, which means that there is a very low electrostatic particle-interface attraction, and that the coalescence rate between droplets is high, and this means that the time available for particles to adsorb to small droplets is reduced.

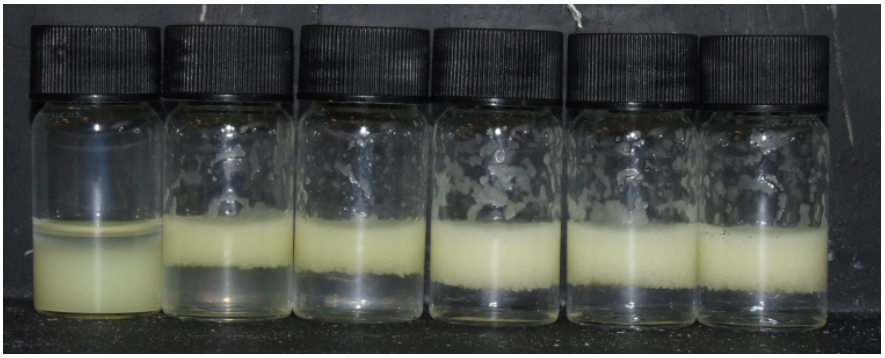

Figure 4.19 *Photograph of emulsions stabilised by Stöber silica at different* pH *values, where the* pH *was changed prior to emulsification. The* pH *values of the samples are, from left to right,* 3, 4.5, 6, 7, 8.5 *and* 10. *In all of the samples* $\phi_p = 1.1\%$, $\phi_o = 20\%$ *and* $\Phi_{IM} = 10\%$.

Figure 4.21 shows confocal micrographs of droplets from the samples where the pH was adjusted prior to emulsification. It can be seen that the droplets are fully

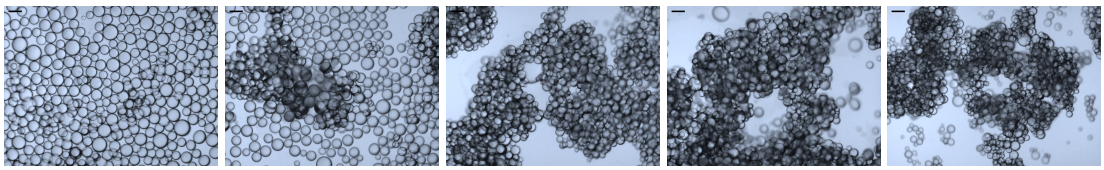

Figure 4.20 *Micrographs of emulsions stabilised by Stöber silica at different* pH *values, where the* pH *has been changed prior to emulsification. The samples are shown immediately following emulsification and the sample* pH *values are, from left to right,* 4.5, 6, 7, 8.5 *and* 10. *In all of the samples* $\phi_p = 1.1\%$, $\phi_o = 20\%$ *and* $\Phi_{IM} = 10\%$. *The scale bars are* 100 μm.

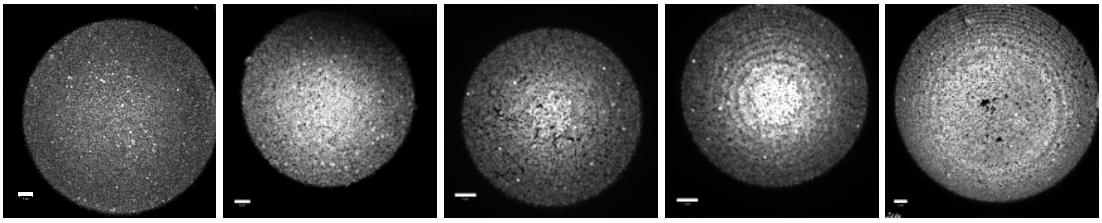

Figure 4.21 *Confocal micrographs of Pickering emulsions stabilised by Stöber silica at a series of* pH *values, where the* pH *has been changed prior to emulsification. The* pH *values are* 4.5, 6, 7, 8.5 *and* 10, *from left to right. The images are z-projections with z-spacings of* 0.9 μm, *constructed using ImageJ. The scale bars are* 5 μm.

covered at all pH values.

The samples shown in Fig. 4.19 were then placed on a roller bank. Figure 4.22 shows the samples after 6 h of rolling, and it is clear that the samples with pH values of 4.5 and 6 have undergone coalescence, with free silica also appearing in the aqueous phase, and that the samples with pH 7-10 have deaggregated. Figure 4.23 shows micrographs of these emulsions.

Post-emulsification When the pH was adjusted following emulsification, few differences were observed in the emulsions compared to the pre-emulsification samples, except at pH 3, the lowest pH studied here. In this case, the emulsion immediately destabilises, yielding droplets which are large enough to be visible with the naked eye and releasing a large amount of free silica into the aqueous phase, as can be seen in the photograph in Fig. 4.24. Micrographs of these samples are shown in Fig. 4.25, and confocal micrographs are shown in Fig. 4.26. After being placed on a roller bank for approximately 20 h, the pH 3 and pH 4.5 samples had destabilised completely. That the pH 3 sample is so unstable suggests that the high positive zeta potential of the particles (see Fig. 3.9 (right))

Figure 4.22 *Photograph of emulsions stabilised by Stöber silica at a series of* pH *values, where the* pH *was changed prior to emulsification and the samples have been rolled for* 6 *h. The* pH *values of the samples are, from left to right,* 3, 4.5, 6, 7, 8.5 *and* 10. *In all of the samples* $\phi_p = 1.1\%$, $\phi_o = 20\%$ *and* $\Phi_{IM} = 10\%$.

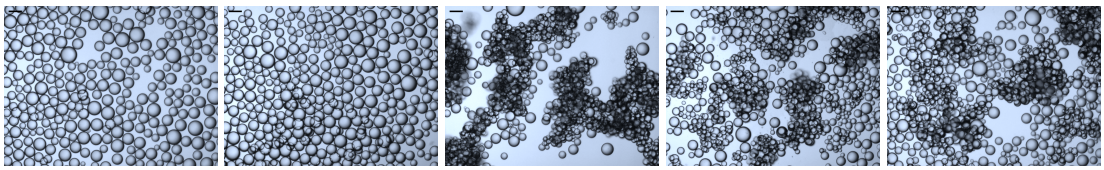

Figure 4.23 *Micrographs of emulsions stabilised by Stöber silica at different* pH *values, where the* pH *has been changed prior to emulsification. The samples have been rolled for* 6 *h and the* pH *values of the samples are, from left to right,* 4.5, 6, 7, 8.5 *and* 10. *In all of the samples* $\phi_p = 1.1\%$, $\phi_o = 20\%$ *and* $\Phi_{IM} = 10\%$. *The scale bars are* 100 μm.

Figure 4.24 *Photograph of emulsions stabilised by Stöber silica at different* pH *values, where the* pH *was adjusted following emulsification. The* pH *values are, from left to right,* 3, 4.5, 6, 7, 8.5 *and* 10.

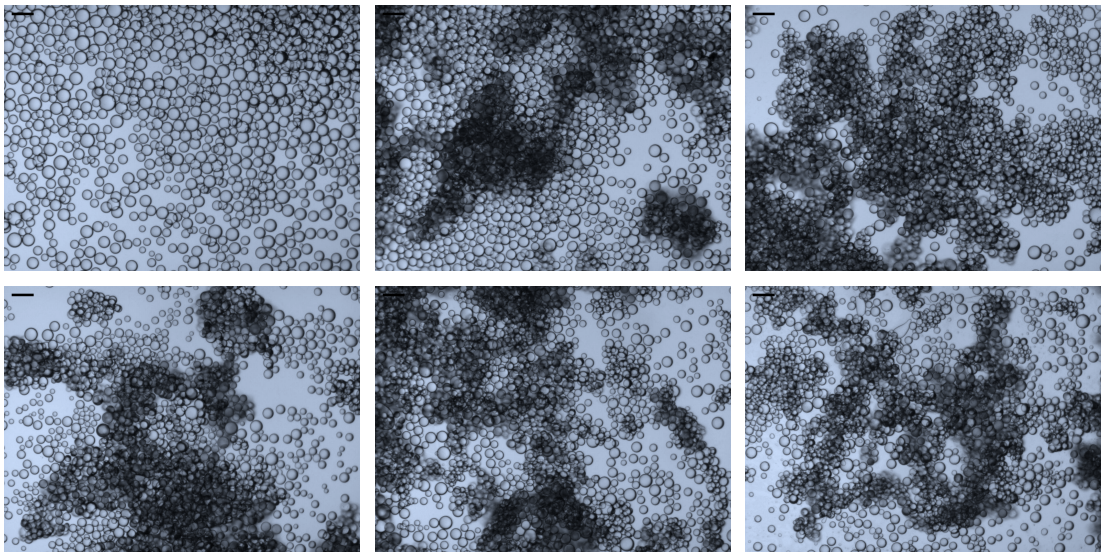

Figure 4.25 *Micrographs of emulsions stabilised by Stöber silica at different* pH *values, where the* pH *was changed following emulsification. The* pH *values of the samples are, from left to right, Top row:* 3, 4.5 *and* 6, *Bottom row:* 7, 8.5 *and* 10. *In all of the samples* $\phi_p = 1.1\%$, $\phi_o = 20\%$ *and* $\Phi_{IM} = 10\%$. *The scale bars are* 100 μm.

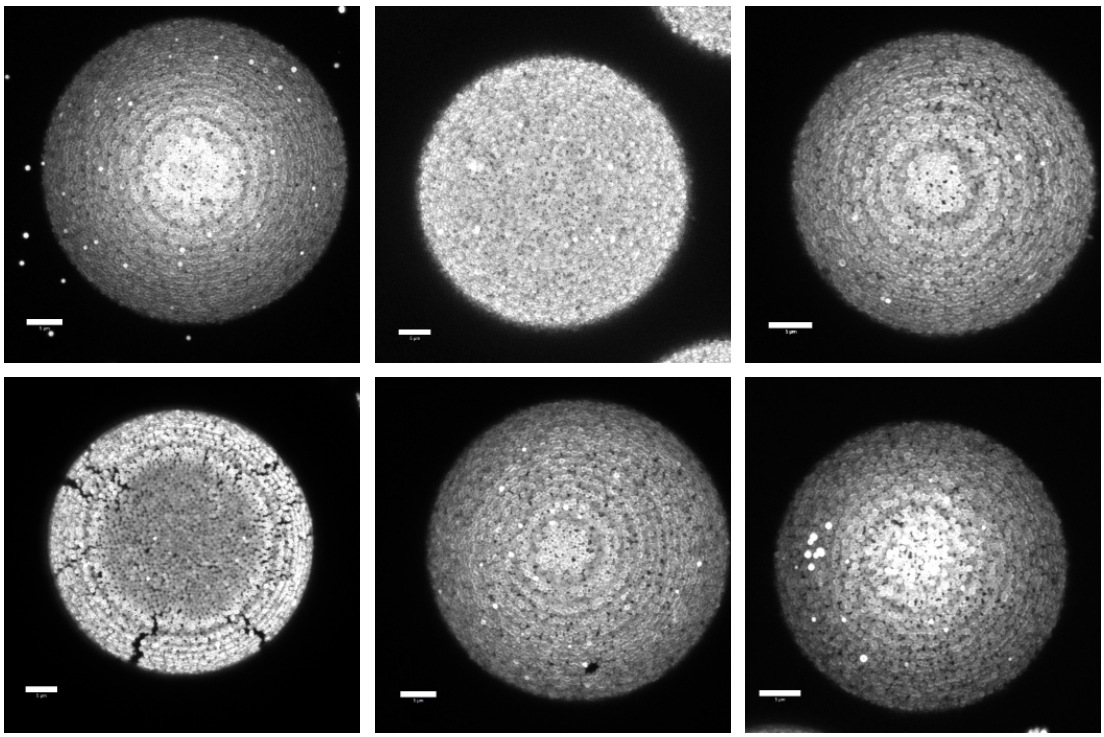

Figure 4.26 *Confocal micrographs of Pickering emulsions stabilised by Stöber silica at various* pH *values, where the* pH *has been changed after emulsification. The* pH *values are, from left to right, Top row:* 3, 4.5 *and* 6*; Bottom row:* 7, 8.5 *and* 10. *The images are z-projections with z-spacings of* 0.9 μm, *constructed using ImageJ. The scale bars are* 5 μm.

here prevents them from adsorbing to the interface and that θ_w will be very low if they do adsorb. However, in the pH 4.5 samples the particles carry only a moderate charge and do initially adsorb to the interface, and it is surprising that they are subsequently removed. It is also interesting that the pH 10 samples, where the particles are also strongly charged, are still very stable. Whilst it may initially be surprising that increasing ζ by means of drying the particles and by decreasing the pH have opposite effects on the emulsion stability, the reason for this is that adjusting the pH also affects the interfacial charge of the droplets, which drying the particles does not.

The samples shown in Fig. 4.24 were also placed on a roller bank. Figure 4.27 shows the samples after 6 h of rolling, and Fig. 4.28 shows the corresponding micrographs. These samples have not destabilised noticeably, despite rolling for a longer time than the samples shown in Fig. 4.23, where the pH values were adjusted prior to emulsification.

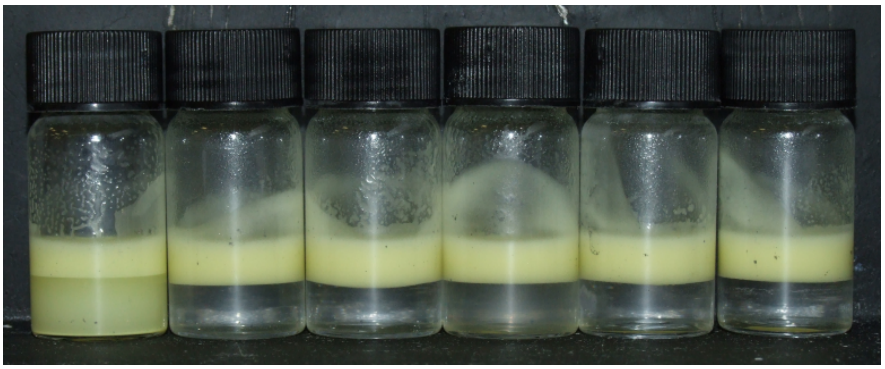

Figure 4.27 *Photograph of emulsions stabilised by Stöber silica at different* pH *values, where the* pH *was modified following emulsification. The samples have been rolled for* 21.5 *h. The* pH *values of the samples are, from left to right,* 3, 4.5, 6, 7, 8.5 *and* 10. *In all of the samples* $\phi_p = 1.1\%$, $\phi_o = 20\%$ *and* $\Phi_{IM} = 10\%$.

The differences between emulsions where the pH has been adjusted prior to and following emulsification show that pH has a greater effect than simply modifying θ_w. The particle-interface interactions during emulsification are highly important, a fact which is missed by oversimplifications such as the necessity for particles to flocculate in order to stabilise a Pickering emulsion.

Discussion: Stöber silica and pH The lack of any significant difference in the behaviour of the emulsions which have had their pH adjusted before or after the

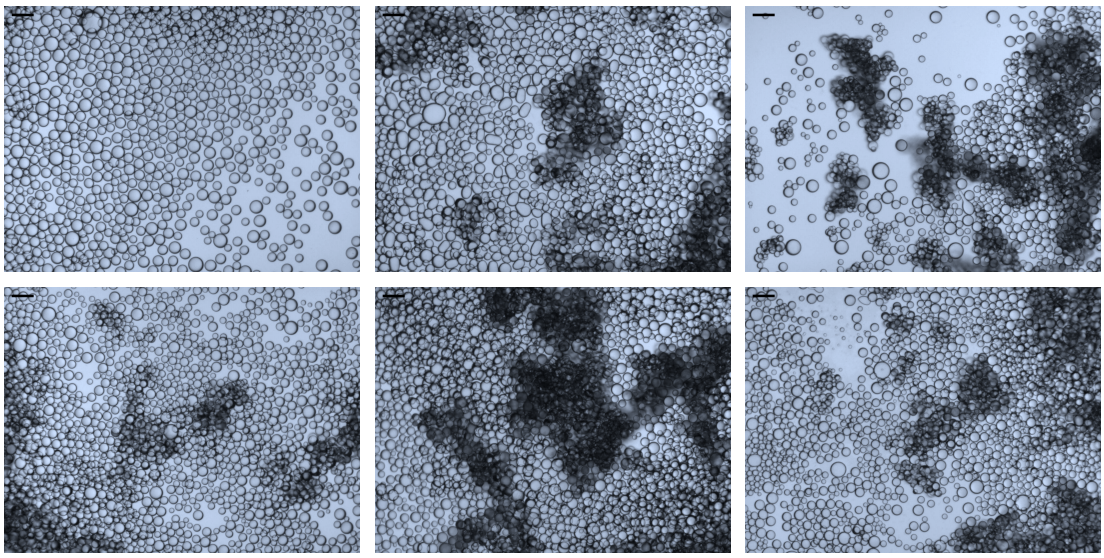

Figure 4.28 *Micrographs of emulsions stabilised by Stöber silica at different* pH *values, where the* pH *has been changed following emulsification. The samples have been rolled for* 6 *h and the* pH *values of the samples are, from left to right, Top row:* 3, 4.5 *and* 6*; Bottom row:* 7, 8.5 *and* 10. *In all of the samples* $\phi_p = 1.1\%$, $\phi_o = 20\%$ *and* $\Phi_{IM} = 10\%$. *The scale bars are* 100 μm.

emulsification process suggests that the particles can freely diffuse rotationally, which would mean that the contact line is not pinned in this system. However, it should be noted that the contact angle of the particles at the interface here is quite low ($\approx 30°$) and that particles with higher contact angles may behave in an entirely different manner.

The lower stability of the samples with acidic aqueous phases, even when the pH is adjusted following emulsification, suggests that the contact angle of the particles in these samples is lower than it is at higher pH values. This might be explained by the fact that charged particles at an interface will repel each other more strongly through the non-polar phase due to the lack of electrostatic screening, and so may tend to sit further into the polar phase.

The degree of aggregation of the particles on a droplet's surface will influence the stability of the emulsion as it is rolled. If a droplet is approximately fully coated and the particles aggregate at the interface then the droplet is less likely to deform and the particles are less likely to leave gaps at the interface which may lead to coalescence [106]. However, this behaviour contradicts the observed behaviour, which is that samples with pH $\approx$ 4-5, where the particles have the lowest $|\zeta|$ and so are most liable to aggregate, are less stable than samples where the particles

have a high negative charge. It therefore seems likely that the contact angle of the particles is lower when the aqueous phase is acidic, which can be attributed to the high charge of the particles causing them to sit further into the aqueous phase, and is in agreement with both theoretical predictions and previous experimental results [89].

4.3.3.2 Fumed silica

The effect of varying the pH on oil-in-water emulsions stabilised by fumed silica has also been studied, and the results of these experiments will be presented briefly here.

Figure 4.29 shows a series of emulsions stabilised by fumed silica where the pH of the aqueous phase has been adjusted prior to emulsification. The pH values are 3, 4.5, 6, 7, 8.5 and 10. Micrographs of the samples in Fig. 4.29 are shown in Fig. 4.30. The emulsions are indistinguishable, except for the pH 3 sample, where the silica which has not adsorbed to an interface has aggregated and sedimented more quickly than the free silica in the other samples. As seen in Chapter 3, the isoelectric point for the fumed silica is at pH ≈ 3, so this result is not surprising. Rolling the fumed silica samples for 24 h does not effect any noticeable changes in the samples.

Figure 4.29 *Photograph of emulsions stabilised by fumed silica at different* pH *values, where the* pH *was adjusted prior to emulsification. In all of the samples* $\phi_p = 0.15\%$, $\phi_o = 20\%$ *and* $\Phi_{IM} = 10\%$. *The* pH *values of the samples are, from left to right,* 3, 4.5, 6, 7, 8.5 *and* 10.

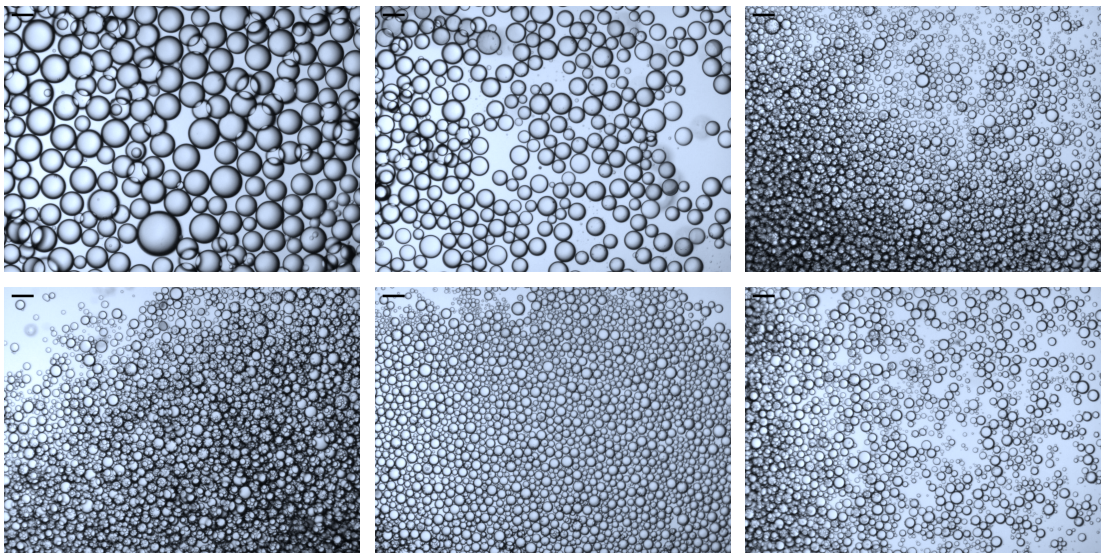

Figure 4.30 *Micrographs of emulsions stabilised by fumed silica at different* pH *values, where the* pH *was changed prior to emulsification. The* pH *values are, from left to right, Top row:* 3, 4.5, 6*; Bottom row:* 7, 8.5 *and* 10. *In all of the samples* $\phi_p = 0.15\%$, $\phi_o = 20\%$ *and* $\Phi_{IM} = 10\%$. *The scale bars are* 100 μm.

4.3.4 Discussion: pH

Adjusting the pH of the aqueous phase of the Pickering emulsions studied here has several effects. At very low pH values, where the Stöber silica has a high positive zeta potential, the emulsions are very unstable and separate completely, as shown in Fig. 4.19. This is attributed to the high charge on the particles, which decreases the contact angle and causes them to repel strongly enough that fully covered interfaces become unstable, so that particles are ejected from the interface. The partially coated droplets which are left are then able to coalesce readily.

The emulsions stabilised by fumed silica become less stable at low pH values, in an apparently similar fashion to those stabilised by Stöber silica. This is not surprising when the zeta potentials of the particle dispersions (shown in Fig. 3.9) and the results of Marinova *et al.* [103] are taken into consideration. An attractive particle-interface interaction is necessary in order to maximise the fraction of particles which adsorb to the oil-water interface. At low pH values, however, the oil-water interface is not charged and so no electrostatic attraction can occur. In the case of Stöber silica, where the particles are strongly charged at pH 3, there will be a repulsive particle-interface interaction due to the image charge, and this

explains why the Stöber silica does not adsorb to the interface at pH 3. At higher pH values there is a strong attraction between the Stöber silica particles and the oil-water interface. This strong attraction occurs because at high pH values the Stöber silica particles are positively charged (see Fig. 3.9 (right) - emulsification is carried out approximately 5 *min* after the particles are added to the water), whilst the oil droplets are negatively charged. Additionally, the particles will sit further into the aqueous phase when they are more strongly charged and these factors explain the high stability of the emulsions at high pH.

The optimal pH for emulsification will naturally depend on several factors, but it is clearly desirable for there to be an attractive force between the particles and the oil-water interface, and this can be achieved by using positively charged particles at a high pH, so that the interface is negatively charged. However, if the particles have a very high positive charge, this effect may be cancelled out by the repulsive image force. If these principles are taken into account, it should be possible to tune the surface chemistry of silica particles to maximise emulsion stability.

4.4 Conclusions and future work

This chapter has presented a study into the effects upon the emulsion phase behaviour of altering the phase behaviour of the particle dispersion used to create oil-in-water Pickering emulsions stabilised by silica. The particle phase behaviour was altered by the addition of a salt, either sodium chloride or sodium iodide, or by adjusting the pH using either hydrochloric acid or sodium hydroxide. The effects these alterations have on the particle phase behaviour was described in Chapter 3.

It has been shown that, in contrast to many statements found in the Pickering emulsions literature [38–43], it is not necessary to use flocculating particles to stabilise a Pickering emulsion. In fact, weakly flocculating particles may even lower the emulsion's stability significantly. This behaviour has been attributed to the particles' surface chemistry. For a full picture of Pickering stabilisation it is necessary to consider various other factors than the particle flocculation, including the particle-interface interactions, the contact angle and the coalescence rate of the droplets as well as the manner in which the particle-particle interactions are affected by the particles being at the interface.

Aqueous phases containing sodium iodide are observed to lead to more stable emulsions than aqueous phases containing sodium chloride, when Stöber silica is used as the emulsion stabiliser. The adsorption of ions at the particle interface is thought to play a rôle in this, but the higher refractive index of sodium iodide solutions may also have an effect.

Unlike in the case of Stöber silica, but in agreement with previous results which have been published by Binks and Lumsdon [43], emulsions stabilised by fumed silica pass through a minimum in stability as the sodium chloride concentration is increased. Due to the fluorescent dye incorporated into the Stöber silica particles, the ion adsorption behaviour at their interface will likely be different from the fumed silica case, and this may explain the observed differences in behaviour between the sets of emulsions.

Differences in behaviour are observed between samples where the sample pH is adjusted prior to or following emulsification. This shows that the pH during emulsification is important, and will affect not only the contact angle of the particles, but the likelihood of the particles adsorbing to the interface during shear.

The enormous variation in emulsion phase behaviour which can be achieved by modifying the surface chemistry of the particles, the salt concentration and the pH highlights once again one of the major advantages of Pickering emulsions - the emulsion phase behaviour can be tuned by tuning the particle phase behaviour. By understanding the coupling between particle and emulsion phase behaviour, it should also be possible to optimise the surface chemistry of particles for specific applications.

Fundamentally, it is an oversimplification to state that flocculating particles are necessary to generate a stable emulsion. The particle-particle interactions are less important than the particle-interface interactions and, whilst aggregating particles may be an indication that the particles will be attracted to the interface, there is a wealth of other aspects at play here which must be considered.

Of great interest in the future will be theoretical and experimental work which further elucidates the relationships between particle phase behaviour in the bulk and the behaviour at an oil-water interface, and builds on the work of Horozov *et al.* [107] and Law *et al.* [108]. This, coupled with research into how the particle interactions at the interface affect the emulsion behaviour will hopefully allow for a far greater understanding of Pickering emulsions to develop. This work would

require a more reliable method of measuring the particle contact angle than has been used here, although such methods may well exist already [70, 72].

It is possible to synthesise Stöber silica particles without dye but with APS still incorporated, and also particles with a fluorescent core surrounded by a non-fluorescent shell which lacks APS. The use of such particles may provide useful insight into the particular effects of changing the particle surface chemistry.

From Eq. (1.3) it can be seen that the energy required to remove a particle which has adsorbed to an oil-water interface has a maximum when the contact angle is 90°. This has led researchers to attempt to tune the particle surface chemistry to obtain neutral wetting. However, it can also be seen that, simply by using larger particles, the trapping energy can be very large even when the contact angle is small. For example, a particle with a diameter of 1 μm and a contact angle of 30° will have a trapping energy of $\approx 10^4\ k_B T$. Therefore, by using larger, non-neutrally wetting particles, stable emulsions can be generated from highly stable particle dispersions and hence reduce the amount of energy needed to disperse the particles. This has the disadvantage of requiring a larger mass of stabiliser, but the use of non-spherical particles, such as clay, may overcome this.

The pH and salt concentration of the aqueous phase both clearly have an effect on the likelihood of particles adsorbing to the oil-water interface. However, the combined effects of varying the pH and the salt concentration have not been studied here, and interesting work could be carried out by doing so. For example, although increasing the particle charge by lowering the pH causes the particles to be less likely to adsorb at the oil-water interface due to the repulsive image charges, adding salt will screen the repulsions and increase the probability of the particles adsorbing to the interface.

Chapter 5

Bridging in Pickering emulsions

5.1 Introduction

As described in Chapter 1, solid particles that exhibit partial wettability with two fluid phases reduce the free energy of the interface between these two fluids, and can become kinetically trapped at the interface. It is therefore possible to create an emulsion stabilised solely by solid particles, where each droplet is coated with a layer of particles [7]. However, if the particles protrude further into the continuous phase than they do into the dispersed phase then it is possible for a particle to be adsorbed at two fluid-fluid interfaces simultaneously, a situation referred to as bridging [28, 110] and shown schematically in Fig. 5.1 (top row).

The potential for particles to form bridges in an emulsion was apparently first identified by Denkov *et al.* [111]. It has since been shown that particle bridging can increase the stability of an emulsion and hence be desirable in some cases [112]. However, bridging will sometimes be undesirable as creaming rates will be enhanced, due to the increase in the effective droplet size and possible formation of a network, and the emulsion may flow poorly. The microstructure of bridged Pickering emulsions has previously been studied using confocal microscopy by Lee *et al.* [113]. Xu *et al.* have demonstrated that bridging can occur when particles on opposing interfaces interlock as they come together, but also that the bridging particles can initially all come from one interface [114]. Work has also recently been done on bridging in immiscible polymer blends. Moghimi *et al.* have shown that the presence of bridging particles significantly alters the rheology of their

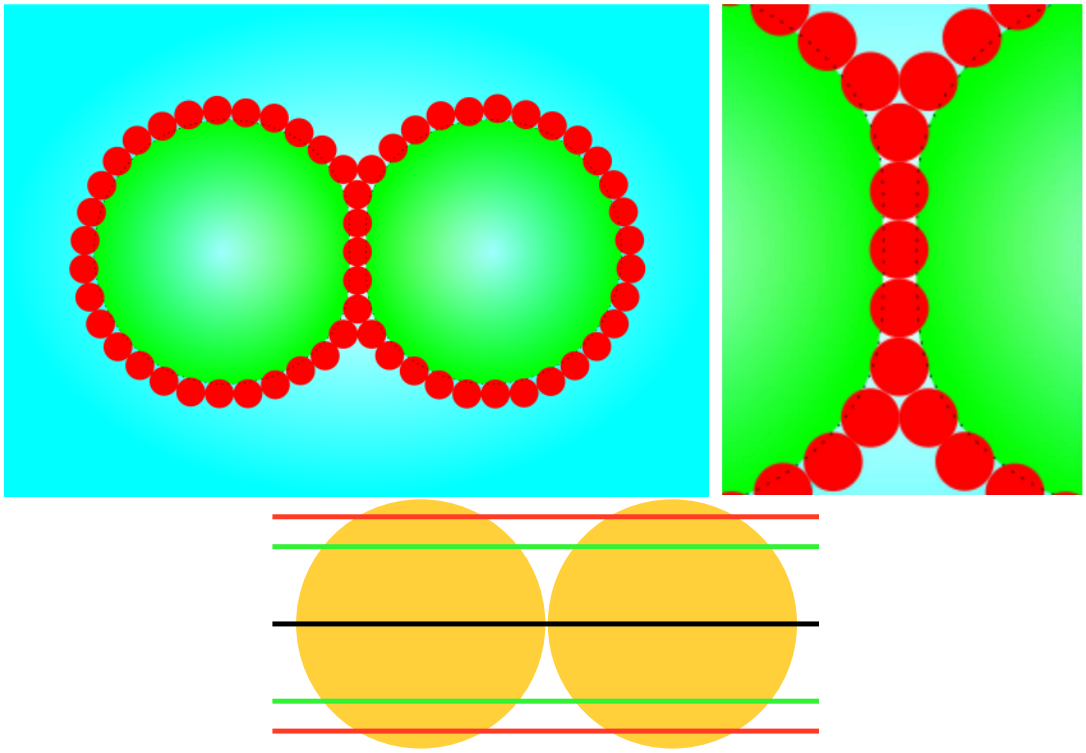

Figure 5.1 *Top left: Cartoon showing two oil droplets bridged by particles; Top right: Enlarged section, showing the layer of water between the two droplets; Bottom: If the contact angle is close to, or above,* 90° *then bridging cannot occur (black line), whilst if it is too small then the particle attachment energy will be too low to maintain stability (red lines). Instead, an intermediate contact angle is required (green lines).*

emulsions, and inhibits flow-induced coalescence [115]. Nagarkar and Velankar have also shown that particle bridges can occur in immiscible polymer blends and lend the blends a solid-like rheology [116]. Destribats *et al.* have investigated the bridging behaviour of emulsions stabilised by soft microgel particles and found that the emulsion's flocculation behaviour is highly dependent on the nature of the particle interactions during the emulsification process [117]. Particle bridging in Pickering systems where one of the fluid phases is an ionic liquid has been studied by Frost *et al.*, who observed clusters of droplets held together by monolayers of particles [118, 119].

Whether desirable or undesirable, it is important to understand the mechanisms involved in creating bridged emulsions, and how to choose system parameters to obtain the desired emulsion characteristics. Therefore various methods of both creating and breaking up droplet aggregates, and the ways these are affected by

system parameters, have been studied, and the results of these experiments will be presented in this chapter. Light scattering and microscopy have been used to study the degree to which emulsions are bridged, and how this is affected by parameters including particle volume fraction, particle wettability and shear rate. Freeze fracture scanning electron microscopy (FFSEM) has been used to look for direct evidence of droplets sharing particles.

In the rest of this chapter some necessary quantitative considerations and the necessary experimental methods which were not covered in Chapter 2 will be described briefly, before experimental results are described in three broad themes: how particle bridges are formed, how particle bridges can be removed from an emulsion and the differences in rheological behaviour between bridged and non-bridged emulsions. These experimental results are used to develop a theoretical understanding of particle bridging based on collisions between partially coated droplets.

5.1.1 Quantitative considerations

In order for particle bridging to occur in oil-in-water emulsions, the particles must have a contact angle of less than 90°, otherwise the two droplets would overlap and coalesce. Bridging will also only occur between partially coated droplets, as fully coated droplets are mechanically stable to coalescence. Shearing of an already emulsified sample will create extra oil-water interface, whilst coalescence between partially coated droplets can reduce the amount of oil-water interface until the droplets are fully coated. Particles on one partially coated droplet can also adsorb to another, also reducing the amount of oil-water interface. Figure 5.1 (bottom) depicts the sensitivity of particle bridging to the contact angle.

In order to achieve collisions between partially coated droplets, the interfacial area generated by shear must be greater than the total cross-sectional area of the particles in the sample. Equation (1.7), Eq. (1.11) and Eq. (1.14) can be used to find the parameters at which this will occur.

The degree of aggregation of droplets in an oil-in-water emulsion can be quantified using the fraction of water resolved, f_w, which is given by:

$$f_w = \frac{h_w}{h_t \phi_w}, \tag{5.1}$$

where h_w is the height of the resolved water, h_t is the total height of the sample and ϕ_w is the volume fraction of water in the sample. Larger f_w values indicate that the emulsion droplets have packed more densely, a process which is hindered by droplet aggregation. For random close packing of monodisperse droplets in a sample with $\phi_o = 0.2$, the expected value is $f_w = 0.85$. Polydispersity will tend to increase packing efficiency (and hence increase f_w). Meniscus effects are ignored here, but will not vary greatly between samples. Similarly, the degree of aggregation can also be quantified using the oil volume fraction of the emulsion (excluding the resolved water), ϕ'_o, which is given by:

$$\phi'_o = \frac{\phi_o h_t}{h_t - h_w} = \frac{\phi_o}{1 - f_w \phi_w}. \tag{5.2}$$

5.2 Methods and materials

The methods which are particular to this chapter will be discussed in this section. Methodology for techniques which are used in this chapter and in other chapters can be found in Chapter 2.

5.2.1 Sample preparation

Oil-in-water emulsions stabilised by fluorescent Stöber silica were prepared by mixing the oil phase with a dispersion of the particles, and shearing the sample using a vortex mixer, as described in Chapter 2.

In most cases, several minutes of vortex mixing are required for all the particles to adsorb to an oil-water interface, but at lower particle volume fractions ($\lesssim 0.75\%$) the process can be completed in 15 s. The volume fraction, Φ_{IM}, of isopropyl myristate in the oil phase is used to control particle wettability [81]. The oil volume fraction was 20%. Subsequent shearing of samples was carried out using the Kinematica Polytron at shear rates between 8 000 s^{-1} and 34 000 s^{-1}. All experiments were carried out at room temperature.

In order to modify the inter-particle electrostatic interactions, sodium chloride was added to some silica dispersions. Glycerol was added in order to modify the van der Waals interactions and the viscosity of the aqueous phase. Hydrochloric acid and sodium hydroxide were added to samples to adjust their pH.

5.2.2 Electron microscopy

Samples for freeze-fracture scanning electron microscopy (FFSEM) were mounted in copper chalices which were used to fracture the samples. A copper collar was placed on a chalice and then the emulsion was added to the chalice using a pipette until the meniscus protruded above the collar. Liquid nitrogen was used to freeze the sample in a Gatan Alto 2500 cryotransfer system and the sample was then transferred to the preparation chamber which was at -124℃ and under high vacuum. Sample fracture was carried out by knocking the copper collar off the chalice with a cooled scalpel blade within the preparation chamber. The sample was then heated to -96℃ for 2 min in order to allow ice to sublime. Following sublimation, the sample was again cooled to -124℃ and sputter coated with $\approx$ 6 nm platinum. The sample was then transferred to a Gatan cold stage in a Hitachi S-4700 field emission scanning electron microscope, where it was maintained at -124℃. The sample was observed using an accelerating voltage of 5.0 kV at a working distance of 5 mm using both upper and lower secondary electron detectors.

5.2.3 Tensiometry

Figure 5.2 shows how the oil-water interfacial tension depends on the oil phase's isopropyl myristate content. These experiments were conducted without adding salt to the aqueous phase and using pure deionised water (pH $\approx$ 6.5).

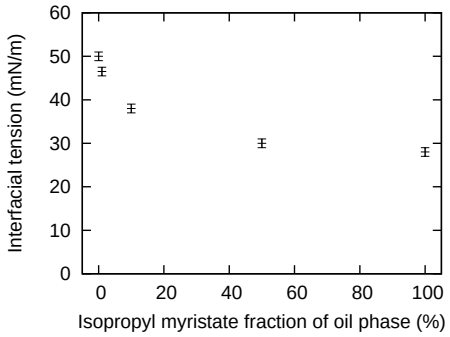

Figure 5.2 *Dependence of the oil-water interfacial tension on* Φ_{IM}.

5.2.4 Rheology

A TA Instruments Discovery HR2 rheometer was used to measure the viscoelastic properties of both bridged and non-bridged emulsions. The experiments were performed using a plate-plate geometry with a sandblasted aluminium bottom plate and a hatched steel top plate with a diameter of 4 cm. The temperature of each sample was maintained at 20℃ throughout the experiments. Strain sweeps were performed with an oscillation frequency of 1 Hz. Measurements were made at strains of 0.01% to 1000%, in logarithmic steps with ten measurements per decade. Samples used for rheological experiments were prepared as described in Section 2.3.1, but with the sample volume increased from 3 mL to 4.5 mL, so that there was enough of each sample to perform two experiments, the results of which were averaged. The initial sample was split into two, and then poured gently from the vial onto the bottom aluminium bottom plate, the top plate was then gently lowered until the gap height was 1.05 mm. Excess water was then removed from the outside of the geometry using a paper towel before the gap height was lowered to 1.00 mm.

5.3 Results and discussion

First, the effects that shear rate, particle volume fraction and particle wettability have on droplet aggregation will be described. These effects are explained in terms of the interfacial area generated during shear, with reference to Eq. (1.9) and Eq. (1.11). Next, the effects of more complex shear histories on samples will be discussed, and it will be shown that the bridged system can be destabilised by adjusting the pH, or by adding small quantities of sodium chloride or glycerol. Finally, some rheological data comparing bridged and non-bridged emulsions will be presented.

5.3.1 Bridge formation

5.3.1.1 Shear rate

As shown in Fig. 5.3, a decrease in emulsion packing fraction is observed when the shear rate is increased, together with an increase in the roughness of the

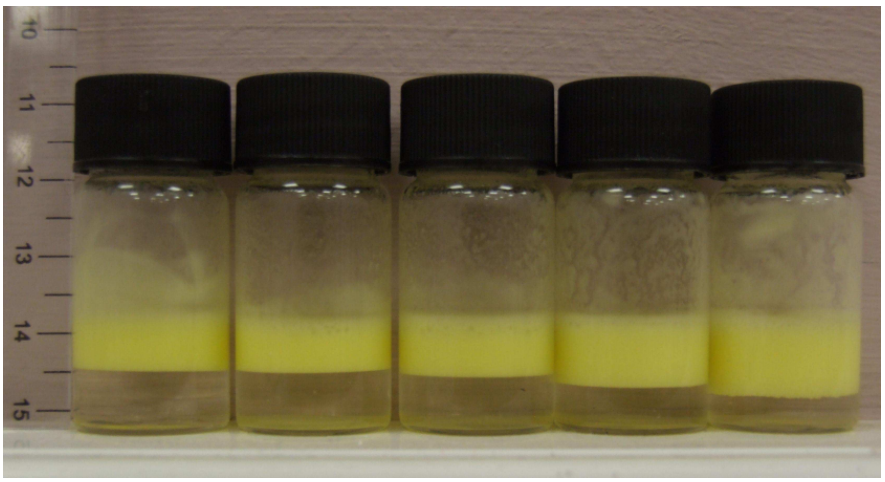

Figure 5.3 *Increasing the shear rate causes a decrease in the emulsion packing fraction. The shear rates are, from left to right, vortex mixer only,* $8\,500\ s^{-1}$, $17\,000\ s^{-1}$, $25\,500\ s^{-1}$ *and* $34\,000\ s^{-1}$. *In each sample,* $\phi_o = 20\%$, $\phi_p = 1.7\%$ *and* $\Phi_{IM} = 10\%$. *The samples were left to settle overnight before being photographed.*

emulsion-resolved water interface. The non-aggregating emulsions formed at low shear rates are reasonably monodisperse (CV≈25%) and have smooth emulsion-resolved water interfaces. The corresponding bright-field micrographs, shown in Fig. 5.4, show that this is because the emulsions' propensity to aggregate increases with shear rate.

The samples shown in Fig. 5.3 were prepared with $\phi_p = 1.7\%$ and $\Phi_{IM} = 10\%$ and then pre-emulsified using a vortex mixer, creating moderately aggregating emulsions with a primary droplet size of $\approx 30\ \mu m$. This droplet size is slightly lower than that predicted by Eq. (1.7), due to droplets sharing particles and a surface coverage which is lower than the theoretical maximum of close-packed spheres. A micrograph of a pre-emulsified sample is shown in Fig. 5.5 (left). These samples were then subjected to a variety of shear rates using a rotor-stator device. Low shear rates ($\approx 8\,500\ s^{-1}$) create smooth, non-aggregating emulsions whilst progressively higher shear rates create increasingly flocculated networks of droplets, as shown in the micrographs in Fig. 5.4 (a-d). This aggregation causes a decrease in the packing efficiency of the emulsion, as shown in Fig. 5.5 (right). Even at the lowest shear rate f_w is only 0.65, notably lower than the value of 0.85 expected for random close packing - even without aggregation effects the samples do not pack closely.

As can be seen from Eq. (1.9) and Eq. (1.11), increasing the shear rate will lower

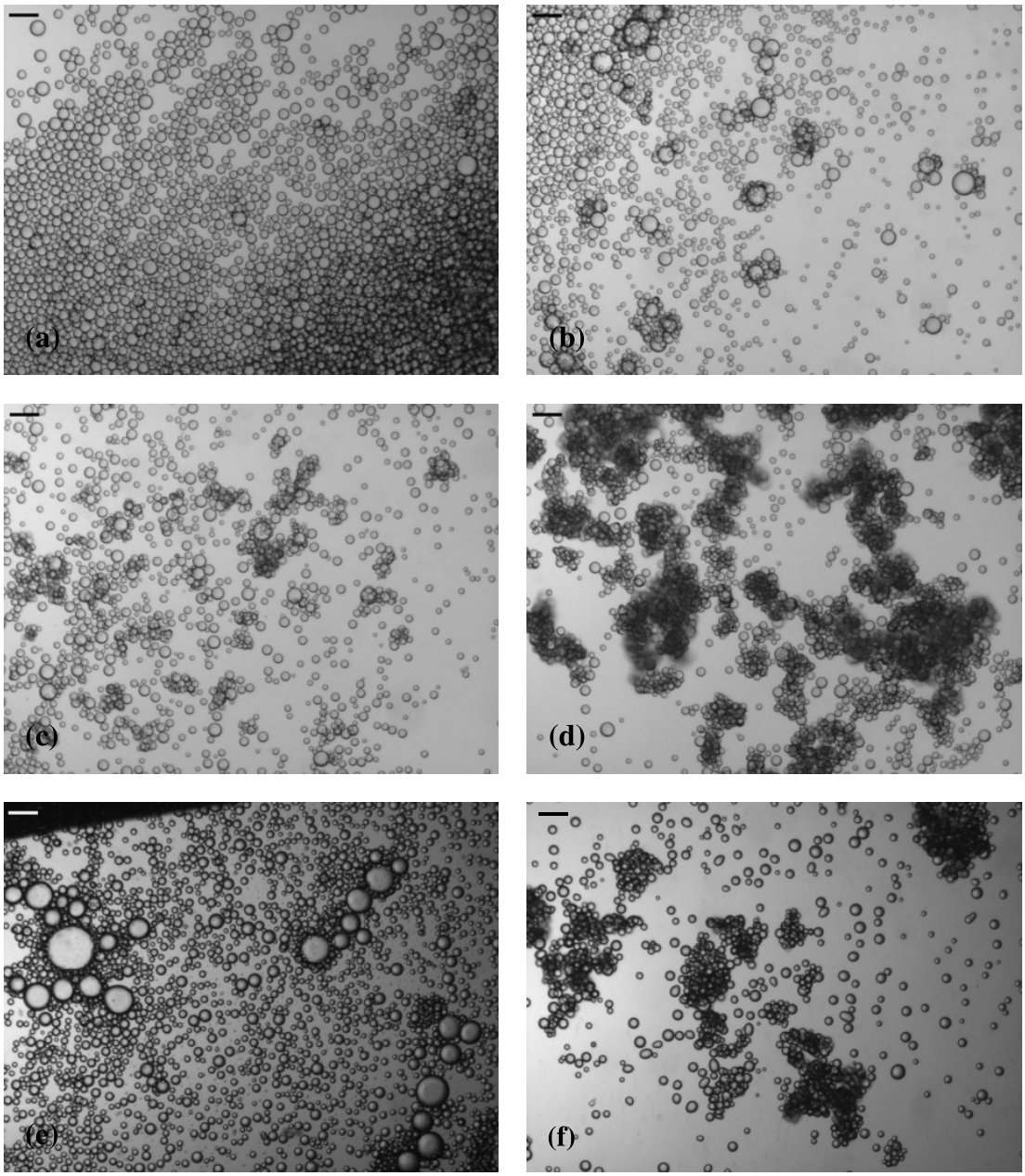

Figure 5.4 *Micrographs of the samples from Fig. 5.3. The shear rates are: (a)* $8\,500\ s^{-1}$*, (b)* $17\,000\ s^{-1}$*, (c)* $25\,500\ s^{-1}$*, (d)* $34\,000\ s^{-1}$*. (e) The same sample as in (d), following further shear at* $8\,500\ s^{-1}$*. (f) The same sample as in (a), following further shear at* $34\,000\ s^{-1}$*. The scale bars are* $100\ \mu m$*.*

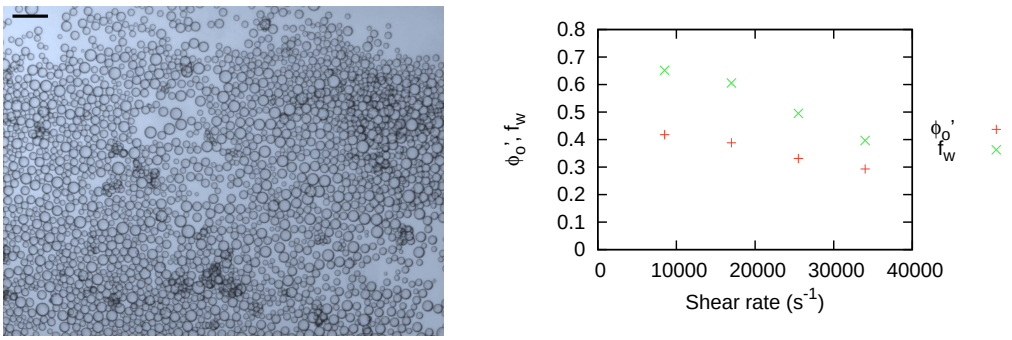

Figure 5.5 *Left: Micrograph of a pre-emulsified sample prepared using a vortex mixer. The scale bar is* 100 μm. *In this sample* $\phi_o = 20\%$, $\phi_p = 1.7\%$ *and* $\Phi_{IM} = 10\%$*; Right: Increasing shear rate causes a decrease in emulsion packing fraction. For the vortex mixed sample,* $f_w = 0.67$ *and* $\phi_o' = 0.43$. *In all samples,* $\phi_o = 20\%$, $\phi_p = 1.7\%$ *and* $\Phi_{IM} = 10\%$.

the droplet radius. This means that at higher shear rates, there will be a greater amount of interfacial area exposed, and so a greater number of collisions between partially coated droplets will take place. Since it is these collisions which lead to particle bridging, the degree of aggregation increases when shear rate is increased.

Using Eq. (1.15), it is found that $Re \gtrsim 1000$ when $\dot{\gamma} \gtrsim 12\,500\ s^{-1}$. Equation (1.7), Eq. (1.11) and Eq. (1.14) have therefore been used to estimate the shear rate at which the interfacial area generated during shear will be greater than that which can be stabilised by the particles during this experiment. The critical shear rate for these parameters, and using a value of 0.86 for C, is found to be $\approx 17\,500\ s^{-1}$, which compares very well with the observed onset of aggregation at $\approx 17\,000\ s^{-1}$.

5.3.1.2 Electron microscopy

FFSEM was used to look directly for particles bridging droplets. Samples were prepared with particle volume fractions of 0.6%, 1.1% and 1.7%, and with $\Phi_{IM} = 10\%$. The electron micrographs, shown in Fig. 5.6, clearly show particles being shared by droplets and that this behaviour is more prevalent at lower particle volume fractions, an observation which will be explained below.

Analysis of the patterns left in the droplets where the particle layer has been ripped off during fracture show that $\theta_w \approx 30°$. It is possible, however, that differences in freezing rates and expansivities between the two liquid phases will affect this.

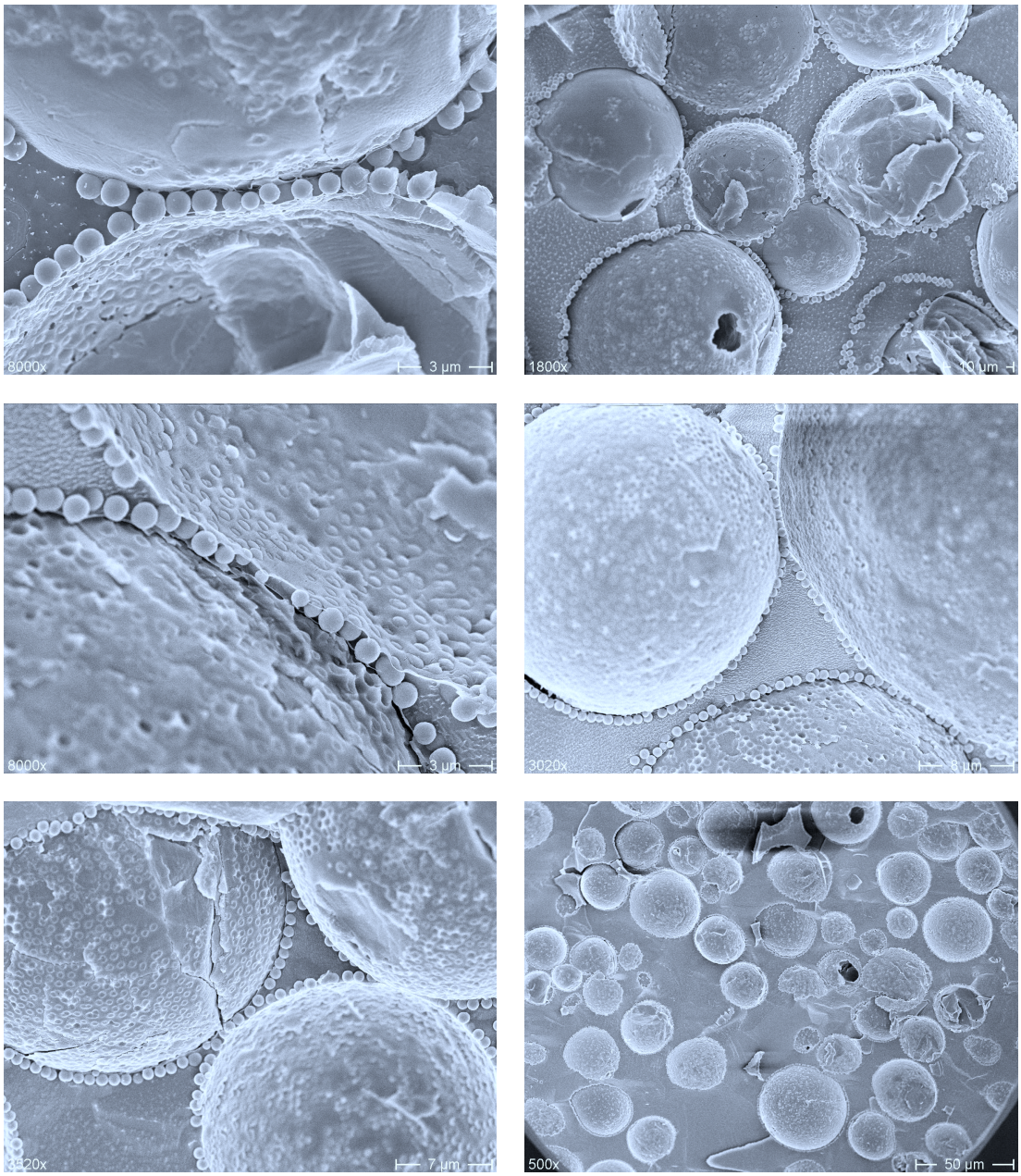

Figure 5.6 *FFSEM images of silica particles being shared by two droplets. The particle volume fractions are:* 0.6% *(top row),* 1.1% *(middle row) and* 1.7% *(bottom row). All samples had* $\phi_o = 20\%$, $\Phi_{IM} = 10\%$ *and were sheared at* $34\,000\ s^{-1}$. *The bottom left image shows that bridging is occurring when* $\phi_p = 1.7\%$, *although the bottom right image shows that the prevalence of particle bridges is reduced at this particle volume fraction.*

5.3.1.3 Particle wettability

It is found that increasing the volume fraction of isopropyl myristate in the oil phase makes particles more likely to adsorb to the interface. When $\phi_p \gtrsim 1.0\%$ and $\Phi_{IM} = 0\%$ it is impossible to sequester all the particles to an oil-water interface using only a vortex mixer, even after 5 *min* of mixing, but if $\Phi_{IM} \gtrsim 10\%$ the sample can be fully emulsified in less than a minute. This can be seen in Fig. 5.7, where it is only at higher isopropyl myristate volume fractions that the resolved water becomes fully depleted of particles. This behaviour is attributed to the lower interfacial tension of isopropyl myristate with water, relative to that of dodecane with water (see Fig. 5.2), as well as its higher dielectric constant. These changes mean that a particular shear rate will generate more interfacial area when isopropyl myristate is included, since the interfacial area is inversely proportional to σ_{ow} when the flow is laminar (Eq. (1.10)), and proportional to $\sigma_{ow}^{-3/5}$ when the flow is turbulent (Eq. (1.12)). Additionally, there will be an increased particle-interface attraction, due to the lower repulsion from the image charge. It is also found that increasing Φ_{IM} increases an emulsion's degree of aggregation, as shown by the reduction in creaming at higher values of Φ_{IM} in Fig. 5.7.

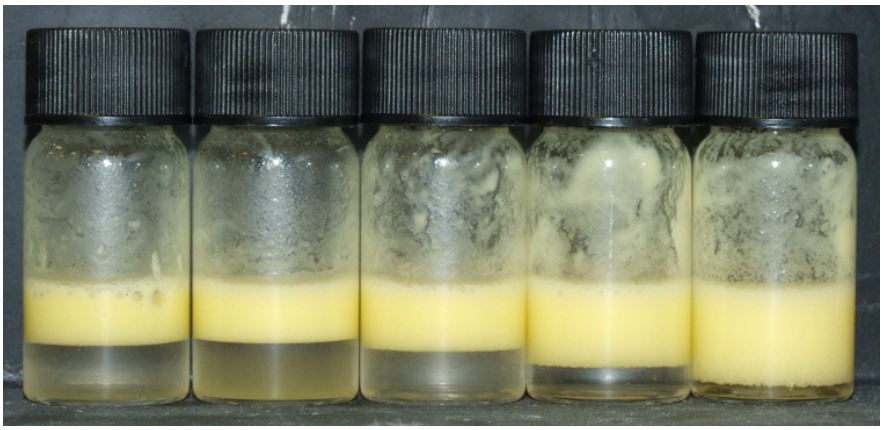

Figure 5.7 *Photograph of emulsions with various values of Φ_{IM}. Increasing particle wettability by the dispersed phase (left to right) causes a decrease in emulsion packing fraction. Φ_{IM} values are 0%, 1%, 10%, 50% and 100%. ϕ_o and ϕ_p are 20% and 1.7% respectively. The samples were sheared at 17 000 s^{-1} for 8 min. The samples were left to settle for 1 h before being photographed.*

The propensity of an emulsion to aggregate via particle bridging will be affected by the three-phase contact angle. If the particles are neutrally wetting ($\theta_w = 90°$) or preferentially wetted by the dispersed phase then it will be impossible for a

particle to be shared between two droplets. On the other hand, if the contact angle is too small, then the attachment energy of the particle decreases and the emulsion becomes unstable. At intermediate contact angles, $\theta_w \approx$ 30-70°, particle bridging should be possible. Increasing Φ_{IM} increases the contact angle of the particles at the interface, and this will affect particle bridging.

Variations in Φ_{IM} therefore affect both the contact angle and the interfacial tension, as well as the particle-interface interactions. Whilst all of these effects, and others, will contribute to the observed changes in particle bridging when Φ_{IM} is varied, it is believed that the most important aspect is the lowering of the interfacial tension, as this leads to a large increase in the number of droplets in the emulsion during the shearing process, and hence increases the number of collisions between partially coated droplets. The other changes, such as contact angle, will be secondary effects to this.

5.3.1.4 Droplet size distribution

The aggregating nature of the emulsions can also be demonstrated using the apparent droplet size, as measured using light scattering. Figure 5.8 shows that the apparent droplet size increases as shear rate is increased. This is because the light scattering apparatus is measuring the size of clusters of aggregated droplets, rather than the primary droplet sizes. It is also interesting to note that the primary droplet size, which can be approximated by the left hand peak on each graph, is roughly unchanged, *i.e.,* aggregation occurs without significant changes in the primary droplet size, which is determined by the particle volume fraction and shear rate.

5.3.1.5 Particle volume fraction

It has been found that increasing ϕ_p lowers an emulsion's propensity to aggregate, for a given shear rate, as shown in Fig. 5.9. The emulsion-resolved water interfaces in the samples with lower ϕ_p values are rough because these samples contain clusters of aggregated droplets, held together by particle bridges. The smoother emulsion-resolved water interfaces in the samples with higher ϕ_p values show that these samples contain significantly fewer particle bridges. The interfacial area during shear is determined by Eq. (1.10) or Eq. (1.12), and the proportion of this area which is covered by particles is determined by ϕ_p. If the interfacial

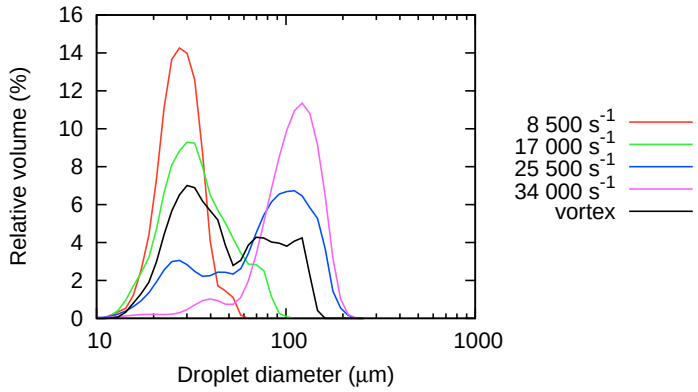

Figure 5.8 *Apparent droplet sizes, measured using light scattering, as a function of shear rate. The emulsions were prepared with* $\phi_o = 20\%$, $\phi_p = 1.7\%$ *and* $\Phi_{IM} = 10\%$.

area exceeds that which can be occupied by particles, then collisions between partially coated droplets will occur, and lead to particle bridging.

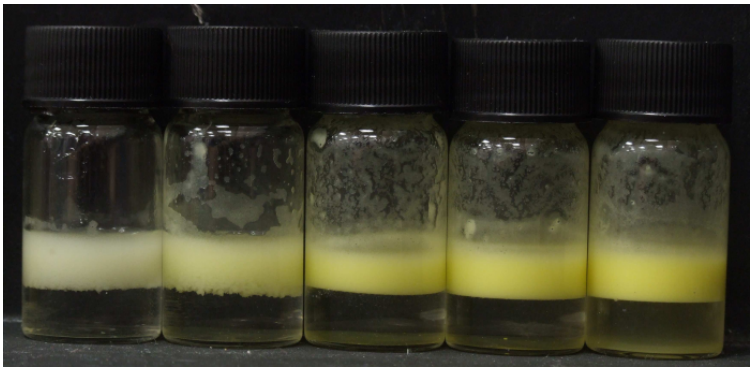

Figure 5.9 *Increasing* ϕ_p *leads to the formation of emulsions which are more densely packed. Particle volume fractions are* 0.3%, 0.6%, 1.1%, 1.7% *and* 2.3%, *from left to right. In all samples,* $\phi_o = 20\%$ *and* $\Phi_{IM} = 10\%$. *All samples were sheared at* 17 000 s^{-1} *for* 8 *min. The samples were left to cream overnight before being photographed.*

When using an oil phase with $\Phi_{IM} = 10\%$ and a particle volume fraction below 1.25%, it is observed that the entire emulsion creams rapidly, suggesting that the vast majority of droplets have formed aggregates. When ϕ_p is 1.25% or greater, however, a single emulsion is observed to have two populations of droplets creaming at different rates: there is a rapidly creaming portion comprised of aggregated droplets and a slowly creaming portion comprised of non-aggregated droplets. This suggests that the population of slowly creaming droplets are those

which quickly become fully coated with particles during emulsification.

The presence of free silica in a sample will also inhibit particle bridging. This can be seen when a sample with $\phi_p = 1.1\%$ is emulsified with a vortex mixer. Following initial mixing for 30 s a smooth emulsion is formed, but not all particles adsorb to a droplet interface. Further bursts of emulsification create increasingly aggregated emulsions with increasingly clear resolved water phases. This shows that free silica can prevent droplet aggregation from occurring between partially coated droplets, because the free silica will lower the rate of collisions between partially coated droplets by adsorbing to areas of bare interface before a droplet can do so.

Particle bridging relies on collisions occurring between partially coated droplets, and so bridging will only occur below a critical particle volume fraction, which will depend on the shear rate. Above this critical particle volume fraction, the applied shear will not create enough bare interface for a significant number of collisions to occur between partially coated droplets, as all collisions will be taking place between fully coated droplets. Using Eq. (1.7), Eq. (1.11) and Eq. (1.14), it is found that the critical particle volume fraction in this case, and using a value of 0.86 for C, is $\approx 1.6\%$, which compares relatively well with the observed onset of aggregation at $\approx 1.1\%$.

These results can be viewed in the context of the wider literature on Pickering emulsions. As outlined in Section 5.1, a small number of researchers have studied bridging in Pickering emulsions. It is thought likely that there are other published results where bridging is likely to play a crucial rôle but where it has not been identified. Furthermore, the sample preparation route is not always sufficiently described to draw any clear conclusion. A case where the preparation protocol is described is Fig. 4 in Ref. [106]. Here, emulsions of PDMS-in-water were prepared under two different shear protocols: one protocol causes dispersed droplets to form whilst the other causes the droplets to form large aggregates which cream rapidly. The sample presented in Fig. 4(b) of Ref. [106] appears to be dominated by particle bridging between droplets. A case where the preparation protocol is not sufficiently described is Fig. 6 of Ref. [120], where the rotation rate used to prepare the emulsion is either 13 500 rpm or 24 000 rpm. In Fig. 6(a,b) the samples containing the lowest concentration of particles have the smallest, most strongly aggregating droplets, which could be a signature of particle bridging. In Ref. [120] all emulsion characteristics were attributed to particle wettability, ignoring the potential importance of the processing route.

Other examples of potentially bridged emulsions which have not been identified as such are Fig. 4 (71% SiOH sample) in Ref. [11], Fig. 3 in Ref. [105], Fig. 16 (0.05-0.2 M TEAB samples) in Ref. [43] and Fig. 10 in Ref. [121]. Additionally, in Ref. [122], the presence of bridging is identified in Fig. 12(g-i), but the flocculation observed in Fig. 12(b) and the decrease in the fraction of resolved water shown in Fig. 13(a,b) are not attributed to bridging. In addition to these examples from the academic literature, it seems likely that the existence of particle bridges will have been overlooked in industrial-scale emulsification.

5.3.1.6 Conclusions: Bridge formation

It has been shown above that particle bridges form in Pickering emulsions, given certain conditions, and that the mechanism of formation is through collisions between partially coated droplets. The conditions are:

- The particles should be preferentially wetted by the continuous phase. This allows a particle to adsorb to two droplet interfaces simultaneously without the droplets coalescing.
- The particles should not protrude too far into the continuous phase, as they need to be strongly enough adsorbed at the oil-water interface to maintain a stable bridge.
- The shear rate during emulsification should be high enough to generate more oil-water interfacial area than can be stabilised by the available particles. For turbulent flow, Eq. (1.7) and Eq. (1.11) show that this will happen when:

$$C\frac{\sigma_{ow}^{3/5}}{\rho^{1/5}\epsilon^{2/5}} \geq \frac{2\pi}{\sqrt{3}}\frac{\phi_o d_p}{\phi_p}. \tag{5.3}$$

5.3.2 Bridge removal

Having described the processes by which particle bridges form, the processes which can lead to their removal will now be described.

5.3.2.1 Complex shear histories

The effects of complex shear histories on emulsions have also been investigated. For example, if an emulsion is subjected to a high shear rate followed by a low shear rate then a bidisperse emulsion is produced, with a small number of larger droplets present, which have a diameter approximately three times that of the main population, as shown in Fig. 5.4 (e). This is believed to be caused by the coalescence of droplets which had previously been bridged together. It is possible for coalescence to occur without any particles being removed from the water-oil interface because some particles in the aggregates are shared by droplets. An aggregated emulsion can therefore de-aggregate without any silica appearing in the resolved water.

The fact that when an aggregated sample is sheared at a relatively low shear rate, the emulsion eventually becomes non-aggregated suggests that these low shear rates are capable of pulling two bridged droplets apart, and that coalescence events dominate over bridging events at lower shear rates. This could be a result of repulsive interactions between particles, which at lower droplet collision energies have enough time to create large bare patches on droplets, but at higher collision energies leave only smaller bare patches more prone to bridging events.

On the other hand, when a sample is sheared first at a relatively low shear rate and then at a relatively high shear rate, enough oil-water interface is created to make particle bridging likely. The sample in this case is also observed to contain non-spherical droplets, as shown in Fig. 5.4 (f), which are not observed when the sample undergoes only the higher shear rate. It is not yet clear, however, if these effects are influenced by emulsion ageing.

5.3.2.2 Changing wettability

Sodium chloride The addition of small concentrations ($\lesssim 40\ mM$) of sodium chloride to the silica dispersions prior to emulsification disrupts the system enough to prevent droplet aggregation occurring. Adding similarly small quantities of sodium chloride to aggregated emulsions, combined with gentle shaking to dissolve the salt, also disrupts the droplet network, creating a non-aggregated emulsion, as shown in Fig. 5.10. When the emulsion de-aggregates, free silica is observed in the resolved water. The addition of salt to the system causes θ_w to decrease, leading to a lower particle trapping energy (see Chapter 3 and Ref. [89]). This

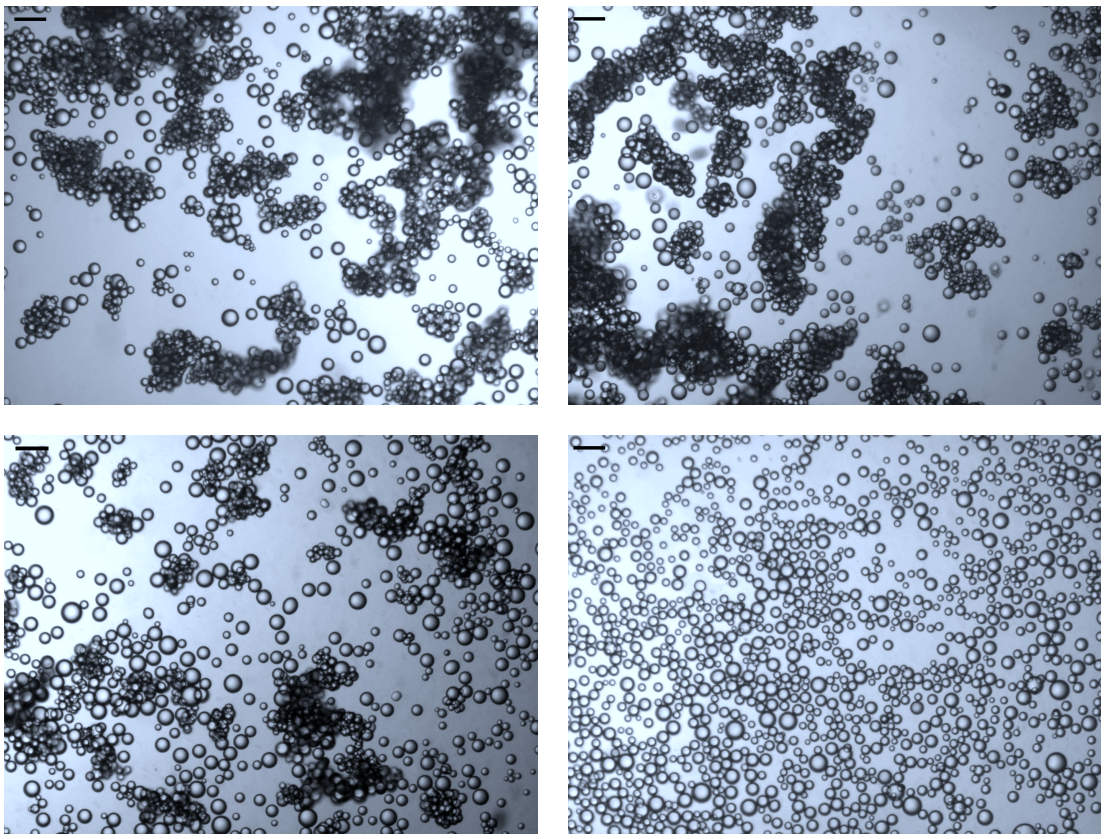

Figure 5.10 *The addition of salt to samples after emulsification destroys particle bridging. The salt concentrations are, from left to right, Top row:* 0 mM *and* 5 mM*; Bottom row:* 10 mM *and* 40 mM*. The sample was created with* $\phi_o = 20\%$*,* $\phi_p = 1.1\%$*,* $\Phi_{IM} = 10\%$*, and sodium chloride was added in* ≈ 5 mM *increments, with the sample being shaken gently after each addition to dissolve the salt. The scale bars are* 100 μm*.*

means that the droplet aggregates are less strongly held together, and so gentle shaking is enough to pull the aggregates apart. When this happens, bridged particles are removed from one, or occasionally both, of the two interfaces to which they had previously been attached, leading to a non-aggregated emulsion with a small amount of free silica in the resolved water.

Adding salt causes electrostatic interactions to be screened, which makes coalescence events between droplets more likely, since there are electrostatic repulsions between the particles on two droplets, and the oil droplets themselves have a slight surface charge. When two partially coated droplets come together, the reduced Debye length may have some influence on the likelihood of coalescence.

Two samples were created with different values of Φ_{IM} - 1% and 50% - so that their interfacial tensions differed (see Fig. 5.2). In both samples $\phi_p = 1.1\%$

and $\phi_o = 20\%$. The two samples were emulsified initially using a vortex mixer, then sheared at 17 000 s^{-1} for 10 min and then again at 34 000 s^{-1} for 2 min, generating strongly aggregated emulsions. Sodium chloride was then gradually added to both emulsions, generally in 5 mM steps, and the emulsions were shaken gently to dissolve the salt. The sample with $\Phi_{IM} = 1\%$ was observed to de-aggregate at a salt concentration of approximately 15 mM, whilst the sample with $\Phi_{IM} = 50\%$ did not de-aggregate until the salt concentration was approximately 50 mM. If the main mechanism involved in de-aggregating the emulsions was the overcoming of an electrostatic repulsion between bridged droplets, then one would expect the sample with the lower interfacial tension to de-aggregate at a lower salt concentration than the sample with the higher interfacial tension. Instead, it seems likely that the mechanism causing de-aggregation is a decrease in θ_w when the salt is added, as was discussed in Chapter 3. This lowering of θ_w leads to a decrease in the attachment energy of the particles and means that the bridged droplets can be pulled apart by gently shaking the sample. However, because the oil phase changes in each case, it is not clear that the amount of charge on a droplet would be constant, although the gradual nature of the de-aggregation also suggests that the mechanism involves changes in contact angle. Furthermore, the separation between bridged droplets when $\theta_w = 70°$, is approximately 300 nm, many times larger than the Debye length for all but the pure water case.

Glycerol Glycerol was added to some samples in order to study the effects of varying the viscosity and refractive index of the aqueous phase, and the results of these experiments are discussed here. Adding glycerol to the samples increases both the viscosity and the refractive index of the continuous phase. The increase in the refractive index means that the strength of van der Waals interactions between particles is reduced.

Glycerol was gradually added to strongly aggregated emulsions - so that the aqueous phase was up to 40% glycerol, by volume - and the samples gently shaken to mix the glycerol into the water. This caused the emulsion to become less aggregated, with a smooth emulsion-resolved water interface forming, as shown in Fig. 5.11.

If water is added to the emulsion instead of glycerol, deaggregation still occurs, but more addition/shaking cycles are required. This is probably because the increase in viscosity, and the associated increase in shear rate during shaking, in the glycerated sample makes disruption of particle bridges more likely. Similar

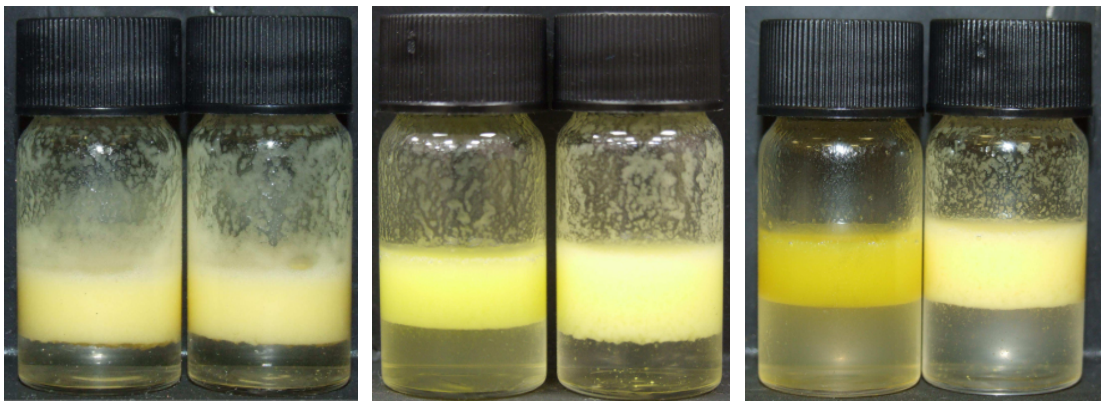

Figure 5.11 *The samples on the left in each image have aqueous phases which are* 0%*,* 25% *and* 40% *glycerol respectively, whilst the samples on the right have had equivalent volumes of pure water added. Adding glycerol clearly accelerates the deaggregation process, as evidenced by the smooth emulsion-resolved water interface in the* 25% *glycerol sample. Initially, both samples have* $\phi_o = 20\%$*,* $\phi_p = 1.7\%$ *and* $\Phi_{IM} = 50\%$*.*

behaviour is observed when the glycerol is added to the aqueous phase prior to emulsification, as shown in Fig. 5.12, suggesting that dilution of the emulsion is not responsible.

These results are consistent with the claim that low shear causes deaggregation, but changes in the strength of particle-particle interactions may also play a rôle, as might changes to θ_w.

pH Changing the pH of the aqueous phase of a Pickering emulsion is known to affect θ_w [89, 123], and is therefore expected to affect the bridging behaviour. To demonstrate that pH adjustment can be used to destabilise the bridged systems, a series of bridged emulsions were made, all with an aqueous phase pH value of 7. The pH of the samples was then adjusted by adding hydrochloric acid or sodium hydroxide, and the samples were gently shaken. Figure 5.13 shows that the bridged emulsions are stable between pH 4 and 10, but become unstable at pH 2, as was also seen in Chapter 4. When these samples are placed on a roller bank for 12 h, the samples with a pH below 5 phase separate completely, with the silica in the aqueous phase. This suggests that even at low pH $\theta_w < 90°$and that the high charge on the particles at low pH causes them to repel each other strongly enough to destabilise the emulsion. In contrast, the samples with a pH above 5 deaggregate but remain stable.

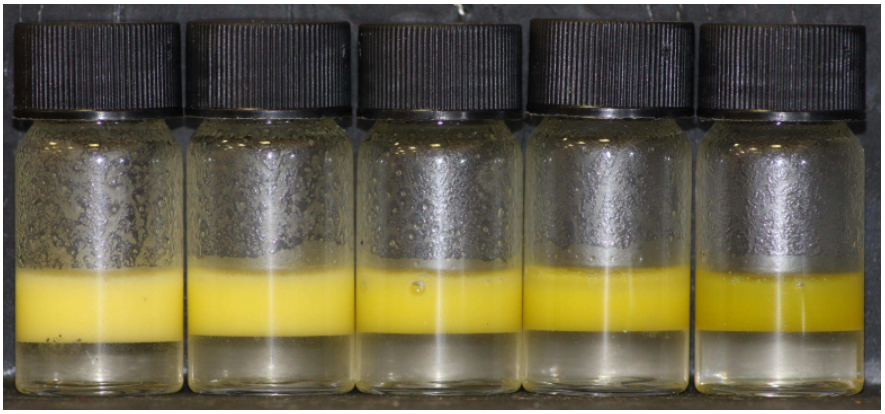

Figure 5.12 *Photograph of a series of samples with aqueous phases comprising, from left to right,* 0%, 10%, 20%, 30% *and* 40% *glycerol. The samples have been emulsified by vortex mixing, followed by* 2 *min of shear at* 34 000 s^{-1} *and being placed in a shaker device for* 1 *h. The increasing packing fraction at higher glycerol concentrations indicates that these samples have deaggregated more thoroughly. In all samples* $\phi_o = 20\%$, $\phi_p = 1.7\%$ *and* $\Phi_{IM} = 50\%$. *Air bubbles are visible in the samples with higher glycerol concentrations. The samples were left to cream for* 1 *h before being photographed.*

Figure 5.13 *Photograph of emulsions taken immediately following adjustment of the* pH *values by addition of either hydrochloric acid or sodium hydroxide. The samples have* pH *values of, from left to right,* 2, 4, 6, 7, 8 *and* 10. *In all samples* ϕ_o, ϕ_p *and* Φ_{IM} *are* 20%, 0.6% *and* 10% *respectively. The sample with a* pH *of* 2 *has undergone coalescence so that the droplets are* $\approx$ 300 μm *in diameter. The samples were left to cream overnight before being photographed.*

5.3.3 Rheology of bridged Pickering emulsions

Rheological experiments on bridged Pickering emulsions have also been carried out, and the results of these experiments have been compared to results for non-bridged samples.

5.3.3.1 Results and discussion

Typical plots of G' and G'' for a bridged Pickering emulsion with $\phi_p = 1.1\%$, $\phi_o = 20\%$ and $\Phi_{IM} = 10\%$ are shown in Fig. 5.14 (left). These can be compared to the data gathered for a non-bridged sample (where the bridging has been suppressed by adding sodium chloride) shown in Fig. 5.14 (right). Both samples were emulsified using a vortex mixer until the aqueous phase was clear of particles. The most striking difference between the bridged and non-bridged rheological behaviour is that there is a pronounced peak in G'' for the bridged samples, which occurs at strains slightly lower than the strain at which G' and G'' cross over. It is believed that this peak is caused by the particle bridges in the emulsion being broken, since it occurs at a lower strain than the yielding point (defined by the crossing point of G' and G''), in a manner reminiscent of the bond-breaking peak observed in attractive colloidal glasses [124].

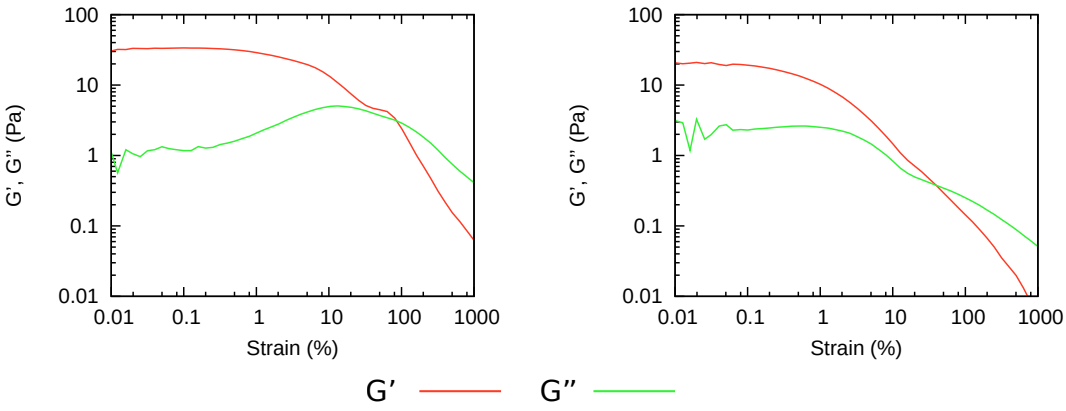

Figure 5.14 *G' and G'' are shown as a function of strain for a bridged Pickering emulsion (left) and a non-bridged Pickering emulsion (right). In both samples, $\phi_p = 1.1\%$, $\phi_o = 20\%$ and $\Phi_{IM} = 10\%$. The bridged sample does not contain salt, and the non-bridged sample has an aqueous phase sodium chloride concentration of 250 mM.*

The rheological behaviour of bridged emulsions has also been studied as a function of Φ_{IM}, as shown in Fig. 5.15. The magnitude of G' in the plateau region decreases

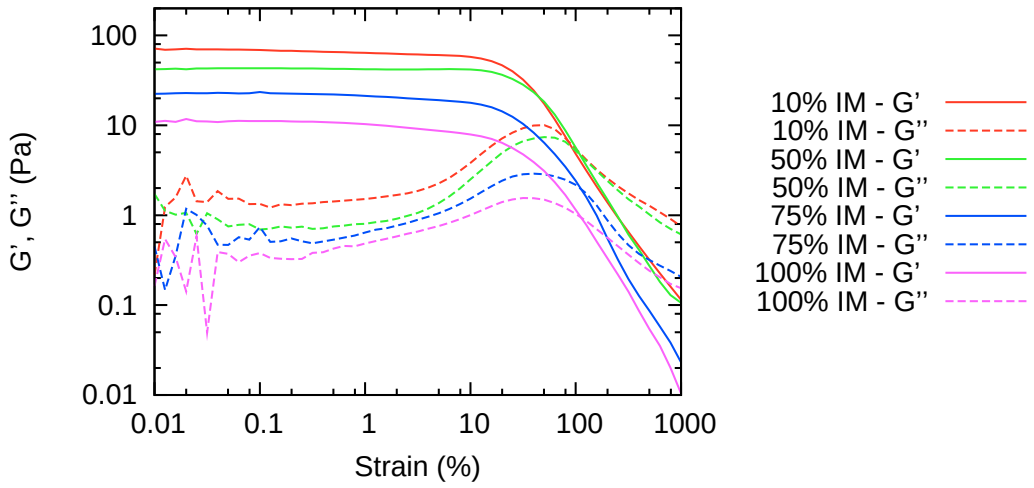

Figure 5.15 *Rheological behaviour of bridged Pickering emulsions at different values of Φ_{IM}. G' and G'' are shown as a function of strain. In all samples, $\phi_p = 0.6\%$ and $\phi_o = 20\%$. All samples were emulsified using a vortex mixer until the aqueous phase was clear of particles.*

as Φ_{IM} increases. This result is to be expected since increasing Φ_{IM} decreases σ_{ow}, which makes deformation of the droplets easier and leads to a more liquid-like behaviour. The peak in G'' also becomes less prominent as Φ_{IM} increases, which may be because the particle bridges are stronger. Since the particle bridges are less likely to break at higher values of Φ_{IM}, the behaviour of the emulsion will be more solid-like. Neither the crossover strain or the strain at which G'' peaks appear to be dependent upon Φ_{IM}.

5.4 Conclusions and future work

A model Pickering emulsion system has been developed which allows the effects of several parameters on the degree of particle bridging between droplets to be investigated. In particular, it has been found that bridging will only occur if the particles have a preference for the continuous phase, but that the strength of a bridge decreases as the particles move further into the continuous phase. This effect can be used to remove particle bridges from an emulsion without destabilising the droplets. Particle bridges can also be removed by applying low shear. The rheological behaviour of the bridged emulsions has been studied, and a bond-breaking peak in the loss modulus has been found, a feature which is not observed in non-bridged samples. Freeze-fracture SEM has been used to directly

observe particle bridging, which has not been published before.

The results presented here show that the most important prerequisites for forming particle bridges are that the particles have a preference for the continuous phase and that more interfacial area is generated during the mixing process than can be stabilised by the particles present - this causes collisions between partially coated droplets to lead to bridge formation. Some of the processes involved in forming bridges have been described quantitatively. From this work it is suggested that bridging may be more prevalent in the Pickering emulsion literature than previously realised, and may have been missed in cases in which the emulsification protocol was not carefully considered (or, in one or two cases, even described). It is strongly argued that the characteristics of Pickering emulsions depend on the shear history of the sample and that this must be documented.

Several methods for removing particle bridges from emulsions have also been investigated. It has been found that shearing a bridged emulsion at a shear rate lower than that necessary to create particle bridges will remove bridges. Modifying the particle wettability by, for example, adding salt to the aqueous phase, can greatly reduce the shear rate and time needed for this to occur.

An understanding of these two processes - making and breaking particle bridges - allows for control over the degree of bridging in a Pickering emulsion. This allows a practitioner to control the emulsion's packing fraction, and hence control an emulsion's macroscopic properties (*e.g.,* the viscosity of an emulsion could be varied independently of dispersed phase volume fraction). The results presented here should therefore be relevant to anyone wishing to design a well-controlled Pickering emulsion system.

It would also be interesting to study the effect upon particle bridging of ϕ_o. Equation (5.3) predicts that an increase in ϕ_o will make particle bridging less likely, as the average droplet size will increase, lowering the oil-water interfacial area during emulsification and hence lowering the number of partially coated droplets. However, increasing ϕ_o is likely to also increase the rate of collisions between droplets, and it is possible that this will lead to an increase in the degree of particle bridging in a sample. Replicating the results presented in this chapter using smaller particles or in different experimental systems (*e.g.*, using fumed silica, or water-in-oil emulsions) would also be interesting. Particle bridging is clearly sensitive to changes in the contact angle, and is likely to be more sensitive when smaller particles are used.

Chapter 6, Chapter 7 and Chapter 8 will expand upon the results which have been presented in this chapter. Chapter 6 will present experiments using emulsions which have been stabilised by two different colours of fluorescent silica particle to elucidate the deaggregation process described above and Chapter 7 will use the same technique to study bridged emulsions as a high shear rate is repeatedly applied. Chapter 8 will present experiments which replicate some of the above findings at a larger scale (sample volumes of approximately 1 L) and using a continuous flow setup, in order to demonstrate the relevance of particle bridging experiments to industrial emulsification processes.

Chapter 6

The secret life of Pickering emulsions: The deaggregation of bridged emulsions

6.1 Introduction

In this chapter a novel technique will be presented which can be used to probe various fundamental aspects of Pickering emulsions, including the fluidity of the particle layer and the rate of particle transfer between droplets. The technique involves the use of two batches of particles which have been fluorescently labelled with different dyes, to study the degree to which a Pickering emulsion is remixed during shear.

In Chapter 5 it was shown that low shear can be used to disrupt particle bridges in a Pickering emulsion, and in this chapter the results of experiments which have applied the two-colour technique to the study of the deaggregation process will be presented.

Pickering emulsions are usually considered to be very stable, due to the large trapping energy of particles at an oil-water interface, which is given by Eq. (1.3). This large trapping energy is usually considered to mean that the particles are irreversibly adsorbed at the interface [4, 24, 113, 125–130]. Yet if the particles which are bridging two droplets are irreversibly adsorbed to both interfaces, then deaggregation at low shear rates should not occur. However, as was shown in

Chapter 5, particle bridges are indeed broken by low shear, and this can even lead to free silica being released into the aqueous phase, which raises questions about the reversibility of particle adsorption and the true stability of these emulsions. The release of silica into the continuous phase is presumably a result of relatively small forces generating relatively large torques, as a result of the bridged droplets experiencing shear, in a manner reminiscent of the shearing of dendritic particle branches by gravitational forces [131].

Bridged emulsions could be useful in applications involving the gradual release of the dispersed phase. A deeper understanding of the deaggregation process is therefore desirable, so that the parameters affecting the deaggregation time can be controlled and tuned. If deaggregation is gradual (*via* an unbridging/rebridging process, for example), then release will also be gradual. Since deaggregation can be triggered by changing the pH or the salt concentration (see Chapter 5), a gradual release mechanism with a lifetime which can be tuned by adjusting the particle wettability would provide a broad spectrum of release behaviours.

The use of two differently labelled batches of particles in this manner also means that the fluidity of the interface in Pickering emulsions, which is currently a major area of research [132–135], can be probed. The fluidity of the Pickering interface is also important in determining the stability of droplets to coalescence during deformation, as well as the rheological properties of the emulsion. It has also been shown that particle jamming at the interface is a separate phenomenon from stable Pickering droplets [136], which contradicts the fundamental assumptions of the theory of limited coalescence. Some of the main open questions surrounding Pickering emulsions pertain to the fluidity of the particle layer at a droplet's surface, as the fluidity of the particles at the interface will be a key influence on the droplets' stability against coalescence during shear. The interface's fluidity is also likely to play a part in the behaviour of the emulsion if the composition of either phase changes, *e.g.,* due to targeted release. Subramaniam *et al.* have studied the minimum dilation necessary for jammed particles at an interface to flow past each other, and showed that the yield stress necessary to effect flow is $\mathcal{O}(\sigma_{ow}/r_p)$ [137]. This yield stress is relatively large, meaning that particle flow is highly unlikely when the droplets are fully covered by particles, although flow will clearly be significantly more likely when surface coverage is below that of close-packed spheres. By using two different colours of particle to stabilise an emulsion, the particles obtain a degree of distinguishability, allowing the fluidity of the particle layer to be probed.

The technique of using two different colours of particles to investigate aspects of Pickering emulsions has previously been used by Maurice *et al.*, who used NBD and $DilC_{18}$ labelled PMMA particles to look for particle bridging in water-in-dodecane emulsions [36]. However, the use of multiple colours of particles to track the homogeneity of droplets and infer information about droplet breakup and coalescence is thought to be novel. A similar technique was previously developed by Taisne *et al.* to study coalescence events in oil-in-water emulsions produced using a high-pressure homogeniser [138]. This technique involved creating two emulsions with differing oil phases, so that the refractive index of one of the oil phases was below that of the aqueous phase and the refractive index of the other oil phase was above that of the aqueous phase. By carefully choosing the refractive indices, Taisne *et al.* were therefore able to create emulsions which became gradually less opaque as coalescence progressed, without simultaneously driving compositional ripening, which allowed them to quantify the degree of coalescence which had occurred. Taisne *et al.* used this technique to gather some interesting results about recoalescence in surfactant-stabilised emulsions, showing that when the sample is rich in surfactant, recoalescence does not occur unless the pressure in the homogeniser exceeded the pressure used to initially create the emulsion. The two-colour technique described in this chapter aims to apply a similar thought process to Pickering emulsions, at both a droplet and particle level.

In the rest of this chapter the necessary quantitative considerations and a description of the experimental methods will be set out, followed by a description of the results of experiments studying how bridged Pickering emulsions deaggregate at low shear rates. Chapter 7 will present the results of similar experiments studying how Pickering emulsions are affected by the repeated application of a higher shear rate.

6.1.1 Theory

The colour-homogeneity of individual droplets can be quantified using:

$$f = |\frac{n_r - n_y}{n_r + n_y}|, \tag{6.1}$$

where n_r and n_y are, respectively, the numbers of red and yellow particles on a droplet. The sample-average will be denoted by $\bar{f}$. For a homogeneous droplet,

f will be exactly 1, whilst for a droplet with equal numbers of red and yellow particles, f will be exactly 0. Another method of quantifying the homogeneity of droplets is to use the number of nearest neighbours of each particle which are the same colour as that particle, n_s, and the number of neighbours which are not of the same colour, n_d:

$$g = \frac{1}{n_p} \sum_{n_p} \frac{n_s - n_d}{n_s + n_d}, \tag{6.2}$$

where the summation runs over every particle on the droplet surface, although in practice a sub-section of the droplet will be more practical to deal with and should provide sufficient precision. The sample average will be denoted by $\bar{g}$. For a homogeneous droplet, g will also be exactly 1, and for a completely heterogeneous droplet, where particles have equal numbers of red and yellow neighbours, g will be exactly 0. Negative values of g would occur if particles are more likely to have neighbours of the opposite colour than of the same colour. Table 6.1 gives the values of f and g for some sample droplets.

Table 6.1 *Table showing some sample values of f and g, assuming a droplet with a diameter of* 100 μm *is fully covered by particles with a diameter of* 1 μm, $n_p = 36\,433$

Droplet type	f	g
Homogeneous, single colour	1	1
Homogeneous, but for one particle	0.99995	0.9998
Droplet with a patch of diameter 25 μm	0.7071	0.9878
Same as above, but with particles randomly arranged	0.7071	0.5
Janus droplet	0	0.9828
Equal numbers of each colour, randomly mixed	0	0

Similar analysis can also be performed at a cluster level:

$$f' = |\frac{N_r - N_y}{N_r + N_y}|, \tag{6.3}$$

$$g' = \frac{1}{N} \sum_{N} \frac{N_s - N_d}{N_s + N_d}, \tag{6.4}$$

where the changes from f, g and n to, respectively, f', g' and N signify that the calculation is being performed at a cluster level, looking at the numbers of red and yellow droplets in each cluster.

The difference between f and g is perhaps best illustrated by considering a Janus droplet which is coated on one hemisphere by yellow particles and the other hemisphere by red particles. In this situation, $f \approx 0$ since $n_r \approx n_y$, but $g \approx 1$, since the vast majority of particles will be completely surrounded by particles of the same colour as themselves. At a cluster level, in particular, g' will be more useful than f', since the bridged droplets often create a sample spanning network, so that $f' = 0$, even if g' is very close to 1.

6.1.2 Possible routes to droplet heterogeneity

The deaggregation of a bridged Pickering emulsion could lead to heterogeneous droplets in several ways. Two of these ways are depicted in cartoons in Fig. 6.1, and repetition of these processes will lead to highly heterogeneous interfaces, yielding low values of both f and g. Once a droplet has become patchy, the particles in the patch might be able to diffuse on the interface, if the interface is not jammed or if the droplet becomes deformed.

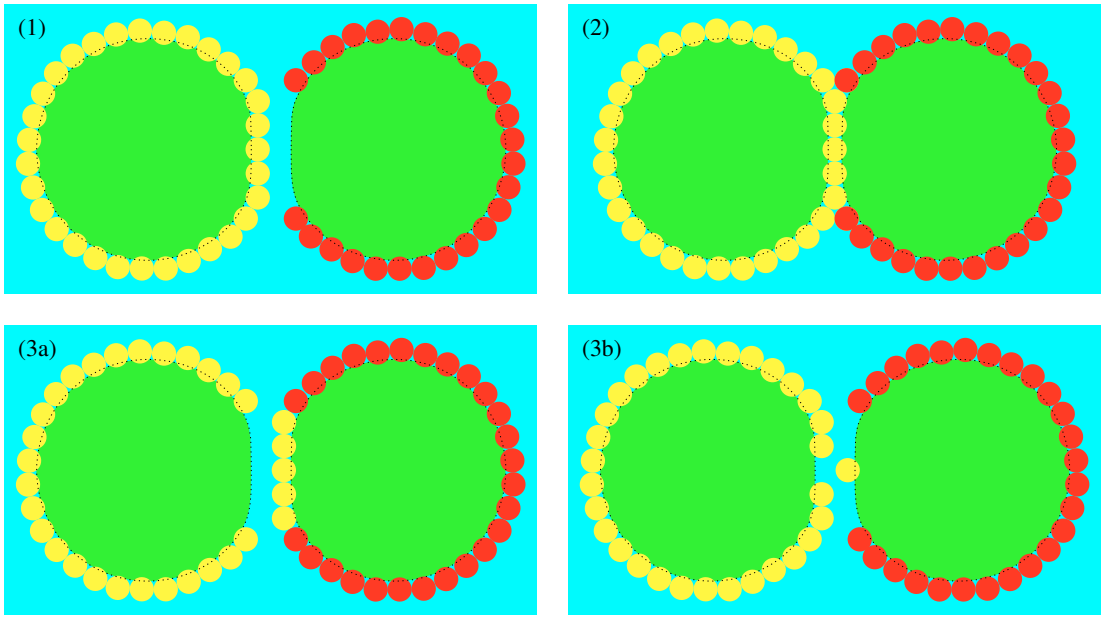

Figure 6.1 *Cartoons showing two possible routes for droplet interfaces to become heterogeneous during deagreggation of a bridged Pickering emulsion. (1-2): A fully coated droplet collides with a partially coated droplet, forming a particle bridge. (3a-3b): The particle bridge is broken, leading to a patchy droplet (3a) or single particle transfer (3b).*

6.2 Methods

The methods which are particular to this chapter will be discussed in this section. Methodology for techniques which are used in this chapter and in other chapters can be found in Chapter 2.

6.2.1 Sample preparation

Two differently dyed batches of Stöber silica have been used in the experiments described in this chapter - one dyed yellow with FITC, the other dyed red with RITC - to study the degree to which a Pickering emulsion is remixed during shear, and also the rate at which particles reorganise at a droplet's surface during shear. In each experiment two separate precursor emulsions of equal volume were created, one with each batch of particles, and these two emulsions were then gently mixed together and subjected to low shear. The use of two different dyes allows the two batches of particles to be observed separately using confocal microscopy. Emulsification was carried out by vortex mixing the samples in 30 s bursts until the aqueous phase was clear of particles. Following emulsification, the precursor emulsions were mixed - with a small amount of water being added to the mixed sample as part of washing out the vials used to emulsify the initial emulsions. The mixed sample was then placed on a roller bank, which causes the emulsion to de-aggregate, if it was initially bridged, and eventually leads to the coalescence of droplets and the appearance of a significant fraction of free oil.

There is a possibility that the volume of the sample will have an effect on the way the emulsion destabilises. The angle that the emulsion-air interface makes with the vial wall could affect how likely droplets are to become stuck to the wall, and the flow conditions near the air-emulsion interface, and unfortunately this effect was not taken into account during these experiments. The shear rate of the samples whilst on the roller bank can be estimated by dividing the circumferential velocity of a vial on the roller bank by the diameter of the vial, which gives a shear rate of $\approx 3\ s^{-1}$. For the system parameters used here, Eq. (1.9) predicts that this shear rate will lead to a droplet diameter of $\approx 5\ m$, so droplet breakup should not occur.

6.2.2 Sample characterisation

Bright-field microscopy, confocal microscopy, photography and light scattering have been used to characterise the emulsions. The Beckman Coulter particle size analyser (see Chapter 2) was used to measure the apparent size distributions of emulsions as they de-aggregate. As was discussed in Chapter 5, this method is only accurate when the droplets are not bridged. When the droplets are bridged light scattering can provide a quantitative measure of the degree of bridging, although this method can be unreliable, since the stirring mechanism in the sizer can break up the aggregates. It should be noted that there are several problems which must be accounted for when using light scattering to measure the apparent size distributions of deaggregating emulsions. Droplets which are incorporated into bridged clusters cream more quickly than droplets which are not aggregated, which means that the emulsion is not homogeneous when it has settled - those droplets which are bridged will generally be above those which are not. Therefore, even though the emulsion was swirled before a pipette was used to extract some of the sample to perform light scattering, on some occasions the extracted emulsion may not be representative of the whole sample. Additionally, droplets above a certain volume will be too buoyant for the stirrer bar in the particle size analyser to drag down into the scattering portion of the chamber, and large droplets are liable to be broken up by the stirrer bar. For these reasons, comparisons with photography and bright-field microscopy have been used to corroborate the light scattering data. In most bridged samples, the fraction of the emulsion which was incorporated into a cluster could be estimated by the area under the bridging peak on the apparent size distributions.

Confocal microscopy was used to qualitatively and quantitatively measure both the colour heterogeneity of individual droplets and the mixedness of clusters of bridged droplets, as well as the packing fraction of particles on the interfaces of droplets.

Photographs of samples were used to track the development of free oil in the samples and can be used to measure the emulsion packing fractions, a signature of bridging, as was explained in Chapter 5.

6.2.3 Image analysis

Figure 6.2 shows a typical image obtained from a two-colour experiment using confocal microscopy. It can be seen that, whilst a small amount of cross-talk between the two channels occurs, it is still obvious when red particles are present on an originally yellow droplet, and *vice versa*. Although the FITC-labelled particles are yellow, it was found that a red and green colour scheme provided better contrast when presenting multicolour confocal micrographs, and for this reason the FITC-labelled particles are shown as green in the confocal micrographs, but will be referred to as yellow in the text.

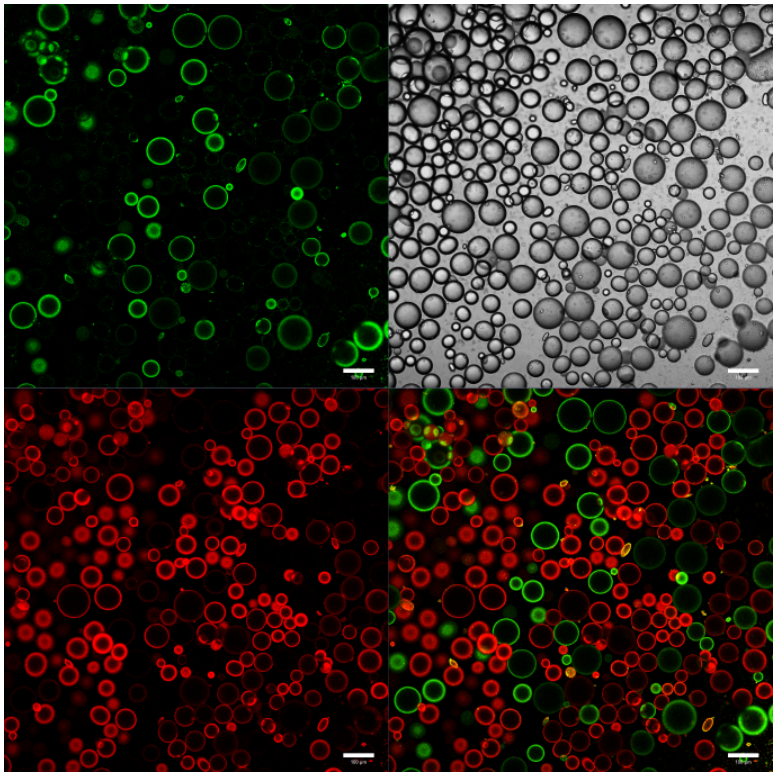

Figure 6.2 *Confocal micrograph of a typical two-colour sample. The quadrants show: the yellow FITC-labelled particles, excited by a* 488 *nm laser (top left); the red RITC-labelled particles, excited by a* 555 *nm laser (bottom left); a transmission image obtained using a dichroic mirror on the transmission side of the sample and the* 488 *nm laser (top right); a merged image of the FITC and RITC channels (bottom right). In this case,* $\phi_o = 20\%$, $\phi_p = 0.6\%$, $\Phi_{IM} = 10\%$, *the aqueous phase contains* 30 *mM of sodium chloride and the sample has been rolled for* 1 *h. The scale bars are* 100 μm.

6.3 Results and discussion

In this section the results of two-colour experiments studying deaggregation in bridged emulsions will be presented and discussed. The insight these provide into the ideas presented in Chapter 4 and Chapter 5 will be highlighted.

The main application for the two-colour technique in this chapter is to further study the de-aggregation process of bridged emulsions which has been described in Chapter 5. Of additional interest is the degree to which particles are transferred between droplets, and the degree to which droplets coalesce during this process.

Several experiments have been carried out in order to study the deaggregation process, with each looking at the effect of a particular variable. The following variables have been studied: isopropyl myristate volume fraction in the oil phase, particle volume fraction, time spent ageing before the rolling process and salt concentration. As shown in Chapter 5, the degree of bridging in a sample depends on both the particle wettability and the particle volume fraction. By varying these parameters, it is possible to compare emulsions with varying degrees of bridging and therefore study the effects of particle bridging on the destabilisation of the emulsion. Furthermore, by varying Φ_{IM} and hence θ_w, the nature of the interactions between particles which are at an oil-water interface is modified, and these modifications will affect the stability of the emulsions to both deaggregation and coalescence (see Chapter 3 and Chapter 4).

If a period of unbridging and rebridging precedes full deaggregation, then when deaggregation occurs in a system formed by mixing a bridged precursor emulsion with a non-bridged precursor emulsion, one would expect that droplets from the non-bridged precursor emulsion quickly become incorporated into the clusters. The rate of incorporation could also be used to calculate the rate of unbridging in the sample. Therefore, systems formed by mixing a bridged precursor emulsion and a non-bridged precursor emulsion will also be studied. Whether the presence of non-bridged droplets accelerates or slows down deaggregation will also be of interest. Alternatively, if rebridging events do not occur at low shear rates, then the expected degree of particle transfer is considerably lower, although coalescence events may still occur.

6.3.1 Particle wettability

As was discussed in Chapter 5, the volume fraction of isopropyl myristate in the oil phase can be used to tune the particle wettability and the interfacial tension, and therefore alter the degree of bridging which occurs in the sample. In this section the effects that Φ_{IM} has on how bridged emulsions deaggregate when subjected to low shear rates will be studied. Two separate particle volume fractions have been studied - one which causes both of the precursor emulsions to be bridged ("bridged/bridged", $\phi_p = 0.6\%$), and another where only one of the precursor emulsions is bridged ("bridged/non-bridged", $\phi_p = 0.9\%$).

6.3.1.1 Bridged/bridged

A higher isopropyl myristate content causes the contact angle to increase, so that the particles sit further into the oil phase and are more strongly held at the interface, but also reduces the interfacial tension, which makes the droplets easier to deform and burst. As was discussed in Chapter 5, an increase in Φ_{IM} increases the degree of bridging in the system.

Bridged Pickering emulsions were made using oil phases of different isopropyl myristate volume fractions, so that the effect this change has on the deaggregation process could be determined. Two samples were made, one using an oil phase with $\Phi_{IM} = 10\%$ and the other with $\Phi_{IM} = 50\%$. In both cases $\phi_o = 20\%$ and $\phi_p = 0.6\%$. The apparent size distributions of the emulsions as they deaggregate are shown in Fig. 6.3.

Both the $\Phi_{IM} = 10\%$ and the $\Phi_{IM} = 50\%$ samples followed a similar behaviour pattern: both samples were initially strongly bridged, and remained so until the cumulative rolling time was at least 30 h. They both then underwent a gradual deaggregation process which lasted until the cumulative rolling time was at least 65 h, as can be seen in the micrographs in Fig. 6.4 and Fig. 6.5. Following deaggregation, both samples were relatively stable, and although a layer of free oil develops and grows in volume throughout the experiment, there is still a significant dispersed volume even after several months of rolling. The similarities and differences between the two samples in each of these stages will now be discussed.

The most striking difference between the two emulsions during the period where

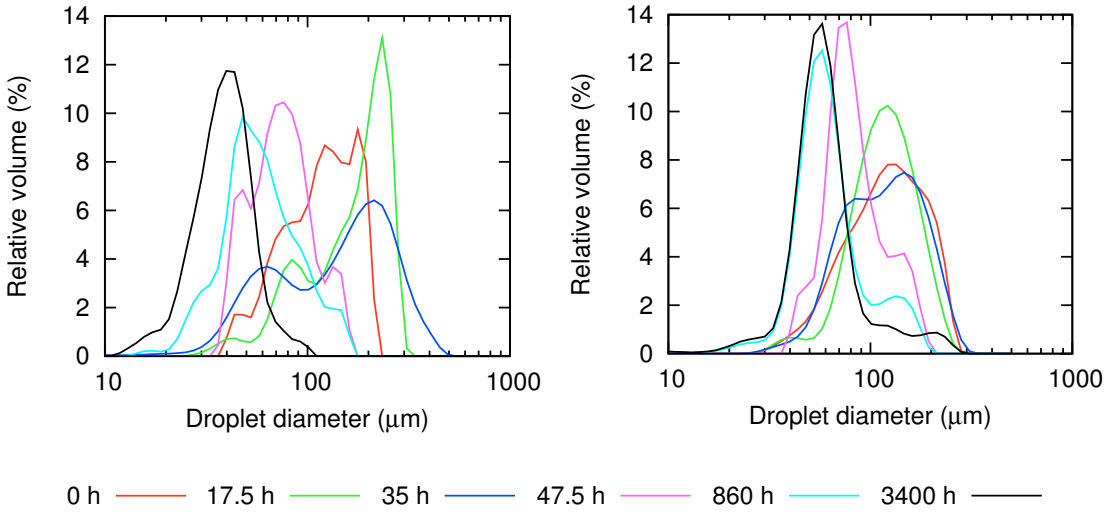

Figure 6.3 *Graphs showing how the apparent droplet sizes in emulsions with different particle wettabilities change as the emulsions are rolled. The Φ_{IM} values are* 10% *(left) and* 50% *(right). The particle volume fraction in both cases is* 0.6%*.*

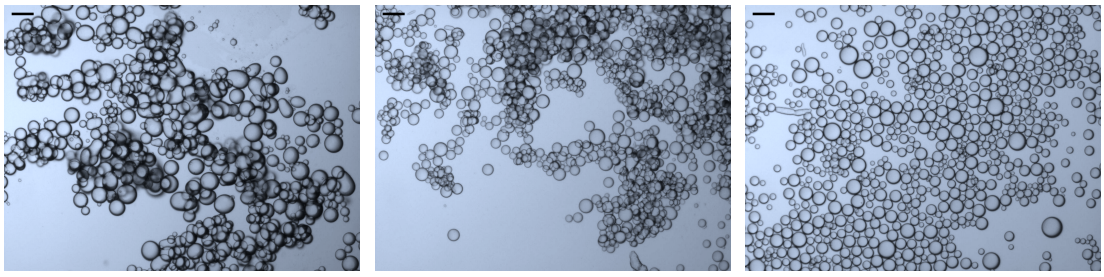

Figure 6.4 *Micrographs of samples with $\Phi_{IM} = 10\%$ at various rolling times. The rolling times are, from left to right,* 1 *h,* 65 *h and* 185 *h. The sample clearly deaggregates between the latter two images. The scale bars are* 100 *µm.*

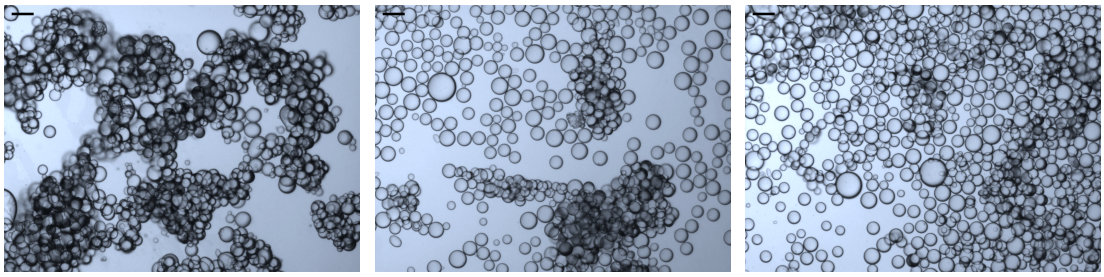

Figure 6.5 *Micrographs of samples with $\Phi_{IM} = 50\%$ at various rolling times. The rolling times are, from left to right,* 1 *h,* 185 *h and* 357 *h. The sample has clearly not fully deaggregated by* 185 *h, and may not even have fully deaggregated by* 357 *h. The scale bars are* 100 *µm.*

the samples are still strongly bridged is that the clusters of droplets in the $\Phi_{IM} = 50\%$ sample are significantly less likely to become mixed, as can be seen in Fig. 6.6. After rolling for 1 h, $\bar{g}'$ values are 0.6 and 0.9 for the $\Phi_{IM} = 10\%$ and $\Phi_{IM} = 50\%$ samples respectively. It takes approximately 15 h of rolling for the clusters in the $\Phi_{IM} = 50\%$ sample to reach a similar level of mixing to that of the $\Phi_{IM} = 10\%$ sample after 1 h of mixing. These results fit well with the hypothesis that a higher isopropyl myristate content leads to a higher contact angle and stronger particle bridges. These stronger particle bridges mean that the clusters are less likely to break up during the rolling process, and so the majority of a droplet's neighbours continue to be from the same precursor emulsion as the droplet itself. In the $\Phi_{IM} = 10\%$ sample, however, the weaker particle bridges are more likely to break during the rolling process, which causes the emulsion to undergo an unbridging/rebridging process as particle bridges continually break and reform, leading to the mixed clusters of droplets seen in Fig. 6.6.

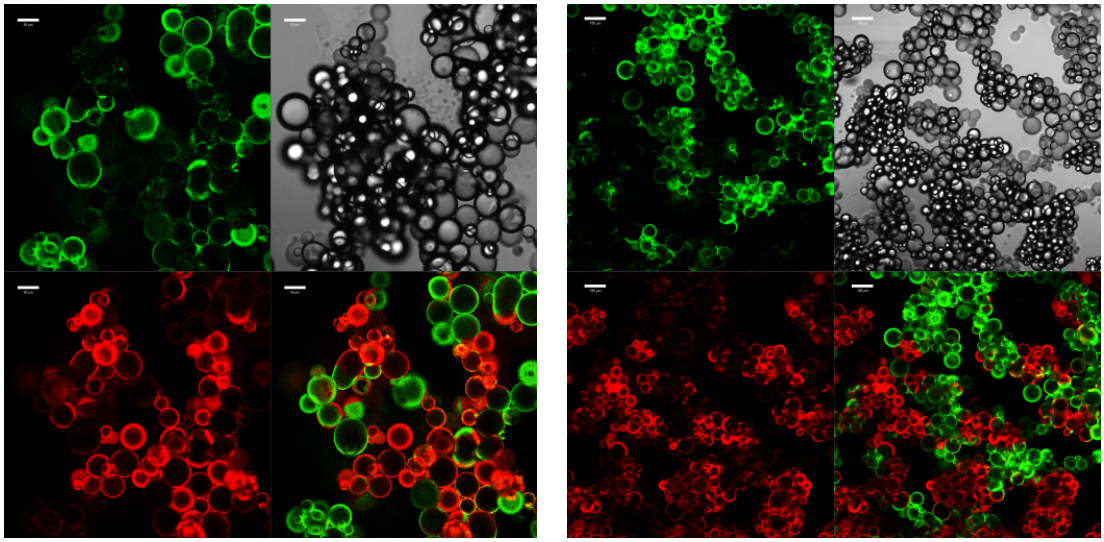

Figure 6.6 *Confocal micrographs of samples with* $\Phi_{IM} = 10\%$ *(left) and* $\Phi_{IM} = 50\%$ *(right), after being on a roller bank for* 5.5 h. *The clusters in the sample with* $\Phi_{IM} = 10\%$ *can clearly be seen to be more thoroughly mixed than those in the sample with* $\Phi_{IM} = 50\%$. *The scale bars are* 50 μm *(left) and* 100 μm *(right).*

In both samples, the droplets become more heterogeneous as the samples are rolled, even prior to deaggregation. Janus droplets are often observed, as can be seen in Fig. 6.7, and are often clearly the result of arrested coalescence. However, the proportion of Janus droplets in most samples is higher than the proportion of droplets with highly heterogeneous interfaces at subsequent rolling times, which suggests that some fraction of these droplets develop during the preparation of

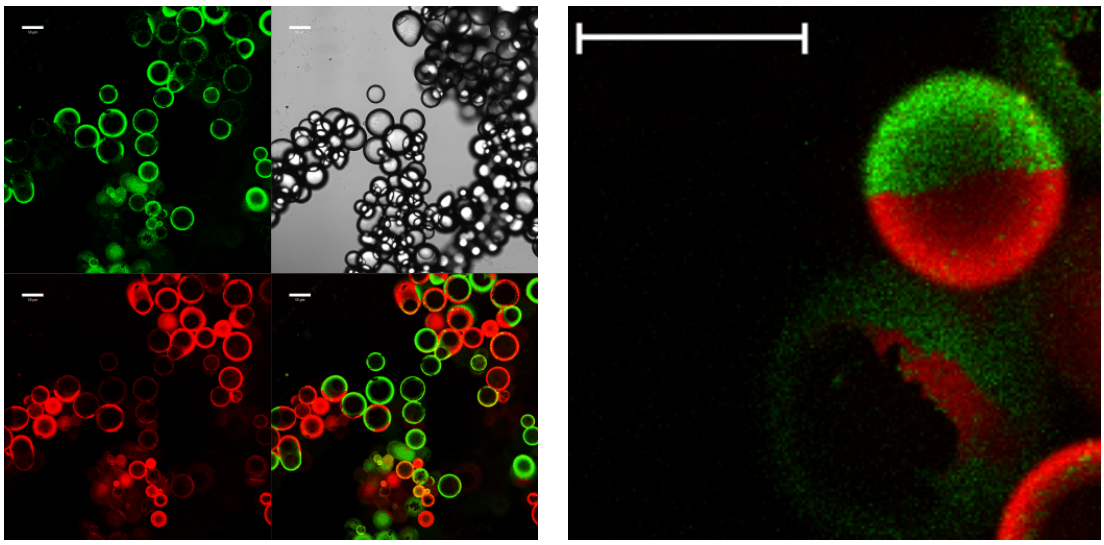

Figure 6.7 *Confocal micrographs showing Janus droplets which have undergone arrested coalescence. Left: Image of the* $\Phi_{IM} = 10\%$ *sample after rolling for* 13 h*; Right: Detail of a Janus droplet from the same sample. The scale bars are* 50 μm*.*

the slides. If the coalescence events are due to the slide preparation, then the increase in droplet heterogeneity is due mainly to particle transfer during the unbridging/rebridging process.

It is difficult to precisely identify the point at which each emulsion begins to deaggregate using the light scattering data, due mainly to the problems relating to the sizing of bridged emulsions mentioned in Section 6.2. However, bright-field microscopy can be used to provide information on both the start and end points of the deaggregation process, and light scattering is more reliable at identifying the presence of a small amount of bridging in an otherwise non-bridged sample, and so can be used to identify the end of the deaggregation process.

Bright-field microscopy shows the $\Phi_{IM} = 10\%$ sample has fully deaggregated after 185 h of rolling (although it should be noted that the previous measurement was taken at 65 h), as can be seen in the micrographs in Fig. 6.4, and which are supported by light scattering measurements. On the other hand, the $\Phi_{IM} = 50\%$ sample does not fully deaggregate until the rolling time is at least 185 h, and possibly isn't fully deaggregated after 357 h, as can be seen in Fig. 6.5. This result again fits well with the idea that the sample with the higher isopropyl myristate content leads to stronger particle bridges, but also with the fact that the particle-interface attractions are stronger when the oil phase has a higher isopropyl myristate volume fraction, which increases the probability of rebridging.

That the two samples both start deaggregating at roughly the same time suggests that a gradual decrease in the contact angle, caused by the particles becoming more hydrophilic as they are immersed in water, may also play a rôle in the onset of deaggregation. This idea will be tested further in experiments involving ageing of the precursor emulsions prior to mixing, which will be discussed below (Section 6.3.2). That there is no observable difference in timing of the onset of deaggregation at different Φ_{IM} values can be attributed to the gradual nature of the deaggregation process, which makes it difficult to precisely define a start point for deaggregation.

When the $\Phi_{IM} = 50\%$ sample deaggregates, the apparent droplet size decreases and free silica appears in the aqueous phase, as can be seen in the photographs in Fig. 6.8. Free silica is also observed following deaggregation of the sample with $\Phi_{IM} = 10\%$, but considerably less free silica is observed than in the $\Phi_{IM} = 50\%$ sample. The deaggregation process seems to occur only after the contact angle has been lowered by a certain amount, which halts the unbridging/rebridging process and instead leads to coalescence events becoming more common. The unbridging/rebridging process could be disrupted by a change in the particle wettability if the particles become hydrophilic enough that the particle-interface attractions are no longer strong enough for the particles to re-adsorb to another droplet. The $\Phi_{IM} = 50\%$ sample has stronger particle-interface attractions than the $\Phi_{IM} = 10\%$ sample, and this means that rebridging will be possible at lower contact angles in the $\Phi_{IM} = 50\%$ sample. This, together with the higher initial contact angle in the $\Phi_{IM} = 50\%$ sample, means that deaggregation will take longer at higher isopropyl myristate values. Additionally, because the contact angle at the point of deaggregation is lower in the $\Phi_{IM} = 50\%$ case, free silica is more likely to be released during deaggregation, since the trapping energy of the particles at the point of deaggregation will be lower.

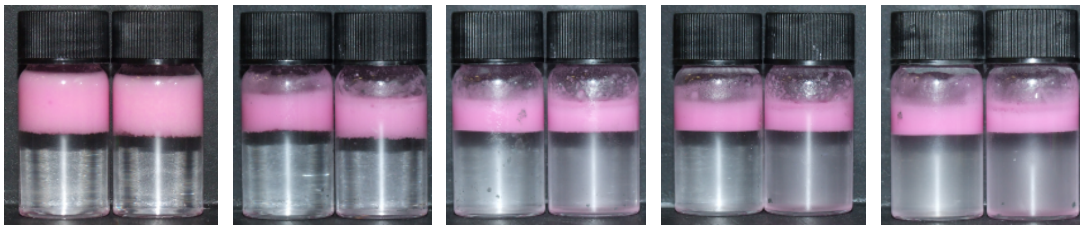

Figure 6.8 *Photographs of samples with* $\Phi_{IM} = 10\%$ *and* 50% *at various rolling times. In each photograph the sample on the left is the* $\Phi_{IM} = 10\%$ *sample and the sample on the right is the* $\Phi_{IM} = 50\%$ *sample. The rolling times are, from left to right,* $0\ h$, $29\ h$, $65\ h$, $185\ h$ *and* $357\ h$.

Light scattering and microscopy show that the apparent droplet size in the $\Phi_{IM} = 10\%$ sample decreases with rolling time, plateauing at the primary droplet size of $\approx 50\ \mu m$ after $\approx 65\ h$ of rolling. This droplet size is notably lower than that predicted by Eq. (1.7), which is $\approx 125\ \mu m$. Comparisons between the light scattering measurements and bright-field micrographs of the emulsions show that the measured primary droplet size is indeed accurate. The discrepancy between predicted and actual droplet sizes is therefore presumably caused by droplets sharing particles and not being fully covered by particles, with droplets which are not fully covered being most likely to coalesce with the free oil. A similar trend is also observed in the sample with $\Phi_{IM} = 50\%$, but in this case the droplet size levels off at $\approx 60\ \mu m$. The greater droplet size at $\Phi_{IM} = 50\%$ relative to $\Phi_{IM} = 10\%$ is presumably linked to the appearance of free silica in the aqueous phase of the $\Phi_{IM} = 50\%$ sample.

Although the droplets in both samples are all clearly heterogeneous following deaggregation of the emulsion, as shown in Fig. 6.9, it is also true that for the majority of the droplets, it is easy to discern whether they are dominated by red or yellow particles, *i.e.,* $f \not\approx 0$. This, together with the gradual change in droplet heterogeneity, suggests that the cause of the heterogeneity in these droplets is a gradual transfer of particles during the deaggregation process rather than coalescence. This conclusion is strengthened by the fact that the droplets which are left at this stage have a mean size which is no larger than that of the mean primary droplet size of the initial emulsion, and are therefore unlikely to have undergone coalescence.

Another intriguing difference between the two emulsions is that, at rolling times greater than 1000 h, the $\Phi_{IM} = 50\%$ sample develops large droplets and colloidal "shells", both of which can be seen in the micrograph in Fig. 6.10 (top right), whilst the $\Phi_{IM} = 10\%$ sample develops neither of these, as shown in Fig. 6.10 (top left). Figure 6.10 (bottom) shows a confocal micrograph of a colloidal shell. The colloidal shells are folded and buckled sheets of particles, and appear to be the left-behind particle layers of droplets which have coalesced with the resolved oil. These shells appear to be formed from aggregated particles, and are possibly the remaining shells of large droplets where the internal phase has coalesced with the resolved oil, leaving behind the particles which have formed bonded sheets so that the oil-water interface is no longer necessary to maintain the particles' structure, as in monogels [139]. Similar structures have been reported by Xu *et al.*, upon removing the internal phase from millimetre-sized droplets in a water-

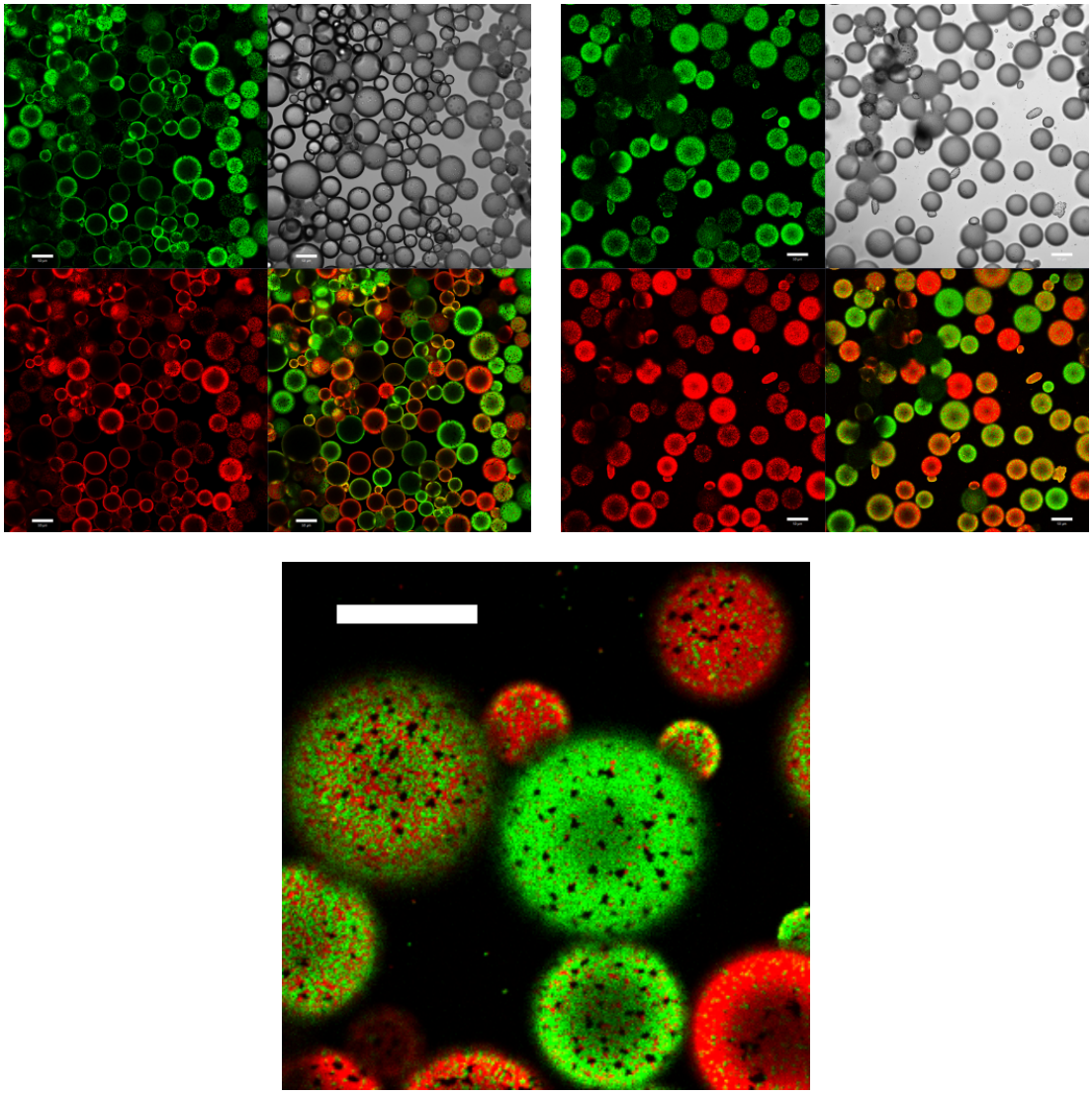

Figure 6.9 *Confocal micrographs of samples with* $\Phi_{IM} = 10\%$ *and* $\Phi_{IM} = 50\%$ *following deaggregation. Top left:* $\Phi_{IM} = 10\%$ *sample following* 185 *h of rolling. Top right:* $\Phi_{IM} = 50\%$ *sample following* 357 *h of rolling; Bottom: Detail of* $\Phi_{IM} = 10\%$ *sample showing bare patches (dark spots) which are thought to be caused by particle transfer. The scale bars are* 50 μm.

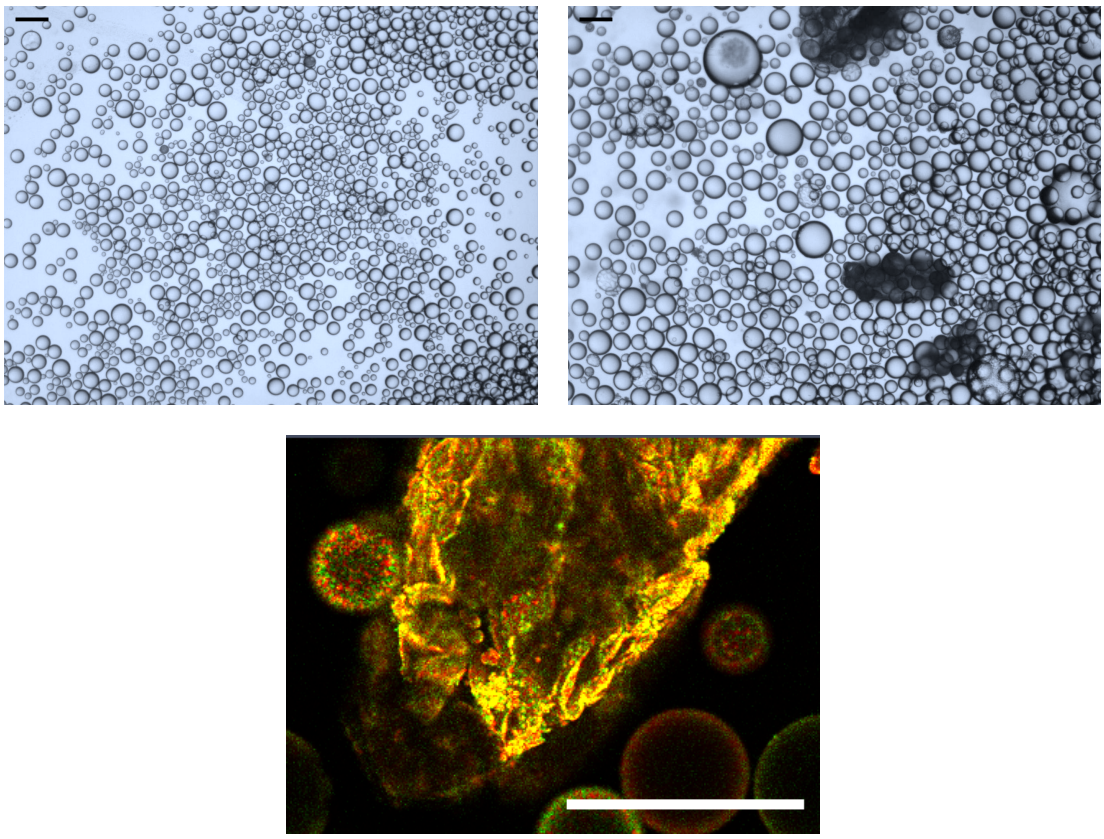

Figure 6.10 *Top row: Micrographs of the* $\Phi_{IM} = 10\%$ *(left) and* $\Phi_{IM} = 50\%$ *(right) samples following* 3400 *h of rolling. Large droplets can be seen in the* $\Phi_{IM} = 50\%$ *sample, as can several of the colloidal "shells" (large dark areas, the two lower ones are out of focus). No such artefacts are observed in the* $\Phi_{IM} = 10\%$ *sample; Bottom: A confocal micrograph showing one of the colloidal "shells". The scale bars are* 100 μm.

decane system stabilised by polystyrene particles [140]. The presence of these shells demonstrates that the particle layer in the emulsions is solid.

Conclusions: Bridged/bridged The application of gentle shear to Pickering emulsions which have been formed by mixing two strongly bridged precursor emulsions, each stabilised by a differently labelled batch of silica particles, has provided some very interesting insight into the deaggregation behaviour of bridged Pickering emulsions, as summarised in the cartoons shown in Fig. 6.11. These experiments have shown that deaggregation is preceded by a relatively long period of unbridging and rebridging, during which substantial droplet rearrangement and particle transfer takes place. The time taken to deaggregate is seen to be higher in the sample with the higher value of Φ_{IM}, which is thought to be due to the

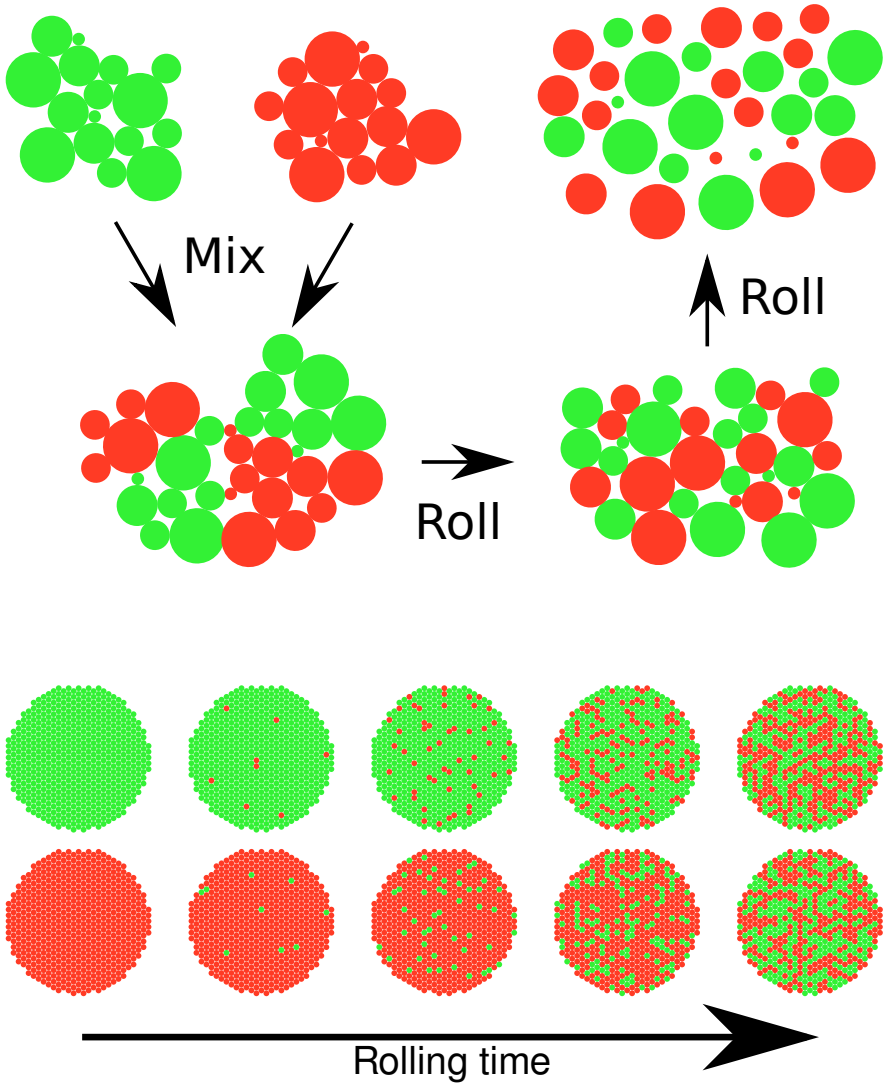

Figure 6.11 *Cartoons showing the effects of rolling on bridged/bridged samples. Top: Clusters of droplets become significantly more mixed as the sample is rolled, due to an unbridging/rebridging process; Bottom: Simultaneously, individual droplets become more heterogeneous as the sample is rolled, due to particle transfer between droplets.*

increased strength of the particle bridges in this sample, and so the deaggregation time can be tuned by modifying the particle wettability. Deaggregation is also probably accelerated in these experiments by a gradual decrease in contact angle due to the particles becoming more hydrophilic as they are immersed in water, but deaggregation should occur eventually without a change in wettability, as was seen in Chapter 5.

The sample with the higher value of Φ_{IM} is also observed to have significantly slower droplet rearrangement within clusters of droplets, and a slower rate of particle transfer between droplets as well. These observations both fit well with the theory that the particle bridges are stronger in the sample with the higher value of Φ_{IM}, which leads to less unbridging/rebridging events and hence a slower rate of rearrangement. The main driver of droplet heterogeneity is the transfer of particles between droplets, since the increase in heterogeneity is gradual.

Although differences between the $\Phi_{IM} = 10\%$ and the $\Phi_{IM} = 50\%$ sample have been noted and explained, the phase behaviour of the two emulsions is admittedly quite similar and it would therefore be desirable to extend the range of isopropyl myristate volume fractions studied in this type of experiment, particularly to lower values (*e.g.,* 0% and 1%). This would allow comparisons with non-bridging and weakly bridging emulsions, but issues with free silica remaining in the aqueous phase would need to be overcome. In the next section, samples with $\Phi_{IM} = 10\%$ and 50% will be studied at a higher value of ϕ_p, which causes one of the precursor emulsions to be non-bridged.

6.3.1.2 Bridged/non-bridged

A similar set of experiments was also carried out with particle volume fractions of 0.9%. In both the $\Phi_{IM} = 10\%$ and the $\Phi_{IM} = 50\%$ samples, the RITC-labelled precursor emulsions were almost completely non-bridged and the FITC-labelled precursor emulsions were strongly bridged. This difference in phase behaviour is caused by the slightly differing wettabilities of the two batches of particles, with the FITC-labelled particles being slightly more hydrophobic, which causes them to form stronger particle bridges. The reason for this difference may be that the RITC carries a charge, which causes the RITC-labelled particles to be slightly more hydrophilic, although APS is added in excess in both syntheses and so is expected to have a dominant effect upon the particles' surface chemistry in both cases. The differing particle wettabilities provide an opportunity to study the

behaviour of a deaggregating bridged emulsion in the presence of a large number of non-bridged droplets, and to test hypotheses about the unbridging/rebridging process, since if this process is indeed occurring, one would expect to see droplets from the non-bridging precursor emulsion become incorporated into the clusters. Other effects caused by changing the particle volume fraction will be discussed in Section 6.3.3.

The apparent size distributions of these samples are shown in Fig. 6.12 for various rolling times. In both cases, the apparent droplet size distributions do not change drastically with rolling time, and some of the changes which are observed can be attributed to the randomness inherent when sampling a bidisperse sample using a pipette. Nevertheless, the decrease in the relative volume of droplets with an apparent diameter greater than $\approx 70\ \mu m$ shows that the emulsions deaggregate as they are rolled, with deaggregation taking at least 147 h in both samples.

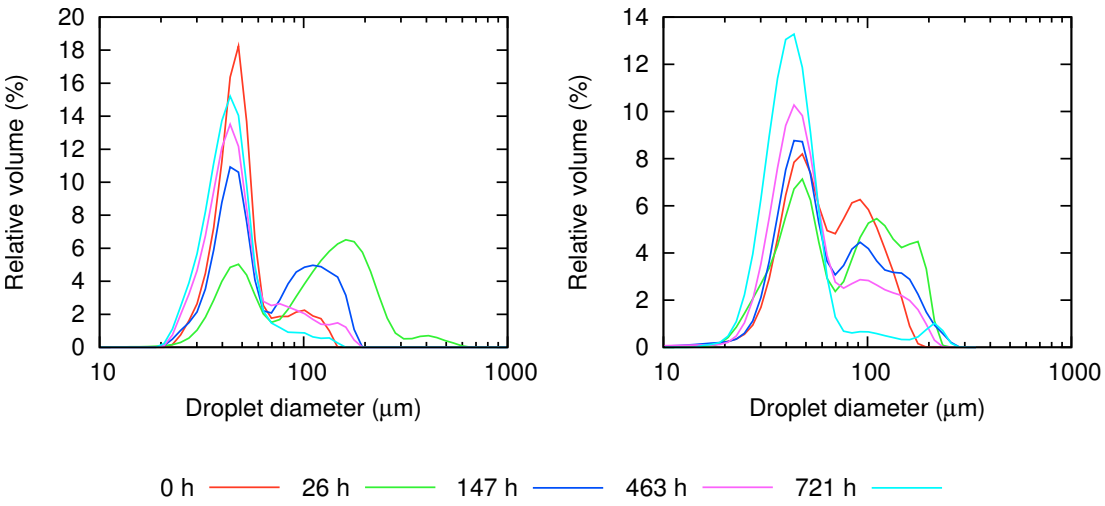

Figure 6.12 *Graphs showing how the apparent droplet size in emulsions with different particle wettabilities changes as the emulsions are rolled. The Φ_{IM} values are 10% (left) and 50% (right). In both cases $\phi_p = 0.9\%$, and both samples are initially a mixture of a bridged emulsion and a non-bridged emulsion.*

Photographs of the samples are shown in Fig. 6.13. There are no rough emulsion-resolved water interfaces because the emulsions are mixtures of strongly bridged and non-bridged droplets and the slowly creaming non-bridged droplets create smooth interfaces. As can be seen in the photographs, this behaviour also creates a colour gradient in the emulsions, which becomes less obvious as the samples deaggregate and the difference in creaming rates decreases. Free silica is also released when the samples deaggregate, and very large oil droplets are seen at

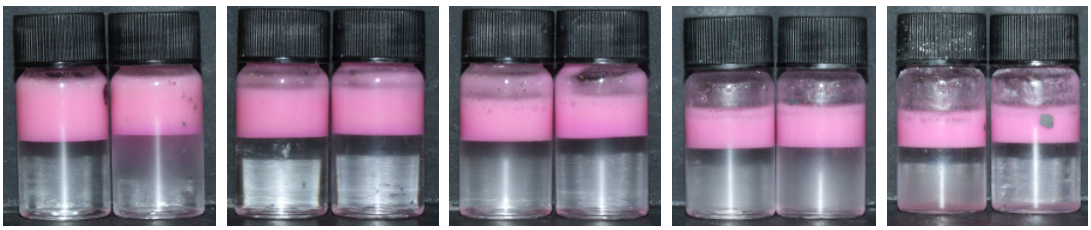

Figure 6.13 *Photographs of the bridged/non-bridged emulsions with* $\phi_p = 0.9\%$. *In each photograph the sample on the left is the* $\Phi_{IM} = 10\%$ *sample and the sample on the right is the* $\Phi_{IM} = 50\%$ *sample. The rolling times are, from left to right,* 1 h, 29 h, 99 h, 463 h *and* 721 h.

the top of the samples, which indicates that coalescence is occurring.

Bright-field microscopy shows that the $\Phi_{IM} = 10\%$ sample does not completely deaggregate until after at least 220 h, as shown in the micrographs in Fig. 6.14. The deaggregation time in the bridged/non-bridged sample is slightly longer than in the bridged/bridged sample (185 h). That the timescales of deaggregation in the bridged/bridged and bridged/non-bridged cases are similar is not surprising, since the yellow precursor emulsions in both cases were strongly bridged and so will take approximately equal times to deaggregate.

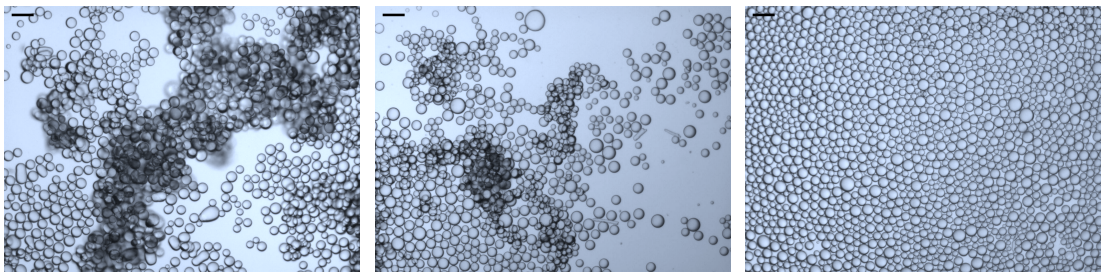

Figure 6.14 *Micrographs of the bridged/non-bridged sample with* $\Phi_{IM} = 10\%$. *The rolling times are, from left to right,* 0 h, 219 h *and* 721 h. *The scale bars are* 100 μm.

As in the bridged/bridged case, the sample with $\Phi_{IM} = 50\%$ takes longer to deaggregate fully than the sample with $\Phi_{IM} = 10\%$ due to the stronger particle bridges in the $\Phi_{IM} = 50\%$ sample. Bright-field microscopy shows that the $\Phi_{IM} = 50\%$ sample does not fully deaggregate until the rolling time is at least 463 h, as can be seen in the micrographs in Fig. 6.15. Again, this deaggregation time is slightly longer than that which was observed in the bridged/bridged system (357 h).

In contrast to the bridged/bridged case, in the bridged/non-bridged case, cluster

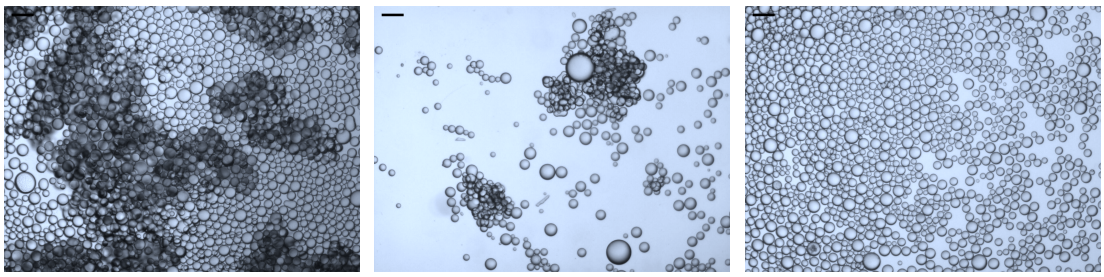

Figure 6.15 *Micrographs of the bridged/non-bridged sample with* $\Phi_{IM} = 50\%$*. The rolling times are, from left to right,* 0 h*,* 463 h *and* 721 h*. The scale bars are* 100 μm*.*

rearrangement does not appear to be significantly slower in the $\Phi_{IM} = 50\%$ sample, relative to the $\Phi_{IM} = 10\%$ sample. However, since the clusters of droplets almost all originate from the same precursor emulsion, cluster rearrangement is not easy to identify in the bridged/non-bridged case. The abundance of non-bridged droplets, which are more mobile than clusters and so more likely to adsorb to a piece of bare interface created by bridge breaking, may also hinder cluster rearrangement. Since the number of free droplets in the $\Phi_{IM} = 10\%$ sample is approximately equal to that of the $\Phi_{IM} = 50\%$ sample, this hindering will be roughly equivalent in the two samples.

Following mixing of the precursor emulsions, droplets from the non-bridged (red) precursor emulsions very quickly become attached to clusters from the bridged (yellow) precursor emulsions, even before the mixed samples are placed on the roller bank, as can be seen in the confocal micrographs in Fig. 6.16 (top row). At early rolling times the red droplets are almost exclusively found near the edges of clusters, where it is easy for them to attach without significant cluster rearrangement. However, after ≈ 150 h of rolling, red droplets are observed to be fully incorporated into the clusters, as shown in Fig. 6.16 (bottom row). This observation confirms that deaggregation is preceded by a period of unbridging and rebridging, as there is no other mechanism by which a droplet from the non-bridged precursor emulsion can become incorporated into a cluster from the bridged precursor emulsion.

Whilst droplets from the non-bridged sample quickly become incorporated into clusters, droplets from the bridged sample mostly remain in the clusters, with the free droplets being primarily from the non-bridged precursor emulsion prior to deaggregation. This can be seen in the confocal micrographs in Fig. 6.17 (top left). As deaggregation progresses, a greater fraction of the free droplets come

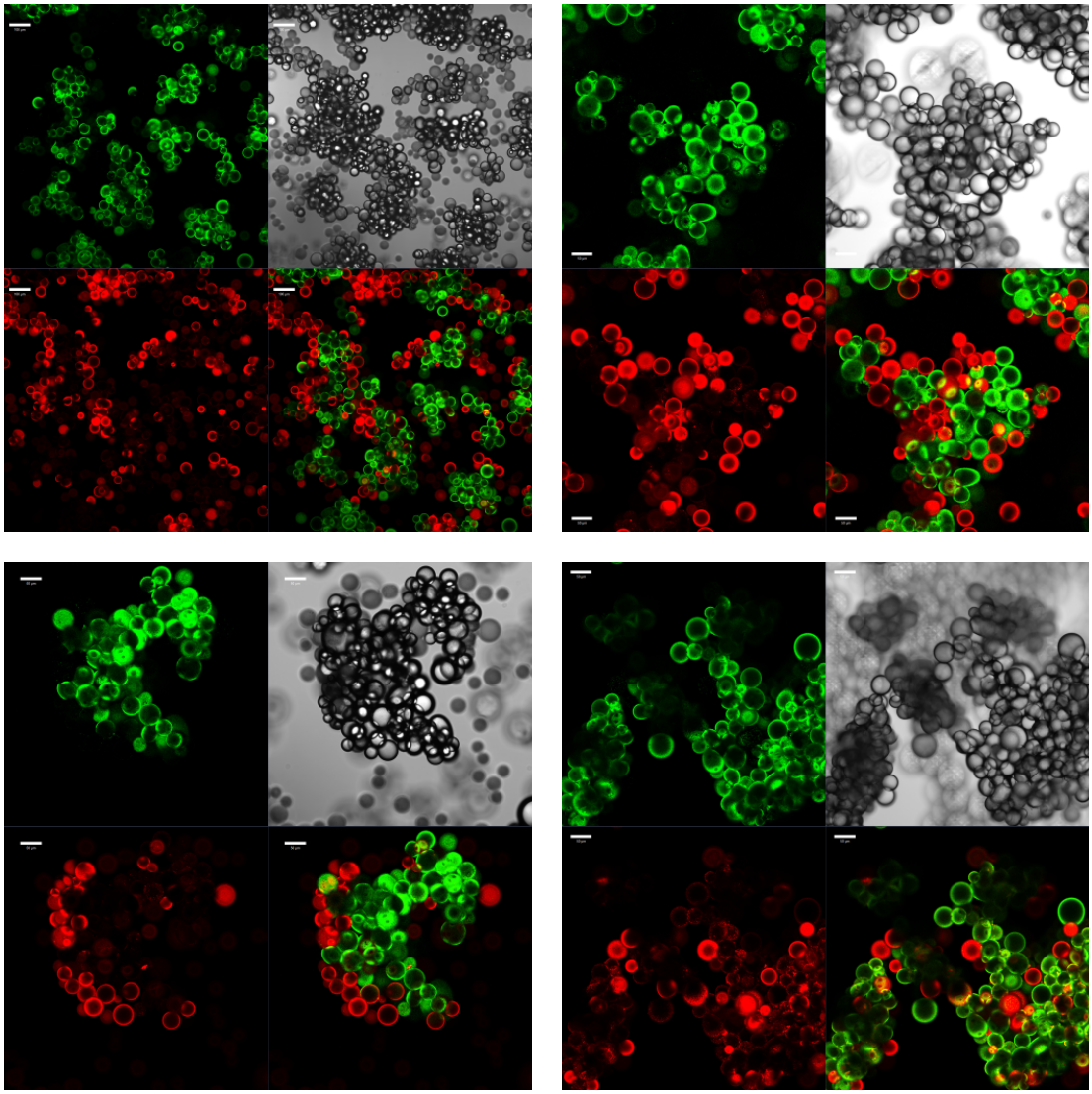

Figure 6.16 *Confocal micrographs of bridged/non-bridged samples showing the rearrangement of droplets and clusters. Top row: Images of the* $\Phi_{IM} = 10\%$ *sample after* 0 *h (left) and* 15 *h (right) of rolling; Bottom row: Images of the* $\Phi_{IM} = 50\%$ *sample after* 1 *h (left) and* 147 *h (right) of rolling. The scale bars are* 50 μm*, except in the top left image, where the scale bars are* 100 μm*.*

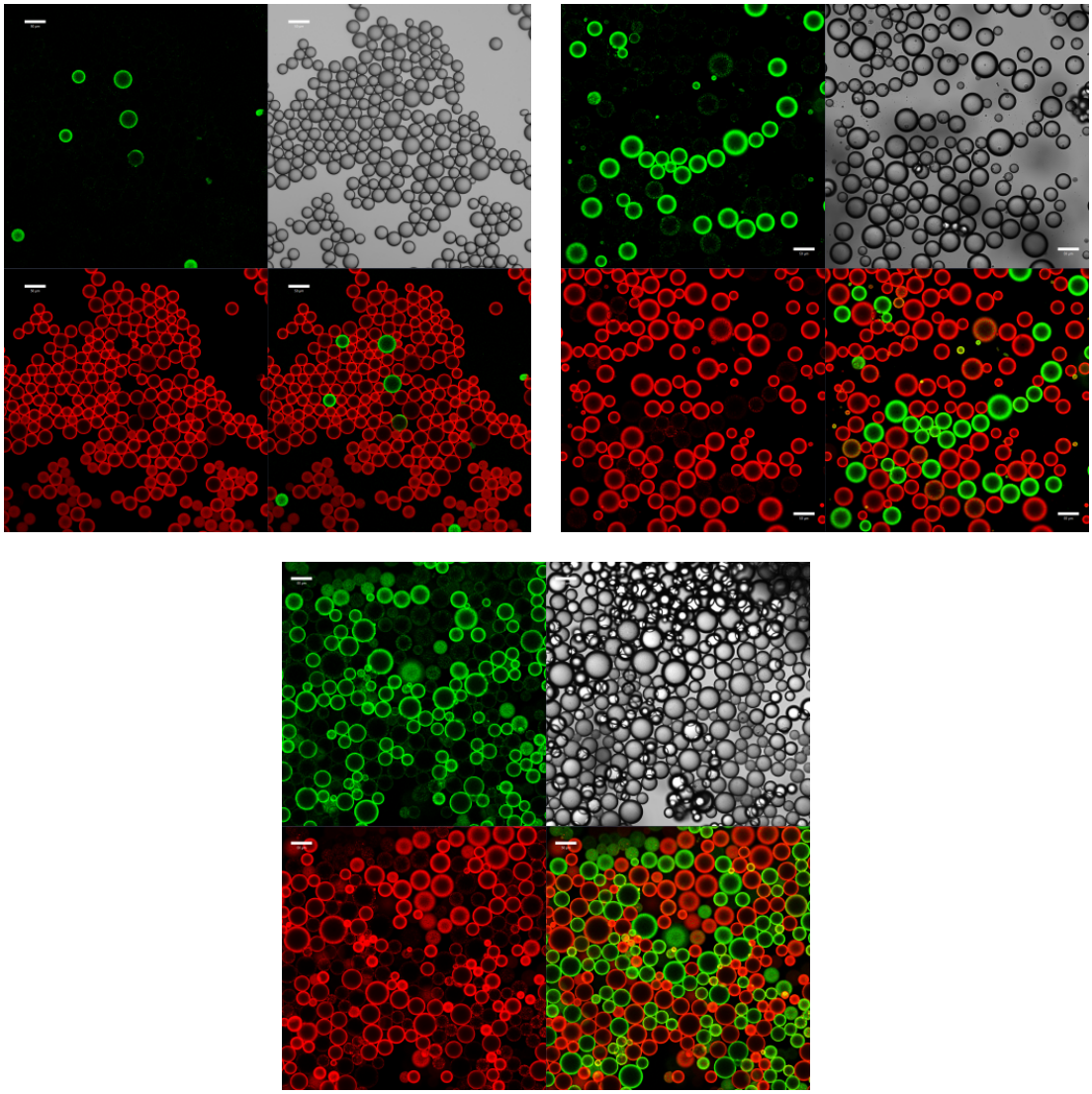

Figure 6.17 *Confocal micrographs of non-bridged droplets in the* $\Phi_{IM} = 50\%$ *sample at various points in the deaggregation process. The rolling times are* 15 *h (top left),* 294 *h (top right) and* 721 *h (bottom). The scale bars are* 50 μm.

from the bridged precursor emulsion and the heterogeneity of the free droplets increases, as shown in Fig. 6.17 (top right and bottom).

As in the bridged/bridged case, droplet heterogeneity in the bridged/non-bridged case is driven almost entirely by particle transfer. In fact, this is more obvious in the bridged/non-bridged case than it is in the bridged/bridged case, where it was not completely clear that coalescence events do not also play a rôle. That particle transfer is the main driver of droplet heterogeneity can be deduced from the slow and gradual increase in heterogeneity with rolling time throughout the experiment, as shown in the confocal micrographs of the $\Phi_{IM} = 10\%$ sample in Fig. 6.18. A very similar trend is observed in the $\Phi_{IM} = 50\%$ sample. There is no discernible difference in heterogeneity between droplets from the bridged and non-bridged precursor emulsions, which suggests that particle transfer occurs during collisions between droplets which do not result in the formation of particle bridges.

The rate of particle transfer appears to be slightly lower in the sample with $\Phi_{IM} = 50\%$ than in the sample with $\Phi_{IM} = 10\%$, which can be attributed to the stronger particle bridges in this sample causing a lower rate of unbridging and rebridging. This difference can be seen in the confocal micrographs in Fig. 6.19.

Janus droplets are observed considerably less frequently when $\phi_p = 0.9\%$ than when $\phi_p = 0.6\%$. This is possibly because the non-bridging droplets are more likely to be fully coated than the droplets in bridged precursor emulsions, and are therefore more likely to attach to the outside of a cluster without coalescing. It is also possible that the increased particle volume fraction means that the bridged precursor emulsion droplets are also more fully coated, which will also decrease the amount of coalescence.

Conclusions: Bridged/non-bridged When a non-bridged precursor emulsion is combined with a bridged precursor emulsion, droplets from the non-bridged precursor emulsion almost immediately become attached to clusters of droplets from the bridged precursor emulsion and, after a relatively short rolling time, become fully incorporated into the clusters. This observation confirms that an unbridging/rebridging process precedes deaggregation, as without an unbridging/rebridging process, the non-bridged droplets could not move into the middle of clusters. Eventually, the sample deaggregates, as in the bridged/bridged case. This behaviour is summarised in the cartoon in Fig. 6.20.

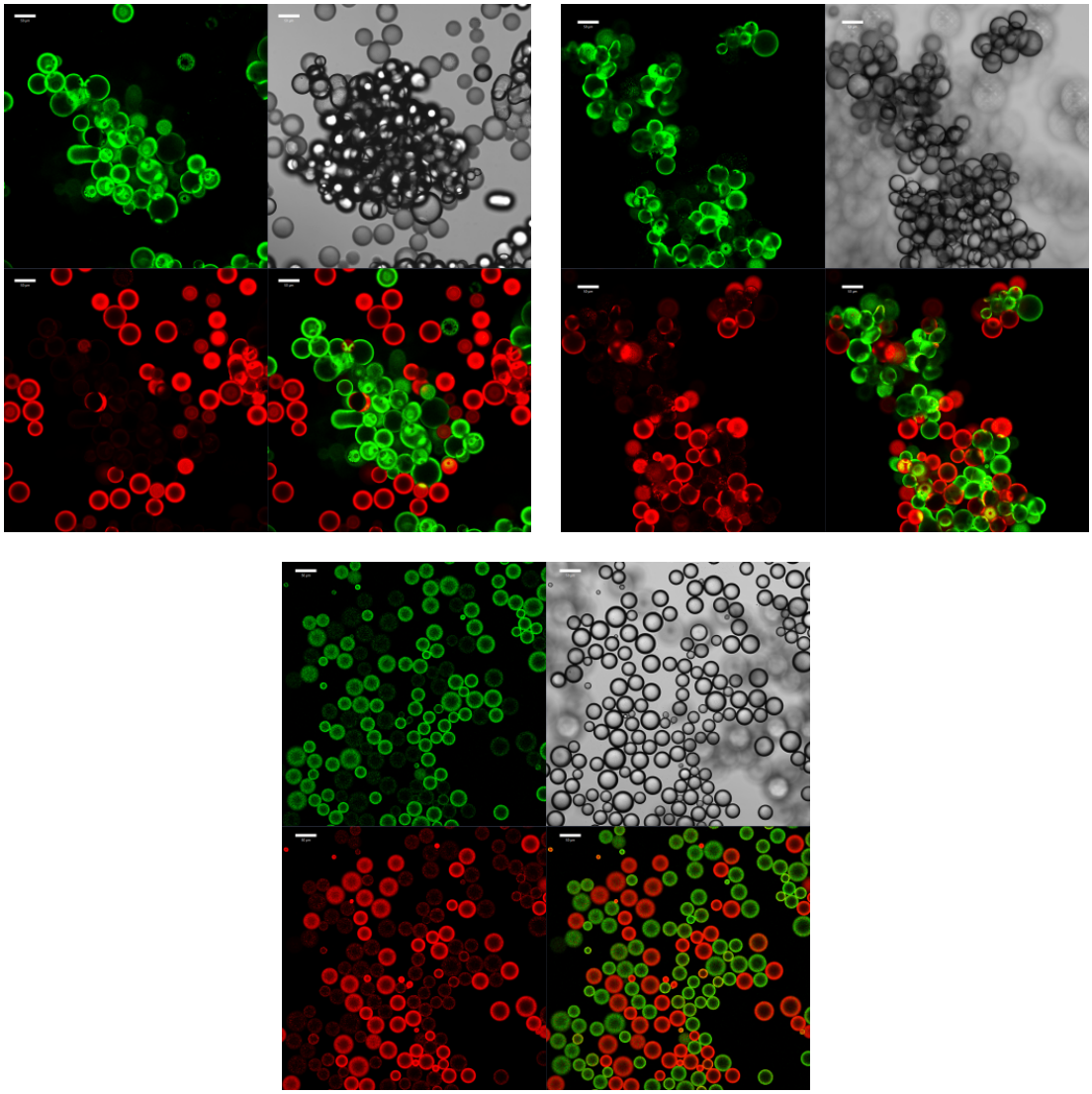

Figure 6.18 *Confocal micrographs taken at various stages of the deaggregation process of the bridged/non-bridged sample with* $\Phi_{IM} = 10\%$. *The rolling times are* 0 *h (top left),* 75 *h (top right) and* 721 *h (bottom). The scale bars are* 50 μm.

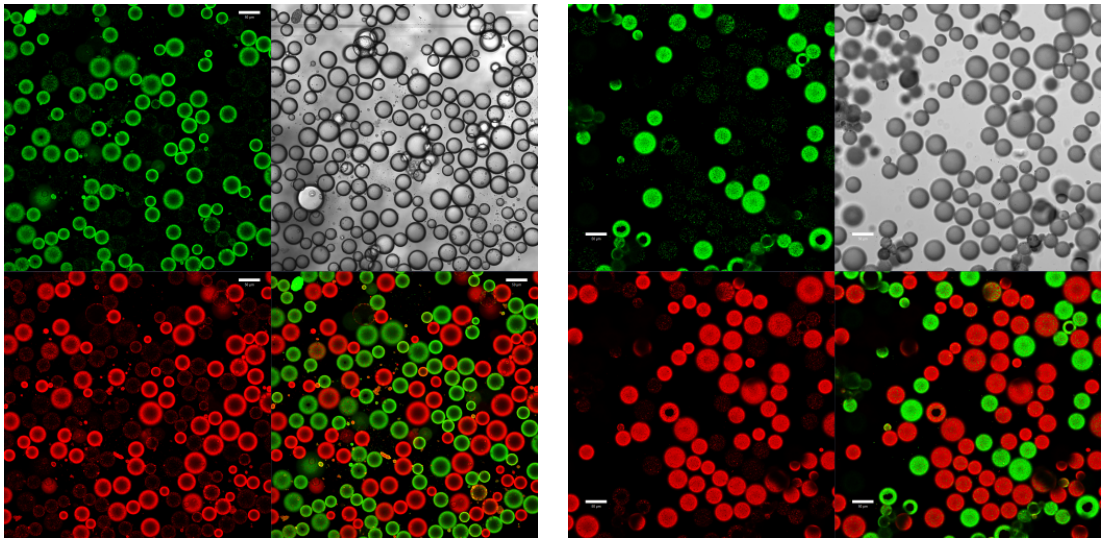

Figure 6.19 *Confocal micrographs showing the difference in rates of particle transfer between bridged/non-bridged samples with different particle wettabilities. The Φ_{IM} values are 10% (left) and 50% (right). The rolling time for both samples is 463 h. The scale bars are 50 μm.*

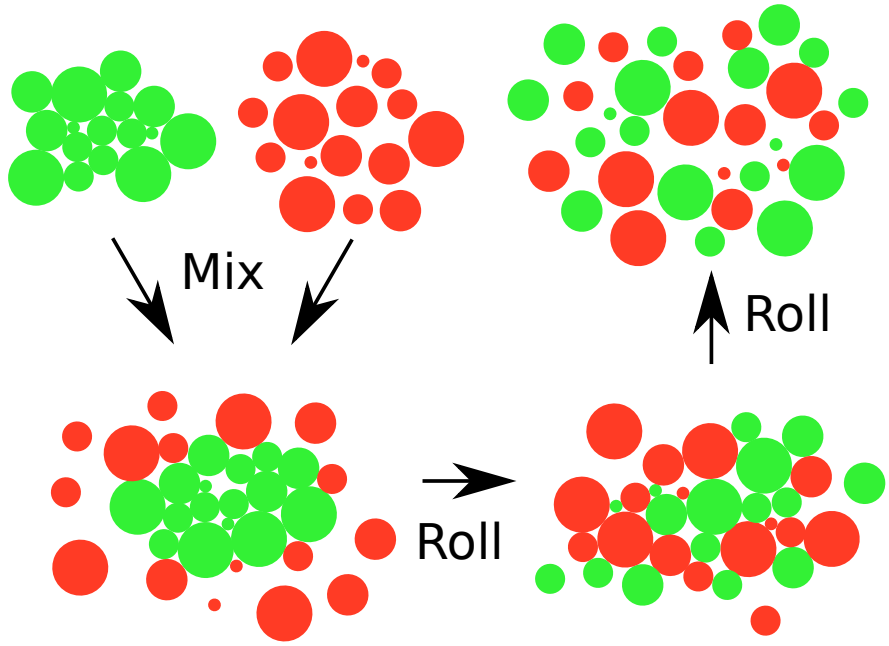

Figure 6.20 *Cartoon showing deaggregation in a bridged/non-bridged emulsion. Droplets from the non-bridged precursor emulsion quickly become attached to the clusters from the bridged precursor emulsion, and the unbridging/rebridging process then leads to fully mixed clusters. Eventually, the sample deaggregates.*

The time taken for the bridged/non-bridged samples to deaggregate is greater than for the bridged/bridged case, which is thought to be because free droplets prolong the lifetime of the bridged system by being more likely to attach to bare patches on a droplet cluster. However, discrepancies in the initial particle wettabilities between the bridged/bridged and bridged/non-bridged samples may contribute to the differing deaggregation times. As in the bridged/bridged case, the increase in droplet heterogeneity in the bridged/non-bridged case is driven almost exclusively by particle transfer, rather than coalescence. Finally, droplets from the non-bridged precursor emulsion are observed to be just as heterogeneous as those from the bridged precursor emulsion, and this suggests that particle transfer can occur without the formation of a stable bridge.

6.3.2 Aged emulsions

It is known that the Stöber silica particles become more hydrophilic whilst they are immersed in water [13], and so ageing the emulsions prior to mixing will allow the effect that this change in hydrophilicity has on the deaggregation and stability of the emulsions to be analysed. Therefore some samples were left to age at room temperature for two months before being mixed and placed on the roller bank. Ageing the samples in this way will also make the particles more likely to become trapped in van der Waals minima, which may cause the particle interfaces to form bonded sheets.

Two samples were used in this experiment, both with $\phi_o = 20\%$ and $\Phi_{IM} = 50\%$, and with particle volume fractions of 0.6% and 1.1%. The precursor emulsions were emulsified, characterised and then left at room temperature for 57 days. Following this period, the precursor emulsions were mixed together and placed on a roller bank.

This two month period is an order of magnitude greater than the rolling time which was necessary to deaggregate other samples, and is approximately a factor of three to four greater than the time elapsed since emulsification of these samples at the point of deaggregation (taking into account both the rolling time and time spent between rolling periods). Therefore, if the deaggregation process is actually effected mainly by a change in contact angle rather than low shear, then the aged samples should deaggregate immediately. If, however, the variation in particle wettability plays no part in the onset of deaggregation, then the aged samples should take the same length of rolling time to cause deaggregation. Additionally,

if the contact line of the particles at the interface is pinned and the particles do not diffuse rotationally, then the surface chemistry of the particles may become heterogeneous, with the areas which are exposed to the aqueous phase becoming more hydrophilic than the areas which protrude into the oil phase. This may even lead to a prolonging of the bridged system, since an amphiphilic particle will be more strongly trapped at the interface [4].

Both of the precursor emulsions which were mixed to form the sample with $\phi_p = 0.6\%$ were strongly bridged, with rough interfaces between the emulsion and the aqueous phase. With the $\phi_p = 1.1\%$ precursor emulsions, the red sample is non-bridged and the yellow sample is partially bridged (approximately 30% of droplets were bridged, estimated from light scattering). The size distributions of the samples are shown in Fig. 6.21 for various rolling times.

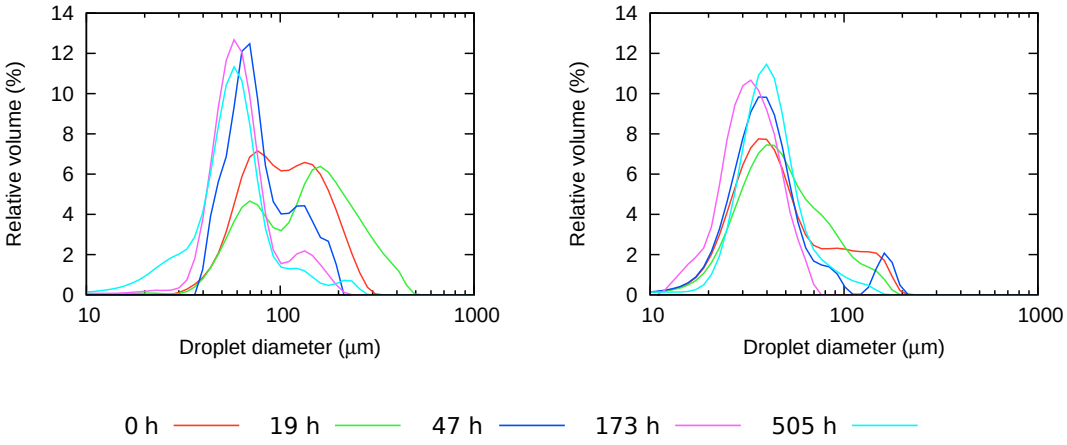

Figure 6.21 *Graphs showing changes in the apparent droplet size distributions in emulsions which have been aged for two months, as the emulsions are rolled. The particle volume fractions are* 0.6% *(left) and* 1.1% *(right).*

Photographs of the samples at various stages of the deaggregation process are shown in Fig. 6.22 and bright-field micrographs are shown in Fig. 6.23. It can be seen that the $\phi_p = 0.6\%$ sample initially has a rough emulsion-resolved water interface, which becomes smoother as the sample deaggregates. It also appears that the red droplets in this sample deaggregate before the yellow droplets, since a colour gradient can be seen in some photographs, and this gradient disappears as the yellow droplets also deaggregate. This two-stage deaggregation process is presumably caused by the RITC-labelled particles being slightly more hydrophilic than the FITC-labelled particles. It can also be seen that free silica appears in the aqueous phase of the $\phi_p = 0.6\%$ sample after approximately 173 h of rolling,

Figure 6.22 *Photographs of the aged emulsions. In each photograph the sample on the left is the $\phi_p = 0.6\%$ sample and the sample on the right is the $\phi_p = 1.1\%$ sample. The rolling times are, from left to right, 0 h, 19 h, 52 h, 173 h and 505 h.*

which coincides with the end of the deaggregation process. Free silica is visible in the $\phi_p = 1.1\%$ sample at all rolling times but the amount of free silica increases considerably following deaggregation.

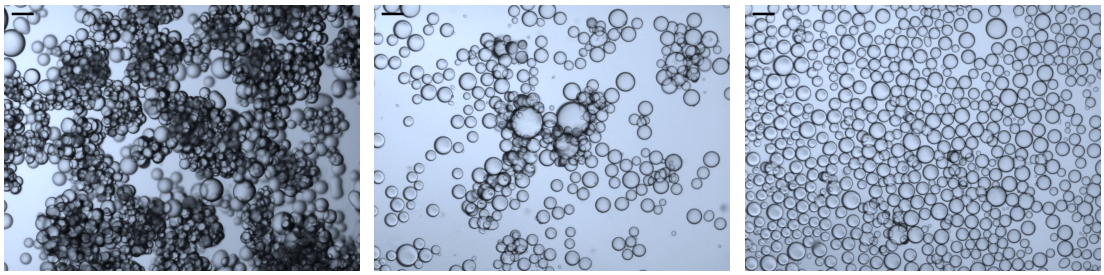

Figure 6.23 *Micrographs of the aged emulsion with $\phi_p = 0.6\%$ at various stages of the deaggregation process. The rolling times are, from left to right, 0 h, 173 h and 340 h. The scale bars are 100 μm.*

There is notably less particle transfer observable in the $\phi_p = 1.1\%$ sample than in the $\phi_p = 0.6\%$ sample, as shown in the confocal micrographs in Fig. 6.24. The difference in particle transfer rates is because there are fewer particle bridges in the $\phi_p = 1.1\%$ sample, which means that the rate at which unbridging/rebridging events occur is lowered, and so particle transfer occurs more slowly. The effects of varying ϕ_p will be discussed further in Section 6.3.3.

Conclusions: Ageing The $\phi_p = 0.6\%$ sample which was aged for two months prior to being placed on the roller bank did not fully deaggregate until after at least 172 h of rolling. This is very similar to the 185 h of rolling required to fully deaggregate the non-aged $\phi_p = 0.6\%$ sample. Therefore, it can be concluded that the deaggregation time does not depend on shelf life. One explanation for this result is that the particles are not able to diffuse rotationally at the interface, possibly because the particles are jammed or have become trapped in

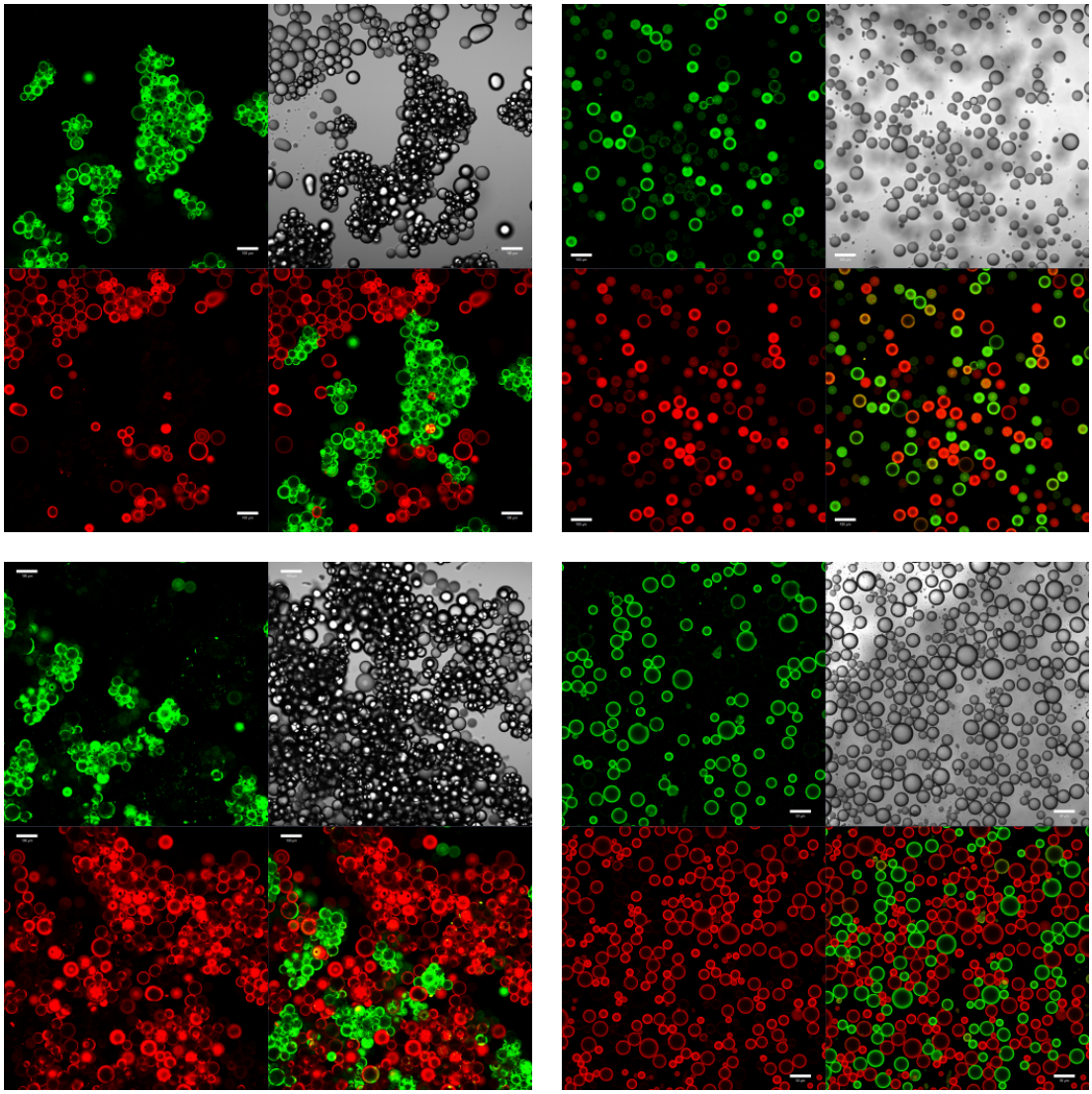

Figure 6.24 *Confocal micrographs of the aged emulsions. Top row: sample with* $\phi_p = 0.6\%$ *after* 0 *h (left) and* 340 *h (right); Bottom row: sample with* $\phi_p = 1.1\%$ *after* 0 *h (left) and* 340 *h (right). The scale bars are* 100 μm.

the primary van der Waals minima of their neighbours. If the particles are not diffusing rotationally, they may develop a Janus-like surface chemistry - with the portions exposed to the aqueous phase becoming more hydrophilic than the portions exposed to the oil phase - which would trap the particles more strongly at the interface.

6.3.3 Particle volume fraction

Comparisons between emulsions differing in particle volume fraction have already been made in Section 6.3.1 and Section 6.3.2, and in this section the effects of particle volume fraction from these and other experiments will be discussed.

Samples were also made with particle volume fractions of 0.3%, 0.6% and 1.1%, and with $\Phi_{IM} = 10\%$. The experiments described below were conducted using different batches of particles from those used in the experiments described in Section 6.3.1 and Section 6.3.2, and so direct comparisons between the different sets of experiments should be avoided because the surface chemistry and hence wettability of the batches of particles may be slightly different.

Varying the particle volume fraction changes the droplet size within the limits set by the shear rate during emulsification, and the likelihood for bridging to occur in an emulsion at a given shear rate (see Chapter 5). The change in droplet size also means that the Laplace pressure of the droplets will change, being higher at higher values of ϕ_p, as given by Eq. (1.1). These changes mean that the droplets in samples with smaller ϕ_p values will be more deformable, which may provide enough elasticity to make deaggregation take longer, although by deforming a Pickering droplet, bare interface will be exposed and this may lead to the emulsion destabilising more readily.

The size of a cluster of droplets as an emulsion is rolled will be determined by the shear rate in the sample and the strength of the particle bridges between droplets, and is expected to be independent of particle volume fraction. This means that the number of droplets in a cluster will increase with ϕ_p, and hence so will the number of particle bridges per cluster. Therefore, one would expect that the droplet rearrangement rate will be lower at higher values of ϕ_p, because if one bridge in a cluster at low ϕ_p breaks, it will lead to the cluster breaking up, whilst if one bridge breaks in a cluster at high ϕ_p, the bridges around it may prevent the cluster from breaking up, and the original bridge is more likely to

reform.

Bright-field microscopy shows that the $\phi_p = 0.3\%$ and $\phi_p = 0.6\%$ samples were both initially fully aggregated and deaggregated fully within 25 h and 144 h of rolling, respectively, whereas the sample with $\phi_p = 1.1\%$ particles was partially aggregated to begin with and did not fully deaggregate until the rolling time as 357 h, as can be seen in Fig. 6.25. Photography also shows that free silica appears in the aqueous phase prior to the end of deaggregation in all three samples. The bright-field micrographs show that the droplet size does not increase significantly during this process, except in the $\phi_p = 0.3\%$ sample, suggesting that coalescence events are mainly occurring with the free oil.

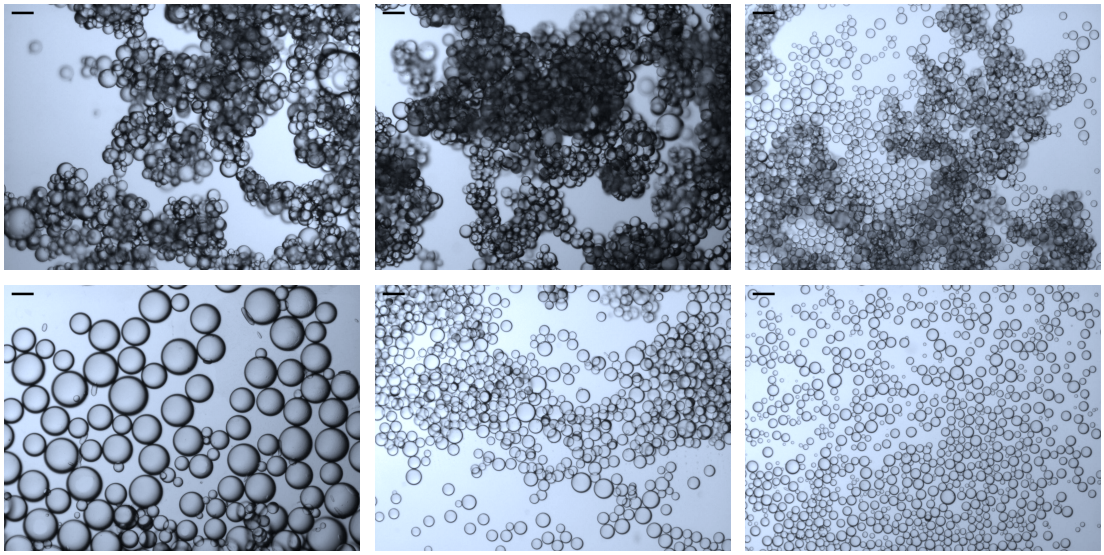

Figure 6.25 *Bright-field micrographs of deaggregating emulsions at varying ϕ_p values. Top row: Samples with $\phi_p = 0.3\%$, 0.6% and 1.1%, from left to right, prior to rolling; Bottom row: Samples with $\phi_p = 0.3\%$, 0.6% and 1.1%, from left to right, after 25 h, 144 h and 357 h of rolling, respectively. The scale bars are 100 μm.*

As can be seen in Fig. 6.26 (top row), in the $\phi_p = 0.6\%$ sample the clusters are generally non-mixed following the mixing of the precursor emulsions ($g' \approx 1$), but are relatively mixed after 1 h, which is the only other measurement time at which the sample was significantly bridged. In the $\phi_p = 1.1\%$ sample, the clusters are slightly mixed following mixing of the precursor emulsions, with many of the clusters being Janus-like in appearance, so that $f' \approx 0$, but $g' \approx 1$, as can be seen in Fig. 6.26 (bottom row). The increased rate of droplet rearrangement in the $\phi_p = 1.1\%$ sample can be explained by the large fraction of non-bridged droplets in this sample. Both precursor emulsions in the ϕ_p sample are partially bridged, and it might therefore be expected that this system behaves in a similar manner

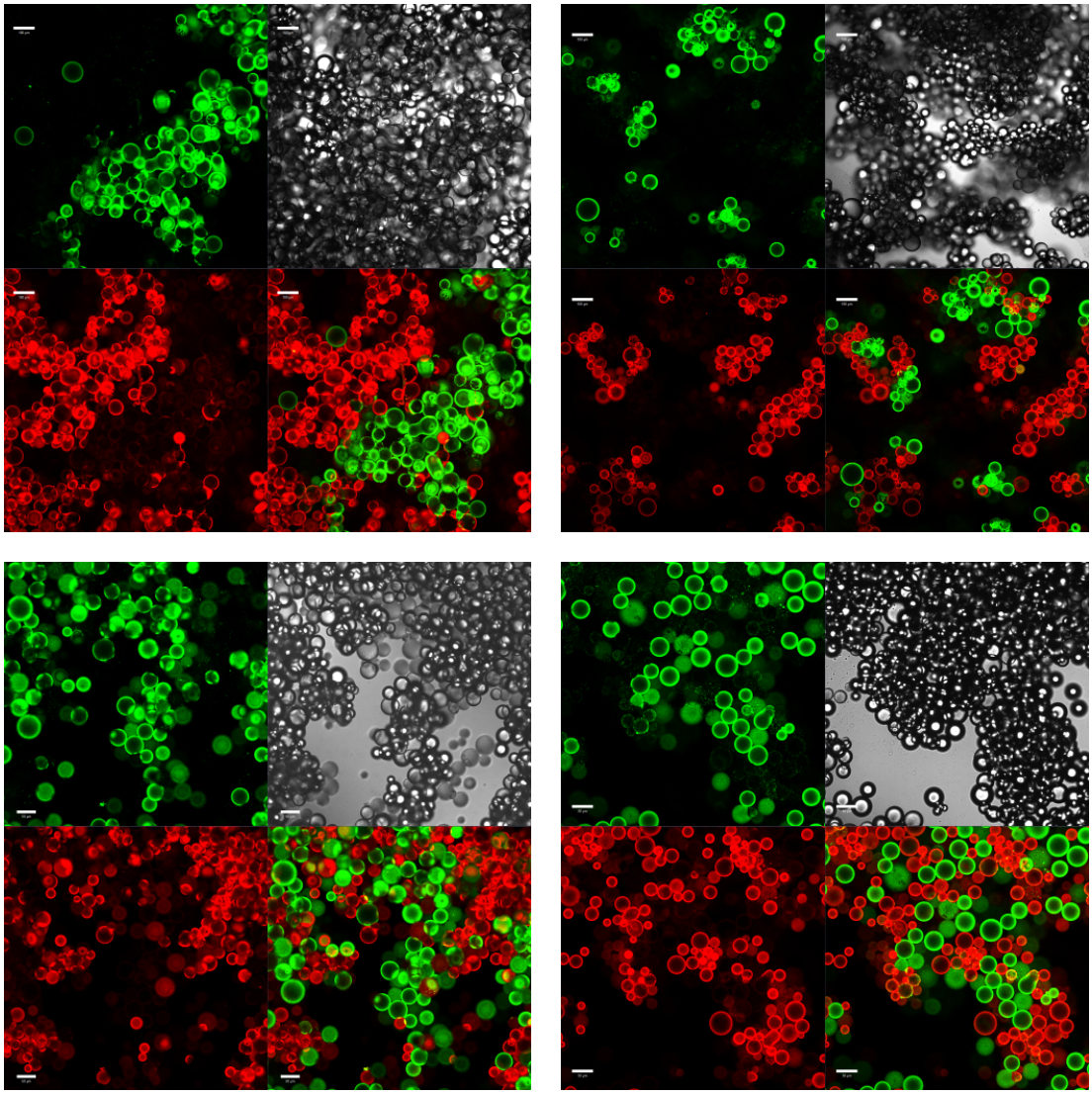

Figure 6.26 *Confocal micrographs of deaggregating emulsions at varying particle volume fractions. Top row: Sample with* $\phi_p = 0.6\%$ *after* 0 *h (left) and* 1 *h (right) of rolling; Bottom row: Sample with* $\phi_p = 1.1\%$ *after* 0 *h (left) and* 23 *h (right) of rolling. The scale bars are* 100 μm *(top row) and* 50 μm *(bottom row).*

to the bridged/non-bridged system described in Section 6.3.1, where non-bridged droplets attached themselves to the fringes of clusters but g' remains relatively high up until deaggregation. However, since it is not possible in this case to differentiate between droplets which were initially bridged and non-bridged, it is not possible to fully evaluate if this situation is what actually happens. Due to the large droplet size and short deaggregation time in the $\phi_p = 0.3\%$ sample, it has not been possible to deduce any useful information about the degree of mixing of the clusters in the $\phi_p = 0.3\%$ sample.

Significant particle transfer is observed at all values of ϕ_p. In particular, in the $\phi_p = 0.3\%$ sample following ≈ 280 h of rolling both $\bar{f}$ and $\bar{g}$ are approximately 0, as can be seen in the confocal micrograph in Fig. 6.27 (top left). In contrast, the droplets in the $\phi_p = 0.6\%$ and $\phi_p = 1.1\%$ samples are all clearly dominated by one colour, even at rolling times greater than 600 h, as shown in Fig. 6.27 (top right and bottom). As was also observed above, the rate of particle transfer is greater prior to deaggregation, when unbridging and rebridging events are common.

Conclusions: Particle volume fraction By comparing emulsions with $\phi_p = 0.3\%$ and 0.6%, it can be concluded that particle volume fraction makes little difference to the deaggregation process when the emulsions are almost completely bridged, or that the differences occur between 1 h and 24 h of rolling. However, by increasing ϕ_p so that the emulsion is only partially bridged, the deaggregation process does change.

At particle volume fractions low enough to produce strongly bridged emulsions, the rate of deaggregation is slower at higher values of ϕ_p. This result is attributed to the increased strength of a cluster of small droplets held together by particle bridges, relative to a similarly sized cluster of larger droplets which is also held together by particle bridges. Free droplets may also hinder deaggregation, and will be more prevalent at higher particle volume fractions. This reasoning is also thought to explain the slower rearrangement of clusters observed at higher values of ϕ_p.

Droplets are also observed to be more heterogeneous following deaggregation at low values of ϕ_p. As with other samples, the main driver of droplet heterogeneity appears to be particle transfer, although coalescence may also play a significant rôle in the $\phi_p = 0.3\%$ sample. The main explanation for this behaviour is thought to be that more unbridging/rebridging events take place in the samples with lower

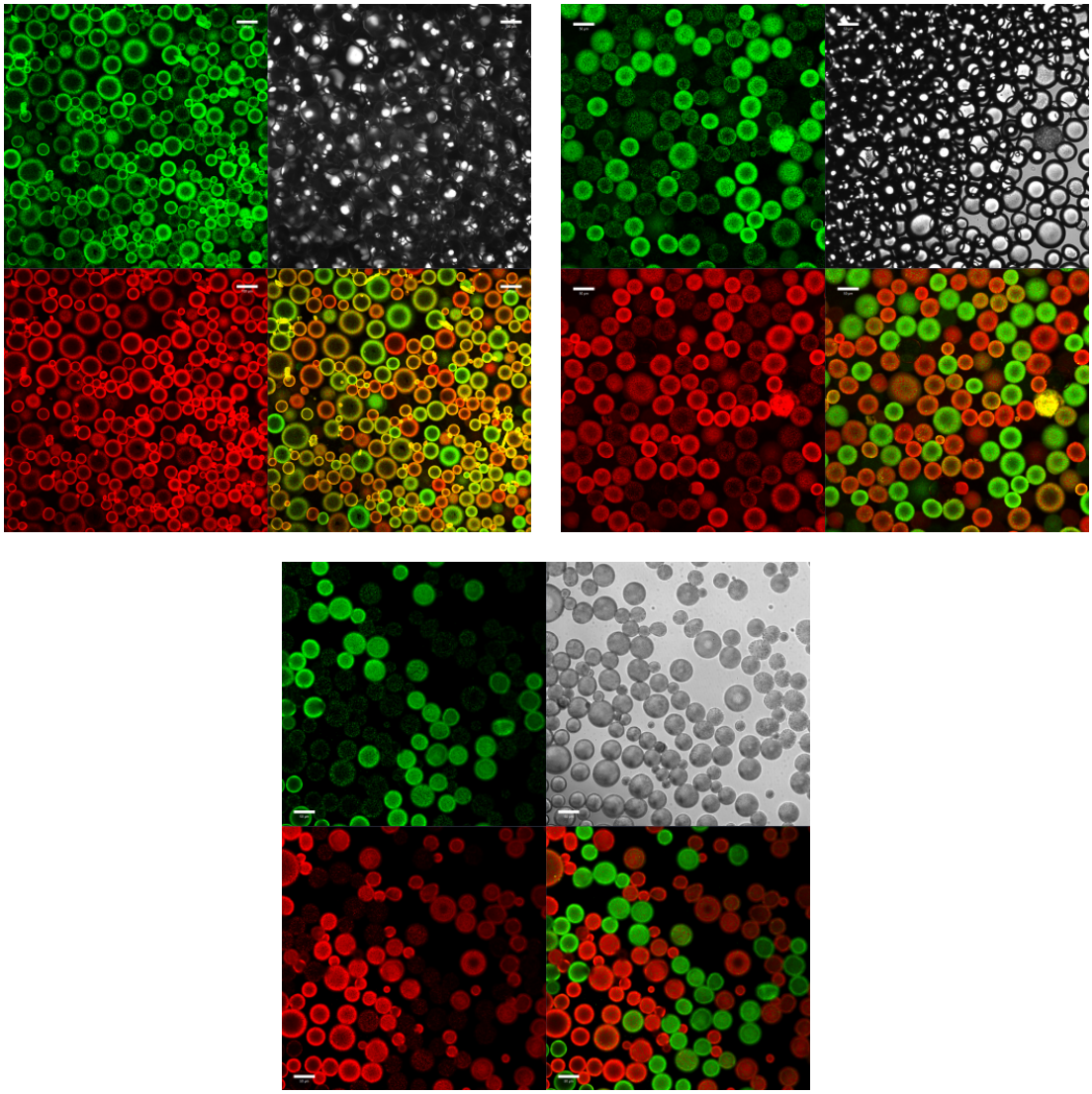

Figure 6.27 *Confocal micrographs of deaggregating emulsions at varying particle volume fractions, at long rolling times. The samples have* ϕ_p *values of* 0.3% *(top left),* 0.6% *(top right) and* 1.1% *(bottom), and have been rolled for* 283 h, 646 h *and* 717 h *respectively. The scale bars are* 100 μm *(top left) and* 50 μm *(top right and bottom).*

values of ϕ_p, since the probability of any given bridge being broken is greater, as there are more bridges in a cluster of a given size when ϕ_p is higher. Furthermore, when the particle volume fraction is lower, the contact area between colliding droplets is larger, and this increases the probability of particles transferring.

6.3.4 Salt concentration

A series of samples was made with sodium chloride concentrations of 10 mM and 30 mM. In both samples $\phi_o = 20\%$, $\phi_p = 0.6\%$ and $\Phi_{IM} = 10\%$, and the salt was added before the particles were dispersed. These parameters were set so that the samples can be easily compared to the $\phi_p = 0.6\%$ sample with no sodium chloride described in Section 6.3.1. Sodium chloride concentrations greater than 30 mM were not studied here because they lead to emulsions which are unstable, for the reasons described in Chapter 4.

By adding salt to the samples, the contact angle is lowered (see Chapter 3) and the particles are less likely to form bridges (see Chapter 5). It is expected that the samples with salt included will deaggregate more quickly and then coalesce more readily than those without salt. However, the strength of the interactions between particles at the interface of a Pickering droplet may increase when the aqueous phase contains salt. The addition of salt means that particle aggregation is more likely and that the particles sit further into the aqueous phase, so that their interactions at the interface are dominated by their interactions through the aqueous phase. When the salt concentration in the aqueous phase is high enough to prevent particle bridging, and if the droplets are fully coated with particles, there will be no unbridging/rebridging process and so it is expected that very little particle transfer will be observed and that droplet heterogeneity will instead be driven by coalescence. However, as was seen in Chapter 4, the addition of salt can lead to droplets with a surface coverage which is substantially below that of close packing, and this situation may still lead to particle transfer.

Figure 6.28 shows how the apparent emulsion droplet sizes change as the samples with different salt concentrations are rolled. Less change with rolling time is observed in the apparent size distributions of the samples with salt, due to the lack of particle bridges in these samples. The length of time taken for the apparent droplet size to reach that of the actual droplet size is also shorter because of the lower degree of bridging and because the particle bridges which are in the samples are weaker and so break more easily.

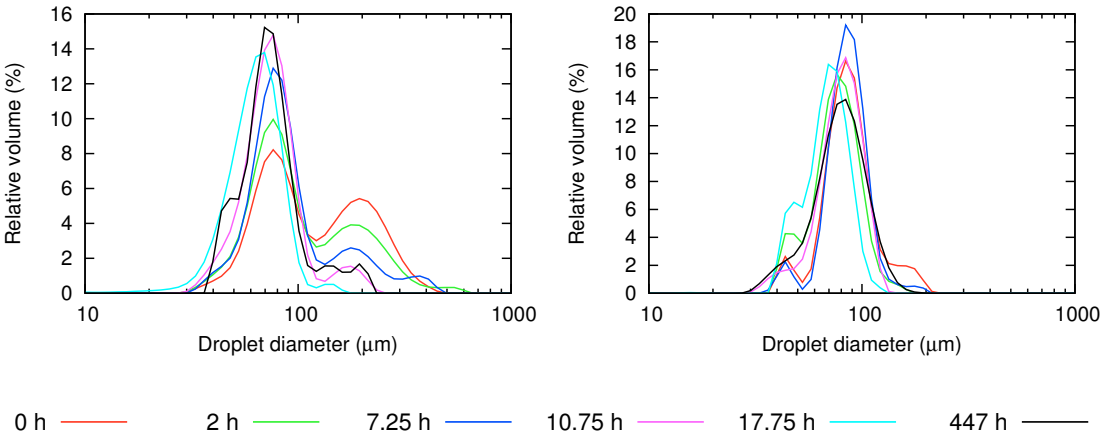

Figure 6.28 *Graphs showing how the apparent droplet size in emulsions with different salt concentrations changes as the emulsions are rolled. The sodium chloride concentrations are* 10 mM *(left) and* 30 mM *(right). In both samples* $\Phi_{IM} = 10\%$ *and* $\phi_p = 0.6\%$.

The precursor emulsions with sodium chloride concentrations of 30 mM were non-bridged. However, the RITC-labelled precursor emulsion with a sodium chloride concentration of 10 mM had a small amount of bridging and the corresponding FITC-labelled precursor emulsion was strongly bridged - which is again because the red particles are slightly more hydrophilic due to the charge of the RITC. The 10 mM sample was observed to deaggregate sooner than the sample with no added salt (after rolling for $\approx$ 4-5 h, rather than $\approx$ 200 h), in agreement with the experiments described in Chapter 4 and Chapter 5. This can be seen from the apparent size distributions shown in Fig. 6.28, and is corroborated by the bright-field micrographs shown in Fig. 6.29.

From Fig. 6.28 it can be seen that, although the 10 mM sample deaggregates quickly, the primary droplet size does not change significantly. Furthermore, the droplet size distribution of the 30 mM sample, which is never aggregated, shows almost no change with rolling time. This lack of change contrasts with the fact that very large droplets of oil can be seen at the top of the samples, as shown in Fig. 6.30 (447 h sample), and the fact that a significant fraction of free oil has resolved at this stage, which shows that coalescence has been taking place. As was discussed in Section 6.2, very large droplets will not be represented in the size distributions due to their buoyancy and the applied shear, which causes them to break up if they do become mixed into the sample. Free silica is also observable in the photographs of the 30 mM sample in Fig. 6.30, which is another sign that coalescence has been happening. It therefore seems that, when salt is included

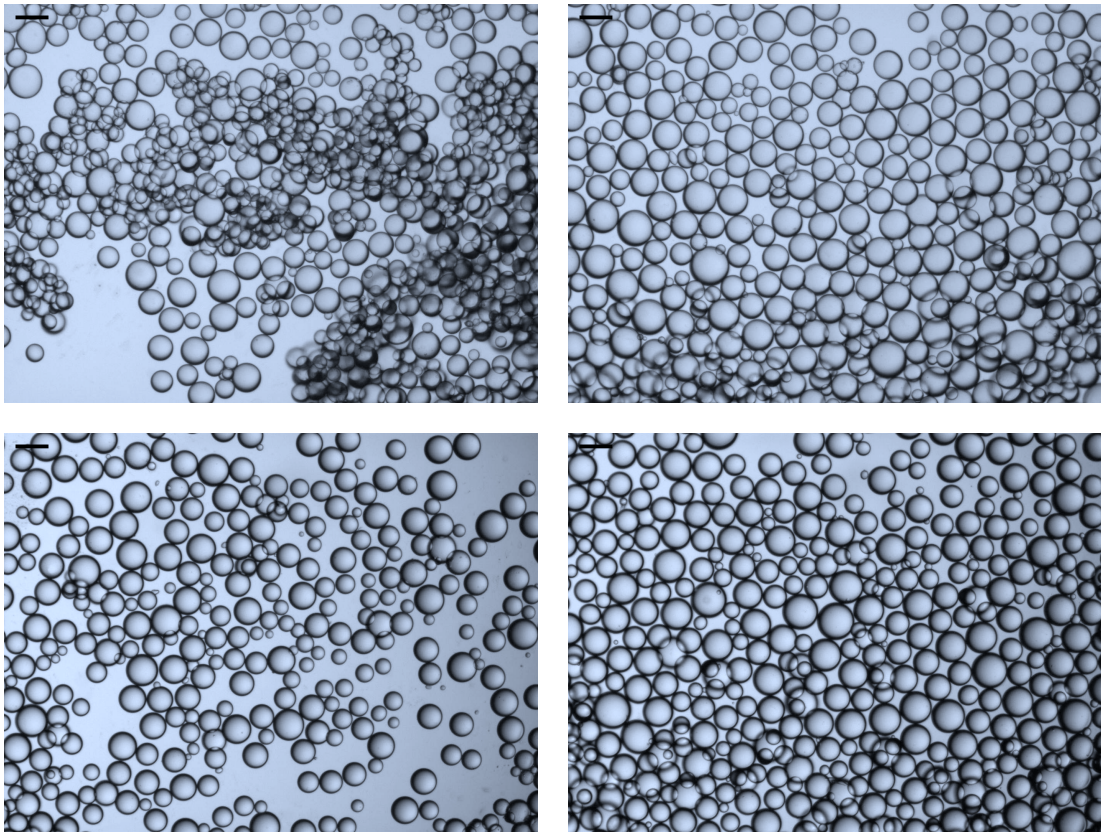

Figure 6.29 *Micrographs showing emulsions with different salt concentrations following* 0 h *(top row) and* 4.25 h *(bottom row) of rolling. Left column: Sample containing* 10 mM *sodium chloride; Right column: Sample with* 30 mM *sodium chloride. The scale bars are* 100 μm.

Figure 6.30 *Photographs showing how emulsions with different salt concentrations change as the emulsions are rolled. In all photographs the sample on the left has a sodium chloride concentration of* 10 mM *and the sample on the right* 30 mM. *The rolling times are, from left to right,* 1 h, 5.25 h, 22.75 h, 38.75 h *and* 447 h.

in the sample, there is no link between the size of a droplet and its likelihood of coalescing with the free oil in the sample. This is in contrast to the situation when there is no salt (*e.g.,* in the $\phi_p = 0.6\%$ sample in Section 6.3.3). Since the particles are expected to aggregate at the interface more strongly when the contact angle is lower, it can be argued that, under certain conditions, the most stable Pickering emulsions will not occur when the contact angle is 90°, despite the particle trapping energy being lowered.

Given the relative ease with which the 10 mM sample deaggregated, it is not surprising that the clusters of droplets in this sample quickly became mixed, with $\bar{g}' \approx 0.3$ after 1 h of rolling, which is significantly lower than the value of $\bar{g}' \approx 0.6$ in the sample with $\Phi_{IM} = 10\%$ which did not contain salt. A confocal micrograph of the 10 mM sample at this stage of deaggregation is shown in Fig. 6.31 (left).

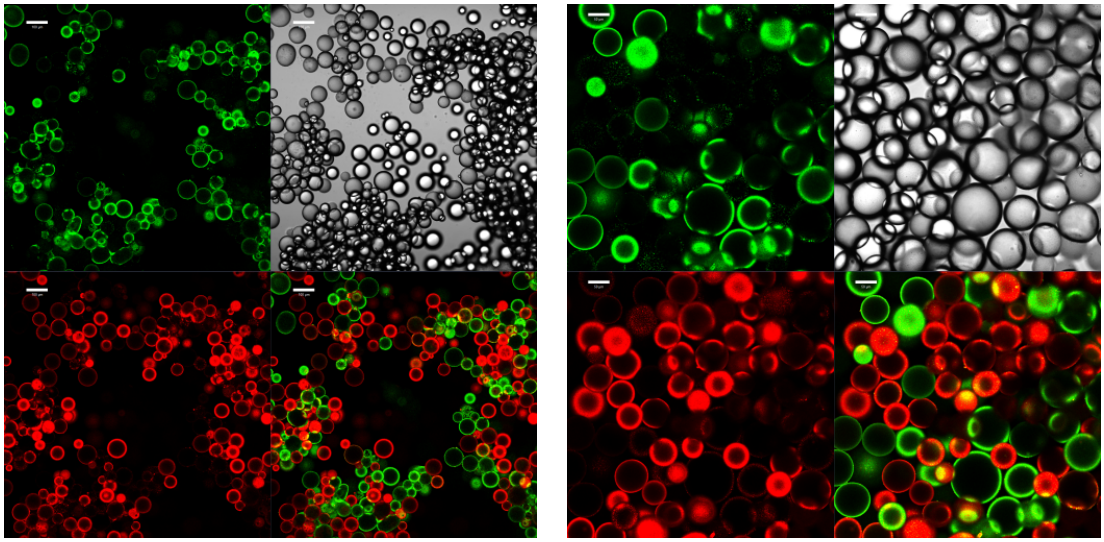

Figure 6.31 *Left: Confocal micrograph of the emulsion containing* 10 mM *of sodium chloride, after* 1 h *of rolling; Right: Confocal micrograph of the emulsion containing* 30 mM *of sodium chloride, after* 735 h *of rolling. The scale bars are* 100 μm *(left) and* 50 μm *(right).*

For a given rolling time, droplets are found to be more homogeneous at higher salt concentrations. For example, in the confocal micrographs shown in Fig. 6.32 it can be seen that the droplets in the 0 mM sample are more heterogeneous than those in the 10 mM sample, which are in turn more heterogeneous than the droplets in the 30 mM sample. This is in spite of the fact that the 0 mM sample had actually been on the roller bank for a total of 185 h, whilst the other two samples had been on the roller bank for a total of 280 h each. These results make sense since the amount of particle redistribution is dependent upon

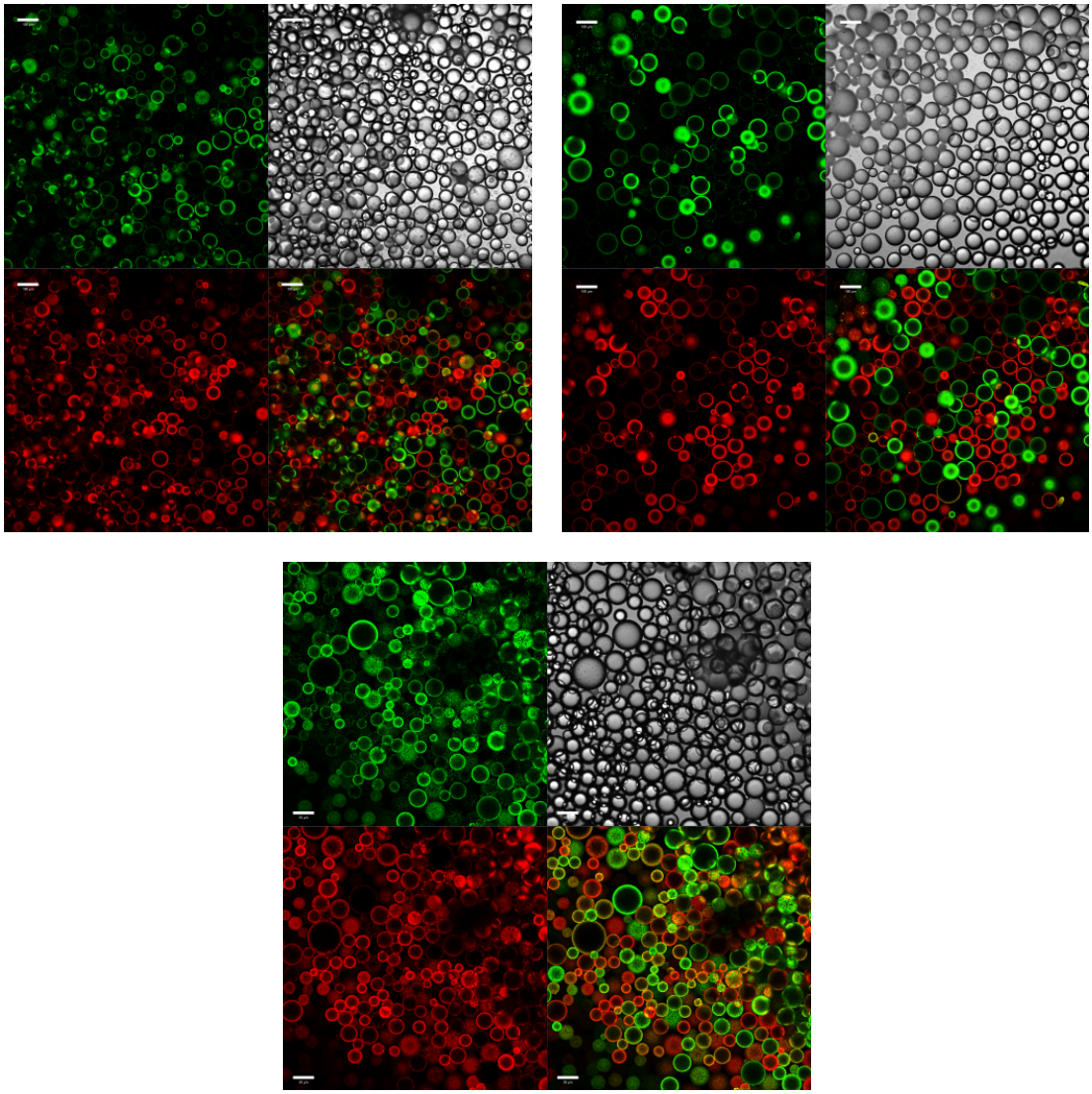

Figure 6.32 *Confocal micrographs of samples with varying salt concentrations. Top row: The* 10 *mM (left) and* 30 *mM (right) samples following* 280 *h of rolling; Bottom: The* 0 *mM sample, following rolling for* 185 *h. The scale bars are* 100 *µm (top row) and* 50 *µm (bottom).*

the degree of bridging in a sample - a non-bridged sample will not undergo the unbridging/rebridging process which accelerates particle transfer. The stability of the 30 mM sample suggests that maximum stability in a Pickering emulsion is not necessarily achieved by using neutrally wetting particles, as in some cases a lower or higher contact angle will result in stronger attractions between the particles at the interface, particularly if the particles can enter into their neighbours' van der Waals minima. This increase in stability in the system described here occurs for different reasons to those given by Binks *et al.* when they argued that particles must be flocculating to create a stable emulsion [39, 41].

It is also worth noting that the rate of particle transfer in the 10 mM samples is greater at earlier rolling times, prior to deaggregation of the sample. This can be explained by the greater rate of particle transfer due to unbridging and rebridging events. The presence of salt also means that the particle bridges in this sample are weaker than in samples with no salt, and this will also lead to a greater rate of particle transfer, since the weaker bridges cause a greater rate of unbridging and rebridging. However, this is balanced by the fact that the lower contact angle decreases the number of bridges in the samples, which will tend to lower the rate of particle transfer.

The droplet size distribution remains largely unchanged whilst the rolling process is occurring, but the droplets' interfaces become gradually less homogeneous. However, it is clear that the heterogeneity is caused mostly by particle transfer rather than coalescence.

Although the droplets are more homogeneous in the samples containing sodium chloride, particle transfer still clearly occurs in both samples, as can be seen in Fig. 6.31 (right) and Fig. 6.32 (top row). Since particle transfer occurs in the 30 mM sample, particle transfer occurs even when neither of the precursor emulsions was bridged. This is despite the large trapping energy of solid particles at an oil-water interface, as given by Eq. (1.3).

Conclusions: Salt The addition of sodium chloride to a sample lowers the particle contact angle and reduces the degree of bridging in the emulsion, as was also shown in Chapter 5. These changes have several important consequences for the deaggregation process. Lowering the particle contact angle causes the particle bridges to be weakened, which means that the emulsion deaggregates more quickly. Furthermore, coalescence is more likely following an unbridging

event at higher salt concentrations, due to the lower Debye length, and this will reduce the likelihood of rebridging. Although weaker particle bridges will make unbridging more likely (which can increase the rate of particle transfer) the samples studied here had a lower rate of particle transfer due to the significant decreases in the number of particle bridges and in the deaggregation time. Since weakening the particle bridges (which will tend to increase the rate of particle transfer) will lead to a decrease in the number of bridges (which will tend to the rate of particle transfer), care needs to be taken when predicting the behaviour of emulsions when the particle wettability is modified. As with the results described previously, droplet heterogeneity in the samples containing sodium chloride is driven by particle transfer rather than coalescence.

When the sodium chloride concentration is 30 mM, neither of the precursor emulsions is bridged, and this means that this sample can be compared to the bridged/bridged and bridged/non-bridged samples described above. Although the lack of bridging in this sample means that the rate of particle transfer is significantly lower than in some samples, particle transfer still occurs, and this shows that particle transfer does not require the creation of a stable particle bridge to occur. The stability of the 30 mM sample, despite its lower θ_w value, implies that the maximum emulsion stability may not necessarily be achieved using neutrally wetting particles, *e.g.,* if the particle-particle attractions at the interface are stronger at non-neutral wettabilities.

6.3.5 Conclusions: Deaggregation by rolling

When a low shear is applied to initially bridged samples, the emulsion deaggregates and droplets are observed to develop heterogeneous interfaces well before deaggregation takes place. Particles are therefore transferring between droplets in the bridged system, which suggests that a process of unbridging and rebridging is taking place, and that this is followed eventually by unbridging and possibly coalescence. It is possible that the contact angle of the particles changes gradually and eventually becomes low enough that rebridging is not favoured. When one of the precursor emulsions is non-bridged and the other is bridged, droplets from the non-bridged emulsion are seen to become fully incorporated into clusters, further confirming that an unbridging/rebridging process precedes deaggregation.

Particle transfer is observed to be faster in samples containing more particle bridges, which shows that particle transfer is driven by the unbridging/rebridging

process, although particle transfer does still occur in non-bridged samples (*e.g.,* the sample with an aqueous phase sodium chloride concentration of 30 mM and post-deaggregation in all samples). The rate of particle transfer is also linked to the strength of the particle bridges, because stronger bridges are less likely to be broken. The number of particle bridges is also related to the strength of the particle bridges, however, which means that care must be taken when predicting the effects of changing the bridge strength upon particle transfer rates.

In every sample, occasional droplets with $g \approx 0$ are observed at early roll times, whilst at the same time almost every other droplet in the sample has $f \approx g \approx 1$ (see, for example, the heterogeneous droplet in the centre-right area of the top right image in Fig. 6.26). This suggests that these heterogeneous droplets are formed by coalescence. Also, since Janus droplets are observed in a lot of samples, which have clearly recently coalesced, coalescence doesn't immediately lead to $g = 0$ droplets, and so the appearance of $g = 0$ droplets (*via* coalescence) shows that particles diffuse on the interface quite significantly.

Janus and patchy droplets are observed in some samples prior to deaggregation, yet at subsequent rolling times very few heterogeneous droplets are observed. This suggests that the development of these Janus droplets is due to coalescence induced during slide preparation, and is not an indication that the sample is coalescing during the rolling process.

In some samples the droplet size does not seem to change significantly as the samples are rolled, yet the emulsion clearly develops a significant fraction of free oil. This suggests that the coalescence which leads to the large amount of free oil is between the free oil itself and droplets of all sizes, rather than a more complicated process of coalescence between small droplets leading to larger droplets which in turn coalesce with the free oil. This makes sense, because when two droplets collide there will be two separate particle barriers preventing coalescence, whilst when a droplet collides with the free oil, there may only be one particle barrier. Furthermore, the Laplace pressure of the free oil in the sample will be considerably lower than that of the droplets, which will make coalescence events between droplets and the free oil more likely than between two droplets. Furthermore, large droplets could be more likely to coalesce with the free oil, due to a Smoluchowski coagulation type behaviour where the coalescence rate is proportional to d_o^N, where $N \gg 1$, so that once d_o begins to grow, so does the probability of it growing further [141, 142].

6.4 Conclusions and future work

A novel technique for studying emulsification and demulsification processes has been described and initial results have been presented. These results compare relatively well with expectations, which provides confidence in the technique. The results also provide new insights into several pertinent aspects of Pickering stabilisation and show, for the first time, the dynamic behaviour of particles in Pickering emulsions.

Particles are shown to be transferred between droplets relatively readily, and particles are shown to be transferred between droplets in all emulsions which have been studied here. The rate of particle transfer is greatest in emulsions which are bridged, as these samples undergo a period of unbridging and rebridging prior to deaggregation. The rate of droplet and particle rearrangement in this period is dependent on the strength of particle bridges, with rearrangement being faster when the particle bridges are weaker. Particle transfer also occurs in samples which are not bridged, or which contain very few particle bridges, as shown by the sample with an aqueous phase sodium chloride concentration of 30 mM.

Increasing the value of ϕ_p, but not by enough to suppress particle bridging, leads to a system with more bridges in a cluster of a given volume, which helps to "share the load", preventing deaggregation and lowering the rate of particle transfer. Further increases in ϕ_p reduce the degree of bridging in the system, and leads to lower rates of particle transfer due to the lack of an unbridging/rebridging process.

The ability to tune the deaggregation time and the fact that the deaggregation time is not strongly linked to the emulsion's shelf life are both beneficial for potential burst release applications. Since deaggregation can also be triggered suddenly by changing the pH or the salt concentration (see Chapter 5), the ability to tune the deaggregation time by adjusting the particle wettability means that a broad spectrum of release behaviours is available.

It is hoped that the results presented above demonstrate the utility of the two-colour technique. There are clearly many applications for this method of studying Pickering emulsions, and a small number of these applications will be highlighted here, along with ways in which the experiments described in this chapter could be improved upon, were they to be repeated.

The results presented above regarding the deaggregation of bridged emulsions are interesting and show that the deaggregation timescale of the emulsions can be tuned using the particle wettability. However, a greater understanding of the deaggregation behaviour could be generated by studying more Φ_{IM} values, particularly values below 10%, where the particle bridges are weaker and less common.

There is a worry that the volume of the sample will have an effect on the emulsion even when the emulsions are not being re-emulsified. The angle that the emulsion-air interface makes with the vial wall could affect the flow conditions near to the vial wall, which could affect whether droplets are likely to become stuck to the wall, and whilst this was not taken into account during these experiments, it should be in any future work.

The inclusion of fluorescent dyes in the oil phases of the precursor emulsions in future experiments would allow for a distinction between coalescence events and extensive particle transfer to be made with more confidence. However, it is also possible that particle transfer occurs simultaneously with a small amount of oil transfer, and such experiments would need to be careful to distinguish such occurrences.

There is also significant room for more quantitative results using these techniques. For example, if image analysis were utilised then it should be possible to measure f for many droplets in a sample. However, this remains difficult because in order to resolve individual particles well enough to use image analysis, the confocal scans need to be made at a slow rate, which makes gathering enough data to obtain good statistics difficult. Figure 6.33 shows an example of an image which could be used to calculate f and g for an individual droplet. Performing image analysis on the bright-field micrographs would also allow the sphericity of the deaggregated droplets to be quantified.

Another obvious improvement to the experiments described in this chapter would be to repeat them whilst ensuring consistency in the sampling points across all of the samples, in order to aid comparisons between samples and experiments.

The two-colour technique described in this chapter has also been applied to the the study of emulsions which are being repeatedly sheared using a vortex mixer. The results of these experiments are presented in Chapter 7.

Finally, Chapter 8 will describe the results of experiments carried out using a

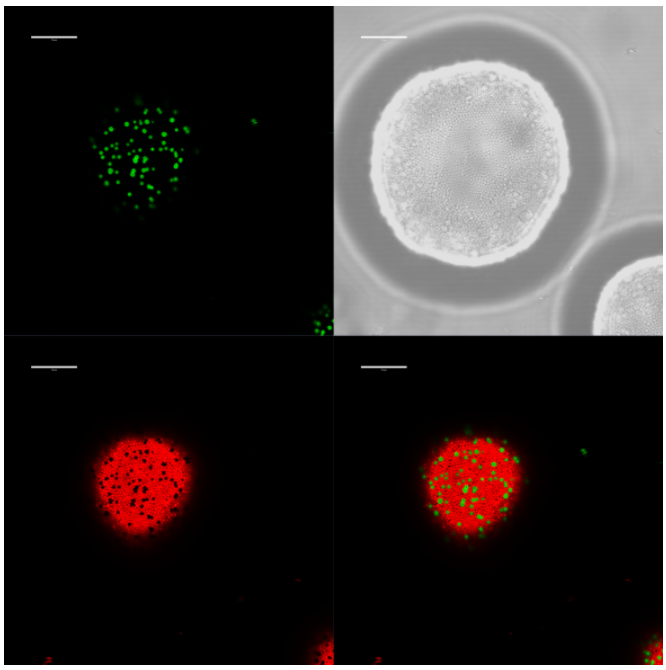

Figure 6.33 *Confocal micrograph showing a two-colour droplet viewed using a* $63\times$ *oil immersion objective lens. In this case,* $\phi_p = 1.1\%$, $\Phi_{IM} = 10\%$ *and the rolling time is* 717 h. *The scale bars are* 10 μm.

continuous flow emulsification device to increase the sample volume from $\approx 3\ mL$ to $\approx 1\ L$. The two-colour technique described in this chapter would provide an interesting additional perspective to these experiments.

Chapter 7

The secret life of Pickering emulsions: Repeatedly shearing an emulsion

7.1 Introduction

Chapter 6 described a novel two-colour technique for studying Pickering emulsions, and the results of experiments applying this technique to bridged Pickering emulsions at low shear. This technique has also been used to study Pickering emulsions undergoing repeated applications of a relatively high shear rate, and the rate at which particles reorganise at a droplet's surface during shear.

When an emulsion is sheared or re-sheared, the degree of droplet breakup will depend upon the size of the droplets prior to the application of shear and upon the shear rate. For low shear rates, a low degree of remixing is expected, and so $\bar{f}$ and $\bar{g}$ are expected to be approximately 1, but for higher shear rates and/or long shear times it is expected that both $\bar{f}$ and $\bar{g}$ will tend to 0. In between these two extremes, there is expected to be a sharp decrease in $\bar{f}$ at the critical shear rate, given by Eq. (1.9), since at this point the shear rate will be high enough to create an excess of interfacial area and so greatly enhance the rates of both droplet breakup and re-coalescence. Comparisons can therefore be made with the results of Taisne *et al.* [138], with the shear rate and the particle volume fraction being analogous to the homogenisation pressure and surfactant concentration,

respectively.

7.2 Methods and materials

The methods which are particular to this chapter will be discussed in this section. Methodology for techniques which are used in this chapter and in other chapters can be found in Chapter 2.

7.2.1 Sample preparation

Two differently dyed batches of Stöber silica have been used in the experiments described in this chapter - one dyed yellow with FITC, the other dyed red with RITC - to study the degree to which a Pickering emulsion is remixed during shear, and also the rate at which particles reorganise at a droplet's surface during shear. In each experiment two separate precursor emulsions of equal volume (3 mL) were created, one with each batch of particles, and these two emulsions were then gently mixed together and repeatedly subjected to high shear. The use of two different dyes allows the two batches of particles to be observed separately using confocal microscopy. Emulsification was carried out by vortex mixing the samples in 30 s bursts until the aqueous phase was clear of particles. Following emulsification, the precursor emulsions were gently mixed - with a small amount of water being added to the mixed sample as part of washing out the vials used to emulsify the initial emulsions. Some of the resolved water was then removed with a pipette so that the component volume fractions were the same as for the precursor emulsions.

The samples used in the experiments described in this chapter were not placed on roller banks, but were instead vortex mixed repeatedly. The analysis techniques described in Chapter 6 were again used to characterise these samples. The vortex mixing times were generally 60 s, except for the first few occasions, where the vortexing times were 5-30 s. The cumulative total vortexing time following mixing of the precursor emulsions will be quoted where appropriate. The period of time between successive mixing periods varied from approximately 10 min to several weeks, but was usually approximately one day. The samples were left for approximately three weeks between the 250 s and 310 s measurements, and this gap will be considered when the results are presented below.

7.3 Results and discussion

The mixing of two emulsions stabilised by differently coloured particles, and the subsequent shearing of the mixed emulsion, allows for the shear rate that is required to re-emulsify a sample to be studied. It is expected that if the initial emulsion droplets are to be burst so that limited coalescence can be re-established, then the subsequent shear rate will need to be great enough to create smaller droplets than the emulsion is initially composed of. Below this shear rate, little re-mixing of the droplets' interfaces is expected, although substantial rearrangement of the droplets in the clusters will presumably still take place, if the emulsion is bridged.

By tracking the proportion of droplets which have heterogeneous interfaces, the degree of remixing which has occurred can be quantified. This information can then be related back to the system parameters to allow information about the elasticity of the particle layer to be deduced, and to gain an understanding of whether limited coalescence can be re-established.

Two samples were used in this work - with ϕ_p values of 0.6% and 1.1%. In both samples $\phi_o = 20\%$ and $\Phi_{IM} = 10\%$. After the precursor emulsions were mixed, a process which involved adding some water to make sure as much of the emulsions were transferred to the new vial as possible, some of the aqueous phase was removed from the samples to maintain the ϕ_o values. Despite this, it should be noted that simply increasing the volume of the samples may change the emulsification conditions, since the flow conditions within the vial will be changed, as the same mixing power is being dissipated in a greater volume of emulsion. The two precursor emulsions which were mixed to form the $\phi_p = 0.6\%$ sample were both strongly bridged, whilst with the $\phi_p = 1.1\%$ sample, the red precursor emulsion was non-bridged and the yellow precursor emulsion was partially bridged - approximately half of the emulsion droplets were attached to a cluster (estimated from light scattering data). Since the $\phi_p = 0.6\%$ sample is strongly bridged, more interfacial area has been generated during shearing than can be stabilised by the available particles, and so a re-application of the same shear rate is expected to be capable of breaking up the primary droplets and re-establishing limited coalescence. In the $\phi_p = 1.1\%$ sample, however, the interfacial area generated by the applied shear will be approximately equal to that which can be stabilised by the available particles, which means that the shear rate generated by the vortex mixer will be approximately equal to the critical shear rate required to cause

droplet breakup, $\dot{\gamma}_{crit}$, given by rearranging Eq. (1.9) to obtain:

$$\dot{\gamma}_{crit} = \frac{Ca_c \sigma_{ow}}{\eta R}, \tag{7.1}$$

which means that limited coalescence is not expected to be re-established by a re-application of the same shear rate in this case.

7.3.1 Re-shearing at $\phi_p = 0.6\%$

Figure 7.1 shows how the apparent droplet sizes, as measured by light scattering, change as a function of total vortex mixing time. These size distributions suggest that bridging has almost disappeared from the $\phi_p = 0.6\%$ sample after 130 s of vortex mixing. However, photography and bright-field microscopy of the sample show that aggregation is still occurring at vortex mixing times up to 370 s, as shown in Fig. 7.2. This result suggests that the bridging becomes weaker over time, presumably as a result of the particles becoming more hydrophilic as water adsorbs to the particle interface, which will lower the contact angle and make it easier for the droplet clusters to be broken up by the stirring mechanism of the particle sizer. Since bright-field microscopy shows that the sample continues to be bridged following each shearing, it can be concluded that the shear conditions do not change drastically despite the increased sample volume.

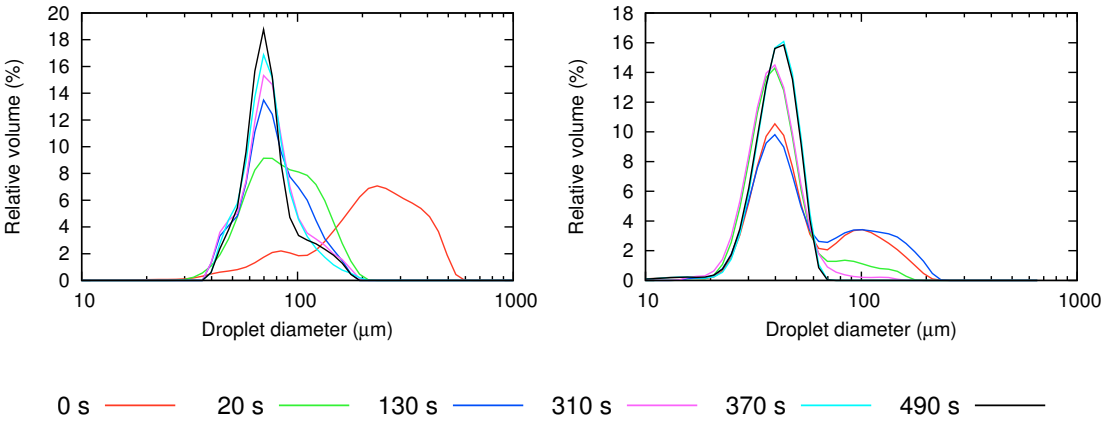

Figure 7.1 *Graphs showing how the measured droplet size distributions in two emulsions with different particle volume fractions (Left: $\phi_p = 0.6\%$; Right: $\phi_p = 1.1\%$) change as the emulsions are repeatedly vortex mixed. The labels give the cumulative vortex mixing time following the mixing of the precursor emulsions.*

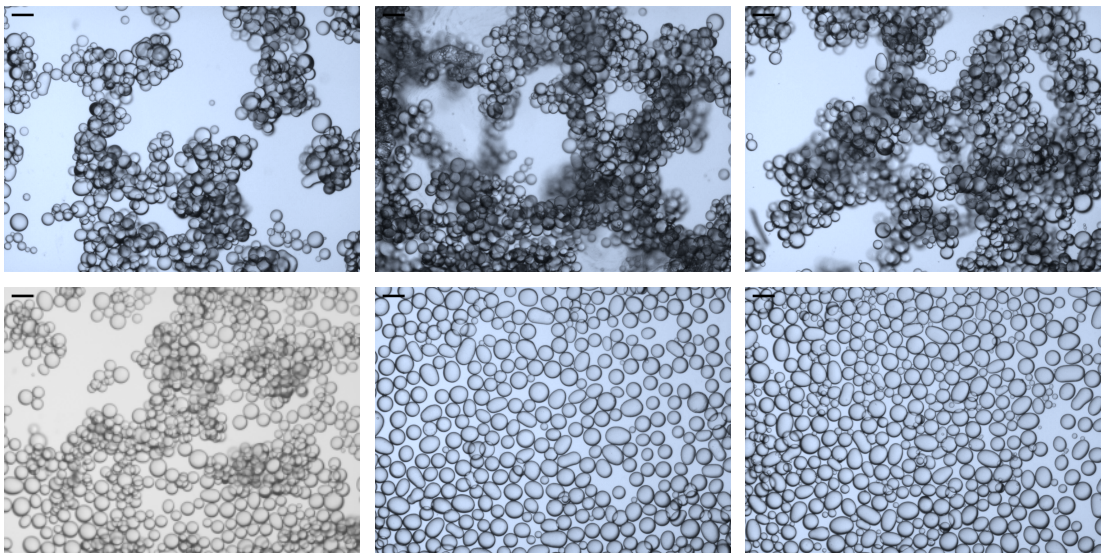

Figure 7.2 *Micrographs of the $\phi_p = 0.6\%$ sample at various cumulative vortex mixing times. The vortex mixing times are, from left to right, Top row: 0 s, 100 s and 190 s; Bottom row: 370 s, 550 s and 610 s. The micrographs in the top row are taken prior to the three week gap and those in the bottom row are taken after the gap. The scale bars are 100 μm.*

Photography and bright-field microscopy of the $\phi_p = 0.6\%$ sample both show that deaggregation occurs gradually during the shearing periods in the time range of 310-550 s. Over this period the interface between the emulsion and the resolved water gradually changes from being rough to smooth and the micrographs show that clusters of droplets become less common. The discussion of the behaviour of this sample will therefore be split into three régimes:

- The initial, bridged, régime, from 0-250 s.
- The transitional period, from 310-550 s, during which the emulsion becomes gradually less bridged.
- The final, non-bridged, régime, from 610 s onwards.

Initial régime Over the initial period, the emulsion changes very little macroscopically, with a rough emulsion-resolved water interface, as shown in Fig. 7.3. Bright-field microscopy and light scattering size measurements of the emulsion throughout this period also reveal very few changes, with the emulsion consistently being aggregated due to particle bridges, and having a primary droplet

Figure 7.3 *Photographs of the re-shearing samples at various cumulative vortex mixing times. In each photograph the sample on the left has* $\phi_p = 0.6\%$ *and the sample on the right has* $\phi_p = 1.1\%$*. The mixing times are, from left to right, Top row:* 0 *s,* 100 *s and* 190 *s; Bottom row:* 490 *s and* 610 *s. The change in the* $\phi_p = 0.6\%$ *sample from having a rough emulsion-resolved water interface to having a smooth emulsion-resolved water interface and the appearance of free silica in the* $\phi_p = 1.1\%$ *sample can both be seen.*

size of $\approx$ 75 μm, as measured by light scattering, and as can be seen in the micrographs in Fig. 7.2 and Fig. 7.4.

However, confocal microscopy reveals that significant rearrangement of droplets and particles is indeed taking place throughout the initial régime, as shown in Fig. 7.5. The vortex mixing process applies the same shear rate which was used to initially create the primary droplets, and therefore is easily capable of breaking up the clusters. The disrupted droplets then reform into new clusters when the shearing ceases, and this leads to the mixed clusters which are observed. Given that the shear rate of the vortex mixer was great enough to create a bridged emulsion, it is expected to be great enough to break up the droplets again. If this were happening, one would expect to see most of the droplets in the emulsion quickly develop heterogeneous interfaces, as coalescence occurs between red and yellow droplets. However, whilst some heterogeneous droplets are observed after just 5 s of vortex mixing, the majority of droplets remain largely monochromatic,

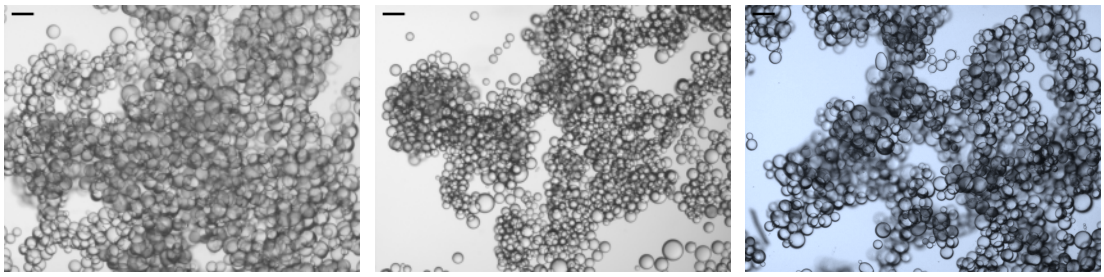

Figure 7.4 *Micrographs of the $\phi_p = 0.6\%$ sample at various cumulative vortex mixing times during the initial régime. The mixing times are, from left to right, 0 s, 20 s and 190 s. The scale bars are 100 μm.*

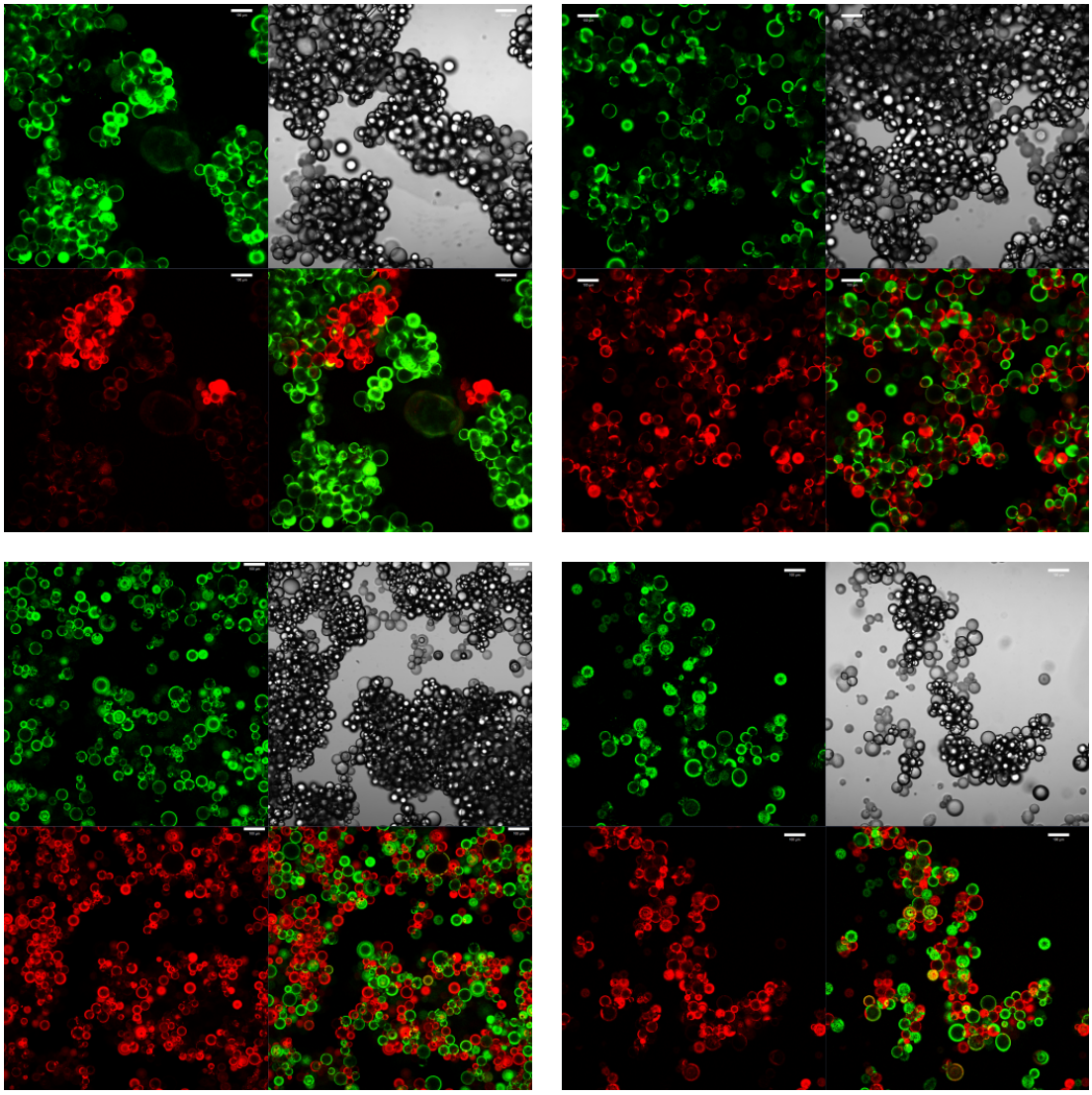

Figure 7.5 *Confocal micrographs of the $\phi_p = 0.6\%$ sample at various vortex mixing times in the initial régime. The cumulative vortex mixing times are, from left to right, Top row: 0 s and 5 s; Bottom row: 10 s and 40 s. The scale bars are 100 μm.*

so that $\bar{f} \approx 1$ throughout the initial régime, with the proportion of heterogeneous droplets being $\approx 15\%$ after 130 s of mixing and $\approx 40\%$ at the end of the initial régime (250 s). The lengths of the mixing periods up to 130 s were all 30 s or below, and it could be that it simply takes longer than 30 s for the shear to cause a reduction in the droplet size, but this would be surprising since the initial emulsification was carried out in 30 s bursts. An alternative explanation is that the presence of the particle layer at the interface significantly inhibits droplet deformation and breakup.

Patchy droplets, such as the ones visible in Fig. 7.6, are seen at some vortex mixing times. Since the fraction of patchy droplets in some samples is much higher than the number of droplets with very heterogeneous interfaces in subsequent samples, and since the mean droplet size remains approximately constant, this may be an indication that the coalescence is occurring during the preparation of the slide, rather than during the vortex mixing process.

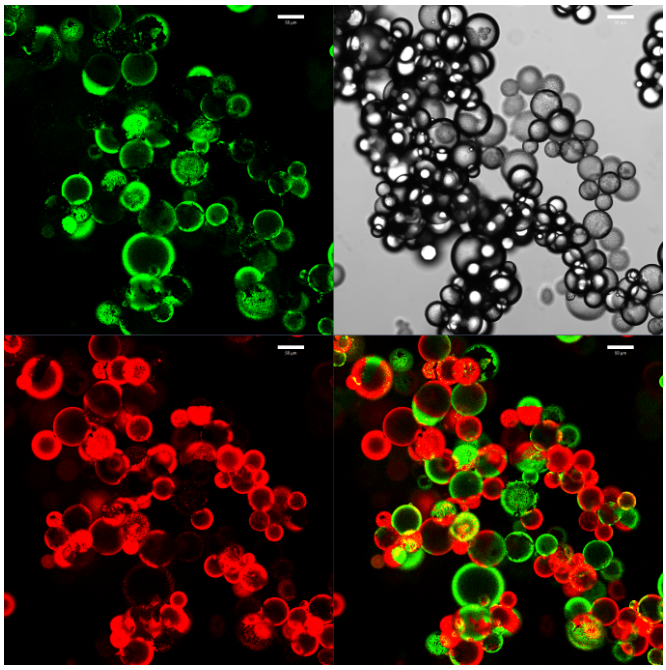

Figure 7.6 *Confocal micrograph of the $\phi_p = 0.6\%$ sample after 40 s of vortex mixing. Patchy, Janus-like, droplets can be seen at multiple points in the image. The scale bars are 50 μm.*

Transitional régime The $\phi_p = 0.6\%$ sample was observed to partially deaggregate after 310 s of vortex mixing, and had fully deaggregated following 550 s of vortex mixing, as shown in the micrographs in Fig. 7.2 and Fig. 7.7. Confocal

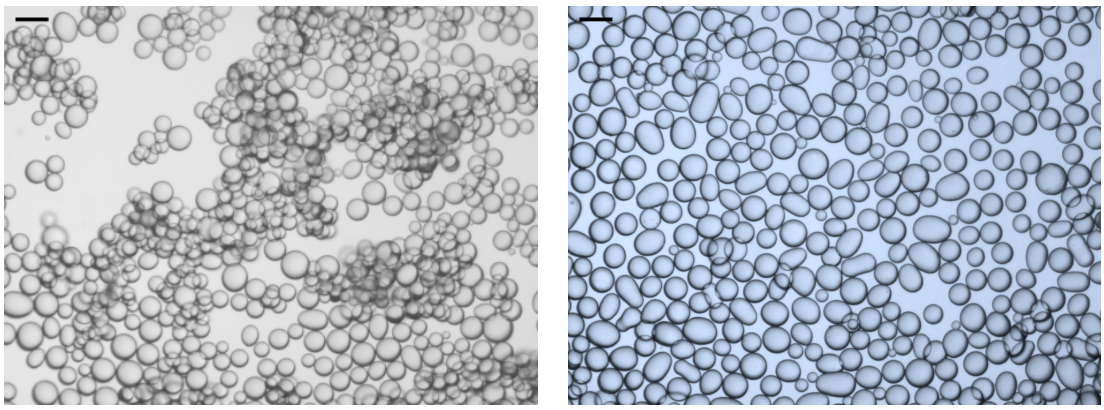

Figure 7.7 *Bright-field micrographs showing the effect of repeated vortex mixing on the $\phi_p = 0.6\%$ sample in the transitional régime. The vortex mixing times are 370 s (left) and 550 s (right). The scale bars are 100 μm.*

micrographs of the sample in this régime are shown in Fig. 7.8. This transitional period immediately follows the three week gap in the taking of measurements mentioned above. It therefore seems likely that the deaggregation is, at least partly, due to changes in the particle wettability, with the particles becoming more hydrophilic as they are immersed in water. During this period, the heterogeneity of the droplets also increases significantly, with an increase in the fraction of heterogeneous droplets from $\approx 40\%$ to $\approx 80\%$ after an extra 60 s of mixing, and then to $\approx 100\%$ after another 60 s. The increase in the heterogeneity which occurs during the deaggregation of the sample suggests that bridge breaking is easier at this stage than it was previously, and may even be a sign that droplet breakup and coalescence is occurring. As mentioned in Chapter 5, particle bridging is sensitive to changes in particle wettability, and so an increase in the hydrophilicity of the particles could easily cause the sample to deaggregate.

Final régime Following deaggregation of the sample, the all of the droplets are heterogeneous, with $\bar{f} \approx 0$, as can be seen in Fig. 7.9, due to either significant particle transfer or to coalescence. Also of interest is that throughout this régime, a significant proportion of the droplets are observed to be non-spherical, often obviously due to arrested coalescence, which confirms that the interface is now rigid, which is expected due to attractions between particles at the interface, especially when θ_w is lowered.

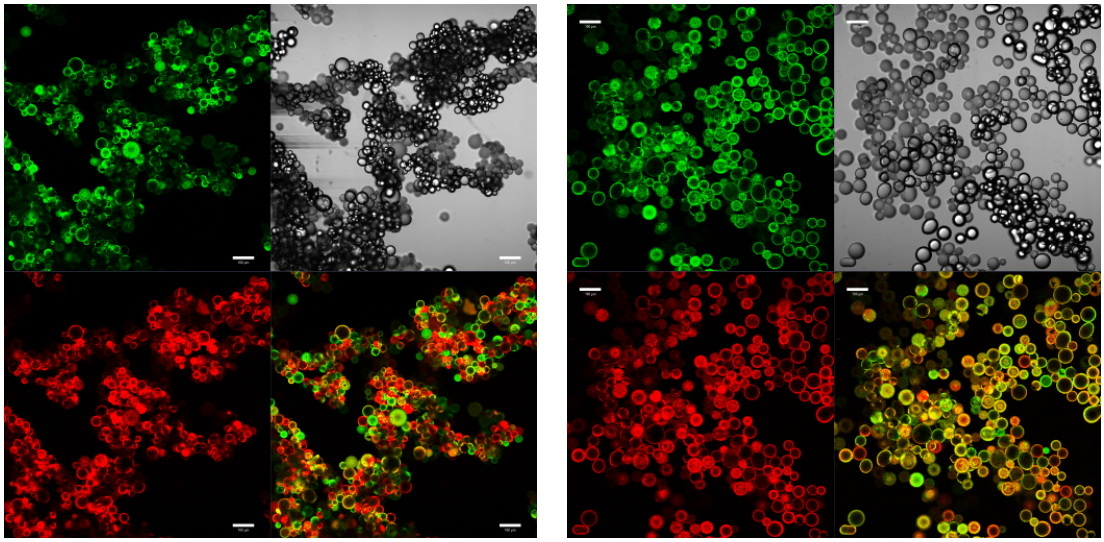

Figure 7.8 *Confocal micrographs showing the effect of repeated vortex mixing on the $\phi_p = 0.6\%$ sample in the transitional régime. The vortex mixing times are 250 s (left) and 370 s (right). The scale bars are 100 μm.*

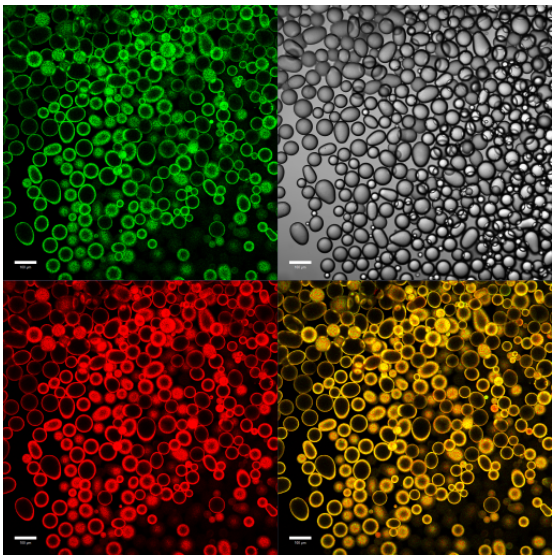

Figure 7.9 *Confocal micrograph showing the effect of repeated vortex mixing on the $\phi_p = 0.6\%$ sample in the final régime. The cumulative vortex mixing time is 610 s. The scale bars are 100 μm.*

7.3.2 Re-shearing at $\phi_p = 1.1\%$

In the case of the sample with $\phi_p = 1.1\%$, bright-field microscopy again shows that the system remains in a partially bridged state until the cumulative vortex mixing time is at least 200 s. This again confirms that the shear conditions are not drastically different when the total sample volume is increased from 3 mL to 6 mL. In fact, the degree of bridging appears to increase following some mixing sessions, most notably between 100 s and 130 s, which is probably due to the ill-controlled nature of vortex mixing meaning more interfacial area was generated during those mixing periods. As with the $\phi_p = 0.6\%$ sample, bridging is not observed after cumulative vortex mixing times greater than 300 s, which coincides with the three week gap between measurements. Photographs of the sample at various mixing times are shown in Fig. 7.3.

The emulsion's behaviour can therefore be split into three régimes:

- From 0 s to 100 s - The system starts off being partially bridged (with approximately 30% of droplets being in a cluster, as estimated from light scattering), and the degree of bridging then decreases (with approximately 10% of droplets being in a cluster). The interface between the emulsion and the resolved water is smooth. Micrographs of the sample in this régime are shown in Fig. 7.10 (top row), and confocal micrographs are shown in Fig. 7.11 (top row).

- From 130 s to 250 s - The system is more strongly bridged (approximately 35% of droplets are in a cluster). The interface between the emulsion and the resolved water is rough. Micrographs of the sample in this régime are shown in Fig. 7.10 (middle row), and confocal micrographs are shown in Fig. 7.11 (middle row).

- From 310 s onwards - The system is non-bridged. The interface between the emulsion and the resolved water is smooth, free silica can be seen in the aqueous phase and a significant proportion of the droplets are non-spherical. Micrographs of the sample in this régime are shown in Fig. 7.10 (bottom row), and confocal micrographs are shown in Fig. 7.11 (bottom row).

Since the flow conditions in the sample during vortex mixing depend on several factors which are difficult to control (*e.g.,* the angle at which the vial is being

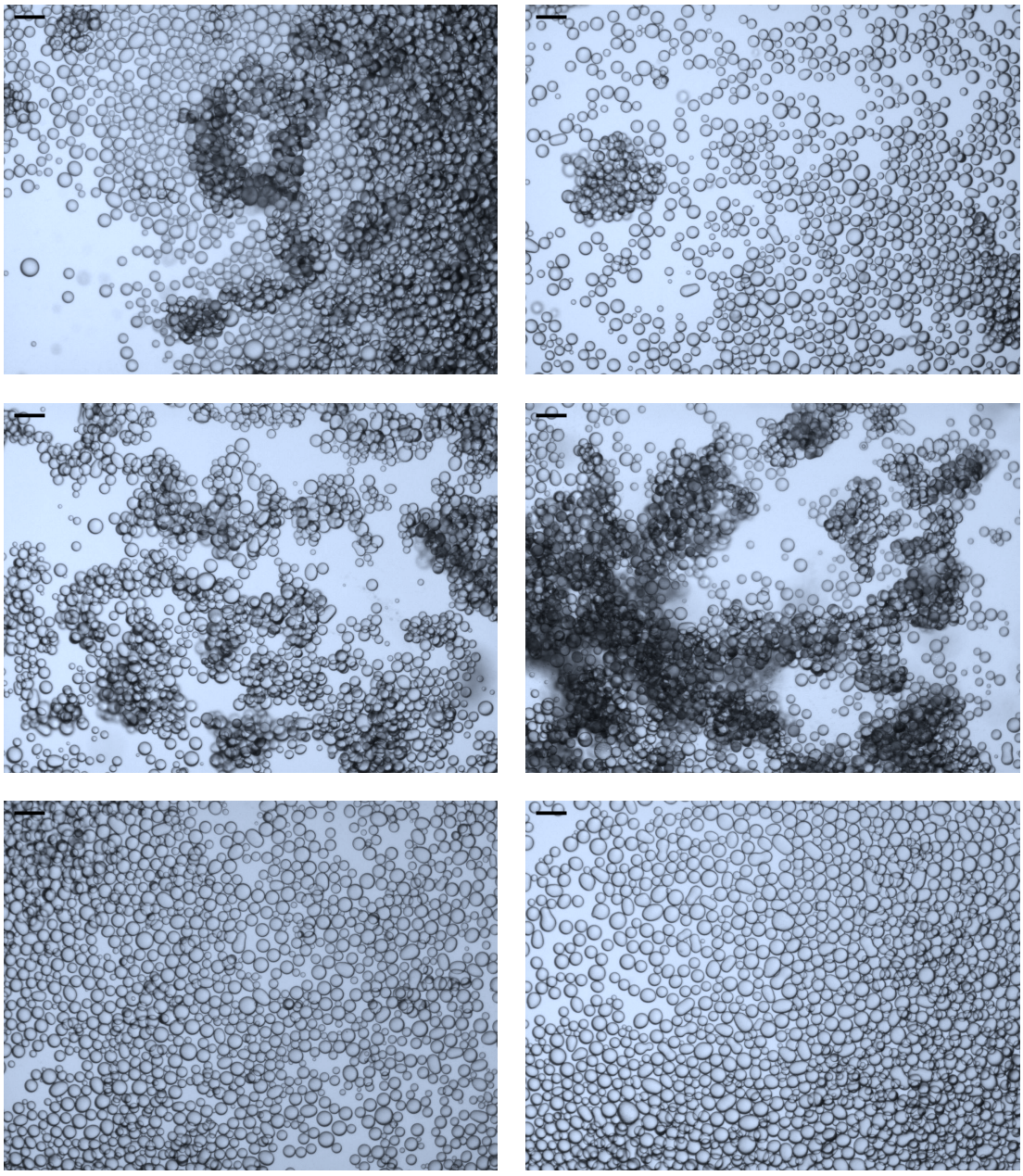

Figure 7.10 *Micrographs showing the effects of repeated vortex mixing on the* $\phi_p = 1.1\%$ *sample. The cumulative vortex mixing times are, from left to right, Top row (initial régime):* 0 *s and* 100 *s; Middle row (transitional régime):* 130 *s and* 190 *s; Bottom row (final régime):* 370 *s and* 610 *s. The scale bars are* 100 μm.

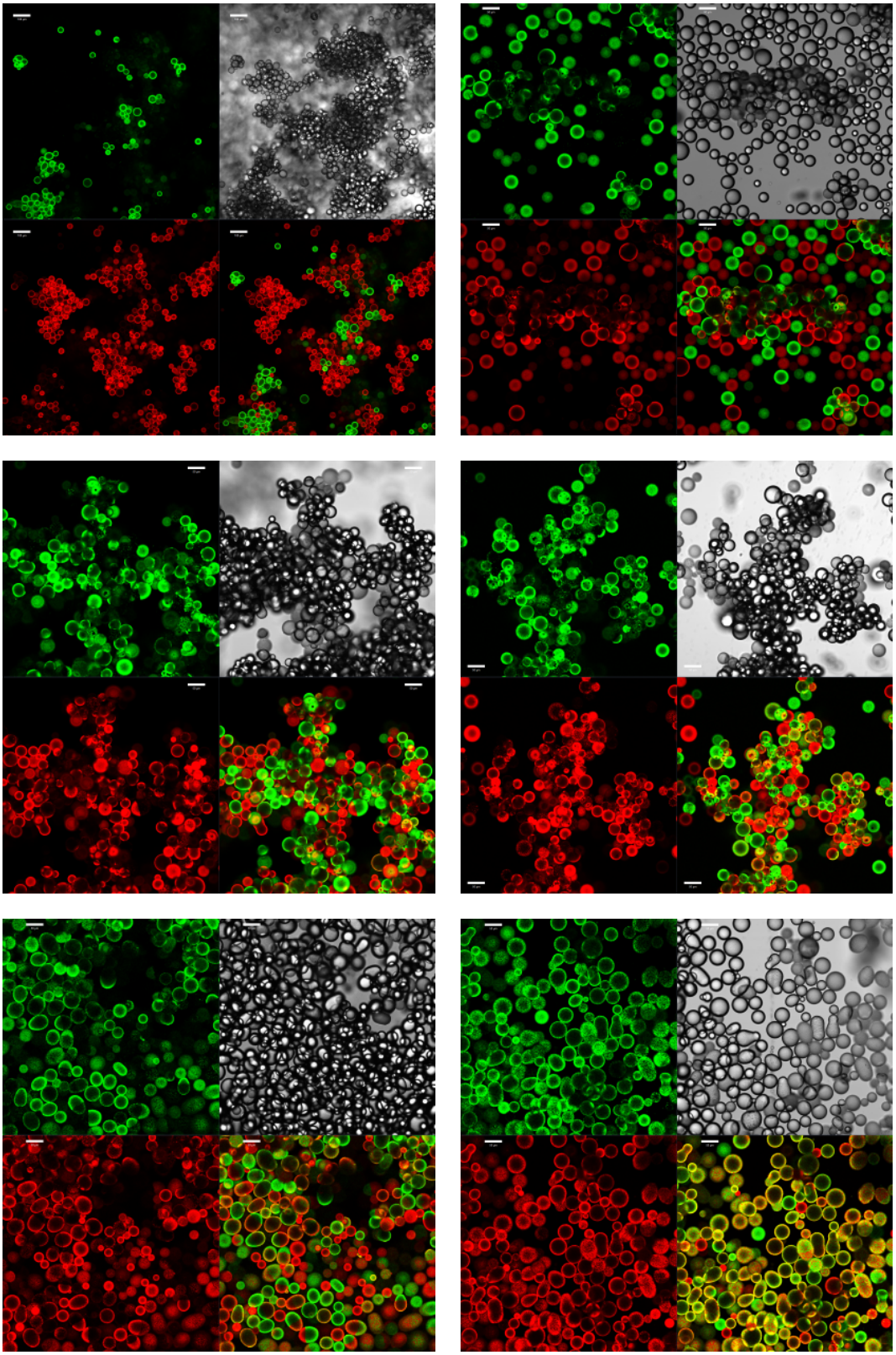

Figure 7.11 *Confocal micrographs of the* $\phi_p = 1.1\%$ *sample. The cumulative vortex mixing times are, from left to right, Top row:* 0 *s and* 100 *s; Middle row:* 130 *s and* 250 *s; Bottom row:* 310 *s and* 610 *s. The scale bars are* 100 μm *(top left) and* 50 μm *(all others).*

held), the transition from the first régime to the second may simply be caused by a particularly 'good' mixing occasion. However, it is also possible that the particle contact angle is changing gradually with time, and that this affects the strength of the particles' aggregation at the interface, and hence the likelihood of a fully coated droplet bursting at a given shear rate.

The transition from the second to third régime immediately follows the three week gap between measurements, and it seems likely that during this period the particles have become too hydrophilic to allow bridging.

In addition to the changes which were observed using bright-field microscopy and light scattering, confocal microscopy shows that a number of changes are occurring as the sample is repeatedly sheared.

In the initial régime, where the emulsion is gradually deaggregating, the droplets generally remain homogeneous, except for a relatively small amount of particle transfer between droplets. This observed particle transfer is in agreement with the observations in other samples where particle transfer takes place as a sample deaggregates (see Chapter 6), and the lower rate which is observed here can be attributed to the lower degree of bridging in this sample.

After 130 s of vortex mixing, there are considerably more patchy and Janus-like droplets in the emulsion. These droplets may be the result of coalescence during slide preparation, but may also be an indication that the droplet stability has been lowered due to a decrease in θ_w.

In the second régime, where the emulsion is consistently bridged, the majority of droplets remain almost homogeneous, but the fraction of droplets which are notably heterogeneous ($f \approx 0$) increases to approximately one third.

Following the deaggregation process which happens after 310 s of vortex mixing, very few homogeneous droplets are observed, with the vast majority of droplets in the sample having completely heterogeneous interfaces. A large fraction of the droplets in this régime are also non-spherical.

The patchy droplets which are observed following the transition to the bridged régime should not be surprising, and in this instance are not thought to be due to coalescence during slide preparation. The increase in the degree of bridging requires an increase in the interfacial area which is generated during the shearing process. This increase could be due to an anomalously efficient mixing period,

although it could also be that the decrease in θ_w leads to droplet breakup being easier. Either way, when this extra interfacial area is generated, it will lead to more coalescence events between partially coated droplets and hence more patchy droplets, as well as the observed increase in particle bridging.

The transition to the third régime appears to be caused mainly by a change in particle wettability which occurred when the sample was left for approximately three weeks between measurements. Although the emulsion did not undergo any noticeable change at a macroscopic level during this period, the first subjection to shear afterwards resulted in a non-bridged emulsion with a notable amount of free silica in the aqueous phase. The release of silica into the aqueous phase fits well with the idea that the particles have become more hydrophilic.

As with the $\phi_p = 0.6\%$ sample, the $\phi_p = 1.1\%$ sample was seen to contain a noticeable number of heterogeneous droplets well before deaggregation took place, but this behaviour was also notably less prevalent than in the lower particle volume fraction sample. This agrees well with the observations above regarding particle transfer between droplets in a bridged system *via* a process of unbridging and rebridging, because the $\phi_p = 1.1\%$ has a lower degree of bridging and so will experience less particle transfer by this mechanism.

7.3.3 Re-shearing summary

Droplet breakup is not observed in the $\phi_p = 0.6\%$ sample until after ≈ 310 s of vortex mixing, despite $\dot{\gamma} > \dot{\gamma}_{crit}$. This behaviour is summarised in Fig. 7.12, and shows that the particles are forming elastic shells at the interface, which hold the droplets together and prevent droplet breakup. This is in contrast to surfactant-stabilised emulsions, where increasing the stabiliser concentration makes droplets more deformable. Droplet breakup does occur at longer vortex mixing times, and this is thought to be caused by a decrease in θ_w making the droplets less stable. Therefore, it can be concluded that in order to re-establish limited coalescence in Pickering emulsions stabilised by particles which aggregate at the interface, it is necessary for $\dot{\gamma} \gg \dot{\gamma}_{crit}$.

In the $\phi_p = 1.1\%$ sample, the degree of bridging increases prior to deaggregation, despite $\dot{\gamma} \approx \dot{\gamma}_{crit}$. This could possibly be explained by the decrease in the contact angle of the particles as they are immersed in water, which will make droplet breakup more likely, increase the amount of interfacial area which is generated

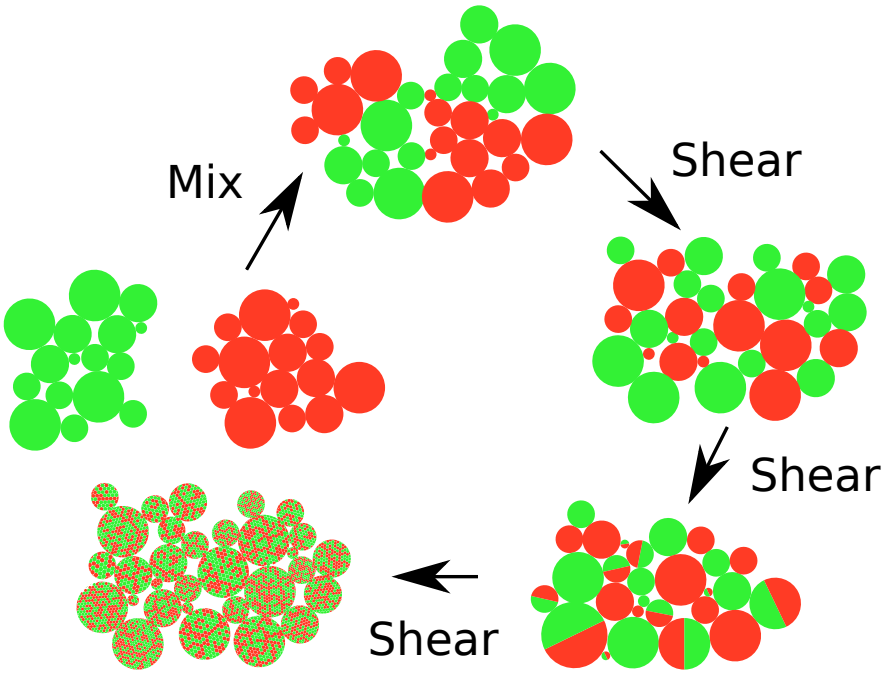

Figure 7.12 *Cartoon showing the effects of repeated shear on a bridged Pickering emulsion. Even when $\dot{\gamma} > \dot{\gamma}_{crit}$, droplet breakup is not observed until the cumulative shearing time is significantly longer than used to initially emulsify the sample.*

and allow particle bridges to form. Alternatively, the particles may rearrange during shear, exposing gaps in the surface coverage which may allow bridges to form, although it is not clear why this would happen after the precursor emulsions have been mixed, but not during the emulsification of the precursor emulsions. As the sample continues to be sheared, it then begins to deaggregate, and this is also likely to be caused by the lowering of the particle contact angle making bridging infeasible.

The lack of any significant change in either sample's behaviour at low shearing times suggests that the shear conditions are not significantly changed when the sample volume is increased from 3 mL to 6 mL. Particle transfer occurs at all vortex mixing times, but the rate of particle transfer increases as θ_w decreases, due to the weaker particle bridges making unbridging more likely. The rate of particle transfer is also higher in the $\phi_p = 0.6\%$ sample than in the $\phi_p = 1.1\%$ sample, which can be attributed to the greater degree of bridging in the $\phi_p = 0.6\%$

sample, which leads to a greater rate of unbridging/rebridging events.

7.4 Conclusions and future work

The two-colour method which was introduced in Chapter 6 has also been applied to emulsions which are repeatedly sheared using a vortex mixer. The results of these experiments show that the particles at a droplet's interface form an elastic shell which hinders droplet breakup. This is in contrast to emulsions which are stabilised by molecular surfactants, where adding stabiliser increases the deformability of the droplets. This resistance to deformation and breakup also means that a surprisingly high shear rate ($\dot{\gamma} > 2\dot{\gamma}_{crit}$) is necessary to re-establish limited coalescence.

Although the results presented in this chapter are highly illuminating, it would be interesting to build upon them by using a rotor-stator instead of a vortex mixer to perform the emulsification. This would allow for precise control of the shear rate, so that the links between droplet size, the critical shear rate and the rate of particle transfer could be investigated further, and would also provide an interesting contrast to the large shear zone of the vortex mixer.

If these re-shearing experiments are repeated, they should be carried out in a more condensed time period, so that the effects of ageing on the particles and droplets are negligible, and/or can be quantified.

Chapter 8

Pickering emulsions created by continuous flow emulsification

8.1 Introduction

Industrial emulsification processes are naturally carried out at very large scales, with batch volumes routinely exceeding 1000 L. However, all of the previous experiments in this thesis have been carried out on a much smaller scale, with emulsion sample volumes typically being 3 mL, and almost all academic research on Pickering emulsions has also been carried out at this scale. Notable exceptions to this rule are the work of Yuan *et al.,* who produced oil-in-water emulsions stabilised by silica particles using two different membrane emulsification devices, with sample volumes of ≈ 1 L [143], and the work of both Thompson *et al.* [144] and Sun *et al.* [145], who used membrane emulsification to produce Pickering emulsions with sample volumes of ≈ 100 mL. In an attempt to further bridge this gap, the laboratory experiments described in Chapter 5 have been scaled up by using a continuous flow setup based around an IKA magicLab homogeniser and sample volumes of ≈ 1 L. This setup also offers the opportunity to further study the fluid mechanics of the emulsification process, but requires far larger volumes of materials and so the cost of each experiment is increased dramatically and the number of experiments that can be carried out in this area using well controlled particles is therefore limited.

The residence times of droplets in the shear zone in a continuous flow setup will

differ from those in batch emulsification setups. This difference is likely to have an effect on the droplet size and polydispersity. More complex effects, such as the particles and the droplets moving at different rates through the shear zone in the continuous flow setup, are also possible.

As was mentioned in Chapter 5, it is believed that particle bridging has been missed in several places in the published literature on Pickering emulsions. It is also possible that particle bridging may occur in industrial-scale emulsification without being identified. Particle bridging can cause the apparent droplet size, as measured using light scattering, to increase, even though the primary droplet size either does not change, or decreases slightly. During emulsification the droplet size will initially be large and will then decrease until the continuous phase is depleted of particles, subject to the limits imposed by mixing power. At this point the interfacial area of the emulsion is equal to that which can be stabilised by the available particles, and so any further increase in the interfacial area will lead to collisions between partially coated droplets and hence particle bridging becomes possible. The appearance of particle bridging in this way could easily be mistaken for an increase in the primary droplet size if using light scattering to measure the droplet size distribution.

The main focus of this chapter will therefore be to show that the results of previous chapters are not limited to the sample size or experimental protocol used in those experiments, putting them on a firmer footing and enhancing their relevance to industrial emulsification procedures.

8.2 Methods and materials

The methods which are particular to this chapter will be discussed in this section. Methodology for techniques which are used in this chapter and in other chapters can be found in Chapter 2.

The main apparatus used in these experiments was an IKA magicLab continuous flow emulsification device, with a 1 L Micro Plant hopper attached, and operating in the basic UTL mode. A schematic of the magicLab is shown in Fig. 8.1. This device is designed for the emulsification of samples with volumes of approximately one litre. The magicLab has a hopper into which the sample is placed, with a rotor-stator beneath the hopper, through which the sample passes before being

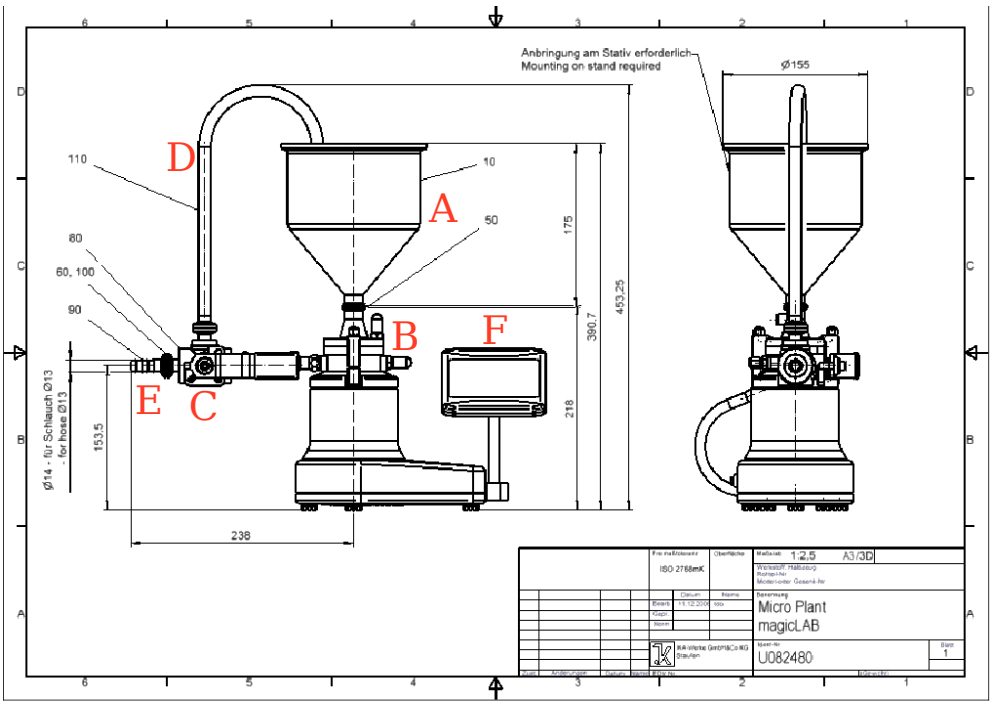

Figure 8.1 *Schematic of the IKA magicLab used in continuous flow emulsification experiments, adapted from the magicLab operating manual [146]. A: Hopper containing the sample, B: Rotor-stator, C: Valve for re-routing the sample, D: Feedback pipe, E: Sampling point, F: Control panel.*

routed through a pipe and back into the hopper. A valve allows the flow to be re-routed to allow samples to be taken as desired. In order to prevent the oil phase from simply accumulating at the top of the hopper an IKA T50 stirrer fitted with a propeller of diameter 6 *cm* was placed with the propeller approximately 5 *cm* below the surface of the sample. The rotor-stator of the magicLab consists of four concentric rings. The first and third rings comprise the rotor and the second and fourth rings comprise the stator. The gaps between the rings are 0.8 *mm* and the inner diameter of the outermost ring has a diameter of 30.8 *mm*. The device operates in the range 3-26 *krpm*, which equates to shear rates of $\dot{\gamma} \approx 6\,000\text{-}52\,000\ s^{-1}$. An integrated thermometer measures the temperature of the sample in the feedback loop. Photographs of the setup are shown in Fig. 8.2.

The larger scale of the continuous flow experiments, compared to the experiments described in previous chapters, means that a larger batch of silica particles was prepared for use in these experiments. As with previous particle batches, this batch was synthesised by Dr. Andrew Schofield. A 20 *L* bottle of silica preparation was used, and yielded approximately 150 *g* of silica. Unfortunately, this batch of

Figure 8.2 *Left: Photograph of the IKA magicLab used in the continuous flow emulsification experiments, showing both the magicLab itself and the IKA T50 stirrer; Right: Photograph showing the inside of the hopper during an experiment. The feedback pipe is on the left, and the IKA stirrer shaft is on the right.*

silica proved to have different chemical properties to previous batches of particles. The particles had a zeta potential of $\approx -65\ mV$ when the pH was above ≈ 5, and a zeta potential of $\approx 70\ mV$ when the pH was below ≈ 4. There was therefore a very narrow range at relatively low pH at which the particle charge may have been strong enough to create a stable dispersion, but low enough to allow the particles to adsorb to the oil-water interface (see Chapter 4). Drying the particles at 170℃ did not make them significantly more likely to adsorb to the interface. For these reasons, these particles were not suitable for the creation of Pickering emulsions. Instead, the experiments described in this chapter were carried out using a mixture of particles from different batches. Unfortunately, only $\approx 10\ g$ of this mixture was available, and this placed a limit on the number of experiments which could be carried out. The particle mixture used for the continuous flow experiments was dried under vacuum at 170℃ for 1 h.

Due to the larger scale of these experiments, the volume fraction of the oil phase was lowered to 5%. The oil phase used was a mixture of unfiltered dodecane and isopropyl myristate, with $\Phi_{IM} = 20\%$. The particles were dispersed in 30 mL of distilled water using the ultrasonic probe. This particle dispersion was then mixed with 50 mL of the oil phase and 900 mL of distilled water in a bottle which was shaken briefly prior to the emulsion being poured into the hopper. The shear rate in the magicLab was maintained at a constant 16 000 s^{-1}, which means that the flow in the pipe was in the transitional régime but was likely to be turbulent

for the reasons noted in Section 8.3. The stirrer speed was maintained at the lowest setting, 500 rpm, so that the production of foam was avoided.

8.3 Quantitative considerations and theory

It was shown in Chapter 5 that particle bridges can form when the interfacial area generated by shear is greater than the interfacial area which can be covered by the available particles. In the experiments described in Chapter 5, where a rotor-stator was used to shear the emulsions, the critical shear rate required to achieve this was usually such that the flow conditions in the shear zone were in the transitional régime between laminar and turbulent flow. Whether the flow is turbulent in the shear zone is determined by Eq. (1.15). For the magicLab, $Re > 1000$ across the entire range of available shear rates, and so the flow in the shear zone will always be turbulent.

The IKA magicLab setup provides an opportunity to probe the effects of the flow conditions further. As can be seen in Fig. 8.1, the sample passes through the shear zone, then through a pipe and back into the hopper. If the flow rate through the pipe is great enough, the flow will be turbulent not only in the shear zone, but in the pipe as well. Whether the flow is turbulent in the pipe is determined by the pipe Reynolds number, Re_{pipe}, which for a pipe of circular cross section is given by:

$$Re_{pipe} = \frac{\rho v d_{pipe}}{\eta} = \frac{\rho Q d_{pipe}}{\eta A}, \tag{8.1}$$

where d_{pipe} is the pipe diameter, Q is the mean flow rate and A is the cross-sectional area of the pipe. When $Re_{pipe} \lesssim 2000$ the flow will be laminar, and when $Re_{pipe} \gtrsim 4000$ the flow will be turbulent [147]. Since the flow at the start of the pipe is likely to be turbulent due to the highly turbulent shear zone, the flow in the pipe is likely to be turbulent as well through most of the transitional régime at $2000 < Re_{pipe} < 4000$.

8.4 Results and discussion

8.4.1 Flow conditions

The flow rate through the pipe was measured at various shear rates by measuring the length of time taken to fill a 500 mL beaker with water. This showed that the flow rate was directly proportional to the shear rate for shear rates below $\approx 40\,000\ s^{-1}$, and plateaued above this value, as can be seen in Fig. 8.3. Using Eq. (8.1), the pipe Reynolds number was calculated at each shear rate, and the flow throughout the pipe was calculated to be laminar below shear rates of $\approx 13\,000\ s^{-1}$ and fully turbulent above shear rates of $\approx 27\,000\ s^{-1}$, with a transitional régime existing between these points. Foam was produced if the shear rate was increased above $\approx 20\,000\ s^{-1}$.

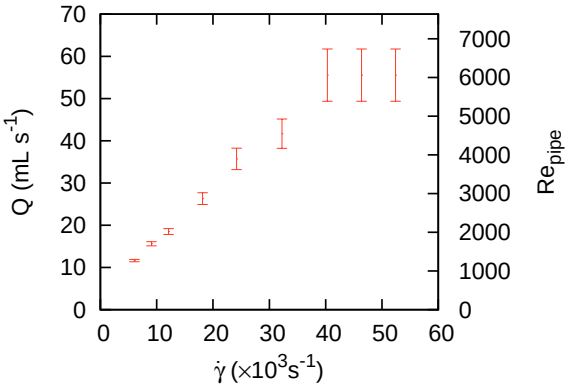

Figure 8.3 *Graph showing the flow rate and pipe Reynolds number in the IKA magicLab as a function of shear rate.*

8.4.2 Bridged Pickering emulsions produced using continuous flow

A photograph of samples taken during a continuous flow emulsification experiment carried out with $\phi_p = 0.2\%$, $\phi_o = 5\%$ and $\Phi_{IM} = 20\%$ is shown in Fig. 8.4. The temperature of the sample was 24℃ throughout the experiment, which means that the viscosities of the fluids will also have remained constant.

The samples in Fig. 8.4 are all clearly bridged, and the amount of free silica

Figure 8.4 *Photograph of Pickering emulsions created using continuous flow. The samples were taken* 2, 5 *and* 10 *min into the emulsification process (from left to right). It can clearly be seen that all of the samples are bridged and that the amount of free silica decreases as the experiment progresses.*

decreases with emulsification time. Free silica is observable at all emulsification times, however, and this may be caused by the mixture of particles used in the experiment leading to a variety of particle wettabilities being present. That the emulsion is so strongly bridged whilst there is still free silica is initially surprising, but particle bridging can occur whenever partially coated droplets collide, and this requires only local depletion of particles. Local depletion of particles may occur more readily in the continuous flow system, as there is a large shear zone which is mostly turbulent, and it would not be surprising if the local particle volume fraction at some points in the flow is very low. Furthermore, entrainment effects may lead to differing flow rates through the shear zone for droplets and particles, and this may also cause local depletion of the particles. These effects may also explain why free silica is always observable, although the variation in particle wettabilities, due to the mixture of particles used, remains the most likely explanation.

Micrographs of the samples are shown in Fig. 8.5 and confocal micrographs are shown in Fig. 8.6. These images confirm that the droplets are bridged, and that the droplet size decreases as the experiment progresses, which is expected since the amount of free silica decreased.

Unfortunately, insufficient silica was available to carry out further experiments at

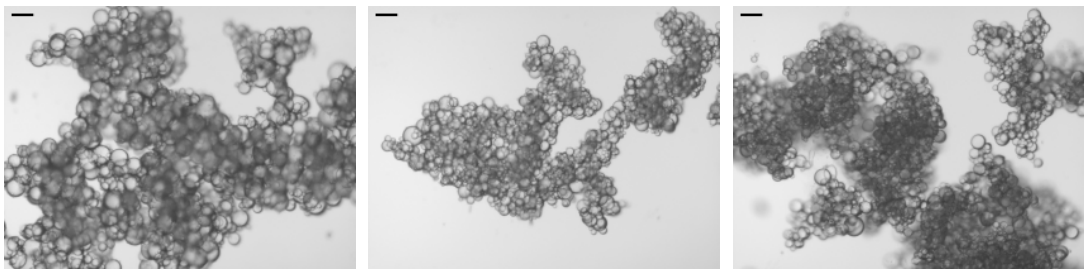

Figure 8.5 *Micrographs of Pickering emulsions created using continuous flow. The samples were taken* 2, 5 *and* 10 *min into the emulsification process (from left to right). The scale bars are* 100 μm.

higher particle volume fractions. Based on the observations in these experiments and those presented in Chapter 5, however, it is very likely that at higher particle volume fractions the degree of particle bridging will reduce. At particle volume fractions approximately equal to the critical particle volume fraction for particle bridging, it is thought that bridging will not be evident initially, but will instead occur only after a certain period of emulsification. If this is the case, then there is clearly a danger of creating unwanted particle bridges if an emulsion is sheared for too long, and this will be of relevance to industrial-scale production of Pickering emulsions.

8.5 Conclusions and future work

It has been shown here, for the first time, that particle bridging is relevant to Pickering emulsions produced using continuous flow. The bridging behaviour described in Chapter 5 has been successfully replicated at a larger scale - with sample volumes increasing from $\approx 3\ mL$ to $\approx 1\ L$ - by utilising a continuous flow emulsification device.

Although it has not been possible to prove experimentally using the continuous flow apparatus, it is thought very likely that an emulsion can transition from a non-bridged state to a bridged state as it is sheared. This will happen when the particle volume fraction is at an intermediate value so that the sample is initially non-bridged, but will become bridged when the system becomes depleted of particles, allowing collisions between partially coated droplets to occur. This should be of relevance to industrial-scale emulsification, as it shows that the time spent in the emulsification device is critical to the emulsion phase behaviour.

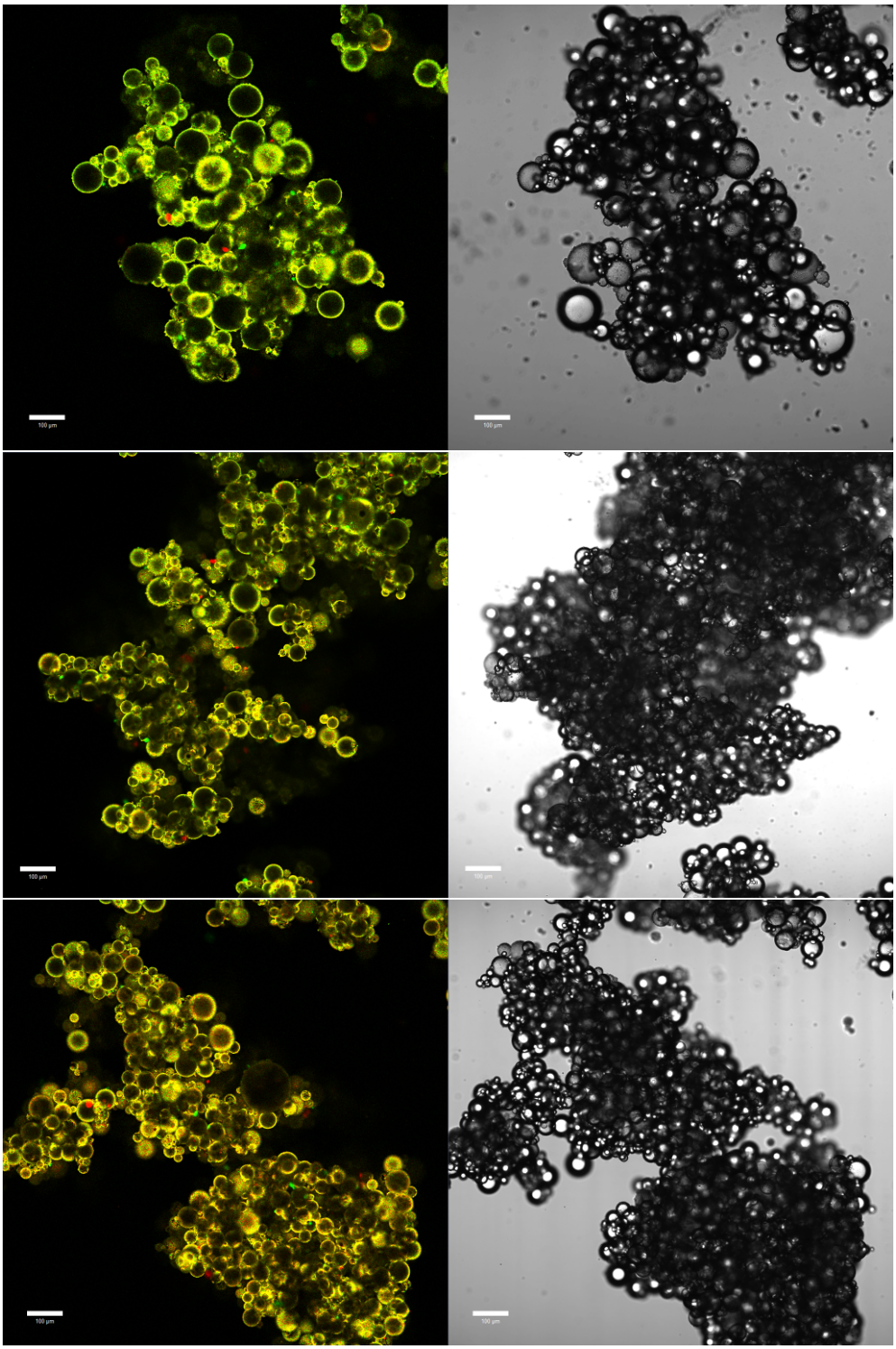

Figure 8.6 *Confocal micrographs of Pickering emulsions created using continuous flow. The samples were taken, from top to bottom,* 2, 5 *and* 10 *min into the emulsification process. The scale bars are* 100 μm.

There are a number of directions this work could take in the future. Perhaps most obviously, the experiments at higher particle volume fractions where the emulsion is either non-bridged or transitions from being non-bridged to being bridged could be carried out to confirm that this occurs. Furthermore, if the problems with foam production at high shear rates can be overcome, which may be possible by adjusting the height and speed of the stirring mechanism, then it would also be interesting to look at the differences in emulsions formed by laminar and turbulent flow. More generally, comparisons could be made between emulsions formed by continuous flow with those formed by batch processes such as vortex mixing and rotor-stator emulsification. The residence times of droplets in the shear zones in each of these emulsification procedures is different and this is likely to have an effect on the emulsion's properties, and may also affect whether inverted emulsions are able to form. Finally, continuous flow emulsification could also be used to further study aspects of particle bridging discussed in Chapter 5. For example, varying the oil volume fraction will alter the frequency of collisions between droplets and the effect of this change on the bridging behaviour may be interesting.

Chapter 9

Conclusions and future work

A model oil-in-water Pickering emulsion system has been developed in order to experimentally study the physics of various fundamental aspects of Pickering emulsions. This model system uses monodisperse, spherical, fluorescently labelled Stöber silica and an oil phase which is a mixture of dodecane and isopropyl myristate. Varying the ratio of the two oils in the oil phase allows the particle wettability to be controlled. The use of fluorescently labelled silica particles allows confocal microsopy to be used to directly observe the particles at the oil-water interface.

In Chapter 3 the phase behaviour of aqueous dispersions of both Stöber and fumed silica particles was characterised at various salt concentrations and pH values. In Chapter 4 the phase behaviour of the particle dispersions was used to explain the differences observed in the emulsion phase behaviour as the salt concentration and pH were varied. This work has shown that a more nuanced view of Pickering stabilisation than has conventionally been put forward is necessary; it is important to take into account factors other than simple maximisation of the trapping energy by using particles which are equally wetted by both fluid phases. Such factors include the particle-interface interactions during emulsification and the strength of interactions between particles at the interface. In disagreement with statements previously made in the literature by, for example, Binks and Lumsdon [43], it is not necessary to have a flocculating particle dispersion in order to stabilise a Pickering emulsion and in some cases causing the particles to weakly flocculate will lower the emulsion stability dramatically. This behaviour is attributed to the positively charged Stöber silica particles, which sequester easily to the (typically)

negatively charged oil-water interface in the absence of salt. Adding salt to this system will make the particles sit further into the aqueous phase and therefore decrease the likelihood of particles adsorbing to the interface, unlike in emulsions stabilised by fumed silica, which is typically negatively charged.

It is not yet clear, however, how the phase behaviour of the particles at the interface will affect the stability and phase behaviour of a Pickering emulsion. It is also not clear how the bulk particle phase behaviour is related to the behaviour at the interface, and systematic studies of the physics involved in these areas could provide considerable new insight into the optimal conditions for creating stable Pickering emulsions.

Significant work on particle bridging in Pickering emulsions has also been carried out and is presented in Chapters 5-8. In Chapter 5 it was shown that particle bridging can occur in Pickering emulsions when partially coated droplets collide, as long as the particles protrude slightly into the continuous phase. Particle bridges can therefore form when the interfacial area generated by shear exceeds that which can be stabilised by the available particles, and so is most likely to occur at high shear or when the particle volume fraction is low. It has also been shown that particle bridges can subsequently be removed by applying low shear or by modifying the particle wettability.

A novel method for studying emulsification and demulsification processes has been developed and was presented in Chapter 6 and Chapter 7. By mixing together two different emulsions, each of which was prepared using a different colour of silica, the surprisingly dynamic behaviour of Pickering emulsions has been observed. Particles are shown to transfer between droplets when a low shear rate is applied to the sample, and various factors which affect the rate of particle transfer are studied and explained. In particular, in Chapter 6 the unbridging/rebridging process which precedes deaggregation in bridged Pickering emulsions was shown to substantially increase the particle transfer rate. This method has also been applied, in Chapter 7, to the study of Pickering emulsions as they are repeatedly sheared, and it is hoped that the understanding of other emulsification processes will benefit from its application in the future.

Finally, Chapter 8 demonstrated the relevance of particle bridging to industrial-scale emulsification processes by replicating the particle bridging behaviour using a continuous flow setup and a sample volume of ≈ 1 L. The use of this setup to study the effects of residence time in the shear zone on emulsification, and

comparisons with other emulsification techniques, could be highly informative.

This thesis describes several novel behaviours in Pickering emulsions and solidifies understanding of several more. It should therefore be relevant to anyone wishing to design or understand a well-controlled Pickering emulsion system.

Bibliography

[1] R.A.L. Jones. *Soft Condensed Matter*. Oxford University Press, Oxford, 2002.

[2] P.M. Chaikin and T.C. Lubensky. *Principles of Condensed Matter Physics*. Cambridge University Press, Cambridge, 1995.

[3] F. Leal-Calderon, J. Bibette, and V. Schmitt. *Emulsion Science Basic Principles*. Springer, New York, 2007.

[4] B.P. Binks and T.S. Horozov. *Colloidal Particles at Liquid Interfaces*. Cambridge University Press, Cambridge, 2006.

[5] S.U. Pickering. Emulsions. *Journal of the Chemical Society*, 91(Part 2): 2001–2021, 1907.

[6] W. Ramsden. Separation of solids in the surface-layers of solutions and 'suspensions' (observations on surface-membranes, bubbles, emulsions, and mechanical coagulation). – Preliminary account. *Proceedings of the Royal Society of London*, 72(479):156–164, 1903.

[7] R. Aveyard, B.P. Binks, and J.H. Clint. Emulsions stabilised solely by colloidal particles. *Advances in Colloid and Interface Science*, 100–102: 503–546, 2003.

[8] J.H. Clint and S.E. Taylor. Particle size and interparticle forces of overbased detergents: A Langmuir trough study. *Colloids and Surfaces*, 65(1):61–67, 1992.

[9] N. Glaser, D.J. Adams, A. Böker, and G. Krausch. Janus particles at liquid-liquid interfaces. *Langmuir*, 22(1):5227–5229, 2006.

[10] R. Miller, V.B. Fainerman, V.I. Kovalchuk, D.O. Grigoriev, M.E. Leser, and M. Michel. Composite interfacial layers containing micro-size and nano-size particles. *Advances in Colloid and Interface Science*, 128–130: 17–26, 2006.

[11] B.P. Binks, P.D.I. Fletcher, B.L. Holt, P. Beaussoubre, and K. Wong. Phase inversion of particle-stabilised perfume oil-water emulsions: Experiment and theory. *Physical Chemistry Chemical Physics*, 12(38): 11954–11966, 2010.

[12] B.L. Holt. *Nanoparticle-stabilised perfume oil emulsions*. PhD thesis, University of Hull, 2010.

[13] K.A. White, A.B. Schofield, P. Wormald, J.W. Tavacoli, B.P. Binks, and P.S. Clegg. Inversion of particle-stabilized emulsions of partially miscible liquids by mild drying of modified silica particles. *Journal of Colloid and Interface Science*, 359(1):126–135, 2011.

[14] B.P. Binks and S.O. Lumsdon. Pickering emulsions stabilized by monodisperse latex particles: Effects of particle size. *Langmuir*, 17(15): 4540–4547, 2001.

[15] A.R. Bausch, M.J. Bowick, A. Cacciuto, A.D. Dinsmore, M.F. Hsu, D.R. Nelson, M.G. Nikolaides, A. Travesset, and D.A. Weitz. Grain boundary scars and spherical crystallography. *Science*, 299(5613):1716–1718, 2003.

[16] R.M. Wiley. Limited coalescence of oil droplets in coarse oil-in-water emulsions. *Journal of Colloid Science*, 9(5):427–437, 1954.

[17] S. Arditty, C.P. Whitby, B.P. Binks, V. Schmitt, and F. Leal-Calderon. Some general features of limited coalescence in solid-stabilized emulsions. *The European Physical Journal E: Soft Matter*, 11(3):273–281, 2003.

[18] B.P. Binks and J.A. Rodrigues. Types of phase inversion of silica particle stabilized emulsions containing triglyceride oil. *Langmuir*, 19(12): 4905–4912, 2003.

[19] B.P. Binks and S.O. Lumsdon. Effects of oil type and aqueous phase composition on oil-water mixtures containing particles of intermediate hydrophobicity. *Physical Chemistry Chemical Physics*, 2(13):2959–2967, 2000.

[20] J.T. Davies and E.K. Rideal. *Interfacial Phenomena*. Academic Press, London, 1963.

[21] E. Vignati, R. Piazza, and T.P. Lockhart. Pickering emulsions: Interfacial tension, colloidal layer morphology, and trapped-particle motion. *Langmuir*, 19(17):6650–6656, 2003.

[22] M.E. Cates. Complex fluids: The physics of emulsions. Preprint at *http://arxiv.org/abs/1209.2290*, 2012.

[23] S.A.F. Bon. Pickering suspension, mini-emulsion and emulsion polymerization. In T. Ngai and S.A.F. Bon, editors, *Particle-Stabilized Emulsions and Colloids: Formation and Applications*, chapter 4. The Royal Society of Chemistry, Cambridge, 2015.

[24] N.P. Ashby and B.P. Binks. Pickering emulsions stabilised by Laponite clay particles. *Physical Chemistry Chemical Physics*, 2(24):5640–5646, 2000.

[25] H. Lamb. *Hydrodynamics*. Dover Publications, London, 1932.

[26] M.M. Robins and D.J. Hibberd. Emulsion flocculation and creaming. In B.P. Binks, editor, *Modern Aspects of Emulsion Science*, chapter 4. The Royal Society of Chemistry, Cambridge, 1998.

[27] B.P. Binks. Emulsions - recent advances in understanding. In B.P. Binks, editor, *Modern Aspects of Emulsion Science*, chapter 1. The Royal Society of Chemistry, Cambridge, 1998.

[28] T.S. Horozov and B.P. Binks. Particle-stabilized emulsions: A bilayer or a bridging monolayer? *Angewandte Chemie International Edition*, 45(5): 773–776, 2006.

[29] P. Walstra. Principles of emulsion formation. *Chemical Engineering Science*, 48(2):333–349, 1993.

[30] R.G. Larson. *The Structure and Rheology of Complex Fluids*. Oxford University Press, New York, 1999.

[31] A.N. Kolmogorov. On the breakage of drops in a turbulent flow. *Doklady Akademii Nauk SSSR*, 66(5):825–828, 1949 [In Russian].

[32] J.T. Davies. *Turbulence Phenomena*. Academic Press, London, 1972.

[33] P. Walstra and P.E.A. Smulders. Emulsion formation. In B.P. Binks, editor, *Modern Aspects of Emulsion Science*, chapter 2. The Royal Society of Chemistry, Cambridge, 1998.

[34] N. Vankova, S. Tcholakova, N.D. Denkov, I.B. Ivanov, V.D. Vulchev, and T. Danner. Emulsification in turbulent flow 1. Mean and maximum drop diameters in inertial and viscous regimes. *Journal of Colloid and Interface Science*, 312(2):363–380, 2007.

[35] T. Sparks. *Fluid mixing in rotor/stator mixers*. PhD thesis, Cranfield University, 1996.

[36] L. Maurice, R.A. Maguire, A.B. Schofield, M.E. Cates, P.S. Clegg, and J.H.J. Thijssen. Squeezing particle-stabilized emulsions into biliquid foams - equation of state. *Soft Matter*, 9(32):7757–7765, 2013.

[37] M. Hermes and P.S. Clegg. Yielding and flow of concentrated Pickering emulsions. *Soft Matter*, 9(31):7568–7575, 2013.

[38] T.R. Briggs. Emulsions with finely divided solids. *Journal of Industrial & Engineering Chemistry*, 13(11):1008–1010, 1921.

[39] B.P. Binks and S.O. Lumsdon. Catastrophic phase inversion of water-in-oil emulsions stabilized by hydrophobic silica. *Langmuir*, 16(6): 2539–2547, 2000.

[40] B.P. Binks. Particles as surfactants - similarities and differences. *Current Opinion in Colloid & Interface Science*, 7(1–2):21–41, 2002.

[41] B.P. Binks and C.P. Whitby. Nanoparticle silica-stabilised oil-in-water emulsions: Improving emulsion stability. *Colloids and Surfaces A: Physicochemical Engineering Aspects*, 253(1–3):105–115, 2005.

[42] I. Kalashnikova, H. Bizot, B. Cathala, and I. Capron. Modulation of cellulose nanocrystals amphiphilic properties to stabilize oil/water interface. *Biomacromolecules*, 13(1):267–275, 2012.

[43] B.P. Binks and S.O Lumsdon. Stability of oil-in-water emulsions stabilised by silica particles. *Physical Chemistry Chemical Physics*, 1(12):3007–3016, 1999.

[44] C.P. Whitby, F.E. Fischer, D. Fornasiero, and J. Ralston. Shear-induced coalescence of oil-in-water Pickering emulsions. *Journal of Colloid and Interface Science*, 361(1):170–177, 2011.

[45] B.V. Derjaguin and L.D. Landau. Theory of the stability of strongly charged lyophobic sols and of the adhesion of strongly charged particles in solutions of electrolytes. *Acta Physicochimica URSS*, 14:633–662, 1941 [In Russian].

[46] E.J.W. Verwey, J.Th.G. Overbeek, and K. van Nes. *Theory of the Stability of Lyophobic Colloids*. Elsevier, Amsterdam, 1948.

[47] W.B. Russel, D.A. Saville, and W.R. Schowalter. *Colloidal Dispersions*. Cambridge University Press, Cambridge, 1991.

[48] H.E. Bergna. *The Colloid Chemistry of Silica*. American Chemical Society, Washington D.C., 1994.

[49] R.F. Probstein. *Physicochemical Hydrodynamics*. Wiley, Hoboken, 2003.

[50] Diagram defining zeta potential and the slipping plane. Online, retrieved 28/5/12, http://en.wikipedia.org/wiki/File:Diagram_of_zeta_potential_and_slipping_planeV2.svg.

[51] J.N. Israelachvili. *Intermolecular and Surface Forces*. Academic Press, London, 1992.

[52] D.J. Shaw. *Introduction to Colloid & Surface Chemistry*. Butterworths, London, 1989.

[53] K.A. White, A.B. Schofield, B.P. Binks, and P.S. Clegg. Influence of particle composition and thermal cycling on bijel formation. *Journal of Physics: Condensed Matter*, 20(49):494223, 2008.

[54] R.K. Iler. *The Chemistry of Silica: Solubility, Polymerization, Colloid and Surface Properties, and Biochemistry*. Wiley, New York, 1979.

[55] D.M. Kaz, R. McGorty, M. Mani, M.P. Brenner, and V.N. Manoharan. Physical ageing of the contact line on colloidal particles at liquid interfaces. *Nature Materials*, 11(2):138–142, 2012.

[56] H. Wang, V. Singh, and S.H. Behrens. Image charge effects on the formation of Pickering emulsions. *The Journal of Physical Chemistry Letters*, 3(20):2986–2990, 2012.

[57] D.R. Lide, editor. *CRC Handbook of Chemistry and Physics*. CRC Press, Boca Raton, 82nd edition, 2001.

[58] M.A. Rivas, T.P. Iglesias, S.M. Pereira, and N. Banerji. On the permittivity and density of the systems {tetraglyme + (*n*-nonane or *n*-dodecane} at various temperatures. *The Journal of Chemical Thermodynamics*, 38(3):245–256, 2006.

[59] P.R. Leroueil, S. Hong, A. Mecke, J.R. Baker Jr., B.G. Orr, and M.M. Banaszak Holl. Electrostatics at the oil-water interface, stability, and order in emulsions and colloids. *Proceedings of the National Academy of Sciences of the United States of America*, 104(8):2585–2590, 2007.

[60] J. C. Fernández-Toledano, A. Moncho-Jordá, F. Martínez-López, and R. Hidalo-Álvarez. Theory for interactions between particles in monolayers. In B.P. Binks, editor, *Colloidal Particles at Liquid Interfaces*, chapter 3. Cambridge University Press, Cambridge, 2006.

[61] M. Oettel and S. Dietrich. Colloidal interactions at fluid interfaces. *Langmuir*, 24(4):1425–1441, 2008.

[62] L. Botto, E.P. Lewandowski, M. Cavallaro, and K.J. Stebe. Capillary interactions between anisotropic particles. *Soft Matter*, 8(39):9957–9971, 2012.

[63] A.J. Hurd. The electrostatic interaction between interfacial colloidal particles. *Journal of Physics A: Mathematical and General*, 18(16):L1055, 1985.

[64] S. Levine, B.D. Bowen, and S.J. Partridge. Stabilization of emulsions by fine particles I. Partitioning of particles between continuous phase and oil/water interface. *Colloids and Surfaces*, 38(2):325–343, 1989.

[65] I. Langmuir. The constitution and fundamental properties of solids and liquids. II. Liquids. *Journal of the American Chemical Society*, 39(9): 1848–1906, 1917.

[66] R. Aveyard, B.P. Binks, J.H. Clint, P.D.I. Fletcher, T.S. Horozov, B. Neumann, V.N. Paunov, J. Annesley, S.W. Botchway, D. Nees, A.W. Parker, A.D. Ward, and A.N. Burgess. Measurement of long-range repulsive forces between charged particles at an oil-water interface. *Physical Review Letters*, 88(24):246102, 2002.

[67] T. Li, M. Kalloudis, A. Zamith Cardoso, D.J. Adams, and P.S. Clegg. Drop-casting hydrogels at a liquid interface: The case of hydrophobic dipeptides. *Langmuir*, 30(46):13854–13860, 2014.

[68] P.G. de Gennes. Wetting: Statics and dynamics. *Reviews of Modern Physics*, 57(3):827–863, 1985.

[69] R. Tadmor. Line energy and the relationship between advancing, receding and Young contact angles. *Langmuir*, 20(18):7659–7664, 2004.

[70] L. Isa, F. Lucas, R. Wepf, and E. Reimhult. Measuring single-nanoparticle wetting properties by freeze-fracture shadow-casting cryo-scanning electron microscopy. *Nature Communications*, 2:438–457, 2011.

[71] B.P. Binks, L. Isa, and A.T. Tyowua. Direct measurement of contact angles of silica particles in relation to double inversion of Pickering emulsions. *Langmuir*, 29(16):4923–4927, 2013.

[72] T.S. Horozov, A.B. Dulce, P.D.I. Fletcher, B.P. Binks, and J.H. Clint. Novel film-calliper method of measuring the contact angle of colloidal particles at liquid interfaces. *Langmuir*, 24(5):1678–1681, 2008.

[73] J. Vermant and Th. Schweizer. Rheology of complex fluids. In *Functional Soft Matter*. 46th IFF Spring School, Forschungszentrum Jülich GmbH, Jülich, 2015.

[74] C.W. Macosko. *Rheology: Principles, Measurements, and Applications*. Wiley-VCH, New York, 1994.

[75] A. Goebel and K. Lunkenheimer. Interfacial tension of the water/n-alkane interface. *Langmuir*, 13(2):369–372, 1997.

[76] W. Stöber, A. Fink, and E. Bohn. Controlled growth of monodisperse silica spheres in the micron size range. *Journal of Colloid and Interface Science*, 26(1):62–69, 1968.

[77] A. van Blaaderen and A. Vrij. Synthesis and characterization of colloidal dispersions of fluorescent, monodisperse silica spheres. *Langmuir*, 8(12): 2921–2931, 1992.

[78] A. Imhof, M. Megens, J.J. Engelberts, D.T.N. de Lang, R. Sprik, and W.L. Vos. Spectroscopy of fluorescein (FITC) dyed colloidal silica spheres. *Journal of Physical Chemistry B*, 103(9):1408–1415, 1999.

[79] N.A.M. Verhaegh and A. van Blaaderen. Dispersions of Rhodamine-labeled silica spheres: Synthesis, chacterization, and fluoresence confocal scanning laser microscopy. *Langmuir*, 10(5): 1427–1438, 1994.

[80] Basic characteristics of AEROSIL fumed silica. Online, retrieved 16/4/15, https://www.aerosil.com/product/aerosil/Documents/TB-11-Basic-Characteristics-of-AEROSIL-Fumed-Silica-EN.pdf.

[81] W.J. Frith, R. Pichot, M. Kirkland, and B. Wolf. Formation, stability, and rheology of particle stabilized emulsions: Influence of multivalent cations. *Industrial & Engingeering Chemistry Research*, 47(17):6434–6444, 2008.

[82] D.J. Fairhurst. *Polydispersity in colloidal phase transitions*. PhD thesis, University of Edinburgh, 1999.

[83] P.N. Pusey and W. van Megen. Detection of small polydispersities by photon correlation spectroscopy. *Journal of Chemical Physics*, 80(8): 3513–3520, 1984.

[84] R.J. Hunter. *Foundations of Colloid Science: Volume I*. Oxford University Press, Oxford, 1991.

[85] http://www.imagemagick.org.

[86] E. Zaccarelli. Colloidal gels: Equilibrium and non-equilibrium routes. *Journal of Physics: Condensed Matter*, 19(32):323101, 2007.

[87] A.G. Mailer. *Colloidal cluster phases and solar cells*. PhD thesis, University of Edinburgh, 2012.

[88] P.N. Pusey. The effect of polydispersity on the crystallization of hard spherical colloids. *Journal de Physique*, 48(5):709–712, 1987.

[89] L.G.J. Fokkink and J. Ralston. Contact angles on charged substrates. *Colloids and Surfaces*, 36(1):69–76, 1989.

[90] E. Serrano-Saldaña, A. Domínguez-Ortiz, H. Pérez-Aguilar, I. Kornhauser-Strauss, and F. Rojas-González. Wettability of solid/brine/n-dodecane systems: Experimental study of the effects of ionic strength and surfactant concentration. *Colloids and Surfaces A: Physicochemical Engineering Aspects*, 241(1-3):343–349, 2004.

[91] G. Hanly, D. Fornasiero, J. Ralston, and R. Sedev. Electrostatics and metal oxide wettability. *The Journal of Physical Chemistry C*, 115(30): 14914–14921, 2011.

[92] F.T. Barranco Jr., H.E. Dawson, J.M. Christener, and B.D. Honeyman. Influence of aqueous pH and ionic strength on the wettability of quartz in the presence of dense non-aqueous-phase liquids. *Environmental Science & Technology*, 31(3):676–681, 1997.

[93] M.C. Phillips and A.C. Riddiford. Temperature dependence of contact angles. *Nature*, 205(4975):1005–1006, 1965.

[94] K. Bai and J. Katz. On the refractive index of sodium iodide solutions for index matching in PIV. *Experiments in Fluids*, 55(4):1704, 2014.

[95] I.M. Abdulagatov, A.B. Zeinalova, and N.D. Azizov. Viscosity of aqueous electrolyte solutions at high temperatures and high pressures. Viscosity B coefficient. Sodium iodide. *Journal of Chemical and Engineering Data*, 51 (5):1645–1659, 2006.

[96] B.W. Ninham and P. Lo Nostro. *Molecular Forces and Self Assembly: In Colloid, Nano Sciences and Biology*. Cambridge University Press, Cambridge, 2010.

[97] R. Sprycha. Electrical double layer at alumina/electrolyte interface I: Surface charge and zeta potential. *Journal of Colloid and Interface Science*, 127(1):1–11, 1989.

[98] R.J. Crawford, I.H. Harding, and D.E. Mainwaring. The zeta potential of iron and chromium hydrous oxides during adsorption and coprecipitation of aqueous heavy metals. *Journal of Colloid and Interface Science*, 181(2): 561–570, 1996.

[99] F. Gautier, M. Destribats, R. Perrier-Cornet, J-F. Dechézelles, J. Giermanska, V. Héroguez, S. Ravaine, F. Leal-Calderon, and V. Schmitt. Pickering emulsions with stimulable particles: From highly- to weakly-covered interfaces. *Physical Chemistry Chemical Physics*, 9(48): 6455–6462, 2007.

[100] M. Destribats, M. Rouvet, C. Gehin-Delval, C. Schmitt, and B.P. Binks. Emulsions stabilised by whey protein microgel particles: Towards food-grade Pickering emulsions. *Soft Matter*, 10(36):6941–6954, 2014.

[101] B.P. Binks, J. Philip, and J.A. Rodrigues. Inversion of silica-stabilized emulsions induced by particle concentration. *Langmuir*, 21(8):3296–3302, 2005.

[102] M.E. Leunissen, A. van Blaaderen, A.D. Hollingsworth, M.T. Sullivan, and P.M. Chaikin. Electrostatics at the oil-water interface, stability, and order in emulsions and colloids. *Proceedings of the National Academy of Sciences of the United States of America*, 104(8):2585–2590, 2007.

[103] K.G. Marinova, R.G. Alargova, N.D. Denkov, O.D. Velev, D.N. Petsev, I.B. Ivanov, and R.P. Borwankar. Charging of oil-water interfaces due to spontaneous adsorption of hydroxyl ions. *Langmuir*, 12(8):2045–2051, 1996.

[104] A. Kumar, B.J. Park, F. Tu, and D. Lee. Amphiphilic Janus particles at fluid interfaces. *Soft Matter*, 9(29):6604–6617, 2013.

[105] S. Arditty, V. Schmitt, J. Giermanska-Kahn, and F. Leal-Calderon. Materials based on solid-stabilized emulsions. *Journal of Colloid and Interface Science*, 275(2):659–664, 2004.

[106] S. Arditty, V. Schmitt, F. Lequeux, and F. Leal-Calderon. Interfacial properties in solid-stabilized emulsions. *The European Physical Journal B: Condensed Matter and Complex Systems*, 44(3):381–393, 2005.

[107] T.S. Horozov, R. Aveyard, B.P. Binks, and J.H. Clint. Structure and stability of silica particle monolayers at horizontal and vertical octane interfaces. *Langmuir*, 21(16):7405–7412, 2005.

[108] A.D. Law, M. Auriol, D. Smith, T.S. Horozov, and D.M. Buzza. Self-assembly of two-dimensional colloidal clusters by tuning the hydrophobicity, composition, and packing geometry. *Physical Review Letters*, 110(13):138301, 2013.

[109] N. Yan and J.H. Masliyah. Creaming behaviour of solids-stabilized oil-in-water emulsions. *Industrial & Engineering Chemistry Research*, 36 (4):1122–1129, 1997.

[110] E.J. Stancik, M. Kouhkan, and G.G. Fuller. Coalescence of particle-laden fluid interfaces. *Langmuir*, 20(1):90–94, 2004.

[111] N.D. Denkov, I.B. Ivanov, P.A. Kralchevsky, and D.T. Wasan. A possible mechanism of stabilization of emulsions by solid particles. *Journal of Colloid and Interface Science*, 150(2):589–593, 1992.

[112] E.J. Stancik, M. Kouhkan, and G.G. Fuller. Connect the drops: Using solids as adhesives for liquids. *Langmuir*, 20(12):4805–4808, 2004.

[113] M.N. Lee, H.K. Chan, and A. Mohraz. Nanoparticle interaction with biological membranes: Does nanotechnology present a Janus face? *Accounts of Chemical Research*, 40(5):335–342, 2007.

[114] H. Xu, M. Lask, J. Kirkwood, and G. Fuller. Particle bridging between oil and water interfaces. *Langmuir*, 23(9):4837–4841, 2007.

[115] E. Moghimi, F. Goharpey, and R. Foudazi. Role of droplet bridging on the stability of particle-containing immiscible polymer blends. *Rheologica Acta*, 53(2):165–180, 2014.

[116] S.P. Nagarkar and S.S. Velankar. Morphology and rheology of ternary fluid-fluid-solid systems. *Soft Matter*, 8(32):8464–8477, 2012.

[117] M. Destribats, V. Lapeyre, E. Sellier, F. Leal-Calderon, V. Ravaine, and V. Schmitt. Origin and control of adhesion between emulsion drops stabilized by thermally sensitive soft colloidal particles. *Langmuir*, 28(8): 3744–3755, 2012.

[118] E.M. Walker, D.S. Frost, and L.L. Dai. Particle self-assembly in oil-in-ionic liquid Pickering emulsions. *Journal of Colloid and Interface Science*, 363(1):307–313, 2011.

[119] D.S. Frost, J.J. Schoepf, E.M. Nofen, and L.L. Dai. Understanding droplet bridging in ionic liquid-based Pickering emulsions. *Journal of Colloid and Interface Science*, 383(1):103–109, 2012.

[120] B.P. Binks and S.O. Lumsdon. Transitional phase inversion of solid-stabilized emulsions using particle mixtures. *Langmuir*, 16(8): 3748–3756, 2000.

[121] B.P. Binks and S.O. Lumsdon. Influence of particle wettability on the type and stability of surfactant-free emulsions. *Langmuir*, 16(23): 8622–8631, 2000.

[122] B.P. Binks, R. Murakami, S.P. Armes, and S. Fujii. Effects of pH and salt concentration on oil-in-water emulsions stabilized solely by nanocomposite microgel particles. *Langmuir*, 22(5):2050–2057, 2006.

[123] A.K.F. Dyab. Destabilisation of Pickering emulsions using pH. *Colloids and Surfaces A: Physicochemical and Engineering Aspects*, 402:2–12, 2012.

[124] K.N. Pham, G. Petekidis, D. Vlassopoulos, S.U. Egalhaaf, P.N. Pusey, and W.C.K. Poon. Yielding of colloidal glasses. *Europhysics Letters*, 75 (4):624–630, 2006.

[125] S. Tsuji and H. Kawaguchi. Thermosensitive Pickering emulsion stabilized by poly(N-isopropylacrylamide)-carrying particles. *Langmuir*, 24(7): 3300–3305, 2008.

[126] Y. He. Preparation and modification of ZnO microspheres using a Pickering emulsion as template. *Materials Letters*, 9(1):114–117, 2005.

[127] F. Jansen and J. Harting. From bijels to Pickering emulsions: A lattice Boltzmann study. *Physical Review E*, 83(4):046707, 2011.

[128] F. Leal-Calderon and V. Schmitt. Solid-stabilized emulsions. *Current Opinion in Colloid & Interface Science*, 13(4):217–227, 2008.

[129] J.H.J. Thijssen and P.S. Clegg. Emulsification in binary liquids containing colloidal particles: A structure-factor analysis. *Journal of Physics: Condensed Matter*, 22(45):455102, 2010.

[130] P.S. Clegg, E.M. Herzig, A.B. Schofield, S.U. Egelhaaf, T.S. Horozov, B.P. Binks, M.E. Cates, and W.C.K. Poon. Emulsification of partially miscible liquids using colloidal particles: Nonspherical and extended domain structures. *Langmuir*, 23(11):5984–5994, 2007.

[131] Z.D. Cheng, P.M. Chaikin, J.X. Zhu, W.B. Russel, and W.V. Meyer. Crystallization kinetics of hard spheres in microgravity in the coexistence regime: Interactions between growing crystallites. *Physical Review Letters*, 88(1):015501, 2002.

[132] F. Ravera, M. Ferrari, L. Liggieri, G. Loglio, E. Santini, and A. Zanobini. Liquid-liquid interfacial properties of mixed nanoparticle-surfactant systems. *Colloids and Surfaces A: Physicochemical and Engineering Aspects*, 323(1–3):99–108, 2008.

[133] J. Krägel and S.R. Derkatch. Interfacial shear rheology. *Current Opinion in Colloid & Interface Science*, 15(4):246–255, 2010.

[134] S. Vandebril, J. Vermant, and P. Moldenaers. Efficiently suppressing coalescence in polymer blends using nanoparticles: Role of interfacial rheology. *Soft Matter*, 6(14):3353–3362, 2010.

[135] A.J. Mendoza, E. Guzmán, F. Martínez-Pedrero, H. Ritacco, R.G. Rubio, F. Ortega, V.M. Starov, and R. Miller. Particle laden fluid interfaces: Dynamics and interfacial rheology. *Advances in Colloid and Interface Science*, 206:303–319, 2014.

[136] H. Yongqiang, W. Fei, S. Xiying, L. Ruqiang, G. Yongqin, L. Chuanbao, Z. Lu, X. Fubao, W. Wei, and G. Jianping. Factors that affect Pickering emulsions stabilized by graphene oxide. *Applied Materials & Interfaces*, 5 (11):4843–4855, 2013.

[137] A.B. Subramaniam, M. Abkarian, L. Mahadevan, and H.A. Stone. Mechanics of interfacial composite materials. *Langmuir*, 22(24): 10204–10208, 2006.

[138] L. Taisne, P. Walstra, and B. Cabane. Transfer of oil between emulsion droplets. *Journal of Colloid and Interface Science*, 184(2):378–390, 1996.

[139] E. Sanz, K.A. White, P.S. Clegg, and M.E. Cates. Colloidal gels assembled via a temporary interfacial scaffold. *Physical Review Letters*, 103(25):255502, 2009.

[140] H. Xu, S. Melle, K. Golemanov, and G. Fuller. Shape and buckling transitions in solid-stabilized drops. *Langmuir*, 21(22):10016–10020, 2005.

[141] M. von Smoluchowski. Versuch einer mathematischen Theorie der Koagulationskinetik kolloider Lösungen. *Zeitschrift für Phyisikalische Chemie*, 92(2):129–168, 1917 [In German].

[142] A. Lips, T. Westbury, P.M. Hart, I.D. Evans, and I.J. Campbell. On the physics of shear-induced aggregation in concentrated food emulsions. In E. Dickinson and P. Walstra, editors, *Food Colloids and Polymers: Stability and Mechanical Properties*, pages 31–44. The Royal Society of Chemistry Special Publications, London, 1993.

[143] Q. Yuan, O.J. Cayre, M. Manga, R.A. Williams, and S. Biggs. Preparation of particle-stabilized emulsions using membrane emulsification. *Soft Matter*, 6(7):1580–1588, 2010.

[144] K.L. Thompson, S. Armes, and D.W. York. Preparation of Pickering emulsions and colloidosomes with relatively narrow size distributions by stirred cell membrane emulsification. *Langmuir*, 27(6):2357–2363, 2011.

[145] G. Sun, F. Qi, J. Wu, G. Ma, and T. Ngai. Preparation of uniform particle-stabilized emulsions using SPG membrane emulsification. *Langmuir*, 30(24):7052–7056, 2014.

[146] IKA magicLab operating manual. Online, retrieved 9/4/15, http://www.masterflex.com/assets/Manual_pdfs/04300-01.pdf.

[147] J.F. Douglas, J.M. Gasiorek, and J.A. Swaffield. *Fluid Mechanics*. Prentice Hall, Harlow, fourth edition, 2001.